



National Library
of Canada

Acquisitions and
Bibliographic Services Branch

395 Wellington Street
Ottawa, Ontario
K1A 0N4

Bibliothèque nationale
du Canada

Direction des acquisitions et
des services bibliographiques

395, rue Wellington
Ottawa (Ontario)
K1A 0N4

Your file - Votre référence

Our file - Notre référence

NOTICE

The quality of this microform is heavily dependent upon the quality of the original thesis submitted for microfilming. Every effort has been made to ensure the highest quality of reproduction possible.

If pages are missing, contact the university which granted the degree.

Some pages may have indistinct print especially if the original pages were typed with a poor typewriter ribbon or if the university sent us an inferior photocopy.

Reproduction in full or in part of this microform is governed by the Canadian Copyright Act, R.S.C. 1970, c. C-30, and subsequent amendments.

AVIS

La qualité de cette microforme dépend grandement de la qualité de la thèse soumise au microfilmage. Nous avons tout fait pour assurer une qualité supérieure de reproduction.

S'il manque des pages, veuillez communiquer avec l'université qui a conféré le grade.

La qualité d'impression de certaines pages peut laisser à désirer, surtout si les pages originales ont été dactylographiées à l'aide d'un ruban usé ou si l'université nous a fait parvenir une photocopie de qualité inférieure.

La reproduction, même partielle, de cette microforme est soumise à la Loi canadienne sur le droit d'auteur, SRC 1970, c. C-30, et ses amendements subséquents.

TERMINAL AND BRIDGING ARYLDIAZENIDO COMPLEXES OF IRIDIUM

by

Xiaoqian Yan

B.Sc., Nanjing University (China), 1980

M.Sc., Nanjing University (China), 1983

A THESIS SUBMITTED IN PARTIAL FULFILLMENT OF
THE REQUIREMENTS FOR THE DEGREE OF
DOCTOR OF PHILOSOPHY
in the Department of Chemistry

© Xiaoqian Yan 1993

Simon Fraser University

June 1993

All right reserved. This thesis may not be
reproduced in whole or in part, by photocopy
or other means, without permission of the author.



National Library
of Canada

Acquisitions and
Bibliographic Services Branch

395 Wellington Street
Ottawa, Ontario
K1A 0N4

Bibliothèque nationale
du Canada

Direction des acquisitions et
des services bibliographiques

395, rue Wellington
Ottawa (Ontario)
K1A 0N4

Your file *Votre référence*

Our file *Notre référence*

The author has granted an irrevocable non-exclusive licence allowing the National Library of Canada to reproduce, loan, distribute or sell copies of his/her thesis by any means and in any form or format, making this thesis available to interested persons.

L'auteur a accordé une licence irrévocable et non exclusive permettant à la Bibliothèque nationale du Canada de reproduire, prêter, distribuer ou vendre des copies de sa thèse de quelque manière et sous quelque forme que ce soit pour mettre des exemplaires de cette thèse à la disposition des personnes intéressées.

The author retains ownership of the copyright in his/her thesis. Neither the thesis nor substantial extracts from it may be printed or otherwise reproduced without his/her permission.

L'auteur conserve la propriété du droit d'auteur qui protège sa thèse. Ni la thèse ni des extraits substantiels de celle-ci ne doivent être imprimés ou autrement reproduits sans son autorisation.

ISBN 0-315-91262-6

Canada

APPROVAL

Name: Xiaoqian Yan
Degree: Ph.D.
Title of Thesis: Terminal and Bridging Aryldiazenido Complexes of Iridium

Examining Committee:
Chair: Dr. T. Bell

Dr. D. Sutton (Professor)
Senior Supervisor

Dr. C.H.W. Jones (Professor)
Committee Member

Dr. L.K. Peterson (Associate Professor)
Committee Member

Internal Examiner: Dr. F.W.B. Einstein (Professor)

External Examiner: Dr. R.J. Angelici
Distinguished Professor
Iowa State University of Science & Technology

Date Approved: _____

2 July 1993

Abstract

Electronic structures for various geometries of coordinated aryldiazenido ligand in complexes are developed by using *Fragment Molecular Orbital Interaction* analysis.

π -acid strengths of the singly bent aryldiazenido and nitrosyl ligands in the identical chemical environment of the compounds $[\text{Cp}^*\text{Ir}(\text{C}_2\text{H}_4)\text{L}]\text{BF}_4$ (L= NO and *p*- $\text{N}_2\text{C}_6\text{H}_4\text{OMe}$) have been compared. It is concluded that the singly bent diazenido ligand is a stronger π -acid than the linear nitrosyl in a low symmetric environment. Further, the singly bent aryldiazenido ligand is shown to undergo re-orientation of the aryl substituent, leading to two observable isomers at low temperature.

The π effect of the ancillary ligands on the geometric preference of the aryldiazenido ligand in the complexes $[\text{Cp}^*\text{Ir}(\text{L})(\textit{p}\text{-N}_2\text{C}_6\text{H}_4\text{OMe})]^0$ or + is demonstrated. This is characterized by following results:

1. When L= CO, a strong π -acid, no stable complex $[\text{Cp}^*\text{Ir}(\text{CO})(\textit{p}\text{-N}_2\text{C}_6\text{H}_4\text{OMe})]\text{BF}_4$ can be isolated. But in EtOH solvent, a diazene complex, $[\text{Cp}^*\text{Ir}(\text{CO})(\text{OEt})(\textit{p}\text{-NHNC}_6\text{H}_4\text{OMe})]\text{BF}_4$, is formed. Further deprotonation of this complex affords a doubly bent aryldiazenido complex, $\text{Cp}^*\text{Ir}(\text{CO})(\text{OEt})(\textit{p}\text{-N}_2\text{C}_6\text{H}_4\text{OMe})$.
2. When L is a weak π -acid, the singly bent aryldiazenido complexes $[\text{Cp}^*\text{Ir}(\text{L})(\textit{p}\text{-N}_2\text{C}_6\text{H}_4\text{OMe})]\text{BF}_4$ (L= C_2H_4 or PPh_3) are produced. Addition of a hydride to $[\text{Cp}^*\text{Ir}(\text{PPh}_3)(\textit{p}\text{-N}_2\text{C}_6\text{H}_4\text{OMe})]\text{BF}_4$ yields $\text{Cp}^*\text{Ir}(\text{PPh}_3)(\text{H})(\textit{p}\text{-N}_2\text{C}_6\text{H}_4\text{OMe})$, with a doubly bent diazenido ligand. The chloro analogue, $\text{Cp}^*\text{Ir}(\text{PPh}_3)(\text{Cl})(\textit{p}\text{-N}_2\text{C}_6\text{H}_4\text{OMe})$, is unstable; but protonation of it at $\text{N}\alpha$,

forming $[\text{Cp}^*\text{Ir}(\text{PPh}_3)(\text{Cl})(p\text{-NHN-C}_6\text{H}_4\text{OMe})]\text{BF}_4$, can stabilize the chloro ligand in the coordination sphere.

3. When $L=\text{X}$, (I or Br), $[\text{Cp}^*\text{Ir}(\text{X})]_2(\mu^2\text{-}\eta^2\text{-}p\text{-N}_2\text{C}_6\text{H}_4\text{OMe})(\mu^2\text{-}\eta^1\text{-}p\text{-N}_2\text{C}_6\text{H}_4\text{OMe})$ are produced, and when $L=\text{Cp}^*\text{Ir}(\text{CO})_2$, $\{[\text{Cp}^*\text{Ir}(\text{CO})]_2(\mu^2\text{-}\eta^2\text{-}p\text{-N}_2\text{C}_6\text{H}_4\text{OMe})\}\text{BF}_4$ is produced.

Complexes produced in the nitrogen extrusion reactions of aryldiazonium ion with certain iridium carbonyls include $[\text{Cp}^*\text{Ir}(\text{CO})_2(\text{Ar})]\text{BF}_4$ and $[\text{Cp}^*\text{Ir}(\text{CO})_2 \rightarrow \text{IrCp}^*(\text{CO})(\text{Cl})]\text{BF}_4$, formed by reactions of the aryldiazonium salt with $\text{Cp}^*\text{Ir}(\text{CO})_2$ in acetone and CH_2Cl_2 , respectively, and $\{[\text{Cp}^*\text{Ir}(\text{CO})]_2(1\text{-}\eta^1\text{-}1, 2\text{-}\eta^2\text{-}\mu^2\text{-}p\text{-C}_6\text{H}_4\text{OMe})\}\text{BF}_4$, formed by a reaction of the aryldiazonium salt with $[\text{Cp}^*\text{Ir}(\text{CO})]_2$.

To my wife, Yichun Dai, and my daughter, Joyce.

Progress in basic natural science is a matter of constantly rebuilding from the very foundations. Significant progress is generally a matter, not of adding further facts, but of changing the frame-work itself....Science in the main develops not by way of cumulation but by way of substitution and replacement.

N. Rescher

in *The Limits of Science*

Acknowledgments

The author wishes to express sincere gratitude to Professor D. Sutton for his patient guidance and assistance and for his encouragement and influence. Special acknowledge is also made to Professor F. W. B. Einstein for his help and encouragement.

It is the author's pleasure to associate with Dr. L. K. Peterson, Dr. R. Hill, Dr. I. D. Gay, Dr. A. S. Tracey, Dr. R. J. Batchelor and Professor S. Wolfe whose expert advice has been very helpful.

Appreciation should also be made of author's colleagues: X. Zhang, R. Nagelkerke, B. A. Palm and Dr. N. D. Lowe for their cooperations.

To the members of his family, especially to his wife, the author is grateful for their selfless sacrifices, support and encouragement during his graduate studies.

TABLE OF CONTENTS

Approval page.....	ii
Abstract.....	iii
Dedication.....	v
Quotation.....	vi
Acknowledgments.....	vii
Table of Contents.....	viii
List of Tables.....	xii
List of Figures.....	xiv
List of Abbreviations and Symbols.....	xix
Chapter 1: Electronic Structure, Properties and Structural Characterization of Aryldiazenido Complexes.....	1
1.1 Introduction.....	1
1.2 Electronic Structure of Aryldiazenido Ligands.....	7
1.2.1 Introduction.....	7
1.2.2 Fragment Orbitals of N ₂ Ar Ligand.....	11
1.2.2.1 Fragment Orbitals of Aryldiazonium Ion N ₂ Ar ⁺	11
1.2.2.2 Fragment Orbitals of the Singly Bent N ₂ Ar Ligand.....	14
1.2.2.3 Fragment Orbitals of the Doubly Bent N ₂ Ar Ligand.....	25
1.3 Mononuclear Aryldiazenido Complexes.....	30
1.3.1 Introduction.....	30
1.3.2 Singly Bent Aryldiazenido Complexes.....	31
1.3.2.1 In Octahedral and Square-planar Geometries.....	31

1.3.2.2	In Trigonal Bipyramidal Geometry.....	52
1.3.3	Doubly Bent Aryldiazenido Complexes.....	60
1.3.4	Side-on Aryldiazenido Complex.....	68
1.4	Structural Characterization of Transition Metal Diazenido Complexes.....	78
1.4.1	Introduction.....	78
1.4.2	X-ray Crystallography of Diazenido Compounds.....	79
1.4.3	Infrared Spectroscopy.....	83
1.4.4	¹⁵ N NMR Spectroscopy.....	85
1.4.4.1	Introduction.....	85
1.4.4.2	¹⁵ N Nuclear Spin Relaxation in Transition Metal Complexes.....	88
1.4.4.3	Nitrogen-Nitrogen Spin-Spin Coupling Constant..	93
1.4.4.4	Nitrogen Chemical Shift.....	101
1.4.4.5	Application of ¹⁵ N NMR Spectroscopy to Aryldiazenido Complexes.....	106
Chapter II	Syntheses, Dynamic NMR and X-ray Structures of [Cp*Ir(C ₂ H ₄)NO]BF ₄ and [Cp*Ir(C ₂ H ₄)(p-N ₂ C ₆ H ₄ OMe)]BF ₄ — A comparison of the π acidity of ligands NO ⁺ and N ₂ Ar ⁺ ..	119
2.1	Introduction.....	119
2.2	Experimental Section.....	121
2.3	Syntheses and Characterization.....	139
2.4	Discussion.....	143
2.5	Conclusion.....	167

Chapter III	Pentamethylcyclopentadienyl Mono- and Di-iridium Aryldiazenido Complexes and Their Derivatives—	
	Ancillary ligand effect on the geometrical preference of the diazenido ligand.....	169
3.1	Introduction.....	169
3.2	Experimental Section.....	171
3.3	Results.....	185
3.3.1	Syntheses and Characterization.....	185
3.3.1.1	The Singly, Doubly Bent Aryldiazenido and Diazene Complexes Containing the Cp*Ir(PPh ₃) Core.....	185
3.3.1.2	Complexes Containing Bridging Aryldiazenido and Aryldiazene Ligands.....	196
3.3.1.2	Metal Base, Cp*Ir(CO) ₂ , as the Ancillary Ligand.....	202
3.3.2	X-ray Crystallographic Analyses.....	205
3.3.2.1	Complex [(Cp*Ir(CO)) ₂ (μ ² -η ² -p-N ₂ C ₆ H ₄ OMe)]BF ₄ (11)....	205
3.3.2.2	Complex [Cp*Ir(I)] ₂ (μ ² -η ² -p-N ₂ C ₆ H ₄ OMe)(μ ² -η ¹ -p-N ₂ C ₆ H ₄ OMe) (7).....	217
3.4	Discussion.....	225
3.5	Conclusion.....	233
Chapter IV	Syntheses and Characterization of Mono- and Diiridium Carbonyl Complexes Formed from the Attempted Syntheses of [Cp*Ir(CO)(p-N₂C₆H₄OMe)]BF₄; X-ray Crystal Structures of [Cp*₂Ir₂(CO)₃Cl]BF₄ and [Cp*₂Ir₂(CO)₂(η¹-μ², η²-μ¹-p-C₆H₄OMe)]BF₄.....	235

4.1	Introduction.....	235
4.2	Experimental Section.....	236
4.2.1	Preparations of the Precursor Materials.....	236
4.2.2	Attempts to Synthesize $[\text{Cp}^*\text{Ir}(\text{CO})(p\text{-N}_2\text{C}_6\text{H}_4\text{OMe})]\text{BF}_4$ (12) through the Reactions of $\text{Cp}^*\text{Ir}(\text{CO})_2$ (14) with $[p\text{-N}_2\text{C}_6\text{H}_4\text{OMe}][\text{BF}_4]$	239
4.2.3	Attempts to synthesize $[\text{Cp}^*\text{Ir}(\text{CO})(p\text{-N}_2\text{C}_6\text{H}_4\text{OMe})]\text{BF}_4$ (12) through the Reactions of $[\text{Cp}^*\text{Ir}(\text{C}_2\text{H}_4)(p\text{-N}_2\text{C}_6\text{H}_4\text{OMe})]\text{BF}_4$ (1) with Carbon Monoxide.....	246
4.2.4	Attempts to synthesize $\{[\text{Cp}^*\text{Ir}(\text{CO})]_2(\mu^2\text{-}\eta^2\text{-}p\text{-N}_2\text{C}_6\text{H}_4\text{OMe})\}\text{BF}_4$ (11) and $[\text{Cp}^*\text{Ir}(\text{CO})(p\text{-N}_2\text{C}_6\text{H}_4\text{OMe})]\text{BF}_4$ (12) through the Reactions of $[\text{Cp}^*\text{Ir}(\text{CO})]_2$ (15) with $(p\text{-N}_2\text{C}_6\text{H}_4\text{OMe})\text{BF}_4$	247
4.3	Results and Discussion.....	248
4.3.1	Syntheses, Properties and Characterization of the Precursor Compounds.....	248
4.3.2	Attempts to Synthesize $[\text{Cp}^*\text{Ir}(\text{CO})(p\text{-N}_2\text{C}_6\text{H}_4\text{OMe})]\text{BF}_4$ (12).....	256
4.3.3	X-ray Single Crystal Structures of Compounds (17) and (20).....	267
4.4	Conclusion.....	281
	Appendix I.....	285
	Appendix II.....	287
	References.....	289

LIST OF TABLES

Table:	page
1.1 Bond Angles of M-N-N in Singly Bent Diazenido Complexes	34
1.2 Comparison of M-Cl Bond Lengths With and Without the Trans Doubly Bent Diazenido Ligand in the Related Compounds	66
1.3 NMR Properties of Some Common Nuclei	87
1.4 Nitrogen-15 Spin Relaxation Time(T_1), in Seconds, for Terminal Dinitrogen Complexes in THF Solution at 297 K	93
1.5 Comparison of Structural Factors and NMR $ ^1J(^{15}N, ^{15}N) $ Values for Diazenide in Different Geometries	101
1.6 Nitrogen Chemical Shifts and $^1J(N, N)$ values of Singly Bent Aryldiazenido Complexes	108
1.7 Nitrogen Chemical Shifts and $^1J(N, N)$ values of Doubly Bent Aryldiazenido Complexes	116
1.8 Nitrogen Chemical Shifts of Bridging Aryldiazenido Complexes	117
2.1 Crystallographic Data for the Structure Determination of (1) and (2)	129
2.2 Positional and Thermal Parameters for Compound (1)	132
2.3 Selected Bond Lengths (Å) and Inter-Bond Angles (°) of (1)	134
2.4 Positional and Thermal Parameters for Compound (2)	135
2.5 Selected Bond Lengths (Å) and Inter-Bond Angles (°) of (2)	137
2.6 Activation Parameters for Compounds (1) and (2)	159
2.7 Some Bond Angles (°) and Distances (Å) for Aryldiazenido	

	Ligand	164
2.8	IR and Structural Data for Linear Monoiridium Nitrosyl Complexes	166
3.1	Crystallographic Data for the Structure Determination of $[\{\text{Cp}^*\text{Ir}(\text{CO})\}_2(\mu^2\text{-}\eta^2\text{-}p\text{-N}_2\text{C}_6\text{H}_4\text{OMe})]\text{BF}_4$ (11)	184
3.2	Positional Parameters of Non-Hydrogen Atoms for $[\{\text{Cp}^*\text{Ir}(\text{CO})\}_2(\mu^2\text{-}\eta^2\text{-}p\text{-N}_2\text{C}_6\text{H}_4\text{OMe})]\text{BF}_4$ (11)	208
3.3	Selected Bond Lengths (Å) and Inter-Bond Angles (°) for $[\{\text{Cp}^*\text{Ir}(\text{CO})\}_2(\mu^2\text{-}\eta^2\text{-}p\text{-N}_2\text{C}_6\text{H}_4\text{OMe})]\text{BF}_4$ (11)	215
3.4	Selected Bond Lengths (Å) and Inter-Bond Angles (°) for $[\text{Cp}^*\text{Ir}(\text{I})]_2(\mu^2\text{-}\eta^2\text{-}p\text{-N}_2\text{C}_6\text{H}_4\text{OMe})(\mu^2\text{-}\eta^1\text{-}p\text{-N}_2\text{C}_6\text{H}_4\text{OMe})$ (7)	222
4.1	Crystallographic and Experimental Data for the complex $[\text{Cp}^*_2\text{Ir}_2(\text{CO})_3\text{Cl}]\text{BF}_4$ (17)	244
4.2	Major Iridium-Carbonyl-Containing Fragment Ions in EI MS of (13)	252
4.3	Selected Bond Lengths (Å) and Inter-Bond Angles(°) for $[\text{Cp}^*_2\text{Ir}_2(\text{CO})_3\text{Cl}]\text{BF}_4$ (17)	270
4.4	Positional Parameters and Bio's of Non-Hydrogen Atoms for $[\text{Cp}^*_2\text{Ir}_2(\text{CO})_3\text{Cl}]\text{BF}_4$ (17)	271
4.5	U_{ij} (x100) for Anisotropic Motion of Atoms of (17)	272
4.6	Positional Parameters and Bio's of Hydrogen Atoms for $[\text{Cp}^*_2\text{Ir}_2(\text{CO})_3\text{Cl}]\text{BF}_4$ (17)	273
4.7	Selected Bond distances (Å) and Inter-Bond Angles(°) for $[\text{Cp}^*_2\text{Ir}_2(\text{CO})_2(1\text{-}\eta^1\text{-}1,2\text{-}\eta^2\text{-}\mu^2\text{-}p\text{-C}_6\text{H}_4\text{OMe})]\text{BF}_4$ (20)	279
4.8	Least-squares plane for the aryl group of $[\text{Cp}^*_2\text{Ir}_2(\text{CO})_2(1\text{-}\eta^1\text{-}1,2\text{-}\eta^2\text{-}\mu^2\text{-}p\text{-C}_6\text{H}_4\text{OMe})]\text{BF}_4$ (20)	281

LIST OF FIGURES

Figure:		page
1.1	The frontier orbitals of NN, NO ⁺ , NNH ⁺ and NNPh ⁺	13
1.2	Singly bending effect on the frontier orbitals of NNPh ⁺	17
1.3	Frontier orbitals of NNPh ⁺ as functions of the bending angle	19
1.4	Perspective views of the molecular structures for (a) CpW(CO) ₂ (N ₂ CH ₃), and (b) RuH ₂ (N ₂ B ₁₀ H ₈ S(CH ₃) ₂)(PPh ₃) ₃	24
1.5	Effect of forming a doubly-bent configuration on the frontier orbitals of NNPh ⁺	27
1.6	Comparison of the bending directions of the singly bent diazenido and the doubly bent hydrazido (2-) ligands on the metal fragment CpM(CO) ₂ , (M = Re and Mn, Cp = Cp or Cp')	29
1.7	Coordination modes of the terminal aryldiazenido ligand	30
1.8	Qualitative orbital interactions of ML ₅ and singly bent N ₂ Ar ⁺	33
1.9	π interaction between a terminal carbonyl and metal centre	38
1.10	The molecular structure of compound CpRe(CO)-(p-N ₂ C ₆ H ₄ OMe)(AuPPh ₃)	42
1.11	The effect of different metals on the bonding between M-CO and singly bent diazenide	44
1.12	Qualitative π interaction of Cl ⁻ ligand and a metal centre	45
1.13	Perspective views of molecules (i) [RhCl(N ₂ C ₆ H ₄ OMe)(PPh ₃) ₂]BF ₄ (ii) MoCl(N ₂ C(O)Ph)(dppe) ₂ and (iii) MoI(N ₂ C ₆ H ₁₁)(dppe) ₂ showing the trans arrangement of the halide ligand and the	

	singly bent diazenido ligand	47
1.14	Effect on the in-plane p orbitals of different orientations of phenyl ring of ligand N_2Ar^+ in a cis-chloro-aryldiazenido arrangement	50
1.15	Molecular structure of $Re(N_2Ph)Cl_2(PMe_2Ph)_3$	51
1.16	The filled frontier orbitals of a ML_5 complex in D_{3h} symmetry without consideration of the π interactions	54
1.17	d- π interaction of metal and ligands in the equatorial plane for a complex in TBP geometry	56
1.18	Correlation of filled metal frontier orbitals in TBP and SP	58
1.19	Molecular orbitals of ML_6 in O_h symmetry, without consideration of the π interactions	61
1.20	The secondary π type interactions along the bonding of Cl-Ir- N_2Ar in $IrCl_2(N_2Ar)(CO)(PPh_3)_2$	63
1.21	The secondary interactions in xz plane of the molecule $IrCl_2(N_2Ar)(CO)(PPh_3)_2$	64
1.22	Molecular structures of (a) $CpTiCl_2(\eta^2-NH_2NPh)$ and (b) $CpTiCl_2(\eta^2-N_2Ph)$	69
1.23	\perp side-on coordination of N_2Ar to the $CpTiCl_2^+$ centre	71
1.24	Qualitative orbital interactions of NH_2NAr and $CpTiCl_2^+$ in a // side-on fashion	73
1.25	View of the molecular configurations of $[CpWMe_3(NH_2NH)]^+$ (a) $CpWMe_4(NH_2NH)$ (b) and $\{CpRe(CO)_2[NHN(Me)Ar]\}^+$ (c)	75
1.26	Important bond lengths (\AA) and angles ($^\circ$) in (a) $CpTiCl_2(NH_2NPh)$, (b) $CpTiCl_2(NNPh)$, (c) $[CpWMe_3(NH_2NH)]^+$ and (d) $CpWMe_4(NH_2NH)$	77

1.27	Different configurations of transition metal aryldiazenido complexes	78
1.28	A perspective view of the distortion of diazenido ligand in $[\text{IrCl}(\text{N}_2\text{Ph})(\text{PMe}_2\text{Ph})_3]\text{PF}_6$	81
1.29	Disordered structure of the doubly bent diazenido ligand in $\text{PtCl}(p\text{-N}_2\text{C}_6\text{H}_4\text{F})(\text{PEt}_3)_2$	82
1.30	Disordered structure of doubly bridged diazenido ligand in $[\text{Cp}^*\text{Ir}(\text{N}_2\text{Ar})\text{I}]_2$	83
1.31	The range of aryldiazenido N=N stretching frequencies in metal complexes	84
1.32	Ranges of $ ^1J(^{15}\text{N}, ^{15}\text{N}) $ values, where the known sign is given in parentheses()	98
1.33	Charge rotation caused by the transitions, $\pi_x \leftrightarrow \pi_y^*$ and $\pi_y \leftrightarrow \pi_x^*$ at the NN group	105
2.1	A perspective view of the cation $[\text{Cp}^*\text{Ir}(\text{C}_2\text{H}_4)(p\text{-N}_2\text{C}_6\text{H}_4\text{OMe})]^+$ of (1)	130
2.2	A perspective view of the cation $[\text{Cp}^*\text{Ir}(\text{C}_2\text{H}_4)(\text{NO})]^+$ of (2)	131
2.3	Qualitative orbital interactions of electrophilic attack of N_2Ar^+ at $\text{Cp}^*\text{Ir}(\text{C}_2\text{H}_4)_2$ (in a C_s symmetry)	146
2.4	Variable -temperature ^1H NMR spectra for (1)	150
2.5	A comparison of the low-limit ^1H NMR spectrum of (1) (top) with the simulated spectrum (bottom)	151
2.6	Hypothetical mechanisms of the fluxional process of the singly bent aryldiazenido ligand (viewed down from the centroid of Cp^*)	153
2.7	Variable -temperature ^{13}C NMR spectra for (1)	156
2.8	Variable -temperature ^1H NMR spectra for (2)	158

2.9	The Dewar-Chatt-Duncanson scheme for bonding in a simple metal-olefin complex	160
2.10	π back-bonding from $\text{Cp}^*\text{Ir}(\text{C}_2\text{H}_4)$ to NO^+	165
3.1	^1H NMR spectrum of (7) in CDCl_3	178
3.2	^1H NMR spectrum of (4) in acetone- d_6 , in a wide window	190
	^1H NMR spectrum of (4) in acetone- d_6 , in a narrow window	191
3.3	^1H NMR spectrum of (6a) in acetone- d_6	194
3.4	^{15}N NMR spectrum of (6a) in acetone- d_6	195
3.5	Molecular structures of (a) $(\mu\text{-H})\text{Os}_3(\text{CO})_{10}(\mu^2\text{-}\eta^2\text{-}p\text{-N}_2\text{C}_6\text{H}_4\text{Me})$ and (b) $(\mu\text{-H})\text{Os}_3(\text{CO})_{10}(\mu^2\text{-}\eta^1\text{-}p\text{-N}_2\text{C}_6\text{H}_4\text{Me})$	200
3.6	A perspective view of the cation of (11)	207
3.7	Two coordination modes of the bridging aryldiazenido ligand found in complex (7)	218
3.8	Two possible modes of the doubly bridging aryldiazenido complex (7)	219
3.9	Perspective view of the molecular structure of compound (7)	221
3.10	The frontier orbitals of the Cp^*Ir fragment	225
3.11	The primary π interaction between Cp^*Ir fragment and singly bent N_2Ar^+ ligand	227
3.12	π interaction between $\text{Cp}^*\text{IrN}_2\text{Ar}^+$ fragment and the ancillary ligand L	228
3.13	The influence of the weak π acid ligand, L, on the primary π interaction between Cp^*Ir and N_2Ar^+ fragments	228
3.14	The influence of a π base ancillary ligand on the metal d_{yz} orbital	231
3.15	An iridium-diazenido MLCT caused by the trans	

	strong π base ligand	231
4.1	The infrared spectrum of (13) in hexanes	249
4.2	The EI mass spectrum of (13)	250
4.3	Two possible structures of the fragment (C)	252
4.4	Molecular structure of the cation of (17)	268
4.5	Molecular structure of the cation of (20)	276
4.6	Possible fluxional process for the molecule (19) in solution	278

LIST OF ABBREVIATIONS AND SYMBOLS

Å	Ångstrom, unit 10^{-8} cm
Ar	aryl or aromatic
B	magnetic field strength
CI	chemical ionization
cm^{-1}	wavenumber
Cp	cyclopentadienyl
Cp*	pentamethylcyclopentadienyl
Cp'	methylcyclopentadienyl
d^n	d-electron configuration
EI	electron impact
Et	ethyl
FAB	fast atom bombardment
<i>fac.</i>	facial
FT	Fourier transform
FMO	fragment molecular orbital
HOMO	highest occupied molecular orbital
Hz	Hertz, sec.^{-1}
I	nuclear spin
IR	infrared
L	unidentate ligand
LUMO	lowest unoccupied molecular orbital
M	central transition metal in complex
Me	methyl
<i>mer.</i>	meridional

MLCT	metal ligand charge transfer
MO	molecular orbital
MS	mass spectroscopy
NMR	nuclear magnetic resonance
NOE	nuclear Overhauser effect
NOBA	<i>o</i> -nitrobenzyl alcohol
OMe	methoxy
Ph	phenyl
PR ₃	phosphine ligand
R	alkyl and aryl
SP	square pyramidal
TBP	trigonal bipyramidal
THF	tetrahydrofuran
X	halogen
δ	chemical shift
γ	gyromagnetic ratio
ν	frequency in cm ⁻¹

(Subscript following a number)

<i>b</i>	broad
<i>d</i>	doublet
<i>m</i>	medium, or multiplet
<i>q</i>	quartet
<i>s</i>	strong, or singlet
<i>sh</i>	shoulder
<i>t</i>	triplet
<i>w</i>	weak

CHAPTER I.

Electronic Structures, Properties and Structural Characterization of Aryldiazenido Complexes

1.1 Introduction

Transition metal aryldiazenido complexes (MN_2Ar) have been of great interest in this group for many years. This research program has been continuously stimulated by two simple facts. First, in organometallic chemistry, relatively little is known about dinitrogen and organodinitrogen complexes compared to carbon atom ligated complexes. Secondly, the close relationship of the aryldiazenido ligand to nitrosyl, dinitrogen and other organodinitrogen species leads to a family of related compounds. In fact, aryldiazenido ligands have been successfully converted into dinitrogen,¹ diazene,² hydrazido(1-),³ and hydrazido(2-)⁴ ligands. It is noteworthy that the hydrogenated forms of these organodinitrogen ligands, including diazenide itself, could be intermediates involved in the nitrogenase mediated reduction of molecular nitrogen.⁵⁻¹⁰

Structural studies of aryldiazenido complexes yield valuable insights into the electronic structure of the ligands and perhaps into reaction mechanisms involving these ligands. Much effort in the study of organodiazenido chemistry has gone into determining which factors influence the geometry and, therefore, the electronic structure of the organodiazenido ligands in various complexes. Undoubtedly, detailed structural and chemical information regarding these ligands in transition metal complexes will not only enrich today's organometallic chemistry, but more importantly, may also contribute to our understanding of the catalytic reduction of dinitrogen, and even to the future development of new and

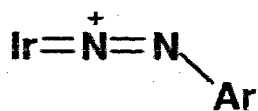
efficient catalysts for the conversion of molecular nitrogen into ammonia, or other useful organodinitrogen compounds, under mild conditions.^{11,12}

Historically, this study has been closely related to nitrosyl chemistry. Since N_2Ar^+ and NO^+ are isoelectronic, very often the mode of coordination of aryldiazenido ligands to transition metals was considered to be similar to that of the NO ligand.¹³ The convenient valence bond (VB) description for the electronic structure of the nitrosyl ligand has been used also equivalently for diazenido ligands. In fact, the analogy between NO^+ and N_2Ar^+ has been found frequently in syntheses and discussions of molecular structure, and it certainly facilitated the development of organodiazenido and nitrosyl chemistry during the early stages of research in this area.

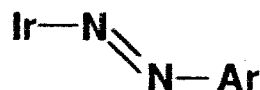
The work presented in this thesis focuses mainly on aryldiazenido iridium complexes with pentamethylcyclopentadienyl (Cp^*) as the main co-ligand. The syntheses, structural characterizations and some typical chemical reactions of these compounds have been investigated. The chemical and structural significance of these pentamethylcyclopentadienyl iridium diazenido compounds is highlighted by observed changes in the coordination mode of the diazenido ligand at the iridium centre, giving rise to various geometries as depicted in Scheme 1.1. The conversions between these modes are dependent upon the identity of the co-ligands in some cases. For comparison with the singly bent diazenido compounds, some nitrosyl compounds have also been synthesized and studied.

The details of the structures of each mode shown in Scheme 1.1, and the relationship between them can be interpreted in terms of the electron configuration of the diazenide ligand and the nature of the bonding between it and the transition metal. During the course of this work, a number of unique

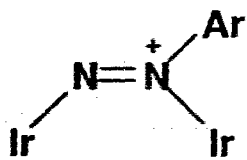
chemical and structural features of the aryldiazenido ligand and other related organodinitrogen ligands have been noticed, and interestingly, some of these



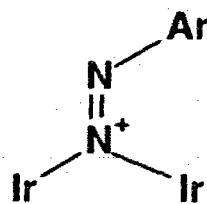
Singly Bent



Doubly Bent



η^2 - μ^2 -Bridging



η^1 - μ^2 -Bridging

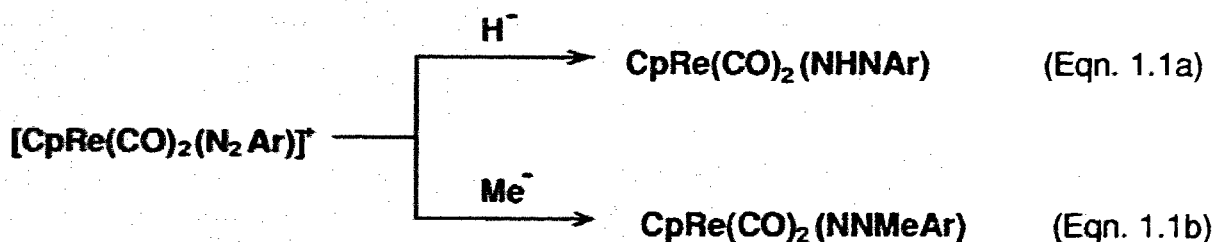
Scheme 1.1

were not satisfactorily explained by the classical picture of the electronic structure of the aryldiazenido ligand that, for example, treats the nitrogen lone pair electrons as non-bonding and does not take into account conjugation of the N=N double bond with transition metals and the aromatic ring. Similarly, in the literature of diazenido compounds, a number of anomalies and uncertainties about the structure and chemical properties are rooted in the classical valence bond framework, and reflect the inadequacy of it in the description of the bonding and electron configuration of the aryldiazenido ligand. Some of these discrepancies are discussed below as examples:

(1). The NO ligand is considered to be a better π acceptor than the N_2Ar ligand due to the greater electronegativity of the O atom in the NO ligand and the greater Lewis acidity of NO^+ over N_2Ar^+ . This apparently simple fact has been confirmed many times.¹⁴⁻¹⁷ However, we found that, at least for $[Cp^*Ir(C_2H_4)L]^+$ ($L=NO$ or N_2Ar), the chemical and spectroscopic evidence suggests that electron transfer from the iridium centre to the aryldiazenido ligand is more extensive than to the NO ligand. This suggests that N_2Ar^+ is a better π acid than the NO^+ ligand in this case.

(2). In aryldiazenido complexes, the singly bent N_2Ar^+ ligand has a small or negligible structural influence on the ligand *trans* to it, such as halide, whereas, there is a significant *trans* lengthening ($\sim 0.10 \text{ \AA}$) of the metal-chloride bonds in $PtCl(N_2Ar)(PEt_3)_2$ ¹⁸ and $IrCl_2(CO)(N_2Ar)(PPh_3)_2$ ¹⁹ where the halide bonds are *trans* to a doubly-bent N_2Ar ligand. How can this be explained?

(3). Similar confusion has also been found in understanding the different reactivities of the ligand in the following reactions (Eqn. 1.1a and 1.1b)



Nucleophilic attack of the diazenido ligand by H^- apparently occurs at the N_α atom forming the expected diazene complex,^{4, 20} whereas attack by the carbanion Me^- seems occurred at the N_β position forming the unusual doubly bent NNR_2 hydrazido(2-) complex.⁴

Clearly, a full explanation of these observations requires a detailed description of the electronic structure and bonding in aryldiazenido transition metal complexes. Previously, the problems of structure and reactivity for aryldiazenido ligands have been mainly discussed in terms of the traditional valence bond theory. The inadequacy of this theory to account for observed discrepancies suggests that this approach may be inappropriate and a more accurate picture of the electron configuration of this ligand may be required. This might be achieved through the use of the Fragment Molecular Orbitals (FMO) approach due to Wolfe, et.al,^{21, 22} based on the Extended Huckel Molecular Orbital (EHMO) calculations by Hoffmann.²³ In fact, Hoffmann, in 1977, has described qualitative molecular orbitals for the structures of a series of isoelectronic species, such as N_2 , NO^+ and N_2H^+ , as well as some complexes of these species by using EHMO.²⁴ Many important conclusions have been drawn from these calculations and they are still valuable in dealing with the molecular structure of the diazenido complexes. In particular, the ideas behind these calculations are very instructive and useful. On the other hand, since an oversimplified N_2H^+ system was used as a model in the calculations, some conclusions suitable for N_2H may not be directly transferable to the aryldiazenido case because it ignores the conjugation of $N=N$ with the aromatic ring. For example, a *cis*-conformation for a doubly bent diazenido ligand was found to be energetically preferred based on the calculation. In fact, no single example of

this conformation has been found in known aryldiazenido complexes, except in the case of a metallacyclic product.²⁵ Clearly, the steric effect of the rather bulky aryl ring must be taken into consideration along with electronic effects when considering aryldiazenido complexes.

While this Thesis was in preparation, a recent paper appeared that also deals with EHMO calculations on *methyldiazenido* complexes.²⁶

In this chapter, an attempt will be made to build up a qualitative molecular orbital picture to describe the aryldiazenido ligand. In order to do this, first, a phenyldiazonium ion, N_2Ph^+ , will be used as a model to develop the fragment orbitals for the aryldiazenido ligand in different geometries. This approach is based on EHMO calculations, with parameters and some details as described in Appendix I. Once the fragment orbitals of the ligand have been constructed, a qualitative FMO analysis approach will be used to combine these orbitals with the well-developed fragment orbitals of transition metal species (ML_n).²⁷⁻²⁹ The relative energy of the latter is approximated by the valence shell, or valence orbital, ionization potential energy (VSIP or VOIP); values are listed in Appendix II with the literature references. This will allow the electronic structure and bonding between the diazenido ligand and transition metal centres to be qualitatively modelled. A particular emphasis will be placed on applying this approach to structure and reactivity problems in aryldiazenido complexes. Many important areas related to diazenido chemistry are only briefly dealt with. For example, a detailed discussion of the structures for hydrazido and diazene type ligands, areas important enough to be discussed in their own right, are only touched on superficially here. No attempt will be made to deal with the theoretical basis of this work here. This has been reported at considerable length elsewhere.³⁰⁻³² Only the results, data and methodology will be discussed here.

It is not intended to give a critical review of the previously published results here. Nevertheless, some previously published contributions on aryldiazenido chemistry have been re-evaluated in the framework of the FMO analysis.

The later part of this chapter includes a discussion of some structural characterization methods commonly used in diazenido chemistry. The potential application of ^{15}N NMR spectroscopy is emphasized, simply because this technique is still not often exploited.

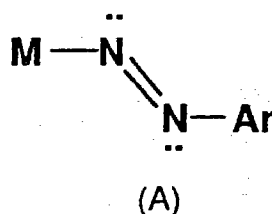
1. 2. Electronic Structure of Aryldiazenido Ligands

1. 2. 1. Introduction

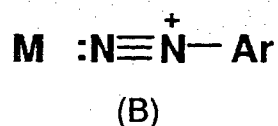
The EHMO method normally does not consider electron-electron interactions in the valence orbitals and does not energetically minimize the molecular geometry. Therefore, when using EHMO calculations to construct valence orbitals for a ligand, it is very important that the fragment for the ligand be chosen carefully; it must be sure to have appropriate geometry and a suitable electron count. The convention used to assign the electron count for the fragment is certainly not unique; however, the total electron count for a complex must stay the same no matter what conventions are used, and the choice will be reflected in the resulting formal oxidation state at the metal. For example, alkyl groups and halogens can be counted as neutral $1e^-$ -donors or, anionic $2e^-$ -donors, provided a formal positive charge is included on the metal centre in the latter case. Treatment of all ligands as Lewis bases, namely, as two electron-donors, is used here whether these ligands are neutral or charged. The virtue in this is that the formal charge on the metal centre directly corresponds to the

formal oxidation state of the metal, and the number of *d*-electrons on the metal centre is also straightforwardly obtained.

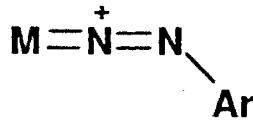
For aryldiazenido complexes, a suitable fragment assignment for the singly or doubly bent aryldiazenido ligand is rather difficult. The N_2Ar ligand can be formally viewed as N_2Ar^+ , N_2Ar^- or $N_2Ar\cdot$. The latter corresponds to an odd-electron configuration and will not be used here because it violates the 2-electron donor concept indicated above. The N_2Ar^- formalism is a closed shell configuration, generates a formal count of 1^+ toward the oxidation state of metal, and has a "doubly bent" geometry when it donates a σ pair as a Lewis base. A trans conformation will be presumed, as shown below in (A)



The closed shell configuration for the N_2Ar^+ ligand shown in (B) corresponds to a linear geometry for this ligand,

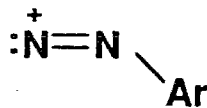


and requires a formal charge of 1^+ on the N_β position. However, there are no known complexes in which the N_2Ar^+ ligand actually adopts the "linear" geometry. The prevailing geometry is "singly-bent" with an angle near 120° at N_β which can be formally represented by the valence structure (C)



(C)

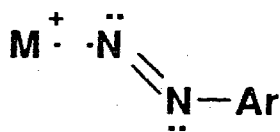
Therefore, it is this singly bent assignment of the ligand which needs to be considered in EHMO calculations for the complexes of this type. The ligand fragment that is suitable is then (D)



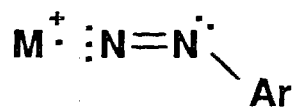
(D)

Note that this is not a closed shell configuration at the terminal nitrogen and is clearly reminiscent of a singlet carbene. In determining the oxidation state and formal electron count of the metal, there is no difference between the linear and singly bent formalisms, but clearly the geometry and the electron distribution in the ligand differs. It is this that needs to be adequately taken into account in formulating the EHMO framework.

It should be clearly understood at this point that the above convention is different from the normal convention for treating the electron count in organometallic compounds, which avoids the notion of a formal oxidation state of the metal centre and simply treats the ligands as $1e^-$, $2e^-$, $3e^-$ etc. donors depending on their electron configuration. For example, NO and N_2Ar are $1e^-$ -donors (E) or $3e^-$ -donors (F) in this convention.

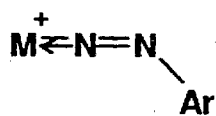


(E) 1e⁻-donor

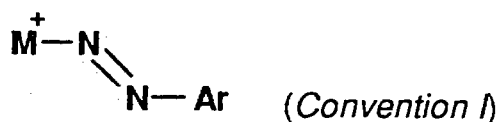


(F) 3e⁻-donor

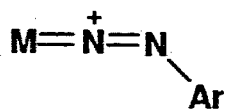
The two conventions are clearly related to each other and their relationship for the aryldiazenido ligand is diagrammed in Scheme 1.2. It is obvious that *Convention I*, the common convention in organometallic chemistry, emphasizes the electric charge neutrality of the N₂Ar ligand, whereas the *Convention II* emphasizes the Lewis base nature of the ligand, as well as the true charge distribution on it. In fact, conversion between *Convention I* and *Convention II* can be easily achieved in the scheme of the valence bond theory by simply relocating the charge on the metal centre or N_α atom, and, meanwhile,



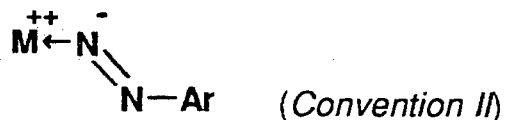
1a. (3e⁻)



1b. (1e⁻)



2a. (2e⁻)



2b. (2e⁻)

Scheme 1.2 Conventions for singly bent (a) and doubly bent (b) aryldiazenido complexes

exchanging the dative bond arrow with the normal covalent bond bar. However, in *Convention I*, the odd number of electrons counted for the ligand to form the bond often leads to an uncommon formal oxidation state for the transition metal centre. For example, in *Convention I*, the formal oxidation state of Fe in $[\text{Fe}(\text{CO})_2(\text{N}_2\text{Ph})(\text{PPh}_3)_2]^+$ will be Fe(I), and in $[\text{Fe}(\text{CO})(\text{NO})(\text{N}_2\text{Ph})(\text{PPh}_3)]$ will be Fe(0), which is clearly confusing. Judicious use of this convention is necessary when ligands like N_2Ar , NO and allyl are present. Unfortunately, indiscriminate use of *Convention I* has caused confusion in this area. For example, N_2R^+ (R= alkyl or aryl) is frequently incorrectly described as a three electron donor ligand and N_2R^- as a one electron donor ligand in the literature.

In this Thesis, *Convention II* will be used throughout, simply because it is convenient and unambiguous in representing the bonding between the metal and the ligand. Therefore, in *Convention II*, the singly bent aryldiazenido ligand (**2a** in Scheme 1.2) will be considered formally as a type of two-electron "cationic carbene" ligand and expressed as N_2R^+ , or aryldiazenido(+1). Correspondingly, the doubly bent diazenido will be assigned as a two-electron anionic ligand of form N_2R^- , or aryldiazenido(-1).

1. 2. 2. Fragment Orbitals of N_2Ar Ligand

1. 2. 2. 1. Fragment Orbitals of Aryldiazonium Ion N_2Ar^+

Hoffmann²⁴ previously used the EHMO method for calculating fragment orbitals for N_2 , NO^+ and N_2H^+ , but not N_2Ar^+ . Here we apply the EHMO method to N_2Ar^+ , but first in order to test the consistency of the EHMO program used here the calculations for the other three species were also computed, and gave results identical to those of Hoffmann. The calculated relative energies of the valence orbitals of N_2 , NO^+ , N_2H^+ and N_2Ph^+ are shown in Figure 1.1. The bond

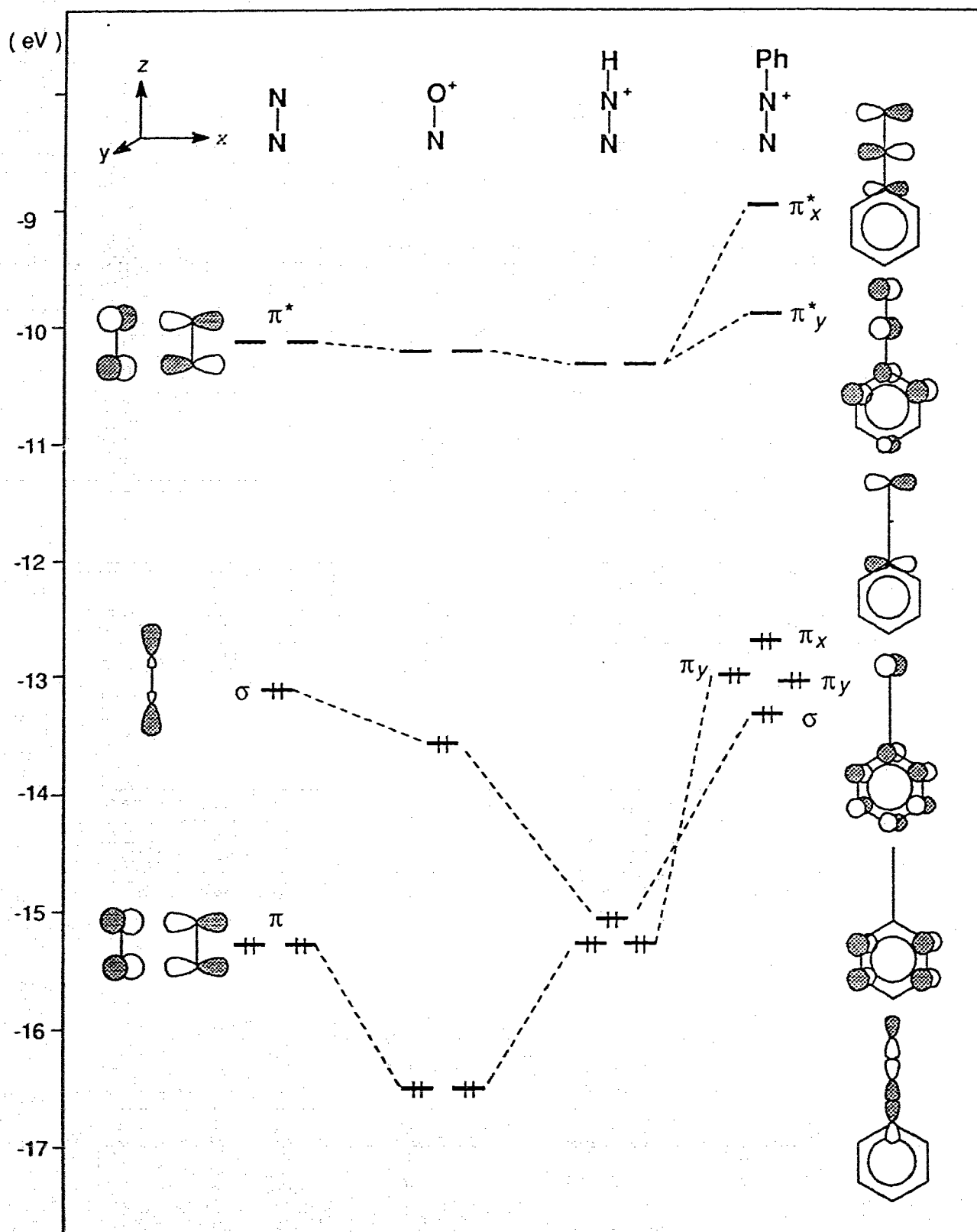


Figure 1.1 The frontier orbitals of NN, NO⁺, NNH⁺ and NNPh⁺

distances and angles used in the calculation for the free phenyldiazonium ion were taken from the X-ray structural data.³³

The molecular orbitals for N_2 , NO^+ and N_2H^+ are filled through the σ level, so the highest occupied molecular orbital (HOMO) for each of these species is a σ -type orbital. When coordinating to a metal, this orbital will be expected to donate electrons to an empty orbital at the metal centre to form a σ bond. However, for the N_2Ph^+ ion, the highest occupied molecular orbital is a non-bonding orbital of π character. In fact, the filled σ orbital of N_2Ph^+ is buried beneath three filled π -type orbitals, one with b_1 symmetry and other two with b_2 symmetry in this C_{2v} system. Interestingly, all these three π orbitals have non-bonding character with respect to the NNC linkage and they are located rather higher than the corresponding π orbitals in N_2 , NO^+ and N_2H^+ (Figure 1.1). Energetically, they are very close to the pure $2p$ orbitals of the nitrogen atom (-13.40 eV), which further indicates the N-N non-bonding character of these orbitals. Another distinguishing feature is that for N_2 , NO^+ and N_2H^+ , the lowest unoccupied molecular orbitals (LUMO's) are two degenerate π antibonding orbitals, but for N_2Ph^+ the corresponding π type orbitals are non-degenerate, (π_x^* and π_y^*); the π_y^* orbital, which is conjugated with the π system of the phenyl ring lies low, and π_x^* , which is perpendicular to it lies high. Clearly, the underlying cause of the differences of the frontier orbitals for N_2 , NO^+ and N_2H^+ from N_2Ph^+ is the conjugation of the π system of the aryl ring with one set of π type of orbitals of the N_2 group (π_y and π_y^* in Figure 1.1) in N_2Ph^+ . It is this delocalization interaction that makes the traditional VB model unsuitable for describing N_2Ph^+ , since it is built upon strictly localizing a pair of bonding electrons between two atoms which are bonded together.

In summary, energetically, the linear phenyldiazonium ion N_2Ph^+ seems to be neither a good σ donor nor a good π acceptor ligand.

1. 2. 2. 2. Fragment Orbitals of the Singly Bent N_2Ar Ligand

Once the MOs for phenyldiazonium ion have been calculated, it is possible to use them, together with the known metal fragment orbitals, to model the molecular orbital interaction in a linear aryldiazenido complex. However, this is not what we are interested in at this stage, because, experimentally, in transition metal complexes, the aryldiazenido ligand has always been observed to bend at N_β in a direction coplanar with N_α , N_β and the aryl ring plane.^{13, 34} This experimental fact simply indicates that a linear aryldiazenido ligand in complexes may not be energetically favorable. In other words, under the influence, or perturbation of a transition metal the aryldiazenido ligand seems to prefer to have a different electronic configuration from that in its free state, *i.e.*, the diazonium ion. This can be fairly easily understood, in principle, in the framework of the perturbation theory.

During coordination of the aryldiazonium ion to a transition metal centre, the electronic configuration on the metal centre will perturb the ligand approaching along the reaction coordinate. Under this perturbation, which includes the symmetry properties of the metal centre, the previous orthogonal condition applied to the basis set of the linear N_2Ar^+ now becomes unnecessary, and hence a reorganization of it into a new set of orbitals could occur, of which the splitting pattern and symmetry properties should be strongly dependent on the nature of the perturbation. Further, a change in the electronic configuration is always accompanied, and reflected by a geometric change in bond lengths

and/or bond angles. For the diazenido ligand this change is indicated by a significant bending of $\angle N_{\alpha}-N_{\beta}-Ar$ from 180° to $\sim 120^{\circ}$.

Clearly, in order to use the FMO method for aryldiazenido complexes, the fragment MOs of a bent aryldiazenido ligand, rather than the linear one, are needed. Calculations on the bent phenyldiazonium were, therefore, carried out by the EHMO method.

The effect of this bending on the π , π^* , and σ orbitals are shown in Figure 1.2 (assuming the bending occurs in the xz plane). Upon bending at the N_{β} position, the local molecular symmetry drops from C_{2v} to C_s . Consequently, the σ type of orbitals and π_x type of orbitals (π_x and π_x^*), which were orthogonal in C_{2v} , will now interact with each other in the C_s system. Energetically, the filled σ and π orbitals are very close to one another in the free diazonium ion, so a strong mixing of the σ orbital and π_x orbital would be expected. The higher orbital $2a'$, actually the HOMO, produced by this mixing is an orbital of σ character, which directly contrasts with the π type of HOMO in the linear aryldiazonium ion. Interestingly, this σ orbital is located in the bending plane and is pointing in the direction slightly *trans* to the phenyl group. The mixing also produces a counterpart orbital of the HOMO, which is a σ orbital $1a'$, primarily bonding between the N_{β} and C atoms. Another primary feature is that the bending decreases the energy of the π_x^* orbital dramatically. The driving forces behind this large energy change of the π_x^* orbital mainly come from: (1) the mixing-in of a higher σ orbital which is primarily antibonding between N_{β} and C atoms, as shown in Scheme 1.3; (2) a weakening of the antibonding π interaction between the N_{β} and C atoms; and (3) a weakening of the antibonding π interaction between N_{α} and N_{β} .

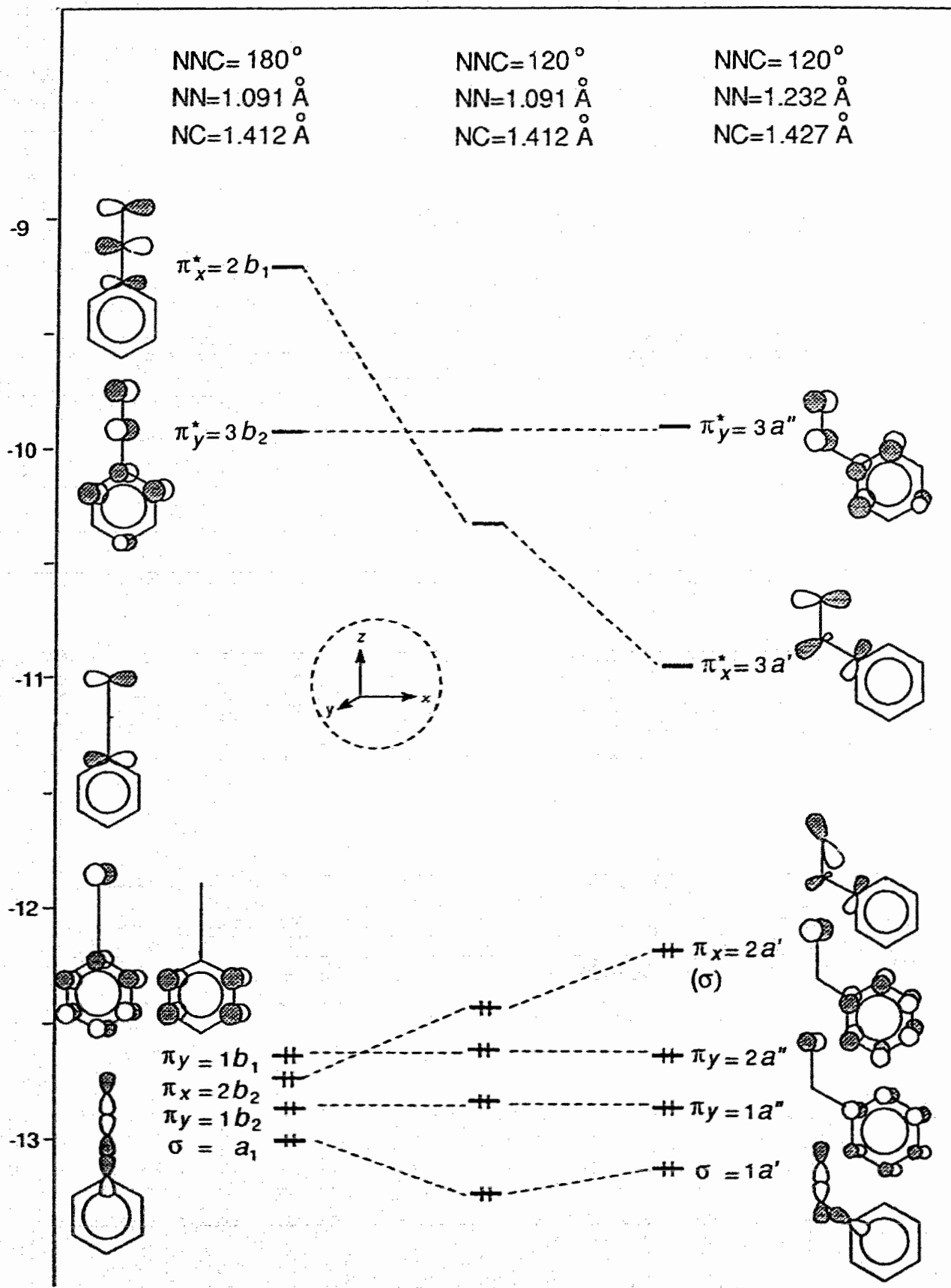
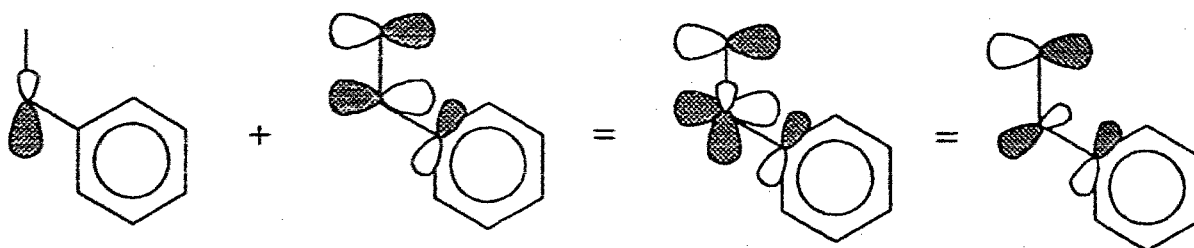


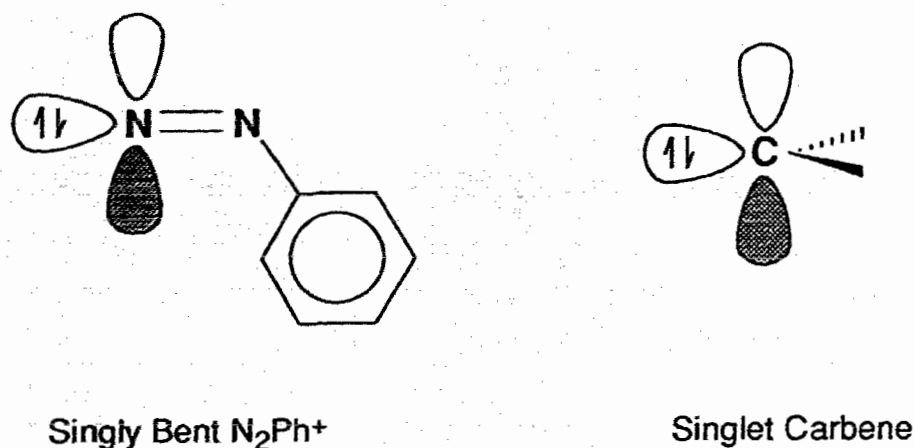
Figure 1.2 Singly bending effect on the frontier orbitals of NNPh⁺



Scheme 1.3

The splitting patterns of the frontier orbitals, shown on the left and middle in Figure 1.2, were calculated by using the dimensions of the free N_2Ph^+ ($\text{N-N} = 1.091 \text{ \AA}$; $\text{N-C} = 1.412 \text{ \AA}$), but $\angle\text{NNC} = 180^\circ$ and 120° separately. In order to construct the fragment molecular orbitals for the singly bent aryldiazenido ligand, which has different NN and NC bond lengths from the free N_2Ph^+ , the values of $\text{N-N} = 1.232 \text{ \AA}$; $\text{N-C} = 1.427 \text{ \AA}$ (averaged from the experimental data for ~40 X-ray structurally determined compounds with singly bent aryldiazenido(+1) ligands,³⁵ were used in the EHMO calculation. The results are shown on the right-hand side of Figure 1.2. Lengthening the NN bond distance will certainly decrease the π antibonding interaction between N_α and N_β and, therefore, again will lead to a further decrease in the π^*_x orbital energy. It is worth mentioning that the π^*_x orbital will be expected to play an important role in the formation of aryldiazenido complexes, since it is much closer in energy to the metal d orbitals than is the π^*_y orbital. It is this large energy difference between π^*_x and π^*_y that distinguishes the bonding to transition metals in the case of the aryldiazenido ligand from other small isoelectronic species NO^+ , N_2 , CO , for which the two π^* orbitals are degenerate.

Considering the shape and arrangement of the HOMO and LUMO of the singly bent aryldiazene in Figure 1.2, these resemble those for carbenes as shown in Scheme 1.4.



Scheme 1.4

The LUMO, $3a'$, of the aryldiazene ligand mainly consist of the empty π_x orbital on the N_α atom lying in-plane with the phenyl ring and it could be considered analogous to the empty p orbital of the carbon atom in the singlet carbene ligand. The HOMO, $2a'$, of the N_2Ph^+ ligand can also be considered analogous to the carbon orbital containing the σ type lone pair of electrons in the singlet carbene. In fact, the electron configuration analysis for the singly bent aryldiazene ligand leads us to the conclusion that aryldiazene(1+) is a carbene type of cationic ligand.

The energy of the frontier orbitals, $3a'(\pi_x^*)$ and $2a'$, the LUMO and the HOMO, as a function of the bending angle of NNC in N_2Ph^+ is shown in Figure 1.3. The greatest change in energy occurs for the LUMO $3a'$. When the bending angle is close to 120° , the energy of this orbital is minimized. When an aryldiazene ligand coordinates to a transition metal centre in a singly bent

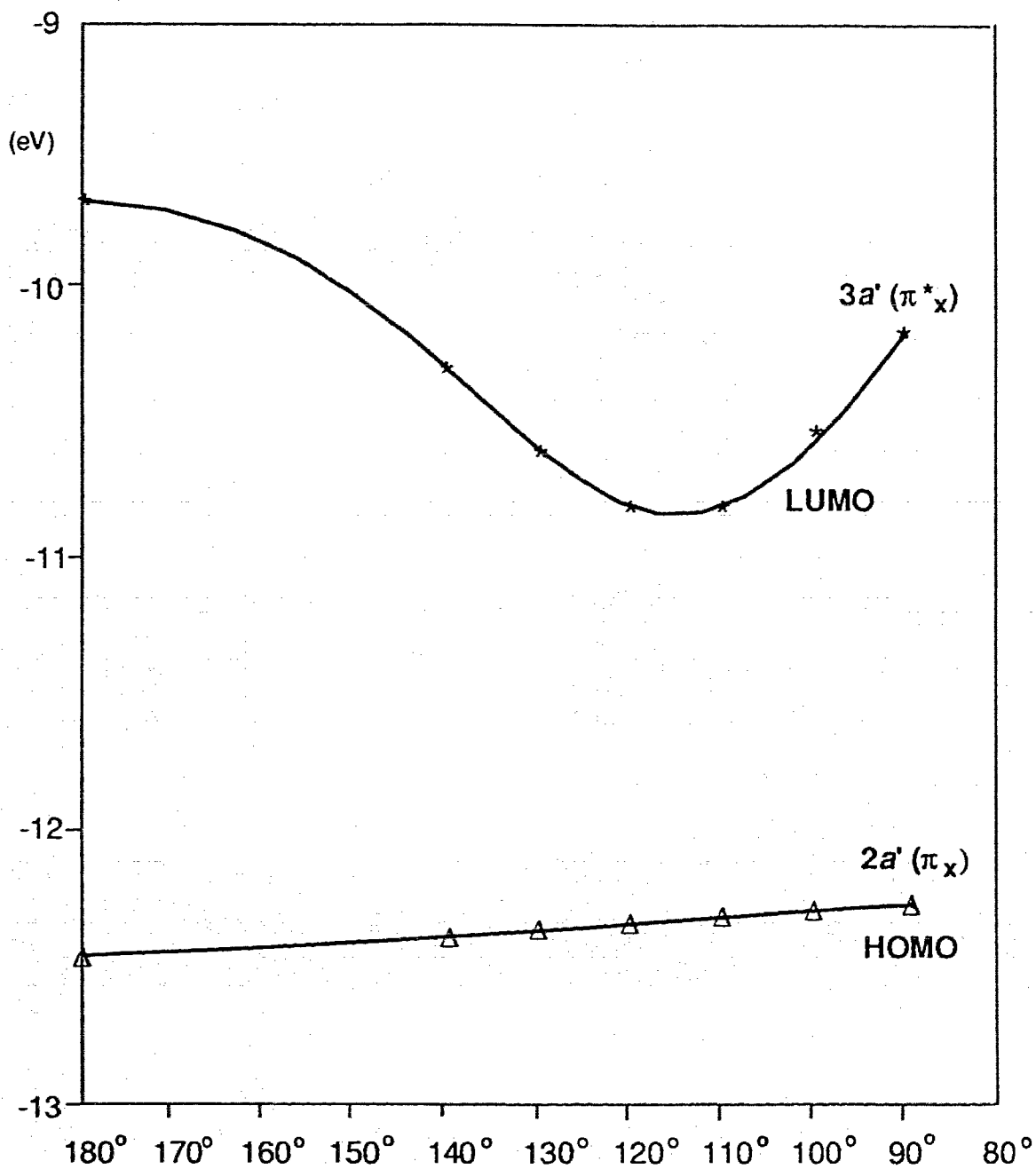


Figure 1.3 Frontier orbitals of NNPh⁺ as functions of the bending angle

fashion, this orbital will be, very often, the highest populated orbital for the ligand *in the complex*. According to Walsh's rule,³⁶ therefore, the singly bent phenyldiazenido ligand will be expected to prefer a 120° bending angle at N_β.

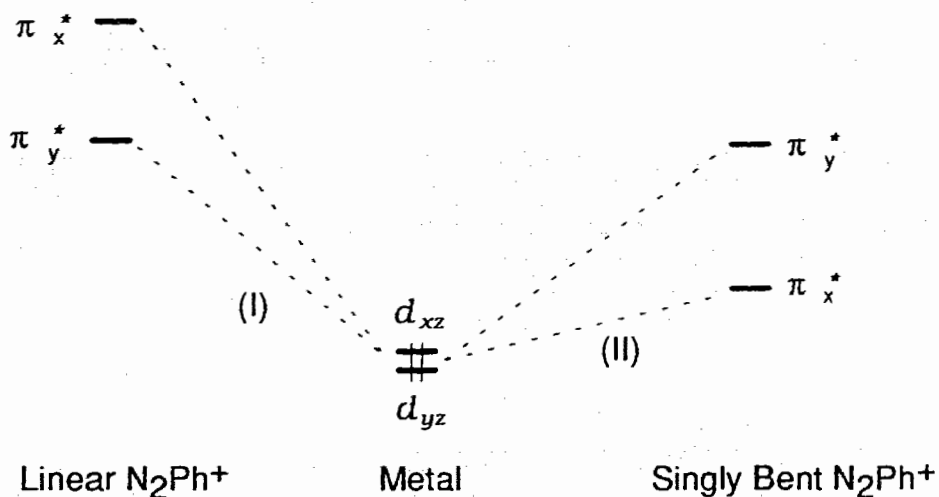
In fact, the orbital 3a" which is orthogonal to the bending plane, as expected, is almost unaffected by the bending. This is also true for the other orbitals with a" symmetry, such as 2a". (This is not shown in Figure 1.3, but it can be seen clearly from Figure 1.2)

Another distinguishing character of this singly bent ligand is that the HOMO and LUMO are located in the same plane defined by the phenyl ring and the dinitrogen group and with the HOMO pointing in a direction trans to the phenyl ring. It is this unique coplanar property of the singly bent aryldiazenido ligand that gives us a chance to use the bending direction of the aryl ring to probe which orbitals on the metal centre are involved in bond formation between the diazenido ligand and the metal centre, and what will be their effects on other ligands. Consequently, based on the same reasoning, any obvious perturbation of the geometry and orientation of the diazenido ligand, *e.g.* by protonation, nucleophilic attack or other reactions at the N atoms, should have predictable effects on the other ligands, especially, on the one trans to the aryldiazenido ligand, and *vice versa*. About this latter point, we will give more detailed discussion in section 1.3.2, when dealing with the aryldiazenido complexes.

Since a bending the phenyldiazenido ligand at N_β will raise its HOMO and lower its LUMO in energy, by considering the relative energies of the transition metals' *d* orbitals (excluding Group VI elements), which, generally, have the energy about -11 ~ -14 eV, obviously, this bending of the

phenyldiazenido ligand at N_β will change the ligand to a stronger π -acceptor and better σ -donor than the linear N_2Ph^+ , and even than NO^+ and N_2 ligands, by reference to Figure 1.1.

Furthermore, the comparison between the linear and singly bent phenyldiazenido ligands indicates another important conclusion, which is that the existence of complexes possessing a *linear* aryldiazenido ligand is highly improbable. It can be seen clearly in Scheme 1.5 that the back bonding



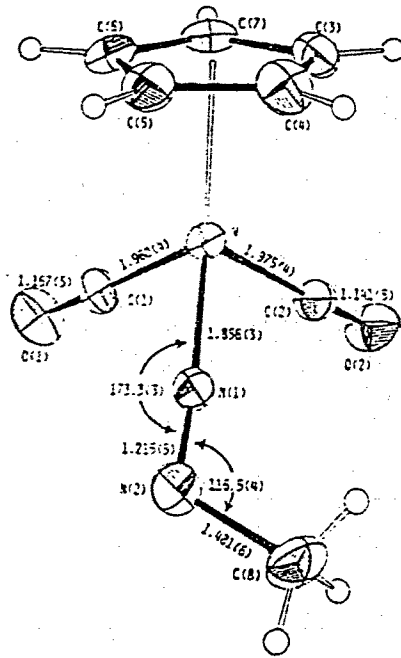
Scheme 1.5

interaction (I) between metal π -type orbitals and empty π^* orbitals on the linear N_2Ph^+ ligand is much less favorable than the interaction (II) between the metal and the singly bent N_2Ph^+ ligand, since the energies of such π -type orbitals for the most of transition metals are lower than that of the LUMO of singly bent aryldiazenido ligand. Although the linear structure would have a smaller steric

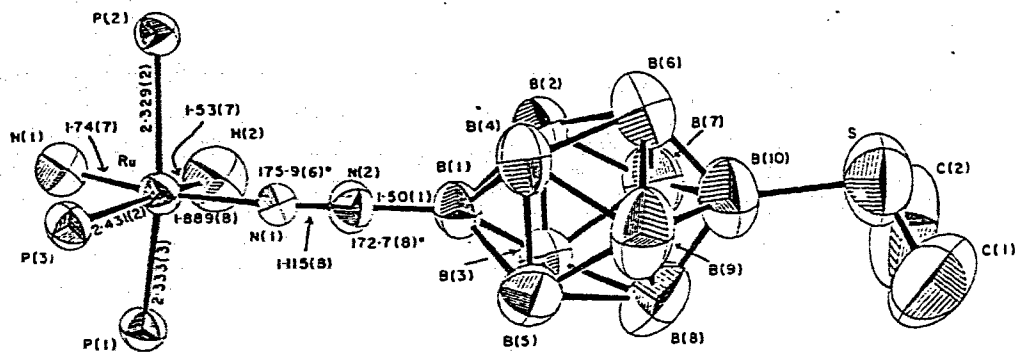
effect, more importantly, the energy lowering by the geometric transformation from linear to singly bent is large. In order to form a complex with a linear N_2Ph^+ ligand, a carefully designed metal centre with a steric "trap" formed by the other ligands would be needed to prevent the favorable energy resulting from the geometric change. There is presently, among more than 40 structurally determined examples, not one aryldiazenido complex in which the MNN system is linear.^{13, 34}

Essentially, this intrinsic bending feature of the aryldiazenido ligand is decided by the non-degeneracy of the in-plane and out-of-plane π systems of the aryl ring. Therefore, for a diazenido ligand, N_2R , as long as the substituent R is such a group that its symmetry is not higher than 2-fold, such as $-CH_2R'$ and $-COR'$ groups, along the N_β -R bonding axis, a similar bending feature as in the aryldiazenido ligand would be expected. So although *aryldiazenido* chemistry is the subject of this Thesis, many conclusions derived from our discussion of the aryldiazenido ligand are also equally applicable to these kinds of *alkyldiazenido* ligands. Therefore, in the discussion which follows, unless particularly specified, "diazenido" ligand will often be used to refer to either aryldiazenido or such kinds of alkyldiazenido ligands. However, for a methyldiazenido ligand where the methyl group contains a C_3 symmetry element, or a ligand having an R group of even higher symmetry, such as $N_2B_{10}H_8S(CH_3)_2$ (which has a C_4 rotation axis in the direction concerned,³⁸ bending at N_β may not be necessarily occur in the coordinated form. In other words, this kind of diazenido ligand could potentially adopt either a linear or a bent geometry when coordinating to a metal centre. However, which one is adopted by such kinds of diazenido ligands in a given

compound would depend on the symmetry of the metal centre. For a metal centre with an asymmetric, or anisotropic, π system perpendicular to the coordination direction, *in principle*, a bent diazenido ligand would be the most favoured. This case can be exemplified by the methyldiazenido compound, $\text{CpW}(\text{CO})_2(\text{N}_2\text{CH}_3)$,³⁷ for which the molecular structure is shown as (a) in Figure 1.4. However, for a metal centre with a symmetric, or isotropic, π system perpendicular to the coordination direction, a linear diazenido would be possible. No example of this case has been observed, possibly due to the critical requirement for an isotropic π electronic system on *both* the ligand and the metal centre. If the π back bonding capability from the metal centre is different in one direction than in the other, but not significantly so, it may not provide enough stabilization energy to compensate the energy loss from removing the degeneracy of the π system as a result of the bending at N_β , so a linear geometry of the ligand also could be possible. For this, rather *weak* π bonding between the metal and the ligand, and an only *slightly* anisotropic π electron distribution of the metal centre are necessary. This situation has been observed in $\text{RuH}_2(\text{N}_2\text{B}_{10}\text{H}_8\text{S}(\text{CH}_3)_2)(\text{PPh}_3)_3$,³⁸ for which the molecular structure has been characterized by X-ray crystallography, and is shown as (b) in Figure 1.4. By comparing with ruthenium-nitrogen bond lengths for six-coordinated singly bent diazenido complexes,³⁴ a significant lengthening, $\sim 0.11 \text{ \AA}$, of the Ru-N_α bond has been observed in this linear diazenido compound, which suggests rather weak π bonding between the ruthenium and the diazenido ligand.



(a)



(b)

Figure 1.4 Perspective views of the molecular structures for (a) $\text{CpW}(\text{CO})_2(\text{N}_2\text{CH}_3)$, and (b) $\text{RuH}_2(\text{N}_2\text{B}_{10}\text{H}_8\text{S}(\text{CH}_3)_2)(\text{PPh}_3)_3$

1. 2. 2. 3. Fragment Orbitals of the Doubly Bent N_2Ar Ligand

Another interesting structural feature of the aryldiazenido ligand in mononuclear complexes is the ability also to bend at the nitrogen atom N_α , bound to the metal. Once again, the bending occurs in the plane defined by N_α , N_β and the aryl ring. The doubly bent aryldiazenido ligand can be conveniently assigned as N_2Ar based upon the *Convention II* established earlier.

Experimentally, almost all neutral doubly bent aryldiazenido complexes can undergo facile protonation on the N_α atom,^{13, 34} which indicates that it is reasonable to assign a lone pair of electrons on this atom. Although, as yet, the free anion N_2Ar^- has not been achieved by either direct or indirect synthesis, use of this anion, N_2Ar^- , as a conceptual approach to build up the fragment molecular orbitals for a doubly bent aryldiazenido ligand is truly instructive.

Figure 1.5 shows the effects of the in-plane bending of the aryldiazenido ligand at N_α . A hydrogen atom was used as a "metal centre" atom in the calculation simply to define the geometry of this diazene type of molecule as either the *cis*- or *trans*-conformation. The orbitals are filled through to the $3a'$ level, as shown in Figure 1.5. Therefore, the HOMO of the doubly bent aryldiazenide, in either the *cis* or *trans* case, is mainly derived from the LUMO of the singly bent diazenido ligand, mixed with some σ character component from the "metal centre". The significance is that the HOMO, in either case, is bent away from the "metal centre", to which the N_α atom is bound, and has a strong n character. Although the HOMO in the *cis* conformation is slightly more stable than in the *trans*, the phenyl ring bends toward the metal centre in the *cis* conformation, and this may

cause significant steric interaction with other coligands in the same plane as the diazenido ligand. This could be the reason that the cis geometry has not been observed yet in the known doubly bent aryldiazenido complexes.^{13, 34}

Note that the LUMO, $3a'(\pi^*_x)$ of the singly bent N_2Ph ligand becomes the HOMO in the double bending transformation, and the "*superjacent*"* antibonding orbital $3a''(\pi^*_y)$ of the singly bent N_2Ph now becomes the LUMO in the doubly bent N_2Ph ligand. Since the geometry change occurs in the nodal plane of $3a''(\pi^*_y)$, the energy and symmetry of this orbital essentially remain the same during this change. On the other hand, the $3a''$ orbital (potentially involved in an unfavorable π back-bonding interaction in the singly bent N_2Ph complex) now becomes the only possible empty orbital in the doubly bent ligand able to accept π back-donation from the metal centre. Keep in mind that the $3a'$ (predominately involved in the back-bonding interaction with metal in the singly bent ligand) and $3a''$ orbitals are perpendicular to each other. Therefore, for an aryldiazenido ligand coordinated to a metal centre in a low symmetric environment, it is predicted that the transformation of a singly bent to a doubly bent N_2Ph ligand would be accompanied by a 90° ligand rotation about the of $M-N\alpha$ bond axis in

*: **Subjacent** was first used by L. Salem in *J. Am. Chem. Soc.*, (1972), **94**, 8917, and **Superjacent** by L. Salem and R. Hoffmann in *J. Am. Chem. Soc.*, (1973), **95**, 3806. They have following definitions

Superjacent Unoccupied Molecular Orbital (SUMO) is the unoccupied MO which is energetically *superior* and *adjacent* to the LUMO.

Subjacent Occupied Molecular Orbital (SOMO) is the occupied MO which is energetically *subordinate* (or *inferior*) and *adjacent* to the HOMO.

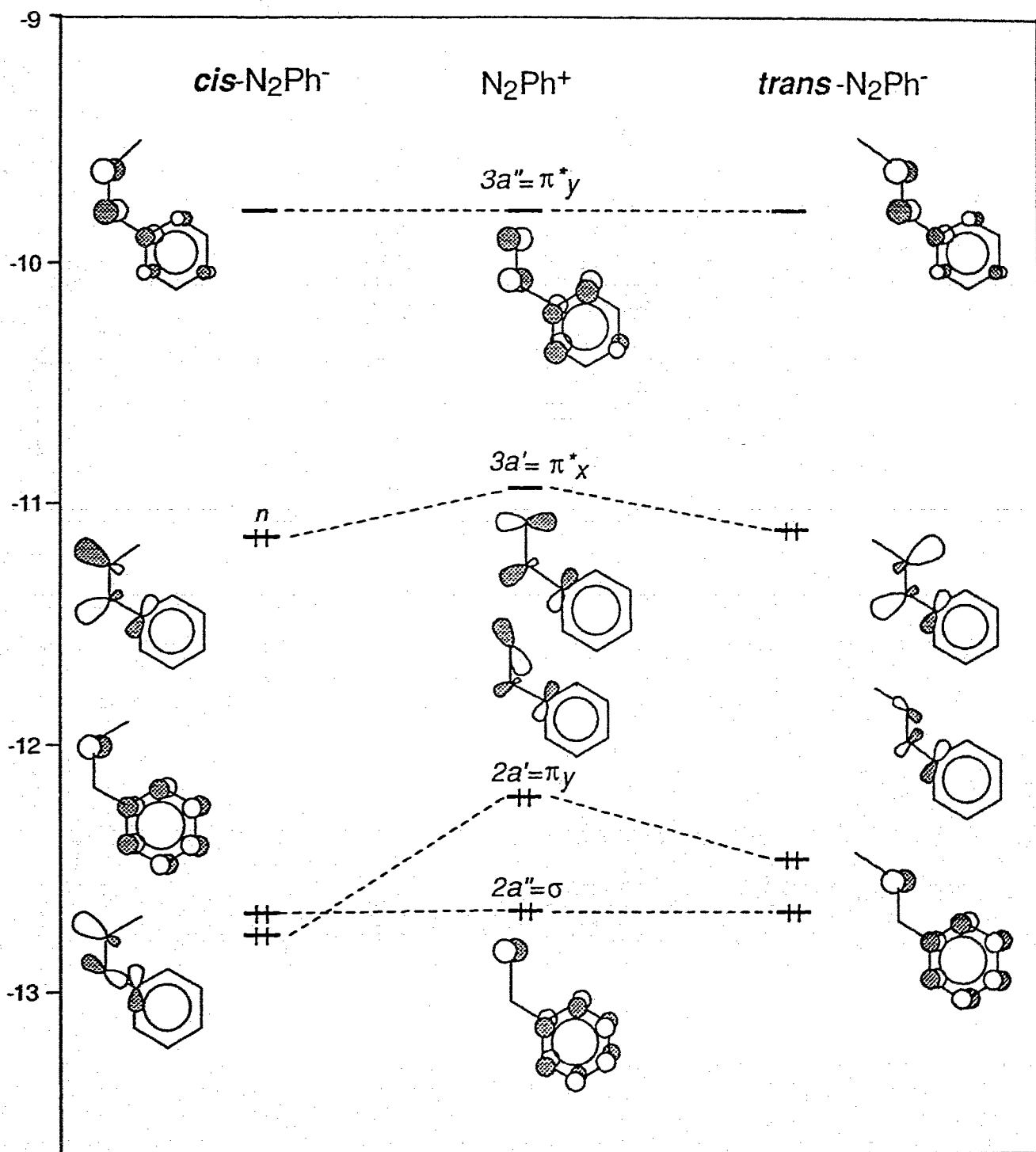


Figure 1.5 Effect of forming a doubly-bent configuration on the frontier orbitals of NNPh⁺

order to achieve better overlap of the filled metal d orbital and the empty π^* orbital of the ligand. This will also avoid an unfavourable antibonding interaction between the filled metal d orbital and the $3a'$ (the filled orbital now in doubly bent N_2Ph ligand). An exception might be when there is a crowded coordination environment around the metal centre which could sterically block such a rotation. Direct experimental evidence for this prediction is absent, because few doubly bent aryldiazenido complexes have been structurally characterized, and there are no known pairs of structures of singly bent and doubly bent aryldiazenido complexes related in this fashion. However, indirectly, it is supported by the examples shown in Figure 1.6. In the singly bent aryldiazenido compound $[Cp'Mn(CO)_2(N_2C_6H_4CF_3)]BF_4$, ($Cp' = C_5H_4CH_3$),^{1, 39} the planar aryldiazenido ligand is located in the position which is pseudo-parallel to the Cp' plane, but in the hydrazido(2-) compound $CpRe(CO)_2(NN(Me)C_6H_4OMe)$,⁴ the hydrazido (2-) ligand, which can be considered structurally similar to a doubly bent diazenido ligand, is in the position perpendicular to the Cp plane.

From the above discussion, we see that doubly bending the aryldiazenido ligand results in a single, weak π -acceptor orbital perpendicular to the bending plane and an n orbital pointed away from the metal centre that the diazenido ligand is bound to. Furthermore, the shapes and the relative orientations of the HOMO and LUMO at the ligating atom, N_α , indicate that the doubly bent diazenido ligand is actually isolobal with the simple arylnitroso compound, $ONAr$, presumably a very weak ligand.

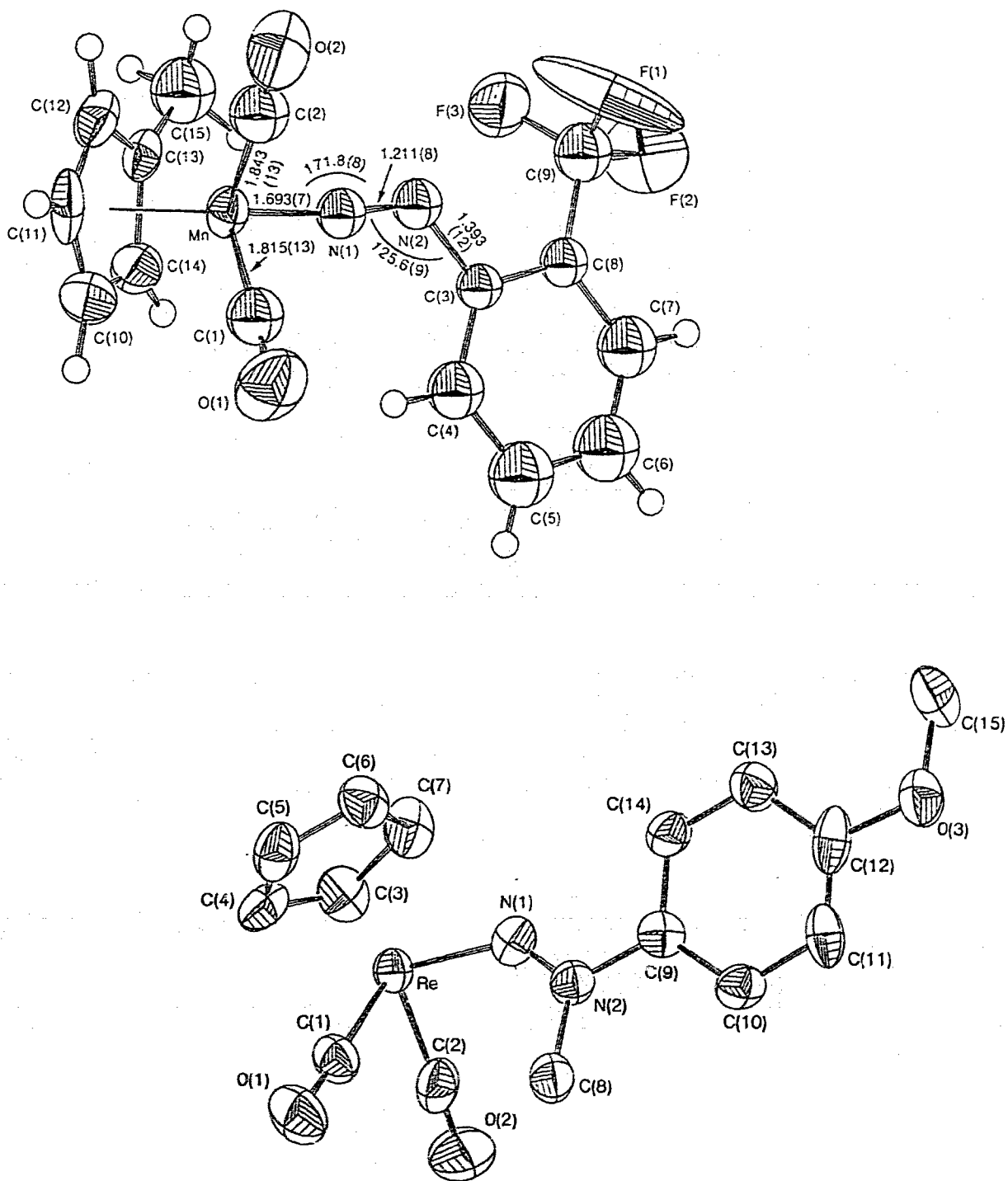


Figure 1.6 Comparison of the bending directions of the singly bent diazenido and the doubly bent hydrazido (2-) ligands on the metal fragment $\text{CpM}(\text{CO})_2$, ($\text{M} = \text{Re}$ and Mn , $\text{Cp} = \text{Cp}$ or Cp')

1.3. Mononuclear Aryldiazenido Complexes

1.3.1. Introduction

As pointed out already, structural studies for terminal aryldiazenido complexes have demonstrated that the aryldiazenido ligand in mononuclear complexes can adopt the two different coordination geometries, singly bent and doubly bent, as shown in Figure 1.7

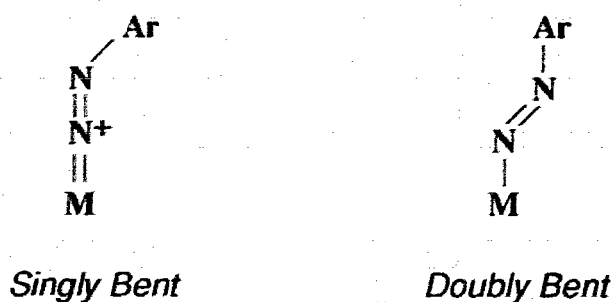


Figure 1.7 Coordination modes of the terminal aryldiazenido ligand

By far the most prevalent bonding mode found is the singly bent geometry (I), with typical parameters: $\angle \text{M-N-N} \approx 170^\circ$; $\angle \text{N-N-C} \approx 120^\circ$; $\text{N-N} = 1.2 \text{ \AA}$. There are only three crystallographically characterized examples of the doubly bent geometry (II),⁴⁰⁻⁴² although more examples have been reported to be observed in solution by spectroscopic methods.^{34,40} Of these two coordination modes, the particular one observed in a given complex presumably depends on the electronic requirement of the metal centre. These two different geometries of terminal N_2Ar ligands in most of the complexes, especially in those of later transition metals, can be easily rationalized by considering only the general requirements of the maximum coordination number and the 18 electron counting rule of the metal

centres. However, when we are dealing with some of the detailed structural and reactivity features of diazenido ligands in the complexes, these general criteria seem less helpful. For example, problems like which nitrogen atom is preferentially attacked by an electrophilic reagent in a doubly bent aryldiazenido ligand, and why no stable compound has been found so far in which a carbonyl ligand is *trans* to a singly bent aryldiazenido ligand, (except for the complexes of Group VI transition metal elements, which will be discussed later as a special case), whereas carbonyl is a common *trans* ligand in many doubly bent aryldiazenido complexes. In order to answer these sorts of questions, fine details of the electronic structure of the molecule concerned must be considered. This consideration should not only include the electronic configuration of the metal centre, but should also include the electronic contributions of various co-ligands around the metal centre. In fact, we believe it is this latter contribution from the co-ligands that plays the key role in stabilizing or de-stabilizing the bonding between the metal and the aryldiazenido ligand.

In the following section, a qualitative fragment molecular orbital description of the nature of the MNNAr linkage will be presented, by means of which the electronic requirement of the aryldiazenido ligand in regard to both the metal and some key co-ligands located in different positions in the molecule will be investigated.

1. 3. 2. Singly Bent Aryldiazenido Complexes

1. 3. 2. 1. In Octahedral and Square-Planar Geometries

For the sake of simplicity, it is convenient to start with a six-coordinate diazenido complex. The molecular orbital interactions between the singly bent N_2Ph^+ fragment and a square pyramidal metal fragment ML_5 are illustrated in

Figure 1.8. On the left of Figure 1.8 are listed the metal-centred d orbitals for a square pyramid ML_5 , and on the right side are the frontier orbitals of a singly bent N_2Ph^+ which we have established in Section 1.2.2.2. The e and b_2 sets are non-bonding d orbitals of the metal and, therefore, to a first approximation with no consideration of π interaction, they should have the same energy as in the free metal ion (which, generally, is around $-12 \sim -13$ eV for the most transition metals)*. Note, however, that Group VI transition metals have higher energy d orbitals, at around $-10 \sim -11$ eV*. When an aryldiazenido ligand approaches the apical position of the ML_5 fragment, two interactions mainly occur, labelled as **A** and **B**, in Figure 1.8. In interaction **A**, the HOMO ($2a'$) of N_2Ph^+ overlaps with the metal orbital a_1 , which is primarily d_{z^2} . Clearly, only when this d_{z^2} orbital is empty, can interaction **A** be a favorable one and the system be stabilized by it. Otherwise, this interaction will be primarily antibonding. Therefore, in order to get a stable singly bent diazenido complex in an octahedral geometry, a d^n ($n \leq 6$) metal centre is essential. This clearly agrees with the 18 electron counting rule. Examples of this type of compound can be found in Table 1.1.

On the other hand, the LUMO of the N_2Ph^+ ligand has the same symmetry as a filled metal d_{xz} orbital, one of the e group orbitals in C_{4v} ML_5 . Mixing between them will produce another bonding interaction, labelled as **B**. Interaction **A** is of σ type and there is only a small energy gap between the two fragment orbitals involved. Interaction **B** is a π type interaction between two rather largely separated fragment orbitals. So, generally, interaction **A** is stronger than interaction **B** and **A** is the dominant component in the "synergic"

*: Refer to the appendix II for the references.

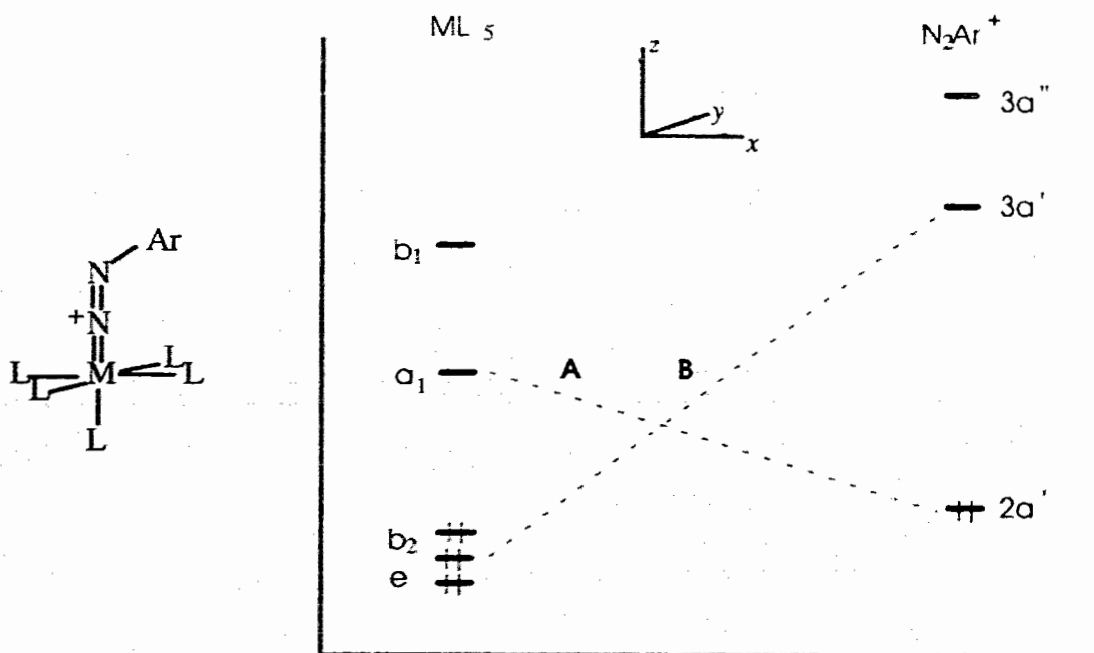


Figure 1.8 Qualitative Orbital Interactions of ML_5 and Singly Bent N_2Ar^+

bonding pattern of $M-N_2Ph^+$. It is worth mentioning that the interaction of the filled metal d_{yz} orbital and another empty π^* orbital ($3a''=\pi_y^*$) *superjacent* to the LUMO of the diazenido ligand is small, albeit not negligible, so that the π back bonding in this "synergic" process mainly occurs in the plane in which a metal d_{xz} orbital and the LUMO of the singly bent N_2Ph^+ are located. This intrinsic property of the singly bent aryldiazenido ligand can be described as an anisotropic or "single-faced" π -back bonding ability, and distinguishes it from those having an isotropic or "cylinder-type" π back bonding ability, such as terminally bonded CO, NO, N_2 , etc ligands. Importantly, the "single-faced" π -type interaction between the singly bent aryldiazenido ligand and the metal centre actually could provide us with some insights into the approximate arrangement of

Table 1.1 Bond Angles of M-N-N in Singly Bent Diazenido Complexes

Compounds	\angle M-N-N ($^{\circ}$)	Reference
a*		
$[(\text{MeC}_5\text{H}_4)\text{Mn}(\text{CO})_2(\text{N}_2\text{C}_6\text{H}_4\text{CF}_3)]\text{BF}_4$	171.8(8)	1
$[(\text{C}_5\text{Me}_5)\text{Ir}(\text{C}_2\text{H}_4)(\text{N}_2\text{C}_6\text{H}_4\text{OMe})]\text{BF}_4$	176.2(6)	37
$\text{RuCl}_3(\text{N}_2\text{C}_6\text{H}_4\text{Me})(\text{PPh}_3)_2$	171.2(9)	38
$(\text{C}_5\text{H}_5)\text{Re}(\text{CO})(\text{N}_2\text{C}_6\text{H}_4\text{OMe})(\text{AuPPh}_3)$	171(1)	39
$\text{ReBr}_2(\text{N}_2\text{Ph})(\text{N}_2\text{HPh})(\text{PPh}_3)_2$	172.4(10)	40
$\text{ReCl}_2(\text{N}_2\text{C}(\text{O})\text{Ph})(\text{PMe}_2\text{Ph})_3$	170(2)	41
$\text{ReCl}_2(\text{N}_2\text{Ph})(\text{PMe}_2\text{Ph})_3$	172(2)	42
b*		
$(\text{HBpz}_3)\text{Mo}(\text{CO})_2(\text{N}_2\text{Ph})$	174.2(1)	43
$(\text{HBpz}_3)\text{Mo}(\text{N}_2\text{C}_6\text{H}_4\text{F})(\text{SC}_6\text{H}_4\text{Me})_2$	170.8(8)	44
$\text{MoCl}(\text{N}_2\text{C}(\text{O})\text{Ph})(\text{NHNC}(\text{O})\text{Ph})(\text{PMe}_2\text{Ph})_2$	174(1)	
	175(1)	45
$\text{Mo}(\text{N}_2\text{C}_6\text{H}_{11})(\text{diphos})_2$	177(1)	46
$\text{Mo}_2(\text{N}_2\text{Ph})_4(\text{acac})_2(\text{OMe})_2$		
isomer A	177.7(11)	
	175.9(11)	
isomer B	173.3(9)	
	176.5(9)	47
$[\text{Mo}_2(\text{N}_2\text{Ph})_4(\text{MoO}_4)_2(\text{OMe})_2]^{-2}$	180	48

*: Group **a** contains compounds having non-Group VI transition metals, and group **b** contains compounds having Group VI transition metals

the metal frontier orbitals in the complexes. It is also apparent that the terms " π -accepting strength" or " π -accepting ability", normally used for π -acid ligands, should be used carefully, with due regard to the nature of the ligand. A simple comparison of this strength when it involves a "single-faced" π -acid ligand on the one hand, and a "cylinder-type" π -acid ligand on the other is not very meaningful, and could even be dangerous because it, sometimes, might lead to a wrong conclusion.

In singly bent aryldiazenido complexes the ligand has a formal positive charge, and a low-lying LUMO, even lower than that of CO or NO⁺ ligands. It therefore would be expected to strongly accept π back donation from the metal centre. The bond lengths of M-N _{α} found in singly bent diazenido complexes (1.8 ~ 2.0 Å) almost all fall into the metal-nitrogen double bond range, indicating that the "single-faced" "synergic" back bonding in the M-N _{α} linkage is quite effective. If we restrict back bonding to only one plane, the singly bent aryldiazenido ligand in this "single-faced" sense may even be better than CO or NO⁺. As part of this work, we have made a direct comparison of the singly bent aryldiazenido ligand with the nitrosyl ligand in low symmetry complexes in which each effectively back-bonds with only one metal orbital (*i.e.* both ligands are effectively in a single-faced situation). The results support N₂Ar⁺ being the better π -acceptor, and are presented fully in Chapter II.

Recalling that the calculated HOMO of the singly bent N₂Ph⁺ ligand is located in the bending plane and slightly pointed away in a direction *trans* to the phenyl ring (see Figure 1.2), it would be expected that the bonding of a singly bent N₂Ph⁺ to a ML₅ fragment, would be dominated by σ interaction A, and should produce a product with a slightly bent M-N-N linkage, *i.e.*, \angle M-N-N < 180°. This is indeed observed for all of those diazenido complexes with a singly

bent diazenido ligand which have been accurately characterized by crystallographic methods. Some examples are listed in group **a** in Table 1. Of course, since this bending deviates only slightly from linearity, it is difficult to judge whether it is truly an electronic effect or is simply a crystallographic phenomenon. For example, terminal carbonyl ligands, in even highly symmetric molecules, are often observed crystallographically to have $\angle\text{M-C-O} \neq 180^\circ$. However, more importantly, the bending of singly bent diazenido ligands in these complexes is overwhelmingly toward one direction, that is the direction trans to the aryl ring. If this were a crystallographically imposed effect, the bending direction would depend on the crystalline packing structure and be expected to be quite variable. On the other hand, if this delicate structural phenomenon is truly due to the dominant σ bonding interaction (**A**, in Figure 1.8) between the HOMO of N_2Ar^+ and LUMO of ML_5 , then as this interaction decreases, the bending angle of the M-N-N linkage should be expected to increase, even to 180° . One way to weaken the interaction **A** is to raise the energy of the d orbitals of the metal centre. This can be simply achieved by using Group VI transition metals which have rather higher VSIP's for their d orbitals. For example, the molybdenum atom has a VSIP energy about 10 eV for its $4d$ orbitals. Therefore, the bonding interaction between a singly bent N_2Ar^+ and a Mo centre in an octahedral or related complex would be expected to have a less effective σ component. In other words, σ bonding between Mo centre and N_2Ar^+ 's HOMO would not be so dominant in the molybdenum diazenido linkage. Not surprisingly, the crystallographic data on the known molybdenum diazenido complexes (listed in Table 1.1 as group **b**) undoubtedly indicate rather larger $\angle\text{Mo-N-N}$ angles, close to 180° , by comparison with the angles for other metal centres.

In organotransition metal complexes, all ligands with the exception of H^- have π -type valence orbitals. These orbitals can participate in bonding, nonbonding or antibonding interactions with metal d_π orbitals, (for simplicity here and later, we will call metal d_{xy} , d_{xz} , and d_{yz} orbitals d_π orbitals). Stabilization or destabilization of a bonding interaction between a metal and a diazenido ligand may not only strongly depend on π interactions of metal with this ligand, but also depend on the π interactions of the metal with the other co-ligands about the metal. If symmetry conditions are satisfied, there are two factors which would decide the magnitude of this π type of interaction. These are the relative energies of the metal d_π and the ligand orbitals, and the electron filling situation in these fragment orbitals. The variations of these two factors in different complexes are the real source of the rich and diverse structural properties and chemical reactivities of organotransition metal complexes.

Until now we have assumed that metal d_π orbitals are nonbonding to other co-ligands. Now it is necessary to remove this restriction and determine the effect of other co-ligands on this synergic bonding process between the metal and diazenido ligand.

In order to do this by using fragment molecular orbital theory, the principal concern will be to evaluate the contribution from a few, and only a few, π -type valence orbitals of co-ligands to the metal d_π orbitals, and hence to the metal diazenido linkage. The σ orbitals from these ligands need not be considered further, since they normally have much lower energy than the metal-based ones.

Two ligands X^- and CO , which are at the opposite ends of the spectrochemical series,⁵⁵ will be used as examples.

A carbonyl ligand has two orthogonal sets of π -type orbitals, say π_x , π_x^* and π_y , π_y^* . When a CO group is coordinated to a transition metal centre, there

is overlap between these π type of orbitals and metal d_{π} (d_{xy} and d_{yz}) orbitals, as shown in Figure 1.9. Consequently, there results 3 sets of π molecular orbitals,

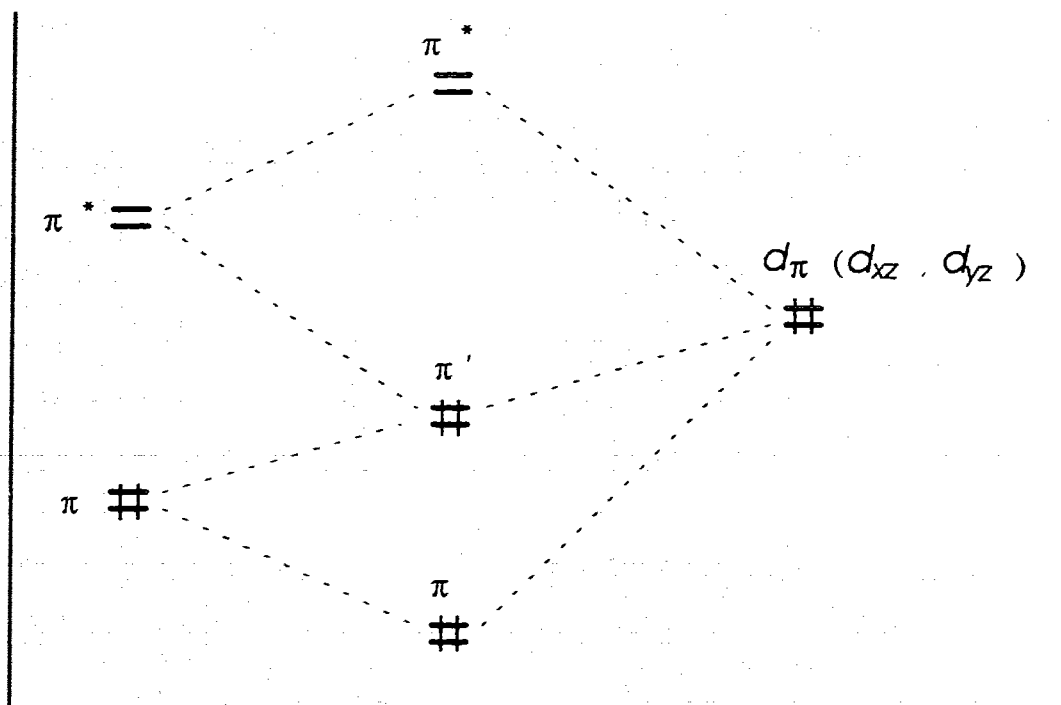
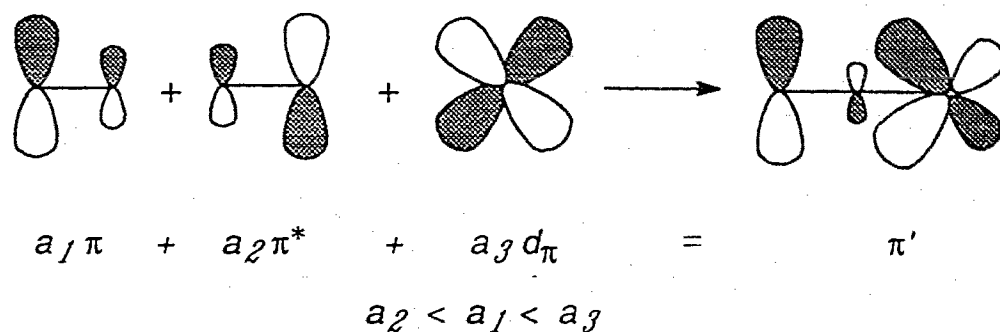


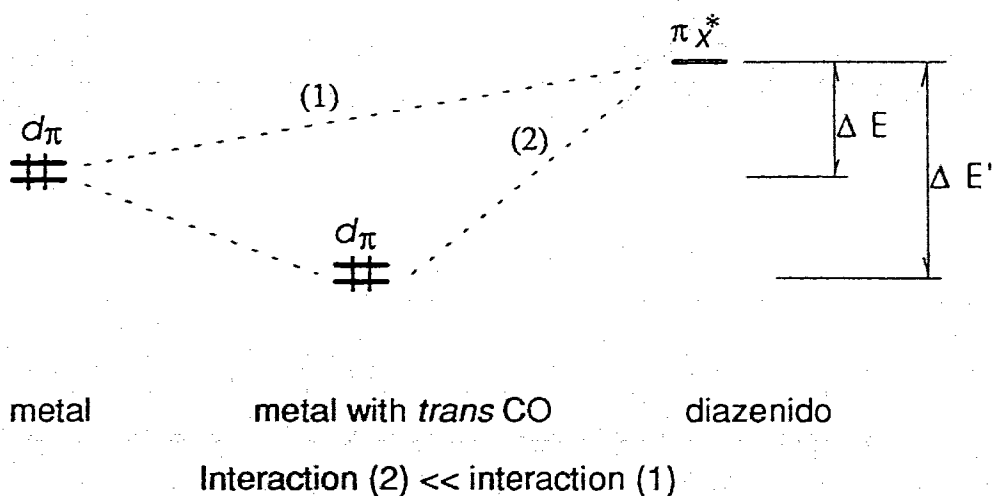
Figure 1.9 π interaction between a terminal carbonyl and metal centre

corresponding to bonding, nonbonding and antibonding, respectively. For a metal centre with filled (d_{π}^6) or partially filled (d_{π}^2 or d_{π}^4) d_{π} orbitals, the nonbonding set, π'_x and π'_y , would be filled or partially filled and, therefore, would become the highest occupied molecular orbital set. Since these two orbitals are primarily metal-centred nonbonding ones, (one of them shown in Scheme 1.6), the electron densities on the metal centre in these orbitals will be expected to be only changed slightly. It is noteworthy that the electron density on the carbon atom in these newly formed HOMOs is substantially decreased. This can be



Scheme 1.6

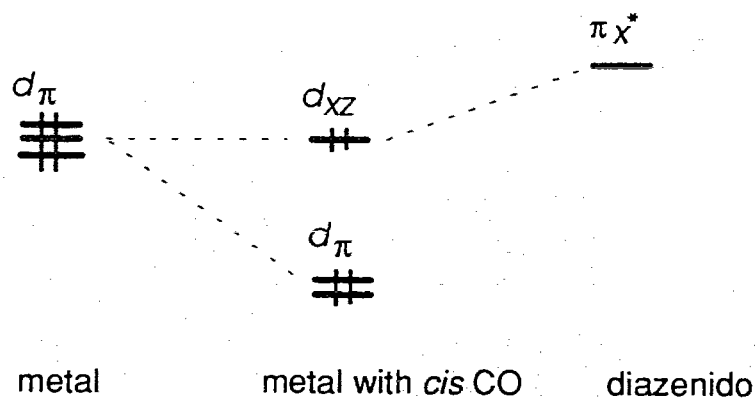
illustrated by the facile attack of nucleophiles at the carbon atom of the terminal CO ligand in later transition metal carbonyl compounds.⁵⁶ It is important to note that as a result of this bonding, the energy of these metal d_π orbitals could decrease dramatically. This would, in turn, directly decrease their back bonding potential to other ligands, particularly, the ligand trans to the CO group. In the case of aryldiazenido complexes, the influence of this trans carbonyl on the π bonding of the metal and diazenido ligand can be clearly seen from Scheme 1.7.



Scheme 1.7

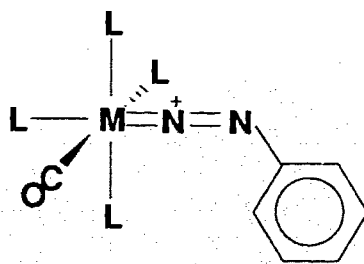
The back bonding from the metal centre to the singly bent diazenido ligand is thus largely reduced by a trans CO ligand. In fact, no matter how the diazenido ligand might be rotated around the axis of the metal-ligand σ bond to bring the LUMO into either the x direction or the y direction to maximize overlap with the d -orbital, the weak back bonding situation will still be the same. Therefore, it is concluded that for most transition metal complexes in low oxidation states, where the d orbitals have energy around -12 eV, a trans arrangement of a CO and a singly bent diazenido ligand is unstable. The experimental evidence is entirely consistent with this conclusion. So far, with the exception of Group VI, in all structurally characterized aryldiazenido transition metal complexes with CO as co-ligand, not one of them has CO trans to the singly bent N_2Ar group.

When a carbonyl ligand is located in a position cis to a singly bent aryldiazenido ligand, the situation may become different. In a cis carbonyl diazenido complex, where the carbonyl, the nitrogen group of diazenido and the metal define a plane, say the xz plane, the two metal d_π orbitals stabilized by the *cis* carbonyl ligand, (assume CO is on the y axis), will be d_{xy} and d_{yz} . The remaining d_π orbital (d_{xz}) on the metal will not be affected by the *cis* carbonyl ligand, as shown in Scheme 1.8. It is this unaffected d_{xz} orbital that will have the same symmetry as the π^*_x orbital (LUMO) of the aryldiazenido, (or this ligand could rotate to achieve the same symmetry). So if, and only if, the metal centre is d^n ($n \geq 6$), the electrons in this d_{xz} orbital could be back donated to the empty π^*_x orbital of the diazenido ligand. Moreover, in this *cis* arrangement, the bending of the aryl ring in the diazenido ligand would be expected to be toward the direction



Scheme 1.8

perpendicular to the plane, as shown in Scheme 1.9, in which the metal, the nitrogens of the diazenido ligand and the CO group are located. An example is $\text{CpRe}(\text{CO})-(\text{N}_2\text{C}_6\text{H}_4\text{OMe})(\text{AuPPh}_3)^{57}$ with a OC-Re-N angle $94.7(6)^\circ$. The $\text{C}_6\text{H}_4\text{OMe}$ ring is bent perpendicular to the plane defined by OC , Re and NN .



Scheme 1.9

The X-ray crystal structure of $\text{CpRe}(\text{CO})(\text{N}_2\text{C}_6\text{H}_4\text{OMe})(\text{AuPPh}_3)$ is shown in Figure 1.10.

A similar argument could also be applied to di-carbonyl diazenido complexes such as $\text{M}(\text{CO})_2(\text{N}_2\text{Ar})\text{L}_3$. When two carbonyls and the diazenido

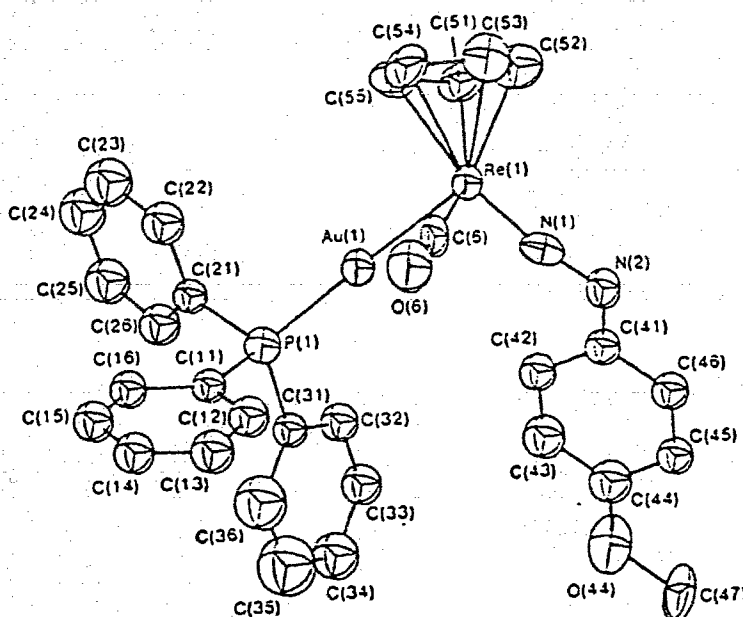
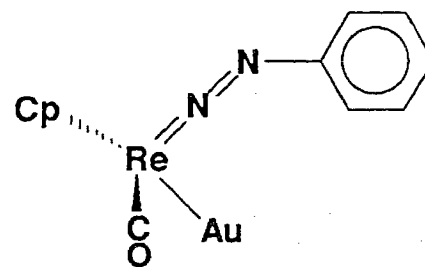


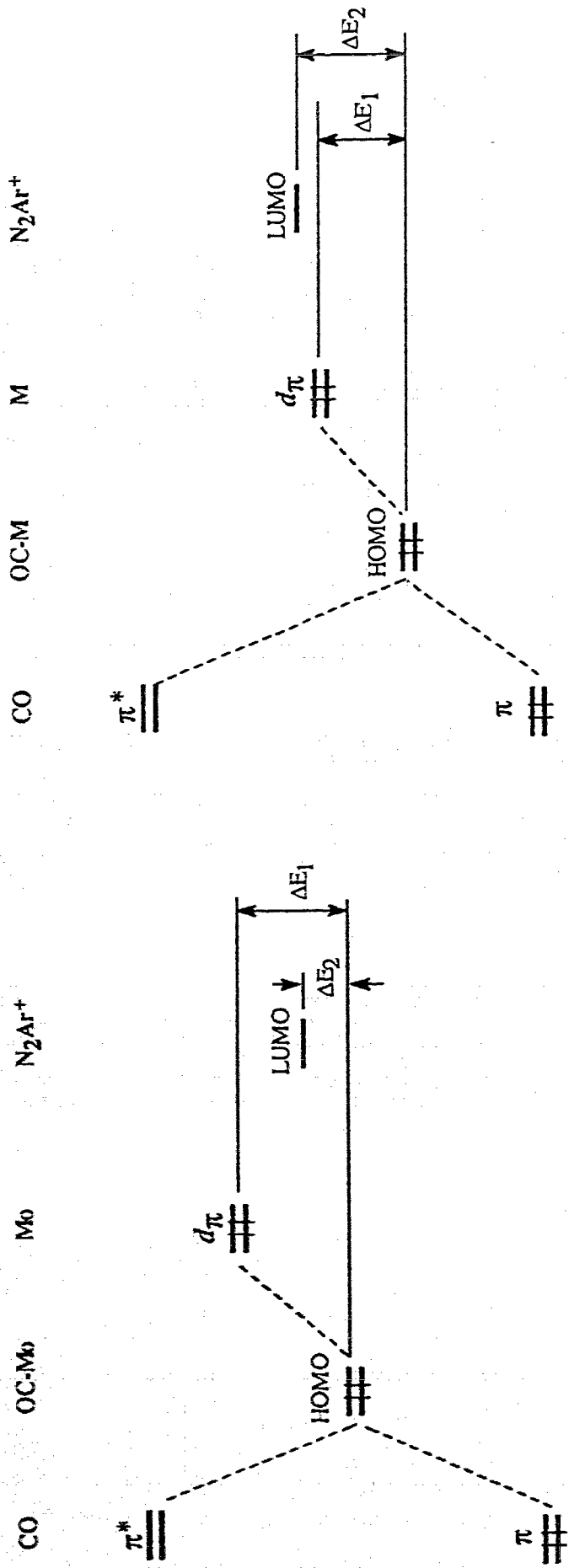
Figure 1.10 The molecular structure of compound CpRe(CO)-
 $(p\text{-N}_2\text{C}_6\text{H}_4\text{OMe})(\text{AuPPh}_3)$

ligand are in a *fac*-arrangement, this would be expected to destabilize the compound. When the two carbonyls and the diazenido ligand are in a *mer*-configuration and the two carbonyls are trans to each other, less effect on the bonding of the diazenido ligand to the metal would be expected. Of course, if some strong π base ligands are present trans to the CO ligands, the

destabilization of the metal d_{π} orbitals due to the carbonyls could be completely offset by the stabilization due to these π donor ligands. An example of this stabilization is dicarbonyl compound $[\text{Cp}^*\text{Mn}(\text{CO})_2(\text{N}_2\text{C}_6\text{H}_4\text{CF}_3)]\text{BF}_4$,¹ in which the two CO's and the diazenido ligand are in a sort of *fac*-arrangement. A detailed analysis of the stabilization of metal d_{π} orbitals by π donor ligands like Cp will be discussed in the next chapter.

It has been mentioned that Cr, Mo and W have rather higher d orbital energies, (Cr: -11.22 eV; Mo: -10.50 eV and W: -10.37 eV) relative to other transition metal elements, which have the VSIP's about 12 eV ~ 14 eV. When these metals, in low oxidation states, are involved in organometallic compounds, the interactions between them and the ligands are slightly different from that of other transition metals. For example, in their aryldiazenido carbonyl complexes,³⁴ the CO group seems to be able to occupy any position.

The differences in the orbital interaction for the Group VI metal Mo and those of other groups in a trans diazenido carbonyl complex are illustrated in Figure 1.11. In the molybdenum diazenido complex, (case **A** in Figure 1.11), a trans CO ligand will cause the metal d_{π} orbitals to lower in energy (ΔE_1). Due to the resulting closeness in energy of the CO LUMO and Mo HOMO, this drop will be larger than that ($\Delta E_1'$) in case **B**, where a non-Group VI transition metal is involved. Since the initial d_{π} energy of the unperturbed Mo centre is higher than the LUMO of the trans diazenido ligand (which is reversed for other transition metals) the π interaction between Mo and the trans CO group, in fact, will push the filled metal d_{π} orbitals to an energy level more favorable for back bonding to the diazenido ligand. This is shown in interaction **A** of Figure 1.11 as a smaller ΔE_2 . For other transition metals, this trans effect of a CO ligand almost surely increases the energy gap between the metal d_{π} orbital and the LUMO of the



(A)

(B)

Figure 1.11 The effect of different metals on the bonding between M-CO and singly bent diazenido

diazenido ligand, and is shown as the larger $\Delta E_2'$ in interaction **B** of Figure 1.11. Clearly, a trans CO ligand in a group VI metal diazenido complex does not weaken the metal-aryldiazenido bond as much as in a diazenido complex with other group metals. The complex $[\text{Mo}(\text{CO})_3(\text{N}_2\text{C}_6\text{H}_4\text{F})(\text{PPh}_3)_2]\text{BF}_4$ ⁵⁸ is a good example, in which the singly bent diazenido ligand is in a *fac*-arrangement with two carbonyl ligands.

Now we consider the halide ligand. Unlike a carbonyl ligand, a halide ligand only has two filled *p* orbitals of π symmetry in the energy range of interest. When it coordinates to a metal centre, π interactions will be expected to occur between the two filled *p* orbitals and metal d_π orbitals. Figure 1.12 shows this kind of interaction for a Cl^- ligand, for which the π orbitals have energy *ca.* -14.2 eV. This interaction will produce two degenerate low-lying bonding orbitals which are mainly Cl^- centred, and two high-lying degenerate antibonding

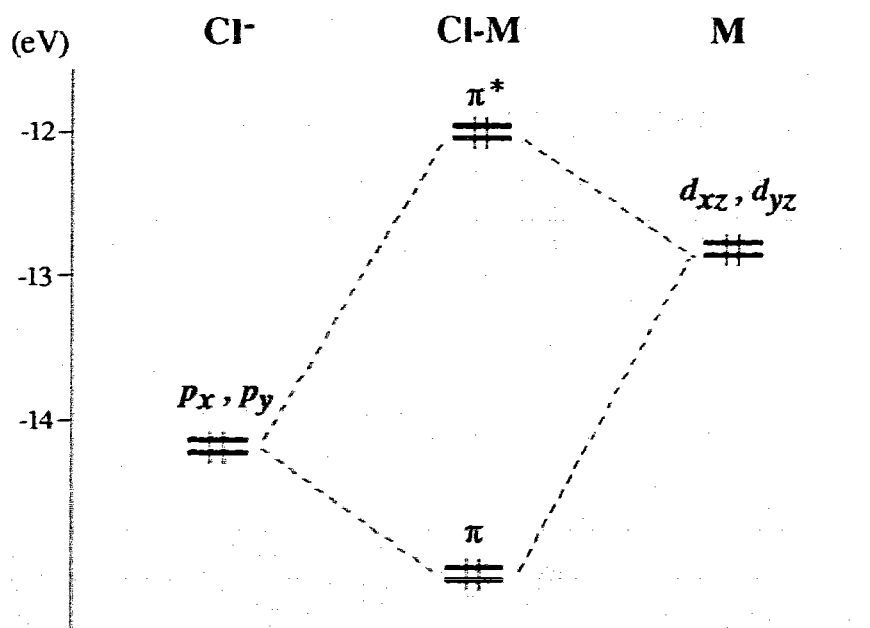
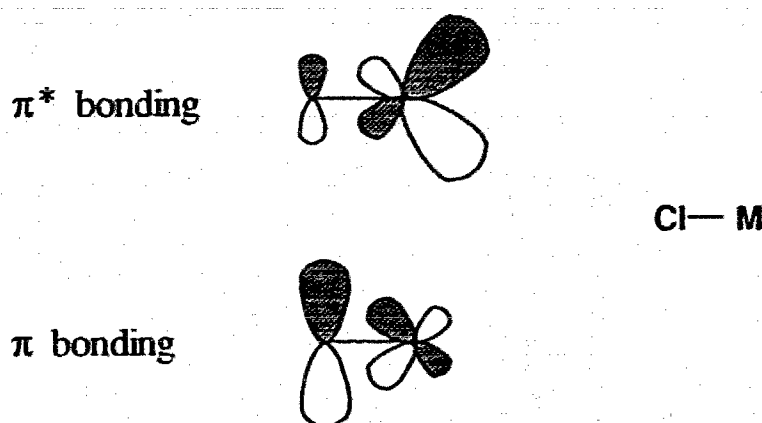


Figure 1.12 Qualitative π interaction of Cl^- ligand and metal centre

π orbitals which are primarily metal centred. One component of each of these two sets of molecular orbitals is diagrammed in Scheme 1.10. In the π bonding orbitals, electron density is mainly distributed between the metal and the chloro ligand, but closer to the latter. In the π antibonding orbitals, the electron density is mainly focussed on the metal centre and is formally concentrated in the two lobes pointed away from the metal-chlorine bond. Since the antibonding orbitals are filled metal-centred ones, coordination of a halide to the metal centre actually pushes the metal d_{π} orbitals into a much higher energy level. In order to release this energy buildup, it will be an advantage for the metal centre to bind



Scheme 1.10

other π acid ligands, like aryl diazenido, in the trans position. For a trans diazenido chloro complex, although this π interaction between the metal and the diazenido ligand may only involve one of the metal d_{π} orbitals raised by the trans chloro ligand, it will surely stabilize the metal-diazenido bonding. Examples to illustrate the structural character of this trans arrangement are

$[\text{RhCl}(\text{N}_2\text{C}_6\text{H}_4\text{OMe})(\text{PPh}_3)_2] \text{BF}_4$,⁵⁹ $\text{MoCl}(\text{N}_2\text{C}(\text{O})\text{Ph})(\text{dppe})_2$ ⁶⁰ and $\text{Mo}(\text{N}_2\text{C}_6\text{H}_{11})(\text{dppe})_2$,⁵² and their X-ray crystal structures are shown in Figure 1.13.

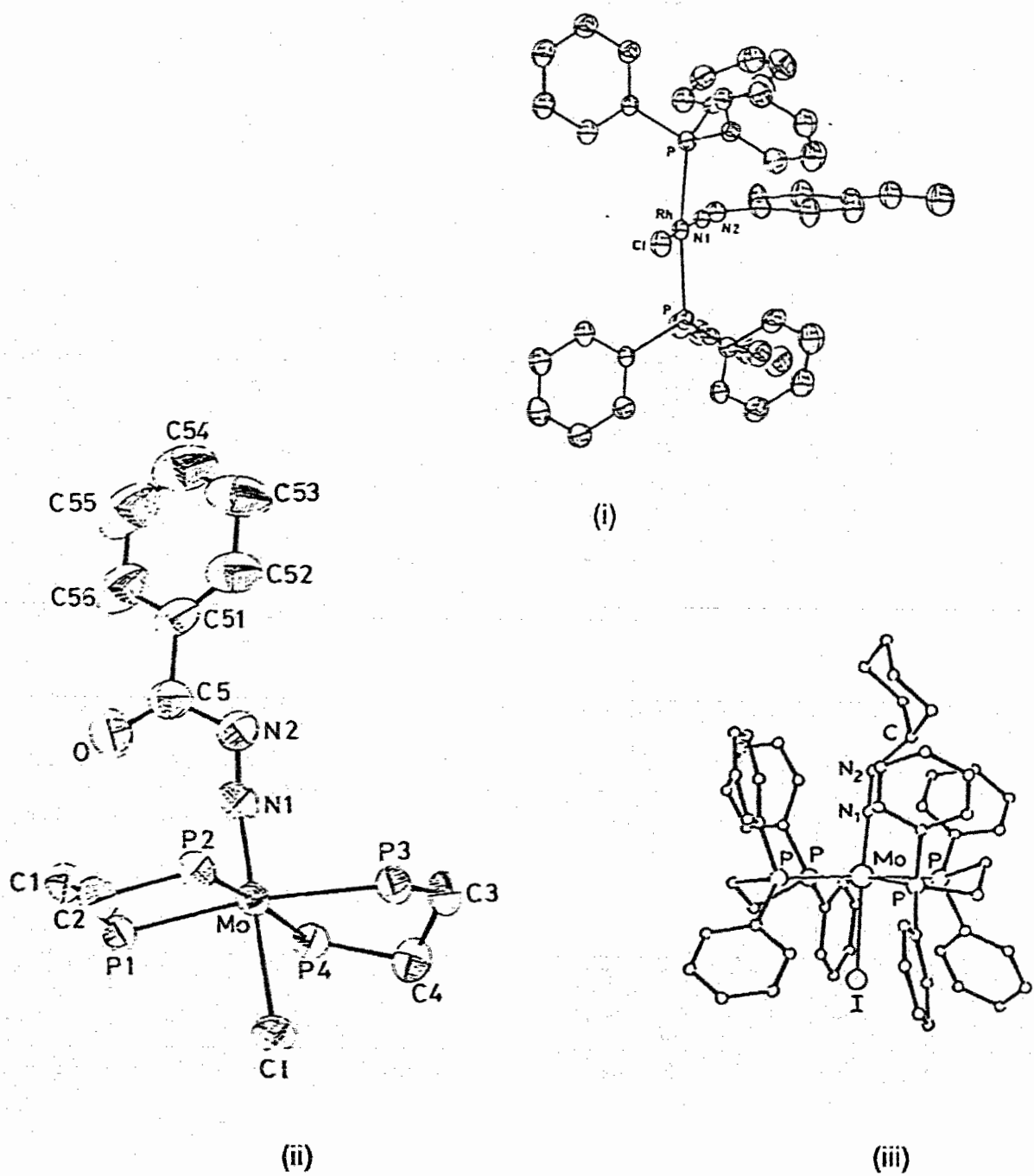
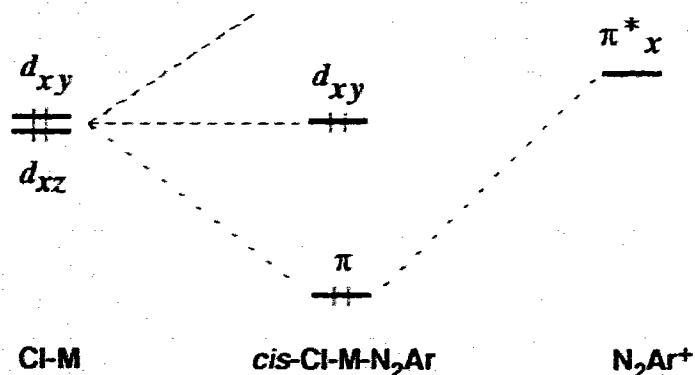


Figure 1.13 Perspective views of molecules: (i) $[\text{RhCl}(\text{N}_2\text{C}_6\text{H}_4\text{OMe})(\text{PPh}_3)_2]\text{BF}_4$, (ii) $\text{MoCl}(\text{N}_2\text{C}(\text{O})\text{Ph})(\text{dppe})_2$ and (iii) $\text{MoI}(\text{N}_2\text{C}_6\text{H}_{11})(\text{dppe})_2$ showing the trans arrangement of the halide ligand and the singly bent diazenido ligand

Furthermore, since the two raised metal d_{π} orbitals are orthogonal and degenerate, each will have equal probability to donate an electron pair into the LUMO of the diazenido ligand. Therefore, the bending direction of the aryl ring of the diazenido ligand trans to a chloro ligand will not be electronically controlled, but will depend on the steric effect or the electronic configuration of other co-ligands in positions perpendicular to the Cl-M-N₂Ar axis. On the other hand, when an aryldiazenido ligand is cis to a halide, (say the halide is in the x direction and the diazenido ligand in the z direction), now only one of the two high-lying metal d_{π} orbitals, d_{xz} , has the same symmetry as the LUMO (π^*_x) of the diazenido group, and the result of overlap between these two symmetry matched orbitals is shown in Scheme 1.11



Scheme 1.11

Considering only the π interactions there is, energetically, no difference between the cis arrangement of a halide and a diazenido ligand, and a trans arrangement. However, the trans halide creates two symmetrically equivalent metal d_{π} orbitals toward diazenido's LUMO, but cis halide only creates one. So, the diazenido ligand cis to a halide will show only an in-plane bending; that is,

the aryl ring plane of the diazenido ligand will stay in the same plane defined by the two ligands and the metal. In fact, all of the singly bent diazenido complexes with a *cis*-halide ligand are in accord with this model. Examples are $\text{RuCl}_3(\text{p-N}_2\text{C}_6\text{H}_4\text{Me})(\text{PPh}_3)_2$ ⁴⁴ and $\text{ReCl}_2(\text{N}_2\text{C}_6\text{H}_5)(\text{PMe}_2\text{Ph})_3$ ⁴⁸.

As a logical extension, we may ask in which direction the aryl ring would prefer to bend — toward the *cis* halide or away from the *cis* halide? In order to answer this question, we have to re-examine the distortion of the metal d_π orbital caused by the π interaction of the *cis* halide.

The repulsion interaction between the halide's filled p_z orbital and the filled metal d_{xz} orbital will result in a distorted metal d_{xz} orbital, which has the same symmetry as the LUMO (π^*_x) of the singly bent aryldiazenido ligand. Consequently, the interaction of this d_{xz} orbital with π^*_x of the diazenido group will form a π back-bond (Figure 1.14). As mentioned in section 1.2.2.2 this π^*_x orbital of the diazenido ligand is also characterized as antibonding between N_α and N_β , (refer to Figure 1.2). So an increase of electron population in this orbital would increase the antibonding character between the two nitrogen atoms. Since the π back bonding orbital is mainly composed of the distorted metal d_{xz} orbital, it will be expected to have an asymmetric distribution of lobes on the two sides along the M-N_α bond. Consequently, the antibonding strength between N_α and N_β atoms will be different with two different orientations of the singly bent aryldiazenido. The two orientations are shown as (A) and (B) in Figure 1.14. In case (A), two large antibonding lobes of the metal and N_β atom are on the same side, so the overlap between them will produce a larger repulsion than that in

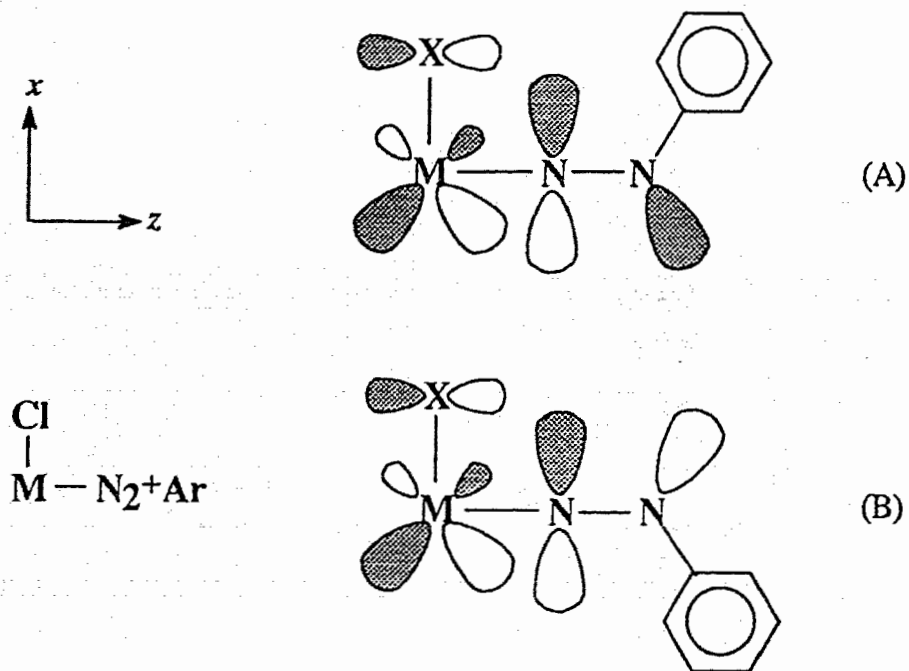


Figure 1.14 Effect on the in-plane p orbitals of different orientations of phenyl ring of ligand N_2Ar^+ in a *cis*-chloro-aryldiazenido arrangement

case (B), where the two large antibonding lobes are located in opposite positions which avoid an efficient overlap between them. Therefore, case (B) is more stable than case (A), namely, the aryl ring is energetically preferred to bend away from the *cis* π base ligand, unless there is a large steric effect in this direction. The latter situation occurs in $\text{Re}(\text{N}_2\text{Ph})\text{Cl}_2(\text{PMe}_2\text{Ph})_3$ ⁴⁸ as shown in Figure 1.15, where the phenyl ring of the phenyldiazenido ligand bends toward the *cis*-chloro ligand, rather than toward the bulky PMe_2Ph group, that is trans to the chloro ligand.

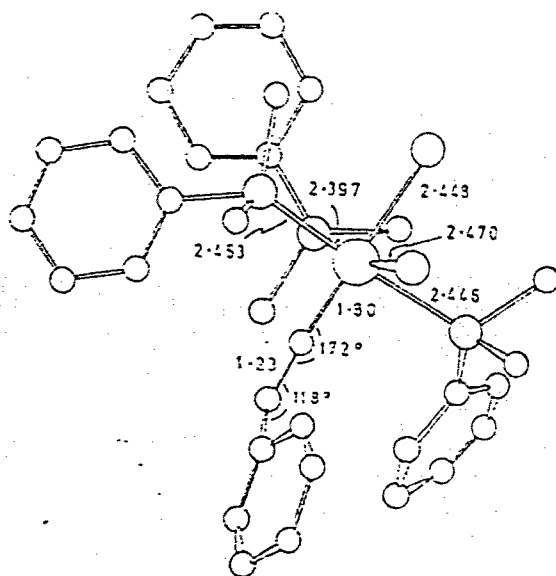


Figure 1.15 Molecular structure of $\text{Re}(\text{N}_2\text{Ph})\text{Cl}_2(\text{PMe}_2\text{Ph})_3$

In general, as a summary for this section we have identified the following:

(a) The position trans to a singly bent diazenido ligand is preferentially occupied by a π base ligand; a strong π acid ligand in this position will strongly destabilize the metal-diazenido bonding. (b) If one π acid ligand is in a position cis to a diazenido ligand, this diazenido ligand will not be destabilized and the aryl ring will bend away from the plane defined by the two ligands and metal centre, and the ring plane will be perpendicular to it. (c) If two π acid ligands are *cis* to a singly bent aryldiazenido ligand in a *fac* structure, they will destabilize the diazenido ligand, whereas in a *mer* geometry with the two π -acid ligands in trans positions, the diazenido ligand will not be destabilized. Further, in the latter case, the aryl ring plane will again bend away in the direction perpendicular to the

plane defined by the two auxiliary ligands and the N_2 group of the diazenido ligand. (d) If a strong π base ligand is cis to a singly bent aryldiazenido ligand, the aryl ring plane will be coplanar with the metal, diazenido and the π -base ligand, but tend to be bent away from this π -base ligand.

1. 3. 2. 2. In Trigonal Bipyramidal Geometry

In organotransition metal chemistry, five coordinated complexes can exhibit both square pyramidal (SP) and trigonal bipyramidal (TBP) geometries.⁶¹ Since a generally soft potential energy surface is believed to connect these two geometric minima, the factors influencing the choice between SP and TBP for a particular penta-coordinated complex has been a fascinating problem.⁶²⁻⁶⁵ For d^8 transition metal complexes, Osborn,⁶⁶ Churchill⁶⁷ and Raymond⁶⁸ have generalized that strong π acceptor ligands will tend to occupy equatorial sites in a trigonal bipyramidal geometry. This conclusion is based on a series of crystal structures as well as static and dynamic NMR studies. The result of a MO calculation by Hoffmann⁶⁹ is consistent with this conclusion. A simple qualitative analysis of the orbital interactions for five coordinated aryldiazenido complexes that is presented below results in the same conclusion, but provides additional insight.

The four crystallographically known five-coordinate aryldiazenido compounds of non-group VI transition d^8 metals, *i.e.*, $[Fe(CO)_2(N_2Ph)(PPh_3)_2]^+$,⁷⁰ $OsH(CO)(N_2Ph)(PPh_3)_2$,⁷¹ $[Fe(N_2C_6H_4Me)\{P(OEt)_3\}_4]^+$ ⁷² and $[IrCl(N_2Ph)(PMePh_2)_3]^+$ ⁷³ are all in TBP geometry and have the singly bent aryldiazenido ligand in an equatorial position. Although the last one was claimed to have a geometry between SP and TBP, it is most probably best described as

a distorted TBP geometry caused by short contacts with other atoms in the molecule.

The sole TBP geometry taken by these five-coordinate diazenido complexes in the solid state indicates that a rather large barrier between the SP and TBP conformations could have been produced by the diazenido ligand. This prompted our interest in examining their electronic structures. A five-coordinate complex of a d^8 metal in a SP geometry can be treated as an octahedral model with one lone pair of electrons occupying a coordination position; since the electronic configuration of this has been discussed in section 1.3.2.1, the discussion, here, will concentrate on the electronic structure of the TBP geometry and on a frontier orbital correlation between the TBP and SP geometries.

Figure 1.16 shows the frontier orbitals for a ML_5 system, presumed to have D_{3h} symmetry, in the absence of π interaction. For the convenience of later discussion, without loss of generality, the y direction is defined by the C_3 axis. Lowest in energy is the set e'' , consisting of the pure metal d_{yz} and d_{xy} orbitals. The e' orbitals are primarily the metal d_{z^2} and d_{xz} orbitals mixed in with some contribution from the metal p_x and p_z orbitals in a bonding sense and with the equatorial ligand σ orbitals in a strongly antibonding sense. Consequently, this e' set occurs at higher energy than the e'' set. When the π interactions between the metal centre and the ligands are considered, the involvement of the two orbitals in the e' set is important because they constitute the HOMO. Geometrically, these two orbitals are located in the equatorial plane of the molecule. Therefore, π interactions between the metal centre and the ligands would be stronger in this plane than in the axial positions. For a π acid ligand, this will directly lead to the

conclusion reached by Osborn, et.al. and Hoffmann,⁶⁶⁻⁶⁹ which we have mentioned at the beginning of this section.

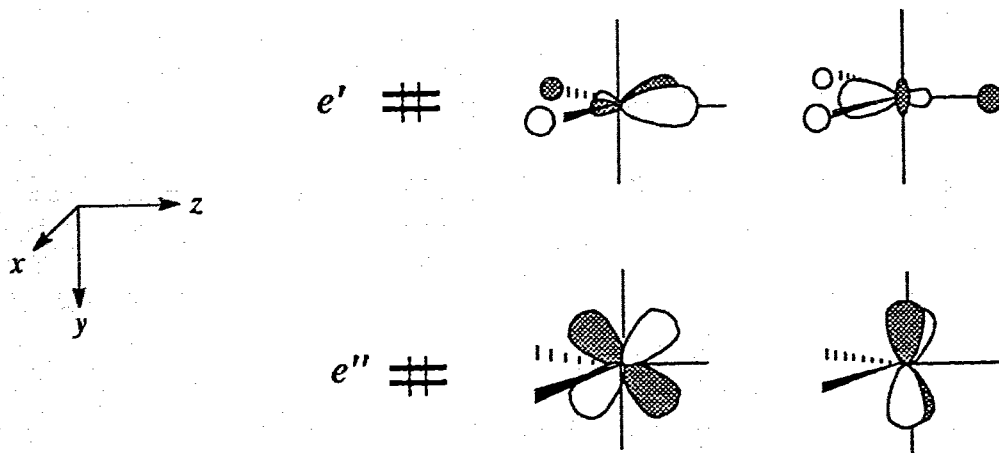


Figure 1.16. The filled frontier orbitals of a ML_5 complex in D_{3h} symmetry without consideration of the π interactions

For a five-coordinate mono-substituted singly bent aryldiazenido compound, the molecular symmetry is at least reduced from D_{3h} to C_s . Following this reduction, the e' and e'' sets of orbitals at the metal centre in D_{3h} symmetry will each be split into a' and a'' orbitals in C_s symmetry, as indicated below :



If we only consider the σ interaction at this stage, although the a' and the a'' components are no longer degenerate, they are still expected to be close to

each other in energy. Namely, the energies of orbitals $1a'$ and $1a''$ are still higher than those of orbitals $2a'$ and $2a''$ in C_s symmetry (excluding π interactions). Now if the π interaction of a singly bent aryldiazenido ligand with the metal is considered for this system, it is evident that the $1a'$ and $1a''$ orbitals of the metal fragment will preferentially be involved rather than the lower energy $2a'$ and $2a''$ ones. The aryldiazenido ligand in a TBP structure is then predicted to be in an equatorial site rather than axial. Furthermore, since the LUMO of the singly bent aryldiazenido ligand is located in the bending plane and co-planar with the aryl ring, the aryl ring plane of the ligand must be coincident with the molecular equatorial plane. These predicted structure features are indeed experimentally observed. In those structurally characterized TBP complexes of non-Group VI transition metals, the singly bent diazenido ligands are exclusively located in the equatorial positions, and the bending of the ligands at N_β occurs exclusively in the equatorial plane and with the aryl rings of the ligands in this plane.⁷⁰⁻⁷³

Once it has been established that the singly bent aryldiazenido ligand will prefer to occupy an equatorial position in TBP complexes, we may further ask: which one of the two metal fragment orbitals, $1a'$ or $1a''$, will be preferentially involved in the π interaction with diazenido ligand? Energetically, these two orbitals are close to each other, however, geometrically, they have different shapes or orientations. The $1a'$ is a distorted metal d_{z^2} orbital. The π interaction of this $1a'$ orbital with the equatorial ligands is shown as (II) in Figure 1.17. This π interaction can be characterized as the sharing of one metal-centred orbital with two equatorial ligands. The $1a''$ orbital is mainly a distorted metal d_{xz} orbital. The π interaction of this orbital with an equatorial ligand is shown as (I) in Figure 1.17. This interaction is characterized by the two lobes of the $1a''$ orbital pointing away from two equatorial ligands and toward a third equatorial ligand in the z

direction. In fact, it is this characteristic feature of the $1a''$ orbital that creates a unique position in the equatorial plane of a five-coordinate compound, and allows a π acid ligand in this position to bear the maximum π back donation from the metal fragment, and a π base ligand to bear the maximum π repulsion from the metal centre.

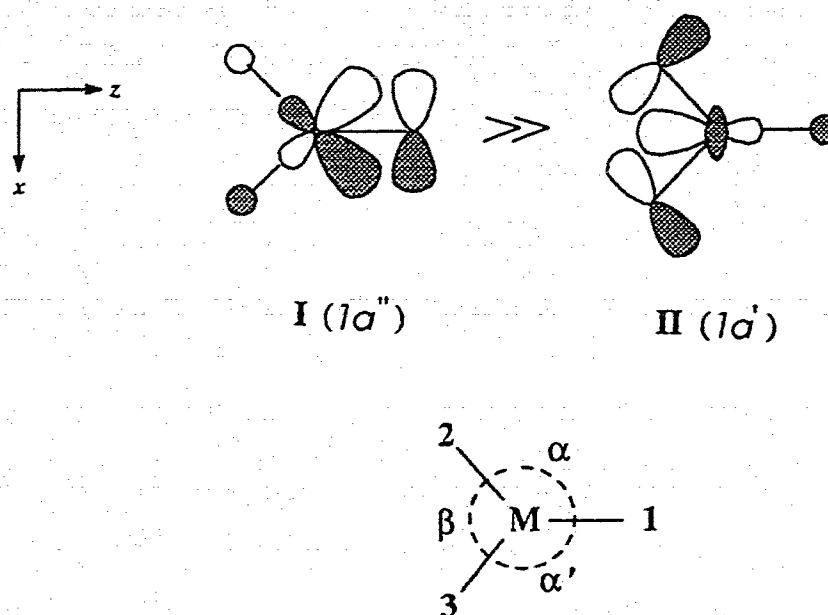


Figure 1.17 d - π interactions of metal and ligands in the equatorial plane for a complex in TBP geometry

Geometrically, a situation in which an equatorial ligand is involved in the specific π interaction of type (I) or type (II) could be easily identified from the different inter-bond angles α or α' and β . For example, the strongest π acid ligand among the three equatorial ones would always occupy position 1 (refer to Figure 1.17) and would always be involved in the π interaction (I), which would result in inter-bond angles α or $\alpha' > 120^\circ$ and $\beta < 120^\circ$. It is also worth mentioning that since the two metal fragment orbitals, ($1a'$ and $1a''$), located in

the equatorial plane, are energetically close to each other, the magnitude of the π interactions of these two orbitals with a specific ligand is mainly controlled by the orbitals' overlap. This can be best demonstrated by the similar complexes $ML_2(CO)_2(\text{olefin})$,⁷⁴⁻⁷⁸ in which the olefin ligand is exclusively located in an equatorial site and involved in the interaction I due to the good $d - \pi^*$ overlap, although the energy of the olefin's π^* orbital could be slightly higher than that of CO ligand.

In the TBP singly bent diazenido complexes,⁷⁰⁻⁷³ the diazenido ligands are always involved in the interaction (I), whereas the other equatorial ligands, even the CO ligands, are involved in interaction (II). This again indicates that the diazenido ligand is a strong π acid.

As we mentioned earlier in this section, all known five-coordinated singly bent diazenido complexes of non-group VI transition metals have TBP geometry with the diazenido ligand in the equatorial position. What is the reason for the absence of a square pyramidal complex with the singly bent diazenido ligand in the apical position? To answer this question, we should examine the differences in the filled frontier π type orbitals in these two situations. A Walsh diagram³² that correlates a SP complex, with a singly bent aryldiazenido ligand occupying an axial position, to a TBP complex with an equatorial diazenido is given in Figure 1.18. For simplicity, we artificially assign the diazenido ligand as a point charge in the $-z$ direction, and analyze only the change of metal fragment orbitals. Correspondingly, in the discussion we use C_{4v} and C_{2v} symmetries, instead of the real symmetry of C_5 .

Let us first examine what happens to the d_{z^2} and d_{xz} orbitals of the metal fragment when the L-M-L angle (β) varies in the directions shown by the arrows in Figure 1.18. Moving the ligands together in the trigonal plane will cause the

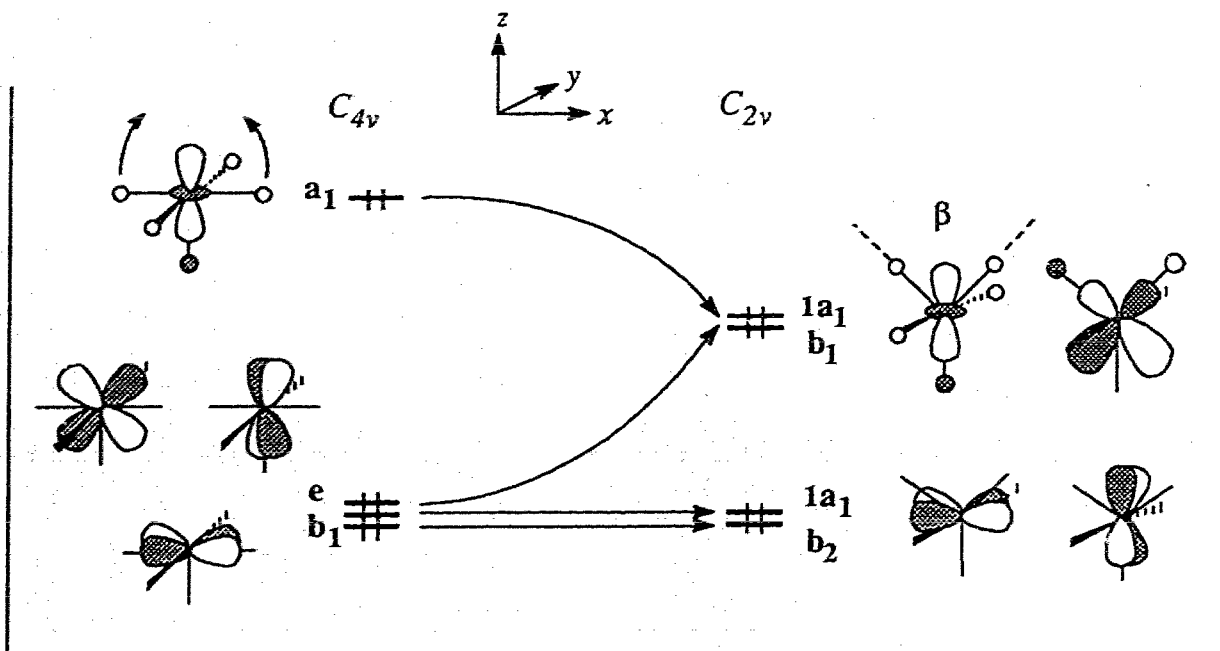


Figure 1.18 Correlation of filled metal frontier orbitals in TBP and SP

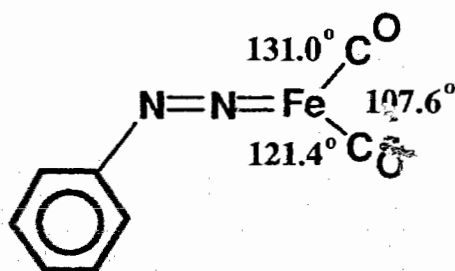
symmetry to drop from C_{4v} to C_{2v} . In doing this, the d_{z^2} orbital will be stabilized by removing the σ antibonding interaction with two of the ligands that were in the plane of the torus of the d_{z^2} orbital, and d_{xz} will be destabilized by the shift of the ligands from nonbonding positions on node of the d_{xz} orbital to strongly σ antibonding positions.

Clearly, if these equatorial ligands are the same, and the stabilization of the d_{z^2} and the destabilization of the d_{xz} are somehow balanced, a regular TBP in D_{3h} symmetry could result.

If a strong π donor ligand is placed in an equatorial position, the π antibonding interaction will occur through either interaction (I) or (II) (refer to Figure 1.17). In interaction (I), the π donor ligand, in the unique equatorial position, would destabilize d_{xz} to a maximum extent. In interaction (II), it would destabilize the d_{z^2} orbital, which had been stabilized by the geometrical change from SP to TBP. Consequently, in either of the interactions, the destabilizations

by the strong π donor ligand will cause the β angle to be larger than 120° . In other words, a strong π donor ligand in an equatorial position of a TBP complex has a tendency to push the TBP geometry back to SP geometry. The square pyramidal compounds, $[\text{Ni}(\text{CN})_5]^{-3}$,^{79a} $[\text{Co}(\text{CNPh})_5]^+$ ^{79b} and $[\text{PtI}(\text{PR}_3)_4]^+$ ^{79c} etc, are examples of this.

For strong π acceptor ligands in an equatorial position, both of the π interactions, (I) and (II) in Figure 1.17, will be favored for the TBP geometry. The stabilized d_{z^2} orbital will be stabilized further by the π interaction (II), and the previously destabilized d_{xz} orbital will be largely stabilized further by the interaction (I). It may be worth to comment that the magnitude of π stabilization by a π -acceptor in the interaction (II) is approximately half of that in interaction (I). Therefore, a strong π -acceptor ligand, like the singly bent diazenido group, will strongly stabilize the TBP geometry by occupying the unique equatorial position. This should leave $\beta < 120^\circ$ and α or $\alpha' > 120^\circ$. In fact, in all four known structures of five-coordinated singly bent diazenido complexes, the β angles are always less than 120° , whereas α or α' larger than 120° . The observed angles in the trigonal plane of $[\text{Fe}(\text{CO})_2(\text{PPh}_3)_2(\text{N}_2\text{Ph})]^+$ ⁷⁰ are indicated in Scheme 1.12 as an example.



Scheme 1.12

1.3.3. Doubly Bent Aryldiazenido Compounds

There are far fewer doubly bent aryldiazenido complexes and their generally low stability in either solution or solid state are reasons why the chemistry of this type of compound is relatively less well understood, compared with that of the singly bent diazenido compounds. There are three structurally established examples^{18, 19, 41} by X-ray crystallography, and others^{19, 80} characterized spectroscopically to be so in solution provide a basis for describing the electronic structures of doubly bent aryldiazenido complexes. An attempt is also made to use the generalized electronic configuration of doubly bent diazenido compounds to illustrate, or to predict, some aspects of the structure and reactivity of this ligand.

For simplicity, as usual, an octahedral complex will be dealt with first to establish the framework of our discussion. The compound $\text{IrCl}_2(2\text{-N}_2\text{C}_6\text{H}_4\text{NO}_2)(\text{CO})(\text{PPh}_3)_2$, reported previously from this group¹⁹, is a good model system for us to use to examine the relationship of the electronic configuration and the structure of the doubly bent aryldiazenido complexes.

First, as an approximation, only considering the primary σ -type interactions, the molecular orbitals of an octahedral ML_6 complex are as shown in Figure 1.19, where L is a σ donor ligand.

Let us replace the metal centre with Ir and replace the two ligands along the z direction with Cl^- and a doubly bent aryldiazenido ligand. Since the primary σ -type interaction of Cl^- ligand and the doubly bent diazenido ligand have already been considered in Figure 1.19, now we will only consider the "secondary" interactions between the frontier orbitals from these two ligands and the metal centre fragment, which are mainly of π -type. Although these secondary interactions may be much weaker than the primary σ -type ones,

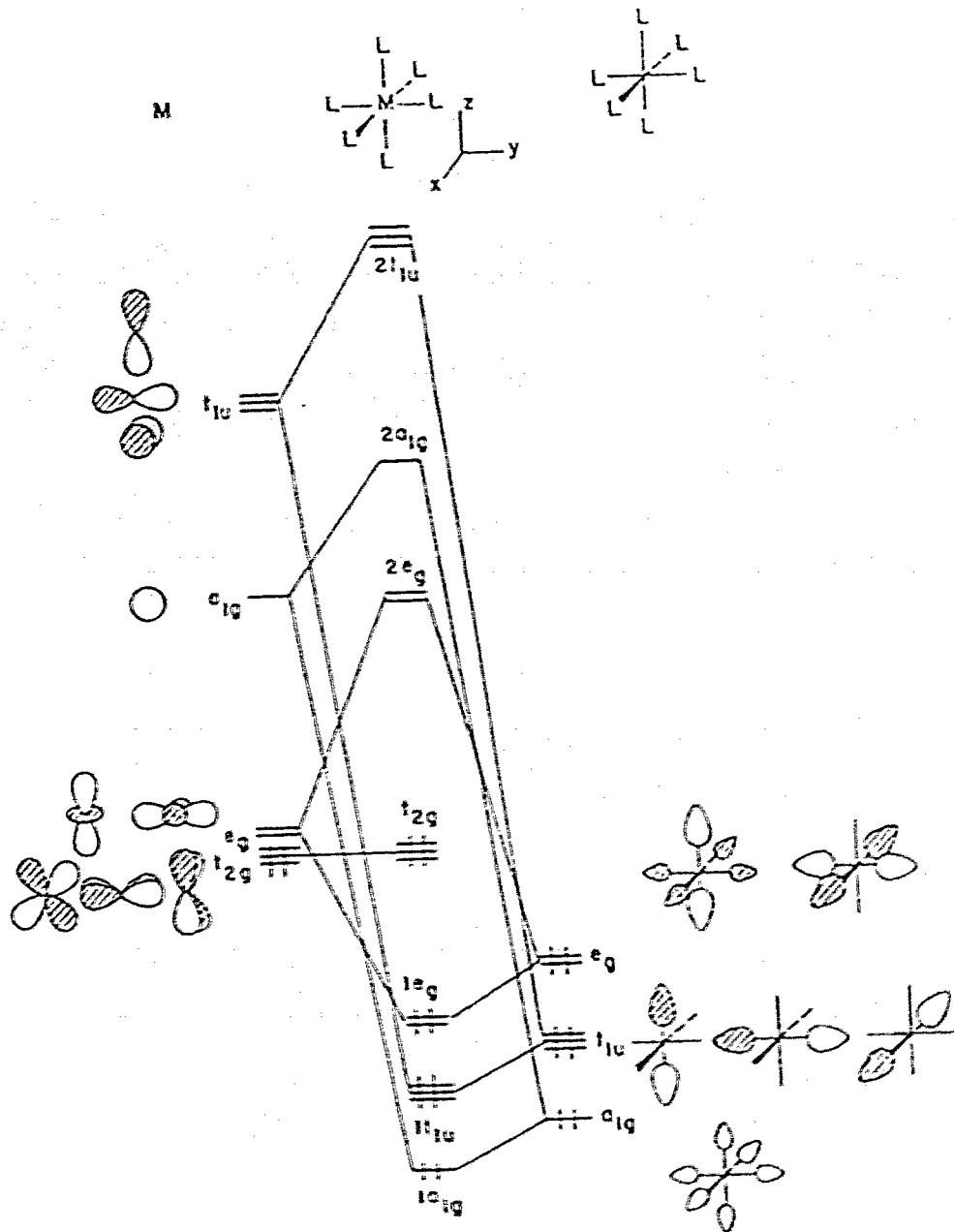


Figure 1.19 . Molecular orbitals of ML_6 in O_h symmetry, without considering the π -type interaction

importantly, these interactions will produce the frontier molecular orbitals as shown in Figure 1.20. It is these orbitals that contain the interesting chemical information about the molecular structure and their reactivity.

In Figure 1.20, the Ir, Cl, N_α and N_β atoms are assumed to lie in the xz plane; the π interactions in this plane are shown on the left, and the π interactions in the plane yz are on the right side. In the yz plane, the net π interactions between the metal and two mutually *trans* ligands result in a destabilization of the M-Cl linkage and a slight stabilization of the M- N_α linkage, due to the low-lying p_y orbital of the Cl^- ligand and the high-lying empty π_y^* orbital on N_2Ar^- , aryldiazenido(-1) ligand. In the xz plane, the d_{xz} orbital of Ir interacts with the lone pair orbital, π_x , of N_2Ar^- and the low-lying p_x orbital of Cl^- , and the overall π interaction in this plane leads to destabilization of the bonds between Ir and the N_2Ar^- and Cl^- ligands. However, the most important electronic feature of the lone pair orbital that is largely localized on the N_α atom of the N_2Ar^- ligand is only faintly apparent in Figure 1.20. In fact, this lone pair orbital is a hybrid orbital, so it can be analyzed into σ and π_x components, as illustrated in Scheme 1.13. In other words, this orbital has both σ_z character and π_x character. The interaction involving the π_x component of this orbital has been considered in Figure 1.20, but the remaining σ_z component of this nitrogen lone pair orbital has yet to be considered. This component has the same symmetry as d_{z^2} , a metal-centred antibonding orbital, (one of the e_g group orbitals in Figure 1.20) and is energetically close to it. Therefore, mixing of these two orbitals will be expected, and since this is a σ -type interaction (as compared to the relatively weak π -type interaction) this interaction would be expected to contribute significantly to the interaction between the metal and ligands in this direction. Also, importantly, the metal-centred empty antibonding orbital is actually the

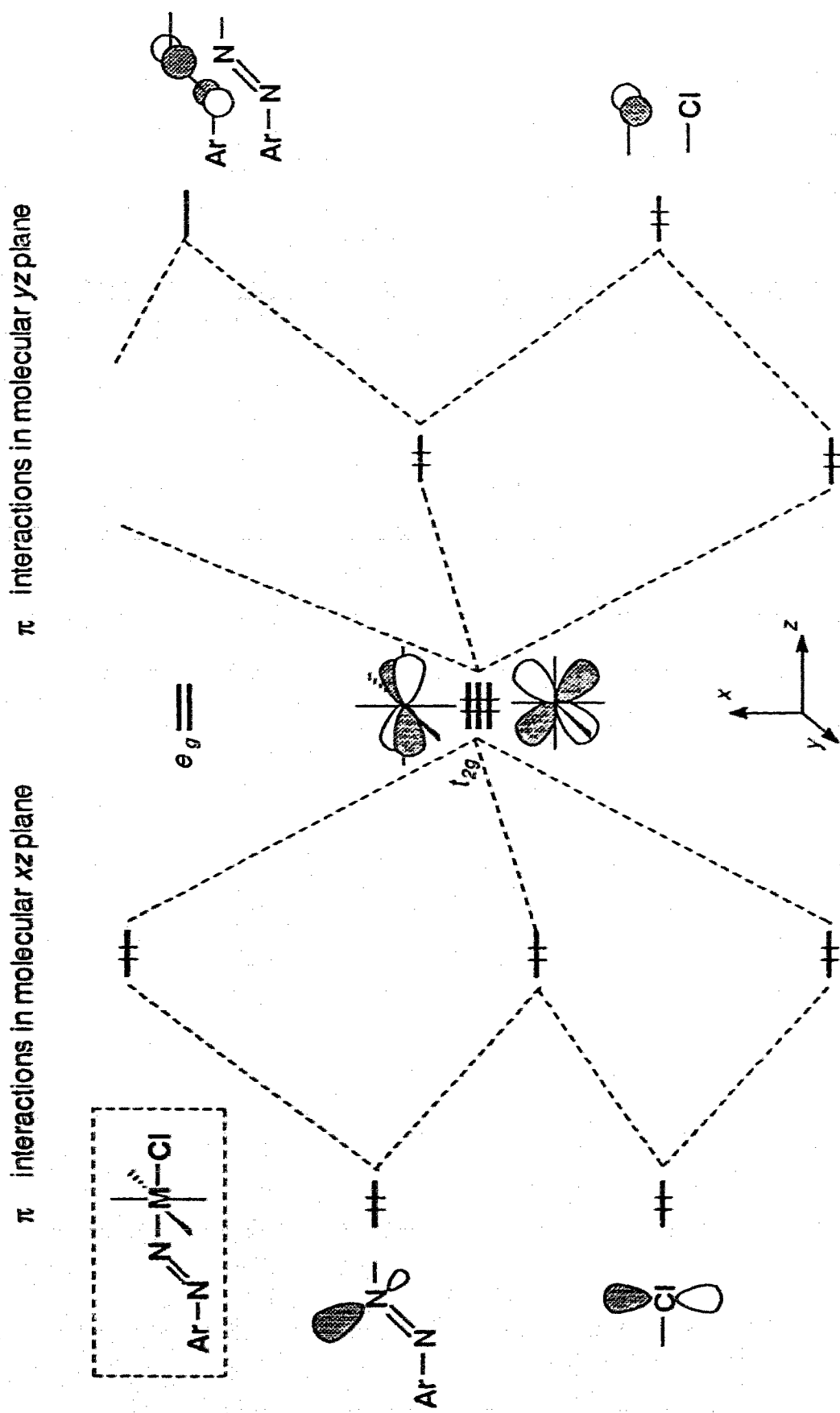
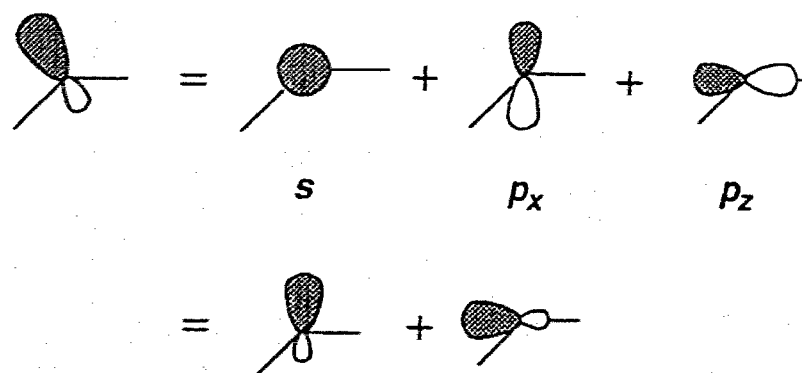


Figure 1.20 The secondary π -type interactions along the bonding of $\text{Cl}-\text{Ir}-\text{N}_2\text{Ar}$ in molecule $\text{IrCl}_2(\text{N}_2\text{Ar})(\text{CO})(\text{PPh}_3)_2$



Scheme 1.13

counterpart of the σ bonding orbital of the metal to two ligands along z axis, *i.e.* the N_2Ar^- and trans Cl^- ligands. For clarity, this kind of secondary σ interaction, together with the π interactions, is shown in Figure 1.21. Clearly, this σ -type secondary interaction between the lone pair orbital, (HOMO), of the N_2Ar^- and metal-centred d_{z^2} orbital is a 2 orbital, 2 electrons one. Its mode of interaction is such as to stabilize the bonding between metal and nitrogen and destabilize the bonding between metal and the *trans* Cl^- ligand. It is also noticed that the bonding orbital resulting from this σ -type secondary interaction is the highest occupied molecular orbital, and therefore it strongly influences the geometry of the molecule.

As a summary of the total effects of these secondary interactions, the metal-Cl bond is largely destabilized, predominantly by the σ -type interaction with some contribution from π -type interaction, and the bond of the metal to α nitrogen atom, *i.e.* to N_2Ar^- ligand, is stabilized marginally due to the mutual cancellation of the stabilization resulting from the σ -type interaction and the destabilization due to the π -type interaction.

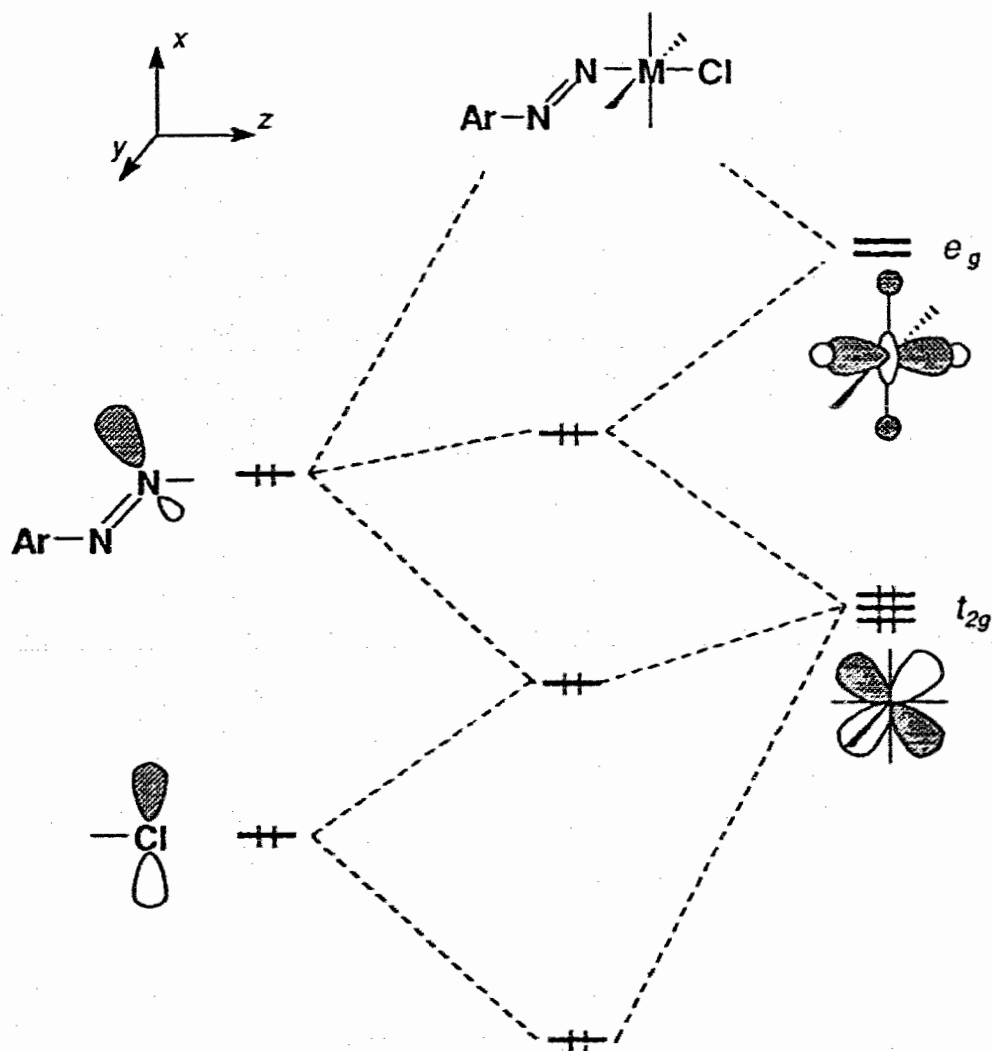


Figure 1.21 The secondary interactions in xz plane of the molecule $\text{IrCl}_2(\text{N}_2\text{Ar})(\text{CO})(\text{PPh}_3)_2$

Experimentally, in the crystal structure of the molecule $\text{IrCl}_2(\text{CO})(\text{N}_2\text{Ar})(\text{PPh}_3)_2$ ¹⁹, a significant trans lengthening (0.10 Å) has been observed for the M-Cl bond, that is trans to the doubly bent diazenido ligand, whereas the Ir-Cl distance for the *cis*-chloro ligand is in the normally expected range (~ 2.37 Å). A similar trans influence of the Pt-Cl bond by the trans doubly

bent diazenido ligand has also been observed in the molecular structure of $\text{PtCl}(\text{N}_2\text{Ar})(\text{PEt}_3)_2$ ¹⁸. The M-Cl bond lengths in some structurally related compounds are compared in Table 1.2.

Protonation at the N_α position of the doubly bent diazenido ligand will have the effect of decreasing the secondary interactions because the lone pair is used to form the N-H bond. Structurally, this will lead to a shortening of the M-Cl bond distance which is trans to the diazene ligand. In fact, this has been seen in the compound $\text{PtCl}(\text{NHNAr})(\text{PEt}_3)_2$ ⁸² and in $\text{PtCl}(\text{H}_2\text{NNAr})(\text{PEt}_3)_2$ ⁸³, where the Pt-Cl bond lengths are significantly shorter than in the corresponding diazenido compound (Table 1.2).

Table 1.2 Comparison of M-Cl Bond Lengths with and without the Trans Doubly Bent Diazenido Ligand in Related Compounds

Compound	Character of the nitrogen ligand	M - Cl (Å)	Ref.
$\text{IrCl}_2(\text{N}_2\text{Ar})(\text{CO})(\text{PPh}_3)_2$	doubly bent N_2Ar	<i>trans</i> 2.48(1)	19
		<i>cis</i> 2.37(1)	
$[\text{IrCl}_2(\text{NO})(\text{CO})(\text{PPh}_3)_2]^+$	linear NO	<i>trans</i> 2.343(3)	81
$[\text{RhCl}(\text{N}_2\text{Ar})(\text{PPh}_3)_2]^+$	singly bent N_2Ar	<i>trans</i> 2.301(3)	59
$\text{PtCl}(\text{N}_2\text{Ar})(\text{PEt}_3)_2$	doubly bent N_2Ar	<i>trans</i> 2.413(6)	18
$\text{PtCl}(\text{NHNAr})(\text{PEt}_3)_2$	η^1 -NHNAr	<i>trans</i> 2.291(2)	82
$\text{PtCl}(\text{NH}_2\text{NAr})(\text{PEt}_3)_2$	η^1 - NH_2NAr	<i>trans</i> 2.303(2)	83

The experimental data listed in Table 1.2 are clearly consistent with the model of the electronic structure we have established for the doubly bent diazenido compounds.

Based on the above analysis of the secondary interactions, or frontier orbital interactions, we know that a doubly bent diazenido ligand actually has a strong trans influence. So ideally, this electronic feature of the doubly bent diazenido ligand is favoured by a trans ligand that should have a relatively strong σ bonding capability to compensate the trans influence caused by the diazenido ligand, and preferably, have a strong π accepting ability to accept electrons from the metal filled d_{π} orbitals in order to strengthen the bonding between it and the metal. Fulfilling these criteria, carbonyl or other strong π acid ligands would be the most plausible candidates. Compounds with trans arranged carbonyl and doubly bent diazenido ligands have been reported by Haymore and Ibers⁸⁰. On the other hand, chloride is not a good trans ligand in doubly bent diazenido compounds. The trans Cl-M bond lengths of the known doubly bent diazenido compounds are comparable with the sum of ionic radii for chloride and these metals. For example, the trans M-Cl bond lengths in $\text{IrCl}_2(\text{CO})(\text{N}_2\text{Ar})(\text{PPh}_3)_2$ ¹⁹ and $\text{PtCl}(\text{N}_2\text{Ar})(\text{PEt}_3)_2$ ¹⁸ are 2.481(3) Å and 2.413(6) Å, separately, and the the sum of the ionic radii of chloride and Ir(III) and Pt(II) are also about 2.49 Å and 2.41 Å⁸⁴, respectively. The long bond lengths of the metals to the trans chloride ligands in these doubly bent diazenido complexes of known structure strongly indicate that the trans chlorides in these compounds are extremely weakly bonded. Chemical lability of the trans chloride ligand in these compounds is also evident. For example, the trans chloride ligand in $\text{IrCl}_2(\text{CO})(\text{N}_2\text{Ar})(\text{PPh}_3)_2$ can be easily extracted by Ag^+ , or substituted by other nucleophilic groups, *e.g.* RO⁻ 19, 23, 85, 86.

Since the bonding of the metal to the N_2Ar ligand is mainly a σ -type interaction, the bending direction of this ligand is not likely to be controlled by electronic factors, but by the steric influence of other ligands. Experimental data seem to be consistent with this. For example, the doubly bent diazenido ligand in all three known structures is bent away from the rather bulky *cis*-phosphine ligands^{18, 19, 41}.

Finally, as a conclusion to this section, although the lack of much experimental data has limited this discussion, the *trans* influence of a doubly bent diazenido ligand and the lability of the *trans* ligand have been adequately elucidated in the qualitative frontier orbital interaction framework. The picture of the electronic structure drawn from this discussion is apparent and important. New evidence of its potential will be demonstrated in the later part of this thesis in designing facile syntheses of new doubly bent diazenido complexes.

1.3.4. Side-on Aryldiazenido Complex

So far, the side-on configuration is rare in mononuclear aryldiazenido complexes. In fact, the only example is $CpTiCl_2(\eta^2-N_2Ph)$ ⁸⁷. However, the close structural relationship of the side-on diazenido group with other side-on organodinitrogen species (*e.g.* hydrazido(1-)⁸⁷⁻⁹⁰, azo or diazene^{91, 92} and hydrazine¹⁹) in transition metal complexes strongly stimulates our interest in the electronic structures of these species.

In this section, we will first analyze the electronic structures of $CpTiCl_2(\eta^2-N_2Ph)$ ⁸⁷ and its hydrazido(1-) analogue $CpTiCl_2(\eta^2-NH_2NPh)$ ⁸⁷ and then try to apply the conclusion derived from this analysis to other related systems. Through the analysis of the orbital interactions between the metal fragment $CpTiCl_2^+$ and the corresponding ligands, we can hopefully understand the

geometrical preference of coordination mode, chemical reactivity, and other structural properties, of these organodinitrogen species in their transition metal complexes. Notably, in the original paper,⁸⁷ a qualitative MO description of the π bonding involved in these two compounds had been given, and a different assignment of the fragments had been used there.

Structurally, there is a remarkable difference between the geometries of these two titanium molecules. The molecular structures of $\text{CpTiCl}_2(\eta^2\text{-N}_2\text{Ph})$ ⁸⁷ and $\text{CpTiCl}_2(\eta^2\text{-NH}_2\text{NPh})$ ⁸⁷ are shown in Figure 1.22.

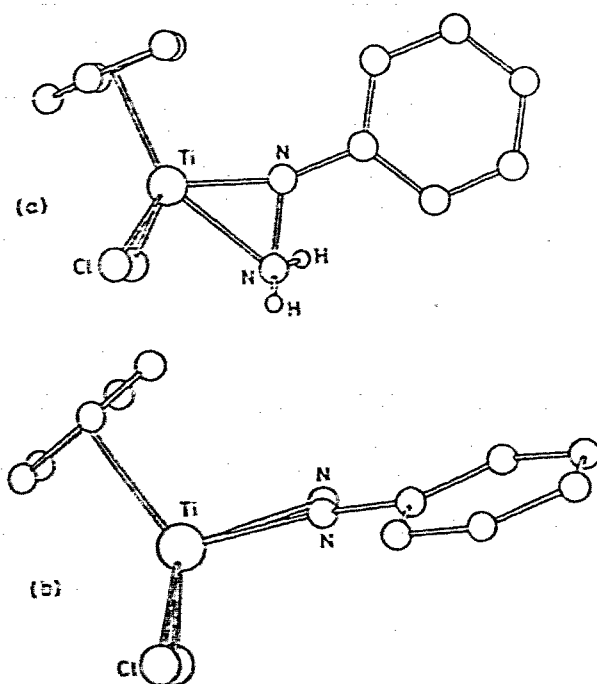


Figure 1.22 Molecular structures of (a) $\text{CpTiCl}_2(\eta^2\text{-NH}_2\text{NPh})$ and (b) $\text{CpTiCl}_2(\eta^2\text{-N}_2\text{Ph})$

In $\text{CpTiCl}_2(\eta^2\text{-N}_2\text{Ph})$ ⁸⁷, the two nitrogen atoms lie in a plane vertical to the idealized symmetry plane of the CpTiCl_2^+ fragment, whereas in $\text{CpTiCl}_2(\eta^2\text{-NH}_2\text{NPh})$ ⁸⁷, they are in this symmetry plane. For convenience in the following discussion, we assign the former as a perpendicular side-on mode, or simply \perp side-on, and the latter as a parallel side-on, or simply $//$ side-on, mode.

We begin with an analysis of the diazenido complex drawing upon the electronic structures of the diazenido(-1) ligand, N_2Ar^- , and the CpTiCl_2^+ fragment. The fragment orbital interactions are diagrammed in Figure 1.23. The metal centre in the CpTiCl_2^+ fragment has a typical 2-1-2 orbital splitting pattern^{28, 29} that results mainly from the π - d interactions between the filled π orbitals of the Cp group and the empty titanium d orbitals. The contributions of the Cl⁻ ligands to each of the d orbitals are approximately the same; consequently, they will not change the 2-1-2 pattern very much, but will push it slightly to higher energy levels. The two low-lying orbitals are metal-centred $d_{x^2-y^2}$ ($1a'$) and d_{xy} ($1a''$) nonbonding orbitals. They are located energetically very close to the pure titanium d orbitals, at about -10.81 eV. The metal d_{z^2} orbital is not destabilized much by the lowest π orbital of the Cp ligand, because this Cp π orbital lies approximately in the d_{z^2} nodal plane. However, d_{xz} and d_{yz} are destabilized significantly by the Cp π -type of HOMOs and are consequently higher in energy. Back donation from the d^0 metal centre to ligands is absent. Therefore, only the filled frontier orbitals of the ligand and the lowest empty metal orbitals are of interest.

For the N_2Ar^- ligand, the HOMO (π_x^*) is π antibonding between the two nitrogen atoms, so it is of high energy and is located close to the empty d orbitals of titanium. The filled subjacent orbital of the ligand is a σ -type orbital, or lone pair (n) (refer to Figure 1.2).

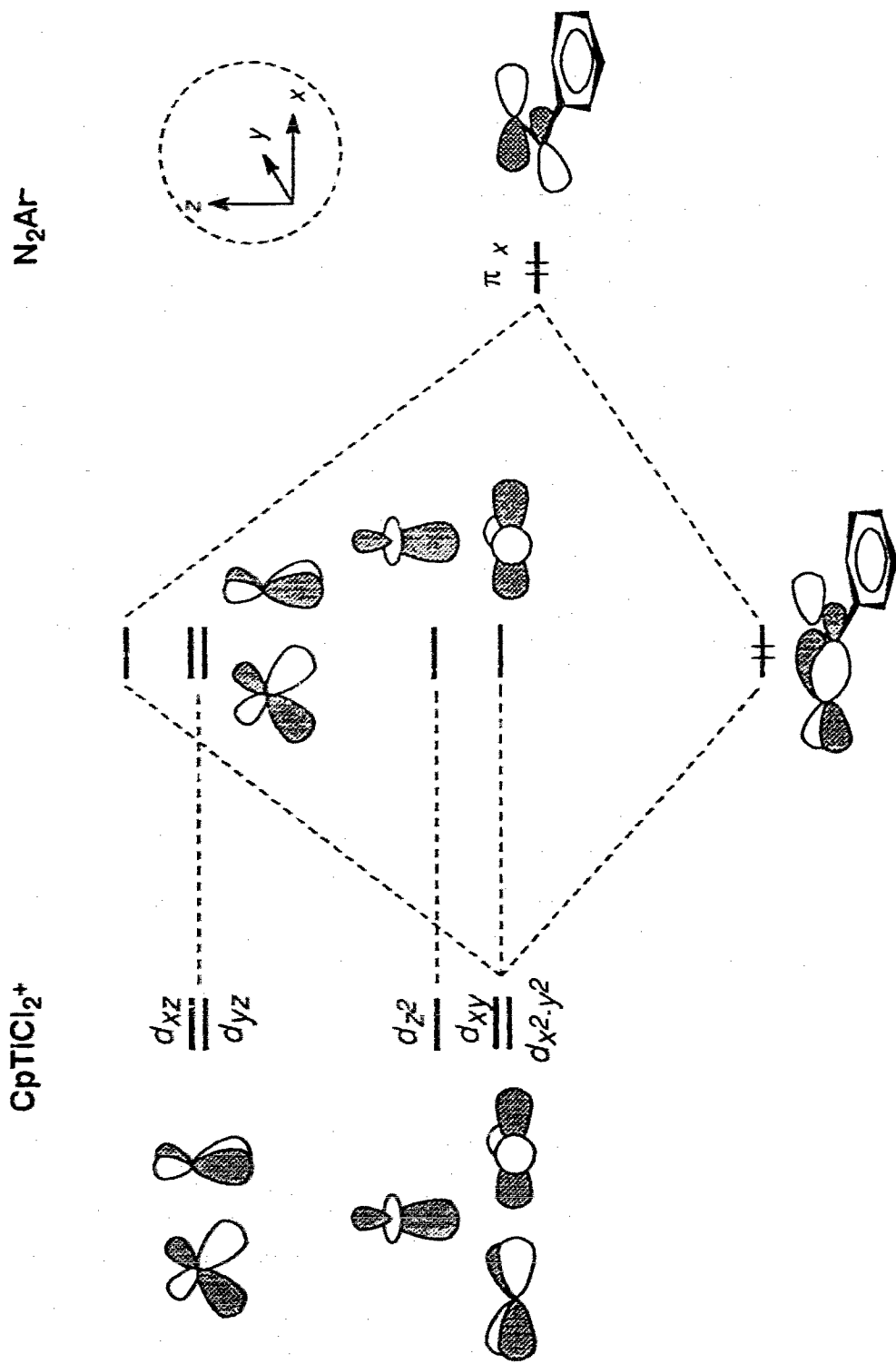


Figure 1.23 \perp side-on coordination of N_2Ar to CpTiCl_2^+ centre

Clearly, coordination of N_2Ar^- to a d^0 metal centre CpTiCl_2^+ could be, symmetrically and electronically, allowed in either end-on or \perp side-on fashions. In end-on coordination, the π_x^* and n orbitals of the N_2Ar^- ligand could interact with $d_{x^2-y^2}$ and d_{xy} of CpTiCl_2^+ , respectively, to form one σ and one π bond as in a singly bent diazenido geometry. This situation might be accounted as either a 4-electron donation of this ligand or a 2-electron donation to a reduced metal centre. In the \perp side-on coordination case, only the two-centred π_x^* orbital of the N_2Ar^- can interact with d_{xy} of the metal fragment. This \perp side-on coordination fashion is the one actually observed in $\text{CpTiCl}_2(\text{N}_2\text{Ar})$ ⁸⁷, which is shown in Figure 1.22 (b). The preference of this \perp side-on coordination could be reasoned as due to its π bonding interaction than for the end-on, and the insignificant σ interaction in the end-on fashion due to the large energy gap between the n orbital of N_2Ar^- and the titanium $d_{x^2-y^2}$ orbital.

The calculated EHMO frontier fragment orbitals of NH_2NPh^- are shown in the centre of Figure 1.24, together with the frontier orbitals of CpTiCl_2^+ on the right and left. Retaining the molecular symmetry (C_s), the frontier orbital interactions involve two different π -type interactions. These are the interactions between the HOMO (π_x^*) of the ligand and two metal fragment d orbitals $d_{x^2-y^2}$ and d_{z^2} , shown as *a* in Figure 1.24, and the interaction between ligand's nitrene type p orbital, *a''*, and meta d_{xy} orbital, shown as *b* in Figure 1.24. The two metal fragment orbitals involved in the interaction *a* could also be schemed in a slightly different fashion. A linear combination of metal $d_{x^2-y^2}$ and d_{z^2} will give a hybrid orbital shown in Scheme 1.14, which will interact with the HOMO of the ligand with *a'* symmetry.

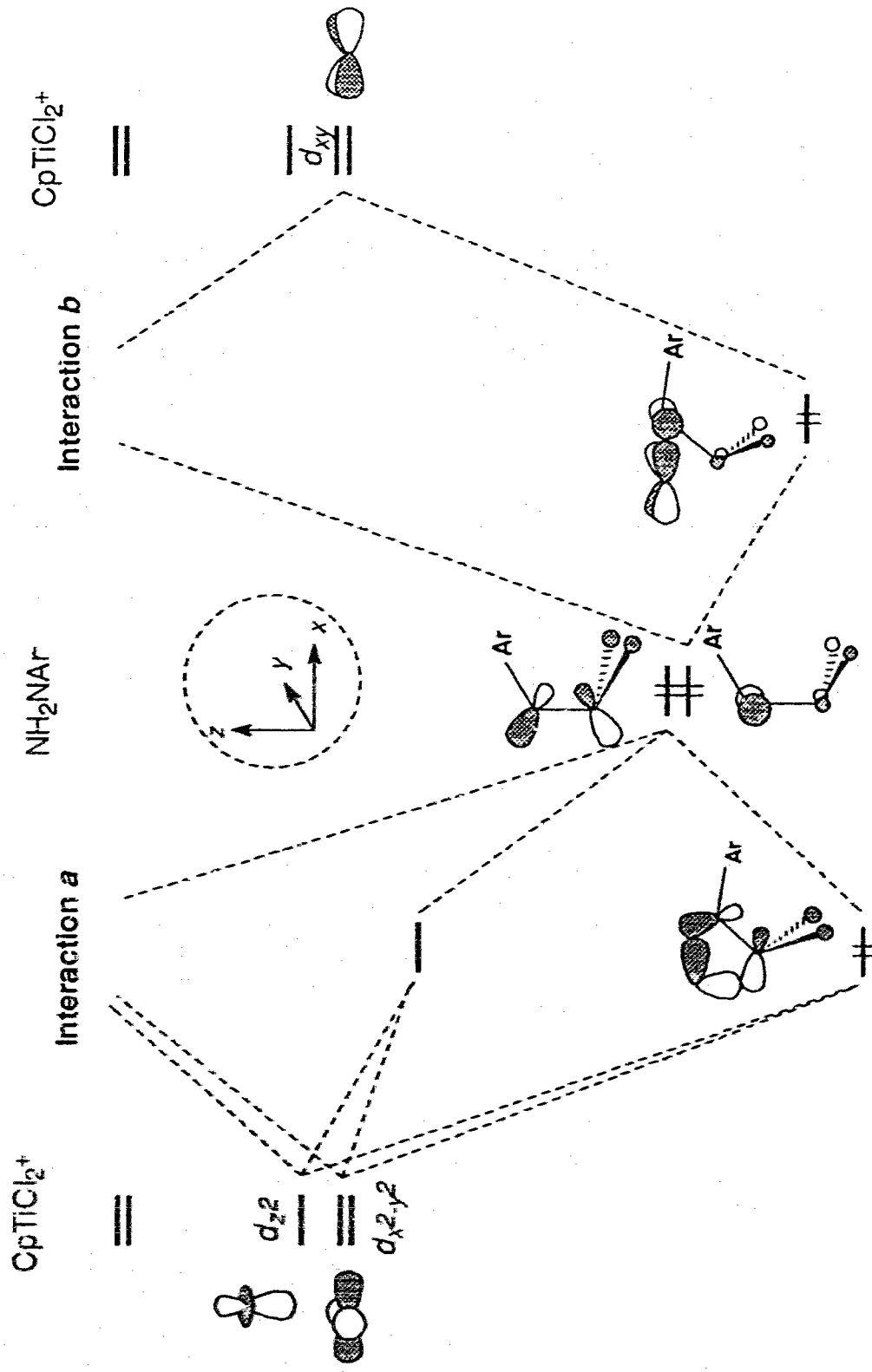
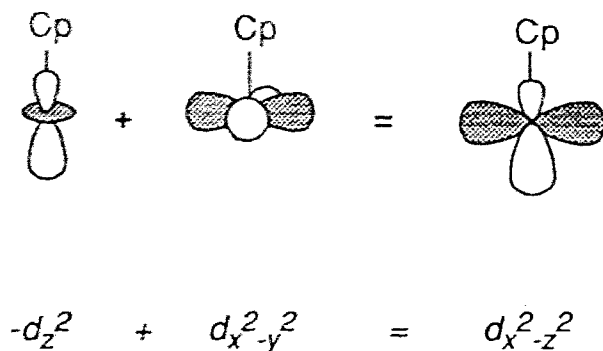


Figure 1.24 Qualitative orbital interactions of NH_2NAr and CpTiCl_2^+ in a // side-on fashion



Scheme 1.14

In $\text{CpTiCl}_2(\text{NH}_2\text{NPh})$ ⁸⁷, a key feature for the NH_2NPh^- ligand is such that the filled nitrene type p orbital (π_y^* , the HOMO) is largely centred on the nitrogen atom adjacent to the phenyl ring but this feature is absent in the N_2Ph^- ligand. The efficient involvement of this orbital in bonding with the metal d_{xy} orbital actually decides the different orientations adopted by NH_2NPh^- and N_2Ph^- with respect to the metal fragment CpTiCl_2^+ . On the other hand, for the metal fragment CpTiCl_2^+ , the only difference in the bonding to NH_2NPh^- and N_2Ph^- is the involvement of the metal d_{z^2} orbital in the bond formation. Clearly, any pre-occupancy of this orbital through either an electronic 'reduction' of the metal centre from d^0 to d^n ($n > 0$) or ligating another ligand in the direction *trans* to the Cp group would make such coordination fashion of NH_2NPh^- impossible, which, however, could lead to either an η^2 -coordination of the hydrazido(1-) ligand in the position that N-N bond is parallel to Cp ligand plane, or an η^1 - (end-on) coordination. The ligating effect on the coordination fashion of the hydrazido(1-) has been seen in the structures of the related compounds $[\text{Cp}^*\text{WMe}_3(\text{NH}_2\text{NH})]^+$

and $\text{Cp}^*\text{WMe}_4(\text{NH}_2\text{NH})$ ⁹⁰, shown in Figure 1.25 as **a** and **b**. The effect of non-zero *d* electrons of the metal centre on the coordination fashion can be demonstrated by the coordination fashion of hydrazido(1-) ligand in compound $\{\text{CpRe}(\text{CO})_2[\text{NHNMe}(p\text{-C}_6\text{H}_4\text{OMe})]\}^+$ ⁹¹ shown in Figure 1.25 as **c**.

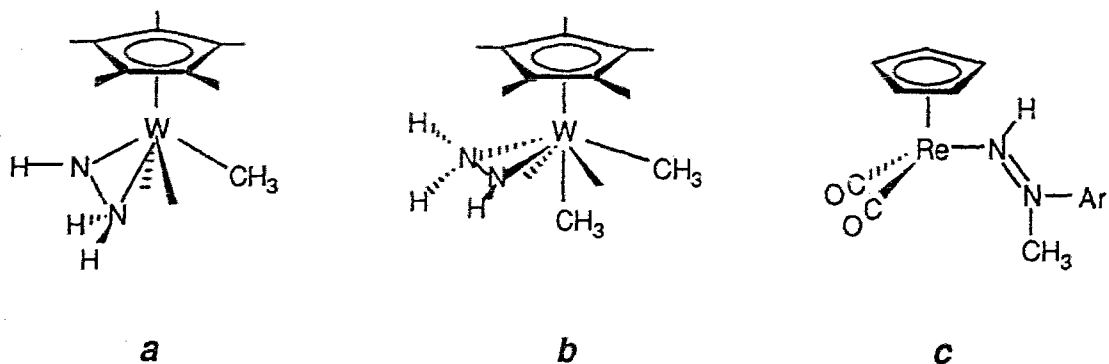
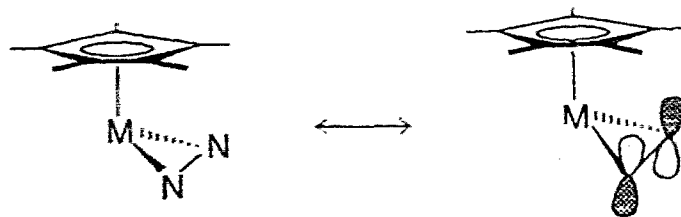


Figure 1.25 View of the molecular structures of $\text{Cp}^*\text{WMe}_3(\text{NHNH}_2)$ (**a**), $\text{Cp}^*\text{WMe}_4(\text{NHNH}_2)$ (**b**) and $\{\text{CpRe}(\text{CO})_2[\text{NHN}(\text{Me})\text{Ar}]\}^+$ (**c**). (for clarity, some methyl groups are omitted)

An important structural feature has been revealed in the above discussion of such side-on coordinated hydrazido (1-) and diazenido ligands that nitrogen-nitrogen bonding is parallel to the Cp or Cp* plane. In both of the ligands, there exists a filled nonbonding π -type molecular orbital which is largely located on the two N atoms in the direction perpendicular to the plane containing metal and the nitrogen group (Scheme 1.15). For the \perp side-on coordinated diazenido ligand, this orbital is located in the lower energy (refer to Figure 1.2) and therefore, it is not chemically active. For hydrazido (1-) ligand, interestingly, this orbital is the subjacent one which indicates it could have a strong influence on the chemical



Scheme 1.15

reactivity of this complex. Furthermore, the electron density, or charge distribution of this orbital between the two nitrogen atoms is significantly different. The presence of a large charge on the nitrogen of the NR group of this type side-on hydrazido(1-) compound has been proved by experimental facts, *e.g.*, $\text{Cp}^*\text{WMe}_4(\text{NH}_2\text{NH})$ ⁹⁴ undergoes facile protonation at NH position, forming a similar \perp side-on coordinated hydrazine compound, and the fast (on NMR time scale) exchange of the hydrogens between two nitrogen positions in $\text{CpWMe}_4(\text{NH}_2\text{NH})$ has also been observed⁹⁰. Furthermore, the structural features revealed by the X-ray crystallographic analyses of such coordinated hydrazido(1-) and diazenido(1-) compounds also indicates that this filled π orbital in either hydrazido(1-) or diazenido(1-) ligands has not been used in bond formation with the metal. The structural dimensions of these compounds are listed in Figure 1.26 as (b) and (c), together with their counterpart compounds, as (a) and (d), in which the corresponding hydrazido(1-) and diazenido(1-) ligands are in the // side-on coordination fashion^{87, 90}. In each of \perp side-on coordination compound, the bond lengths of the metal to the two different

nitrogen atoms are very close and are within the single bond range, regardless of the large unevenness of the electron density in the perpendicular π orbital at these nitrogen atoms.

Finally, such \perp coordinated diazene, or azo ligand has also been observed in complex $\text{CpRe}(\text{CO})_2(\eta^2\text{-NPhNPh})$.⁹¹

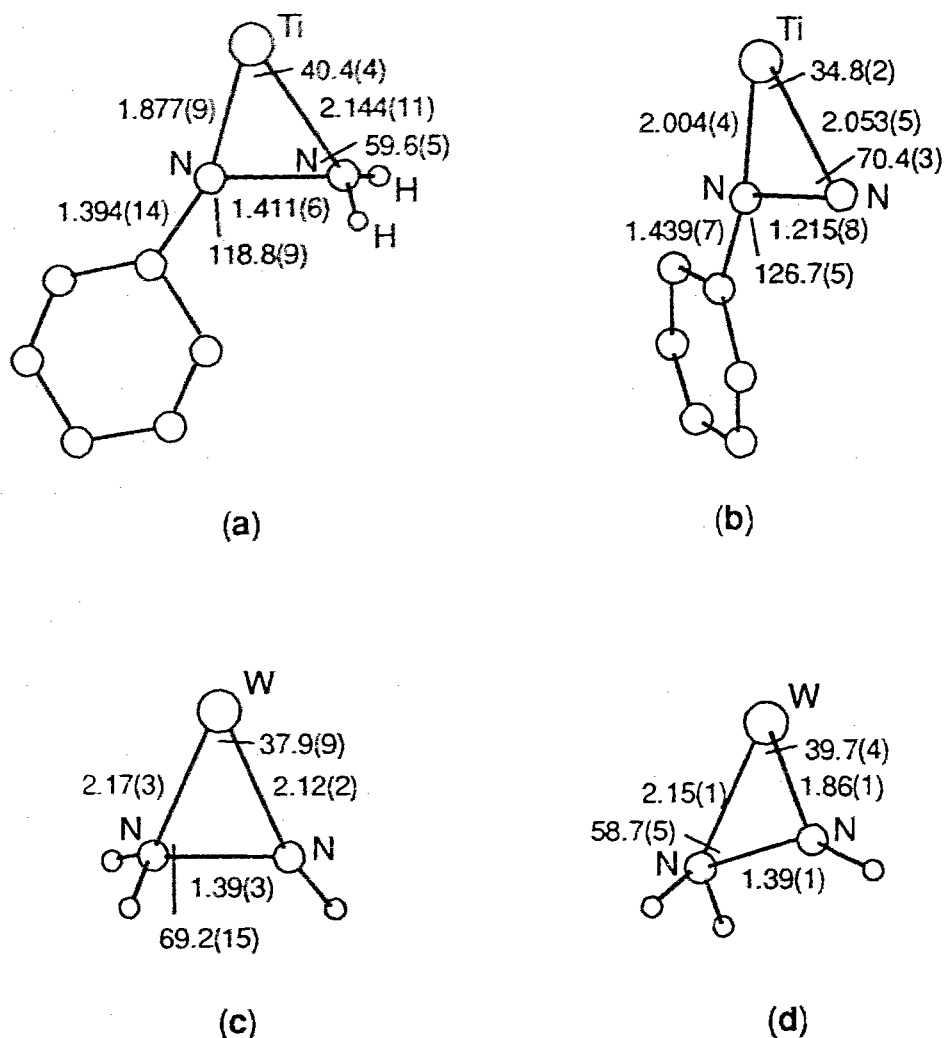


Figure 1.26 Important bond lengths (Å) and angles (°) in (a) $\text{CpTiCl}_2(\text{NH}_2\text{NPh})$, (b) $\text{CpTiCl}_2(\text{NNPh})$, (c) $[\text{CpWMe}_3(\text{NH}_2\text{NH})]^+$ and (d) $\text{CpWMe}_4(\text{NH}_2\text{NH})$

1. 4. Structural Characterization of Transition Metal Diazenido Complexes

1. 4. 1. Introduction

In mononuclear aryldiazenido compounds, three different coordination modes of the diazenido ligand to the metal have been observed. There are many examples of complexes with singly bent diazenido geometry, but far fewer with doubly bent and only one with a side-on coordination mode. These are shown as (1), (2) and (3) in Figure 1.27.

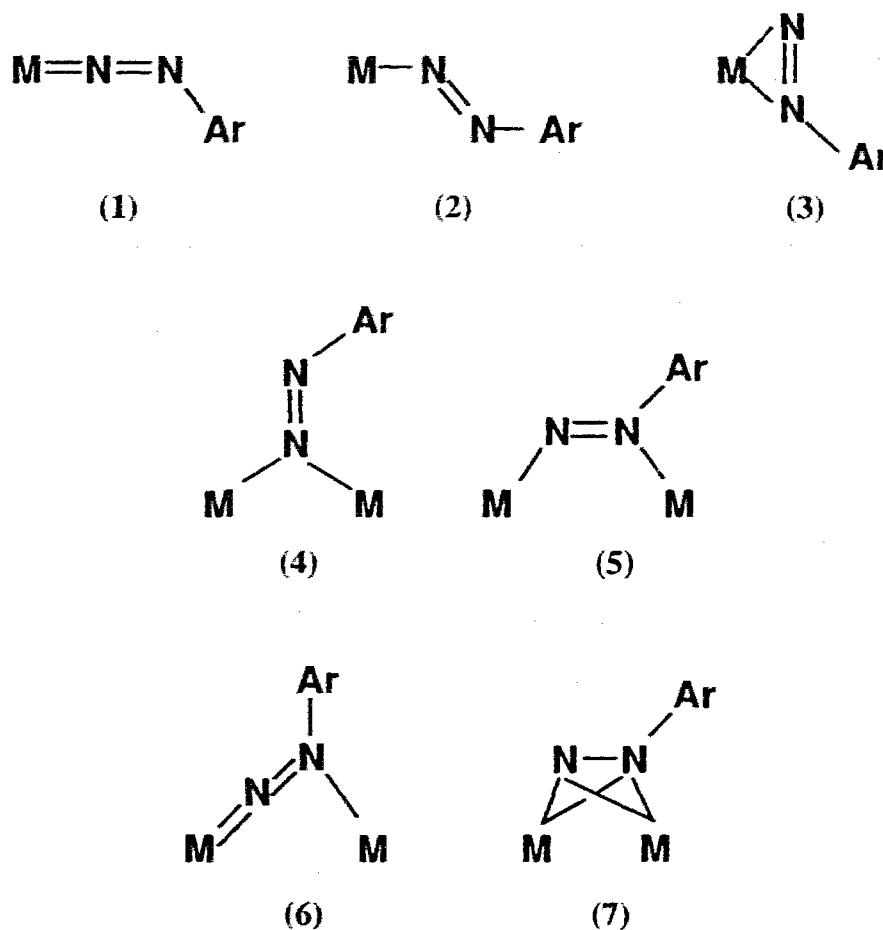


Figure 1.27 Different structures of transition metal aryldiazenido complexes

In dinuclear complexes, aryldiazenido can act as a bridging ligand between two metal centres. Four different bridging modes have been observed so far and they are illustrated in Figure 1.27 as (4), (5), (6) and (7). Different bonding modes directly reflect the different electronic configurations and the different charge density distributions in the metal-diazenido linkages, which is of considerable importance in understanding the chemistry of the aryldiazenido complexes.

A variety of spectroscopic and structural techniques normally used for characterization of transition metal complexes are, in principle, also suitable for diazenido compounds. Among these methods, X-ray crystallography, infrared spectroscopy and ^{15}N NMR spectroscopy are particularly useful. In the following section, some common problems associated with the application of the first two methods in structural characterizations of the diazenido complexes will be briefly discussed, and then emphasis will be given to illustrate the potential applications of ^{15}N NMR spectroscopy.

1. 4. 2. X-ray Crystallography of Diazenido Compounds

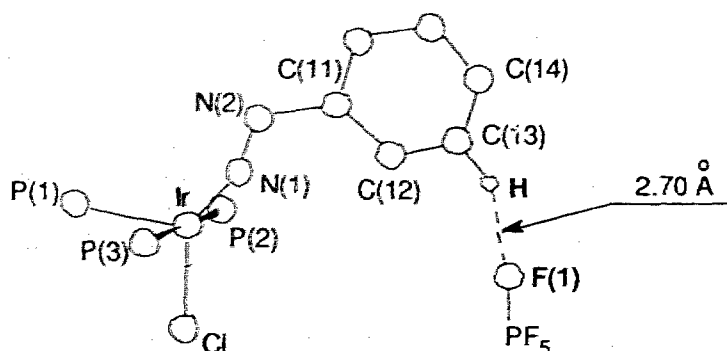
So far, single crystal X-ray crystallography has been the most reliable method for the characterization of diazenido compounds in the solid state. It often gives precise molecular structures and an unambiguous assignment of the coordination mode of the diazenido ligand. Typical parameters for the singly bent diazenido compounds are $\angle\text{M-N-N} = 170^\circ \sim 180^\circ$; $\angle\text{N-N-C} = 118^\circ \sim 125^\circ$ and $\text{N-N} = 1.20 \text{ \AA}$ (NN double bond length is 1.23 \AA). The M-N bond length is generally in a typical double bond range. For the doubly bent ligand, the parameters are $\angle\text{M-N-N} = 115^\circ \sim 125^\circ$; $\angle\text{N-N-C} = 115^\circ \sim 120^\circ$; $\text{N-N} = 1.17 \sim 1.19 \text{ \AA}$ (which is between the double (1.23 \AA) and triple (1.09 \AA) bond length); the M-N

distance is in the single bond length range. For bridging diazenido complexes, very limited structural data are known and they will be given in Chapter III, where they will be compared with new compounds synthesized in this work.

For X-ray crystallography, a suitable single crystal of the compound is necessary. This is sometimes difficult to obtain for unstable or short-lived compounds, as are most of the doubly bent diazenido complexes. Most of these are only stable in the solid state when stored at low temperature in the dark. In solution, decomposition of these compounds is apparently promoted by light exposure, ambient temperature or even solvents. In fact, only three crystal structures of doubly bent aryldiazenido complexes have been determined so far by X-ray diffraction.^{18, 19, 41}

In suitable cases, X-ray crystallography can provide information about connectivity, symmetry and geometry, but it does so only for the crystal studied in a very specific situation. That is, it gives us only a frozen picture of a molecule or ion in the form it adopts under the anisotropic pressure of forces exerted by its neighbors. In solids, many molecules take up different conformations or even have structures which are completely different from those existing in solution. The compound $[\text{IrCl}(\text{N}_2\text{Ph})(\text{PMe}_2\text{Ph})_3]\text{PF}_6$ ⁷¹ has been characterized in the solid state as having a structure shown in Figure 1.28, which contains a "half doubly bent" aryldiazenido ligand with $\angle\text{M-N-N}=155.2(7)^\circ$. This compound has been used as an example of the idea that the aryldiazenido ligand can adopt an intermediate geometry between the ideal singly bent and doubly bent geometries. However, a careful examination of the crystal structure revealed that this intermediate structure could also be the result of the non-bonding interaction between a hydrogen atom on the aryl ring of the diazenido ligand and a fluorine

atom in the counter ion PF_6^- , which is shown as the dashed line in Figure 1.28. In solution, the IR spectrum of this compound gave two stretching frequencies at 1569 and 1644 cm^{-1} , which shifted to 1561 and 1624 cm^{-1} , respectively, upon ^{15}N isotope substitution at the N_α position.^{41, 71} This indicates that the diazenido ligand likely adopts a singly bent geometry in solution, and this has been further confirmed by ^{15}N NMR spectroscopy.⁹⁵



Important Structural Parameters:

Van der Waals Distance: H-F = 2.67 Å, ($R_{\text{H}}=1.20$, $R_{\text{F}}=1.47$ Å)

Plane defined by atoms: Ir, N(1), N(2), C(11), C(14)

Deviation: -0.002, 0.003, -0.003, 0.002, -0.001 (Å)

Distances from the plane: C(12), C(13), H, F(1)

0.063, 0.062, 0.110, -1.170 (Å)

Figure 1.28. A perspective view of the distortion of diazenido ligand



Crystallographic disorder can also lead to some characterization problems. When molecular morphology shows approximately a higher symmetry than it really is, a compound may crystallize out in a higher symmetric lattice which may cause some local or internal disorder in the X-ray crystal structure. The molecular symmetry of the doubly bent diazenido compound $\text{PtCl}(\text{p-N}_2\text{C}_6\text{H}_4\text{F})(\text{PEt}_3)_2$ should not have a two-fold rotation axis, but crystallographically it has been observed in the single crystal structure of this compound which has been characterized in space group $C_{2/c}$.¹⁸ An internal crystallographic disorder of the nitrogen positions produces this higher symmetry as is shown in Figure 1.29.

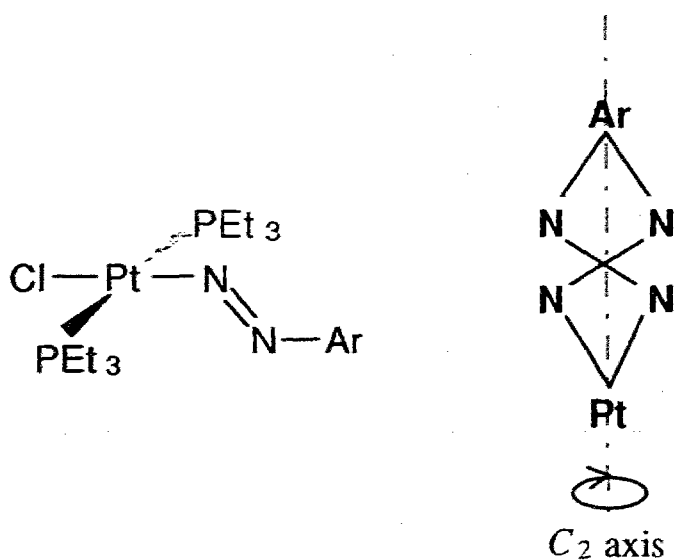


Figure 1.29 Disordered structure of the doubly bent diazenido ligands in $\text{PtCl}(\text{p-N}_2\text{C}_6\text{H}_4\text{F})(\text{PEt}_3)_2$

The diazenido compound, $[\text{Cp}^*\text{Ir}(\text{N}_2\text{Ar})\text{I}]_2$, made in this work, has been characterized in solution to have two different bridging diazenido ligands.

However, this non-centrosymmetric molecule was crystallized in a centrosymmetric space group $P\bar{1}$. The molecular structure shows an internal disorder of the nitrogen groups for both diazenido ligands which is related by a crystallographic centre, as is shown in Figure 1.30.

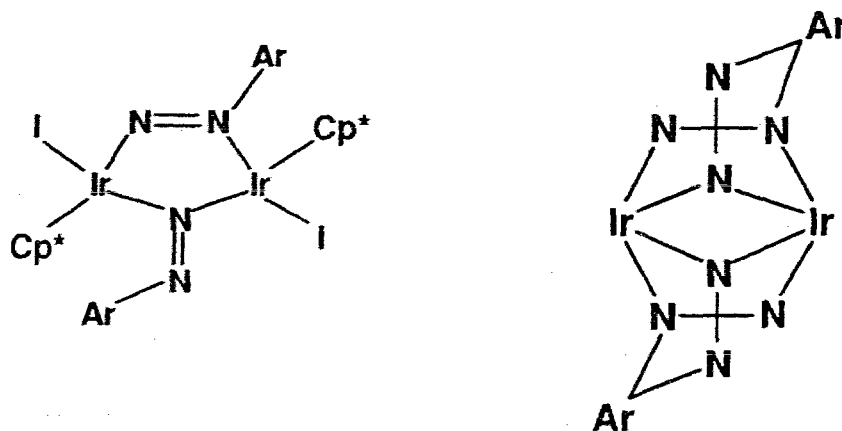


Figure 1.30 Disordered structure of the doubly bridged diazenido ligand in $[\text{Cp}^*\text{Ir}(\text{N}_2\text{Ar})\text{I}]_2$

Although this kind of disorder can be often sufficiently solved by suitable modeling of the molecular structure, without doubt, the strongly correlated mean-square vibrational amplitudes of those disordered atoms in the molecule will certainly leave ambiguity in the accuracy of the bond lengths and angles involving those atoms.

1. 4. 3. Infrared Spectroscopy

The free aryldiazonium ion (N_2Ar^+) shows one infrared absorption frequency near 2260 to 2300 cm^{-1} owing to triple-bond NN stretching. Upon coordination of this ligand to a metal centre, this NN stretch shifts to a lower frequency in a range of 1400 to 1900 cm^{-1} . The typical frequency ranges for the

different coordination modes of the aryldiazenido groups are diagrammed in Figure 1.31.

Generally, two problems hinder infrared spectroscopy from being a reliable structural method for diagnosing the coordination modes of aryldiazenido ligands. First, regions of considerable overlap, as shown in Figure 1.31, preclude any definitive assignment of the coordination mode based on the NN frequencies in the IR range of ca. 1500~1680 cm^{-1} . Secondly, the vibrational coupling of N=N stretch with other vibrational modes of the ligand could cause difficulty in assigning the N=N stretch. For example, coupling of N=N stretch with the C-C skeleton stretch of the aryl ring is often observed in aryldiazenido complexes. In the free diazonium salt, N_2ArBF_4 , one of the carbon-carbon

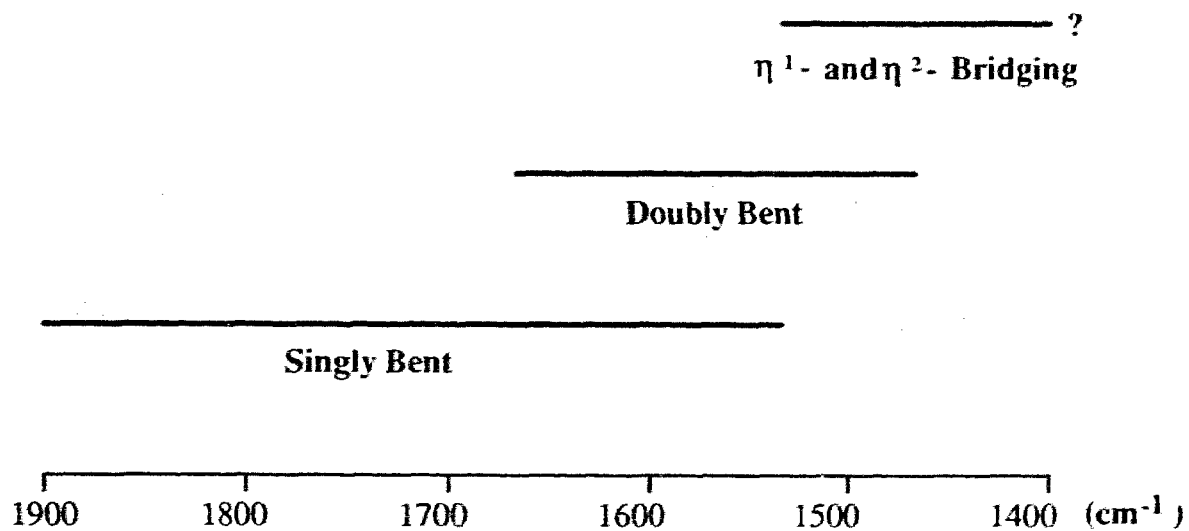


Figure 1.31 The range of aryldiazenido N=N stretching frequencies in metal complexes

stretches of the aryl ring occurs at $1580 \sim 1600 \text{ cm}^{-1}$, which obviously falls into the NN vibration range of the singly bent and the doubly bent aryldiazenido ligand. Furthermore, when a ^{15}N -substituted aryldiazenido ligand is used, a synchronic isotopic shift of this skeleton vibration band together with the band primarily due to the N=N stretch has often been observed. An empirical formula for the assignment of the N-N band has been postulated by Haymore,⁹⁵ on the basis of a careful analysis of the shifts of the individual IR bands upon isotopic substitution.

Despite its limitations, IR spectroscopy in most cases can still provide useful structural information about aryldiazenido complexes, and due to its convenience, it is always among the first methods of characterization.

1. 4. 4. ^{15}N NMR Spectroscopy

1. 4. 4. 1. Introduction

^{15}N NMR spectroscopy has been a particularly useful technique for studying transition metal complexes with dinitrogen and organodinitrogen ligands.⁹⁶ The rapid growth in the numbers of new aryldiazenido compounds, together with the availability of their ^{15}N NMR data, especially those from this laboratory, make this an opportunity for a brief review of ^{15}N NMR of aryldiazenido complexes in different structures with a wide range of transition metals. Previously, the discussion of the ^{15}N NMR spectra of diazenido compounds has been mainly limited to distinguishing the coordination modes and geometries of the complexed diazenido ligand.⁹⁷ Here, an attempt is also made, with help of molecular orbital theory, to relate the ^{15}N NMR parameters such as *nuclear shielding* and *spin-spin coupling constant* to properties of the metal-ligand bond, especially the π back bonding strength, in structurally similar

compounds. ^{15}N NMR is still a rather new technique for studying aryldiazenido and related complexes, so that the ^{15}N chemical shift has been the most reported NMR parameter, and only a few nitrogen-nitrogen spin-spin coupling constants are known. Obviously, this situation will restrict our discussion to a certain extent. In this section some introductory information about the ^{15}N nucleus and the potential of the technique, as well as some problems associated with it will be discussed.

Interestingly, nitrogen was the first NMR nucleus to be reported. In 1950, two well separated ^{14}N NMR signals were observed for the two nitrogen environments in an ammonium nitrate solution,⁹⁸ thus indicating that the signal position depends upon the chemical environment of the nucleus. However, some intrinsic problems prevented nitrogen NMR from becoming a useful structural method in earlier days. A comparison of the NMR properties of nitrogen nuclei with other common NMR nuclei is listed in Table 1.3. The low natural abundance (0.37%) of ^{15}N and its negative low gyromagnetic ratio ($-2.711 \text{ rad}\cdot\text{T}^{-1}\cdot\text{s}^{-1}$) make the ^{15}N nucleus very low in NMR sensitivity, as can be seen from equation 1.2.

$$\text{NMR receptivity} = \text{natural abundance} \cdot \gamma^3 \cdot I(I+1) \cdot B_0^2 \quad (\text{Eqn.1.2})$$

The sensitivity is only 2% of that of the ^{13}C nucleus. The negative gyromagnetic ratio of the ^{15}N nucleus also possibly gives rise to a negative *nuclear Overhauser effect* (nOe), as indicated in the following equation: (Eqn. 1.3)

$$\text{nOe} = 1 + \frac{\gamma_H}{2\gamma_N} \frac{T_{1\text{obs}}}{T_{1\text{cd}}} \quad (\text{Eqn. 1.3})$$

Table 1.3. NMR Properties of Some Common Nuclei

Isotope	Spin (I)	Natural abundance (a%)	Gyromagnetic ratio $\gamma/10^7$ (rad.T ⁻¹ .s ⁻¹)	Quadrupolar coupling constant ($\times 10^{-28}$ m ²)	Relative sensitivity	Operating frequency ^a (MHz)
¹ H	1/2	99.98	26.751	..	5676	400
¹³ C	1/2	1.11	6.726	..	1	100.6
³¹ P	1/2	100	10.83	..	377	161.9
¹⁴ N	1	99.63	1.932	1.56 $\times 10^{-2}$	5.69	28.9
¹⁵ N	1/2	0.37	-2.711	..	0.02	40.5

^a: at 9.4 Tesla magnetic field.

where T_{1obs} is the overall observed ^{15}N spin-lattice relaxation time, and T_{1dd} is that from (^{15}N and ^1H) dipolar interaction only. Without other mechanisms, the ^{15}N nOe reaches its maximum value, -3.93, on proton decoupling. However, when other mechanisms have rather large contributions to the total T_1 (as in the cases of transition metal complexes) the signal 'enhancement' could become negative, so that the signal could even be completely lost, due to $T_{1obs} \ll T_{1dd}$. The long relaxation time of the ^{15}N nucleus has been the most significant problem for those compounds in which the relaxation process is controlled by the inter- or intra-molecular dipole-dipole interaction mechanism. For example, NH_3 has a T_1 about 186 seconds⁹⁹ and for PhNO_2 it is about 420 seconds¹⁰⁰.

With the advent of high-field NMR spectrometers and ^{15}N isotopically enriched samples, the NMR signal of the ^{15}N nucleus has been greatly enhanced. For example, a 95% enriched ^{15}N sample in a 9.4 Tesla (400 MHz spectrometer) magnetic field will have an NMR signal 5.6 times that of ^{13}C nucleus at its natural abundance. In principle, the long relaxation time of the ^{15}N can be overcome by using relaxation reagents, such as $\text{Cr}(\text{acac})_3$.^{101, 102} However, for transition metal complexes, especially for those compounds with ligands containing a multiply bonded NN group, much faster relaxation of ^{15}N nucleus is often observed in practice anyway.^{105, 106} The detailed discussion of this aspect will be given in the next section.

1. 4. 4. 2. ^{15}N Nuclear Spin Relaxation in Transition Metal Complexes

In practice, the more rapid relaxation of the ^{15}N nucleus in transition metal complexes indicates that dipole-dipole relaxation may not be the only mechanism operating. In simple cases where other mechanisms contribute to

the spin relaxation, the rates due to these different mechanisms are additive:

(Eqn.1.4)

$$\frac{1}{T_1} = \sum_m \frac{1}{T_{1m}} \quad (\text{Eqn 1.4})$$

Although possible relaxation mechanisms for ^{15}N in some metal- N_2 complexes have been discussed,^{96, 107} the relative contributions of different relaxation pathways in complexes have not been systematically explored. We believe that, in addition to the common *dipole-dipole* relaxation mechanism, a *scalar coupling* mechanism and a *nuclear shielding anisotropy* mechanism could also be the most likely pathways for complexes. Since a discussion of the various relaxation mechanisms can be found in most NMR textbooks, here we will only pay attention to the applications of these three relaxation mechanisms to the nitrogen ^{15}N nucleus.

A). Relaxation by the Dipole-Dipole Interaction

Nuclear magnetic dipole relaxation of a ^{15}N nucleus may occur through either intra- or inter-molecular interactions with other nuclei. Normally, the intra-molecular interactions are of interest for small molecules, in which the ^{15}N nuclei are connected with protons either directly, such as NH_3 and its complexes, or indirectly, such as $^{15}\text{N}_2\text{R}$ and its complexes in a protonated solvent.

If a nucleus I is relaxed by a nucleus of spin S at distance r, the intra-molecular dipole-dipole relaxation time for I, T_{1dd} (intra), is given by equation¹⁰³ (Eqn. 1.5)

$$\frac{1}{T_{1dd}(\text{intra})} = \frac{\mu_0^2 \gamma_I^2 \gamma_S^2 \hbar^2 S(S+1) \tau_c}{12\pi^2 r^6} \quad (\text{Eqn.1.5})$$

where μ_0 is the permeability of free space. For $^{15}\text{N}_2$ ($r_{\text{NN}}=1.1 \text{ \AA}$), when $\tau_c = 50$ ps, $T_{1dd}^{-1} = 5.1 \times 10^7 \tau_c$, so $T_{1dd} = 400$ seconds. However, experimentally, $^{15}\text{N}_2$ at $-196 \text{ }^\circ\text{C}$ shows a T_1 value of 12 seconds.¹⁰⁴ The significant difference between these data indicates that the dipole-dipole interaction mechanism may not be the dominant one in the relaxation of $^{15}\text{N}_2$. Similar phenomena have also been found in transition metal complexes with either dinitrogen or some organodinitrogen ligands for which the typical relaxation time is about 10 seconds at room temperature in a 9.4 Tesla field.¹⁰⁶

B). Mechanism of Relaxation by Scalar Coupling of "the Second Kind"

The mechanism of "relaxation by scalar coupling of the second kind" relates the fast relaxation of the ^{15}N nucleus to quadrupolar nuclei to which the ^{15}N is bonded. This is distinct from that of the "first kind", involving time dependent chemical exchange or rotation processes. This is perhaps especially important for transition metal compounds with a structural unit such as $\text{Mq-}^{15}\text{N-}^{14}\text{N}$, where ^{15}N is adjacent to two quadrupolar nuclei, ^{14}N and a transition metal. For molecules undergoing isotropic tumbling, characterized by τ_1^s , the scalar coupling relaxation time, T_{1sc} , is given by equation 1.6

$$\frac{1}{T_{1sc}} = \frac{8}{3} \pi^2 J^2 S(S+1) \left[\frac{\tau_1^s}{1 + (\omega_I - \omega_S)^2 (\tau_1^s)^2} \right] \quad (\text{Eqn.1.6})$$

where ω is the corresponding *Larmor* frequency. Obviously the rate of this kind relaxation is field dependent because of the denominator $1+(\omega_I - \omega_S)^2(\tau^{S_1})^2$. So a small frequency difference, $\Delta\omega$, of the coupled nuclei will be important for this mechanism to be operative.

For a linkage of $M^q-^{15}\text{N}-^{14}\text{N}$, the contributions to this mechanism from the quadrupolar metal centre, M^q , and the ^{14}N nucleus can be separated as in equation 1.7

$$\frac{1}{T_{1sc}} = \sum_i \left(\frac{1}{T_{1sc}^i} \right) = \left(\frac{1}{T_{1sc}} \right)_{M^q} + \left(\frac{1}{T_{1sc}} \right)_{^{14}\text{N}} \quad (\text{Eqn.1.7})$$

Since for most transition metal NMR nuclei, the value of J , the coupling constant to ^{15}N , and S , the metal nuclear spin, are rather large and both of them are field independent, therefore, the unfavorable $(\Delta\omega)^2$ term in Eqn. 1.6 will make this mechanism more efficient at lower field. For example, the 'most magnetic' of the transition metal nuclei is rhenium, since ^{185}Re is 37% abundant and ^{187}Re 63% abundant, and both have spin 5/2 and relatively large gyromagnetic ratios. In *trans*- $\text{ReCl}(^{15}\text{N}_2)(\text{PMe}_2\text{Ph})_4$, the relaxation time for the metal bonded $^{15}\text{N}_\alpha$, relative to $^{15}\text{N}_\beta$, is shorter at the lower field ($T_1(^{15}\text{N}_\alpha)/T_1(^{15}\text{N}_\beta) \approx 0.5$ at 2.1 T) than at higher field ($T_1(^{15}\text{N}_\alpha)/T_1(^{15}\text{N}_\beta) \approx 1$ at 9.4 T).¹⁰⁵

For the ^{14}N term in Eqn.1.7, the difference of the *Larmor* frequencies between ^{15}N and ^{14}N , $\Delta\omega$, is much smaller at lower field than at higher field, *e.g.* $\Delta\omega \sim 2 \text{ MHz}$ at 2.1 T, but $\sim 10 \text{ MHz}$ at 9.4 T, which also makes this mechanism more favored at low field.

C). Relaxation by Nuclear Shielding Anisotropy

The relaxation by nuclear anisotropy is important for complexes with a multiply bonded nitrogen group, or the presence of lone pair electrons on the ^{15}N atom, such as the dinitrogen, singly bent and doubly bent diazenido compounds. In these compounds, the shielding anisotropy $\Delta\sigma$ at the ^{15}N nucleus could be as large as *ca.* 1000 ppm ¹⁰⁷ (more discussion on nitrogen nuclear shieldings will be given in the next section). The contribution of this mechanism to T_1 is given by T_{1sa} , (Eqn.1.8), or simply by Eqn.1.8a.

$$\frac{1}{T_{1sa}} = \frac{\mu_0 \gamma_I^2 B_0^2 \Delta\sigma^2 \tau_c}{30 \pi} \quad (\text{Eqn.1.8})$$

$$\frac{1}{T_{1sa}} \propto (B_0 \cdot \Delta\sigma)^2 \quad (\text{Eqn.1.8a})$$

The dependence of T_{1sa} upon B_0 means that this relaxation mechanism may be distinguished from others if measurements are made as a function of the applied field. In fact this has been well demonstrated for dinitrogen complexes,¹⁰⁵ as listed in Table 1.4. The most striking feature of the data in Table 1.4 is the dramatic decrease of the relaxation times for the measurements at higher field. This shows the importance of the anisotropic shielding mechanism for nitrogen-ligated complexes.

Finally, it is worth mentioning that although relaxation by both scalar coupling and by shielding anisotropy are field dependent, their dependences on the applied field are different. This indicates that, in principle, the relative

contributions from each relaxation mechanism could be evaluated by appropriately designed experimental measurements at different field strengths.

Table 1.4. Nitrogen-15 Spin-Relaxation Time (T_1), in Seconds, for Terminal Dinitrogen Complexes in THF Solution at 297 K ^a

Complex	$B_0 = 2.1 \text{ T}$		$B_0 = 9.4 \text{ T}$	
	$T_1 (^{15}\text{N}_\alpha)$	$T_1 (^{15}\text{N}_\beta)$	$T_1 (^{15}\text{N}_\alpha)$	$T_1 (^{15}\text{N}_\beta)$
<i>trans</i> -Mo($^{15}\text{N}_2$) ₂ (depe) ₂	26	31	8.3	9.0
<i>trans</i> -W($^{15}\text{N}_2$) ₂ (depe) ₂	< 54 ^b	< 62 ^b	8.9	8.5
<i>cis</i> -W($^{15}\text{N}_2$) ₂ (PMe ₂ Ph) ₄	33	37	5.4	7.2
<i>trans</i> -ReCl($^{15}\text{N}_2$)(PMe ₂ Ph) ₄	9	20	3.8	4.1
<i>trans</i> -OsCl ₂ ($^{15}\text{N}_2$)(PMe ₂ Ph) ₃	23	31	5.7	4.0

a: Data from reference 105

b: Value overestimated because of a deterioration in resolution during the course of the experiment.

1. 4. 4. 3. Nitrogen-Nitrogen Spin-Spin Coupling Constant

The spin-spin coupling constant is a very valuable NMR parameter in modern NMR spectroscopy, because of its sensitivity to the structure and chemical environment of the coupled nuclei. This also should be so for the nitrogen-nitrogen spin-spin coupling constant, but systematic studies on this, either experimentally or theoretically, have been sparse, although many nitrogen-nitrogen coupling constants have been measured.^{108, 109} This situation might be caused by two reasons. First, the small gyromagnetic ratio of the nitrogen nucleus will intrinsically cause the magnitude of $J(\text{N}, \text{N})$ to be small,

due to the relationship $J(N,N') \propto \gamma_N \gamma_{N'}$. So experimentally, nitrogen-nitrogen spin-spin coupling constants for different compounds are spread in a rather narrow range ($|J(N, N)| \cong 0 \sim 35$ Hz). Secondly, the rationalization of $J(N, N)$ values has been difficult, as in Ramsey's model they are the resultant of three coupling components which can differ in magnitude and sign.⁹⁶ These three coupling components in Ramsey's model¹¹⁰ are the Fermi contact, orbital and dipolar terms. This can be expressed as equation 1.9

$$J(A, B) = J_c(A, B) + J_o(A, B) + J_d(A, B) \quad (\text{Eqn.1.9})$$

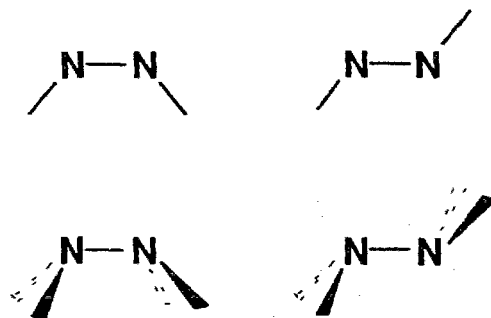
However, examination of the present experimental data for $J(N, N)$, and $J(N, C)$ due to their mechanistic similarity, revealed that some correlations can be drawn between structural factors and the spin-spin coupling constants in different organodinitrogen species, and even in their transition metal complexes. Even more astonishingly, these regular variations of the relative magnitudes and signs of $J(N, N)$ in respect to the structures for different compounds can be explained or even predicted at a qualitative level by considering only the Fermi contact term in a framework of molecular orbital interactions. In other words, a consideration of the molecular orbital interactions provides a good insight into the Fermi contact interaction, the dominant term in the coupling mechanism. For reasons of space, and for the practical purpose of using $J(N, N)$ as a structure probe, the detailed qualitative molecular orbital analysis of the Fermi contact term is omitted here. Instead, some important conclusions are given below:

- (1). $^1J(^{15}\text{N}, ^{15}\text{N})$ of free molecular $^{15}\text{N}_2$ (2.4 Hz) will be used as a reference to classify other groups of compounds.
- (2). Group I, This group comprises species with a linear N-N-X linkage (X \neq transition metal).

When X is a substituent with a higher VSIP, or smaller electronegativity than nitrogen, the magnitude of $^1J(^{15}\text{N}, ^{15}\text{N})$ will be smaller than that of $^{15}\text{N}_2$, and when X is a substituent with a lower VSIP, or larger electronegativity than nitrogen, the magnitude of $^1J(^{15}\text{N}, ^{15}\text{N})$ will be larger than that of $^{15}\text{N}_2$. Dinitrogen itself also belongs to this group (X is null). The sign of $^1J(^{15}\text{N}, ^{15}\text{N})$ for species in this group is negative.

Terminal coordination of species in this group to transition metals in a linear pattern, *i.e.* M-N-N-X, results in a slight increase of the magnitudes of $^1J(^{15}\text{N}, ^{15}\text{N})$ for these species. The smaller the difference of VSIPs between the metal and nitrogen, the less will be the increase in the magnitudes of the $^1J(^{15}\text{N}, ^{15}\text{N})$. The sign still remains negative.

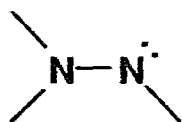
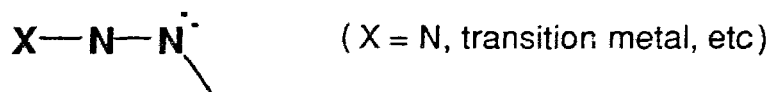
- (3). Group II, comprises species where both of the nitrogens bear π -type of lone pairs with *s* character in either cis or trans arrangement, for example, diazenes and hydrazines shown below



The magnitudes of $^1J(^{15}\text{N}, ^{15}\text{N})$ for species in this group are greatly enhanced compared with N_2 and group I. Where the substituents have smaller VSIPs than nitrogen, increasing the number of substituents decreases the relative enhancement. Where the substituents have larger VSIPs than nitrogen, increasing the number of substituents increases the relative enhancement. With a transition metal substituent, a larger enhancement will be expected than without such a substituent. Coordination of the group II species to a transition metal centre always leads to a slight decrease of $|^1J(^{15}\text{N}, ^{15}\text{N})|$.

The signs of the J values will be negative for cis and trans diazene type of compounds, but for hydrazine type of compounds, will be negative for cis and positive for trans. The magnitudes of J for intermediate conformations, *e.g.* *gauche* conformations, are always smaller than either the cis or trans conformation, and the sign of J is unpredictable.

- (4). Group III species are those in which only one of the coupled nitrogens bears a π -type of lone pair with s character, *e.g.* the planar species shown below



Their $|^1J(^{15}\text{N}, ^{15}\text{N})|$ will be larger than that of completely linear species (Group I), but smaller than those where both nitrogens bear lone pairs (Group II). The substitution effect for this group is similar to that of Group II. The sign is negative.

The above classification, based on the electronic structures of different species, shows good agreement with the NMR experimental results, as will now be illustrated.

The ranges of experimental $|^1J(^{15}\text{N}, ^{15}\text{N})|$ values for Group I, II and III species are listed in Figure 1.32 for a comparison.

The J value of molecular $^{15}\text{N}_2$ can not be obtained directly by experimental measurement, but it can be deduced from the experimental value of $^1J(^{15}\text{N}, ^{14}\text{N})$ for the molecule $^{15}\text{N}^{14}\text{N}$,¹¹¹ which is +1.8 Hz, and equation 1.10⁹⁶ neglecting the isotope effects because they are small and of the order of experimental uncertainty.¹¹²

$$^1J(^{15}\text{N}, ^{15}\text{N}) = -1.403 \ ^1J(^{15}\text{N}, ^{14}\text{N}) \quad (\text{Eqn.1.10})$$

This gives $^1J(^{15}\text{N}, ^{15}\text{N}) = -2.5 \text{ Hz}$.

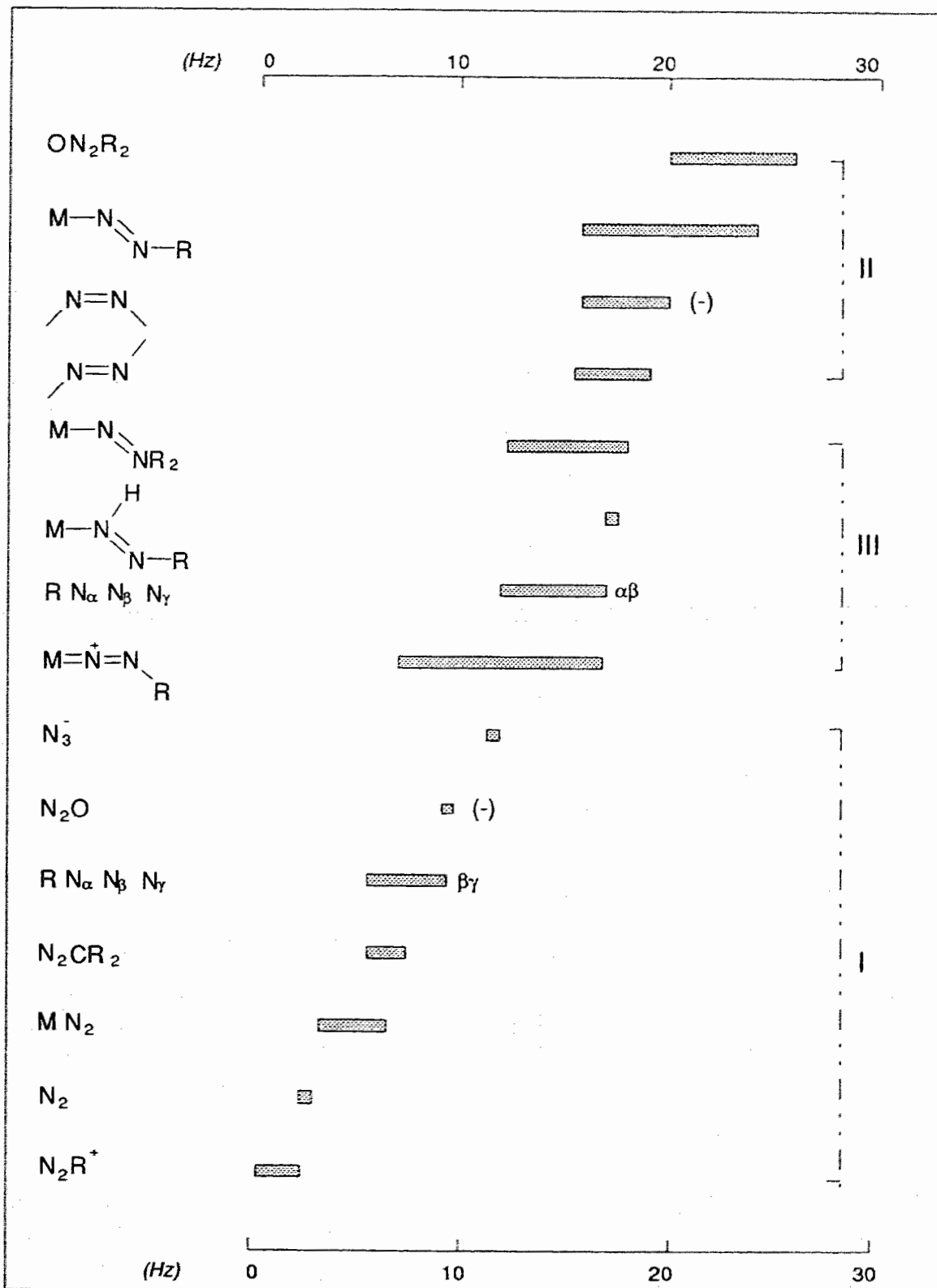
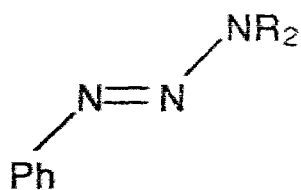


Figure 1.32 Ranges of $|^1J(^{15}\text{N}, ^{15}\text{N})|$ values, where the known sign is given in parentheses ()

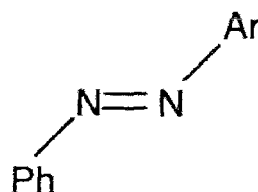
The aryldiazonium ion N_2Ar^+ (Group I) has a less electronegative carbon atom bonded to the N_2 in a linear fashion, its $|^1J(^{15}N, ^{15}N)| \cong 0 \sim 1.6$ Hz,⁹⁷ and as expected, is lower than that of molecular $^{15}N_2$. Among the same group, but with a more electronegative substituent O attached to the N_2 , N_2O shows $J = -9.16$ Hz.¹¹³ Similarly, the $|J|$ value for N_3^- has been observed to be 11.3 Hz¹¹⁴⁻¹¹⁷ and $|^1J(^{15}N_\alpha, ^{15}N_\beta)|$ for N_3R , $(N_\alpha N_\beta N_\gamma R)$, are in the range 5 ~ 8 Hz,¹¹⁴⁻¹¹⁷ depending upon different R, separately. Importantly, the J values found for terminally coordinated dinitrogen compounds are in the range of 4 ~ 7 Hz,^{118, 119} compared with the $|^1J(^{15}N, ^{15}N)| = 2.5$ Hz for $^{15}N_2$. This kind of increase due to coordination to a transition metal is expected to carry over to other Group I species.

Compounds of Group II are generally expected to have the highest J values for the coupled nitrogen atoms based on our classification. In fact, the largest ^{15}N - ^{15}N coupling constant is observed in N-nitrosoamines ($|J| = 20 \sim 23$ Hz),^{120, 121} in which both of the coupled nitrogens are bearing lone pairs with s character. Experimental data for diazene or azo type compounds also show high J values, ($|J| = 14 \sim 17$ Hz),¹²²⁻¹²⁴ and generally, this value is higher for the cis arrangement than for trans. More informatively, the sign of some of the *cis*-azo compounds has been shown to be negative,⁹⁶ tallying with our prediction.

The substituent effect on the J value in this group can be demonstrated by the following examples.¹²² The more electronegative substituent NR_2 causes an increase of the magnitude of the J value.



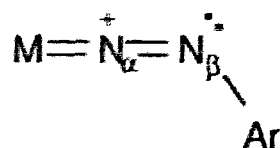
$$|J| = 19.0 \text{ Hz}$$



$$|J| = 14.6 \text{ Hz}$$

For hydrazine types of compounds, the cis and trans geometries considered in theory and mentioned in Group II above are not the observed ground state conformations. The experimental J values are only available for the observed *gauche* geometries, and are in the low range of 3 ~ 7 Hz,¹¹³ in agreement with our prediction. Theoretical calculations by an INDO¹²⁵ and an *ab initio*¹²⁶ method on the parent molecule $^{15}\text{N}_2\text{H}_4$ arrived at the same conclusion as that of our qualitative analysis. The results of the calculations showed a large negative J value for *cis*- $^{15}\text{N}_2\text{H}_4$ and a large positive J for *trans*- $^{15}\text{N}_2\text{H}_4$, separately, whereas for the *gauche* and other intermediate geometries, the calculation resulted in rather small J values.

Group III covers a large variety of compounds. Structurally, this group lies between Group I and Group II. Correspondingly, the J values of this group of compounds also lie between that of group I and group II. One of the typical examples is the singly bent aryldiazenido ligand,



which has a lone pair on N_β with both s and $p\pi$ character. Its $|J|$ value ranges from 7 ~ 17 Hz,^{97, 127} depending on the different metals and aryl groups. Correspondingly, linear diazonium N_2Ar^+ , without such lone pair (Group I), and the doubly bent diazenido ligand, with two such lone pairs (Group II), have J values ranging, separately, from 0 to 2 Hz and 16 to 23 Hz.⁹⁷ The comparison of these species is illustrated in Table 1.5.

Table 1.5 Comparison of Structural Factors and NMR $|^1J(^{15}N, ^{15}N)|$ Values for Diazenide in Different Geometries

Diazenide	$N \equiv \overset{+}{N} - Ar$	$\overset{+}{N} = \overset{+}{N} - Ar$	$\overset{\cdot\cdot}{N} = \overset{\cdot\cdot}{N} - Ar$
Group	I	III	II
No. of lone pairs	0	1	2
Range of J	0 ~ 3 Hz	7 ~ 17 Hz	16 ~ 23 Hz

1.4.4.4. Nitrogen Chemical Shift*

Compared with the relaxation data and spin-spin coupling constant, the nitrogen chemical shift has been used most often in structure assignments for nitrogen containing compounds, since the wide range of nitrogen chemical shifts is a sensitive measure of the electron shielding situation at an individual nitrogen nucleus in these compounds. Generally, the electron shielding effect on a nucleus can be expressed as a sum (Eqn. 1.11)¹²⁸

*: Nitrogen chemical shift data used in this thesis are all referenced to $MeNO_2$.

$$\sigma = \sigma^d + \sigma^p \quad (\text{Eqn.1.11})$$

where σ^d and σ^p are diamagnetic and paramagnetic contributions respectively.

In nitrogen NMR spectroscopy, the paramagnetic term is dominant and it has a negative contribution to the total shielding effect, whereas the diamagnetic term has a positive contribution to it. Since the diamagnetic term arises only from the ground state electronic function,¹²⁸ as such it can be considered as the counterpart of the *Larmor* formula¹²⁹ for the shielding of atomic nitrogen (Eqn 1.12)

$$\omega_N = \gamma_N B (1 - \sigma) \quad (\text{Eqn.1.12})$$

where ω_N and γ_N are *Larmor* frequency and gyromagnetic ratio of the ^{15}N nucleus, B is the applied magnetic field and σ is the shielding. In contrast to this, the paramagnetic term depends upon both the ground and the excited electronic states of the molecule concerned. When the molecule is present in an applied magnetic field, the orbital angular momenta of the molecule are perturbed. Under this perturbation, the ground state angular momenta of occupied orbitals will be mixed-in with some previous excited state angular momenta, and will produce rotations of electron charge around the nucleus. For example, in the case of p atomic orbitals, and assuming the applied magnetic field is in the z direction, we have $L_z |p_x\rangle = -|p_y\rangle$; $L_z |p_y\rangle = |p_x\rangle$ and $L_z |p_z\rangle = 0$, with the similar relationship for the operators L_x and L_y . The interactions of such electron density currents with the magnetic dipole of the nucleus will cause changes in the effective field experienced by the nucleus, which are measured

as changes in the shielding. Since the paramagnetic term requires the presence of electrons with non-zero orbital angular momentum, it will not be operative for s valence electrons. Thus the chemical shift of the hydrogen nucleus is dominated by the diamagnetic shielding.

For a qualitative description of the paramagnetic shielding interaction in a wide range of nitrogen compounds, equation (1.13), after Pople ¹¹²,

$$\sigma_N^p = -A \langle r^{-3} \rangle_{p_N} \frac{\Sigma Q}{\Delta E} \quad (\text{Eqn.1.13})$$

is the most commonly used one, where A is a constant ($\mu_0 e^2 h^2 / 8\pi m^2$), ΔE is the averaged exciting energy and ΣQ is the bond order, or charge density term which can also be understood as the imbalance of the valence electrons in the nitrogen 2p orbitals at the average distance $\langle r^{-3} \rangle_{p_N}$ from the nucleus. In nitrogen NMR the term $\langle r^{-3} \rangle_{p_N}$ is generally not expected to vary much from compound to compound, but the terms ΔE and ΣQ are important in understanding the trend in chemical shifts, due to their direct relationship to the electron environment experienced by the nitrogen nucleus. Furthermore, for a given series of molecules, the ΔE and ΣQ terms are often correlated to each other. A larger ΔE is often accompanied by a smaller ΣQ . So, either ΔE or ΣQ have been used in interpretation of the chemical shift changes. This has led to a correlation between the chemical shifts (δ) and the photoelectron absorption bands (ΔE) for certain types of compounds, such as, RNO ,¹³⁰ R_2CN_2 ¹³¹ and RN_3 .¹¹⁷ The energy differences, ΔE , obtained from a theoretical calculation for N_2H_4 (*gauche*), N_2 and N_2H_2 are 25, 23 and 12 eV, respectively.¹³² Correspondingly, the chemical shifts are *ca.* -300 and -70 ppm for N_2H_4

(*gauche*)¹³³ and N_2 ⁹⁷, respectively, and *ca.* +120 ~ +170 ppm for azo compounds, $RNNR'$ (where the R and R' are aryl groups).⁹⁷

Higher chemical shifts, *i.e.* lower paramagnetic deshieldings, have been observed for saturated compounds with a tetrahedral electron distribution at nitrogen (NH_4^+ , NH_3 and N_2H_4 (*gauche*) *etc.*). This can be understood as a result of the smallest ΣQ for the highly symmetric electron environment around nitrogen nuclei, and relatively large ΔE due to the low-lying $\sigma(N_s-H_s)$ bonding orbitals and the high-lying $\pi^*(N_p-H_s)$ antibonding orbitals.

In linear molecules, such as N_2 , N_3^- and CN^- *etc.*, the multiple bonding often indicates low-lying π^* orbitals and high-lying π orbitals. For these compounds, although the energy gap, ΔE , between HOMOs (π orbitals) and LUMOs (π^* orbitals) is small, the paramagnetic deshielding from the transitions between them ($\pi \leftrightarrow \pi^*$) are magnetically quenched. The entire paramagnetic contribution therefore comes from the transitions of σ type orbitals to low-lying π^* orbitals. Consequently, chemical shifts of these compounds are more downfield than those of saturated compounds due to their relatively smaller ΔE term.

In compounds N_2Ar^+ , N_2CR_2 and $1,1-N_2R_2$ *etc.*, the low symmetry substituents bonded to the nitrogen group will cause the $\pi \leftrightarrow \pi^*$ transitions at nitrogens to be magnetically allowed. So, generally, lower chemical shifts are expected for these compounds. Furthermore, for these compounds, the charge imbalance, ΣQ , on different nitrogen atom has also been largely changed by bonding to the substituents. This will result in a significant chemical shift difference between two nitrogen atoms. This can be exemplified by the free phenyldiazonium ion N_2Ph^+ . Its frontier orbitals have been shown in Figure 1.1. and the magnetically allowed transitions between these orbitals are given schematically in Figure 1.33

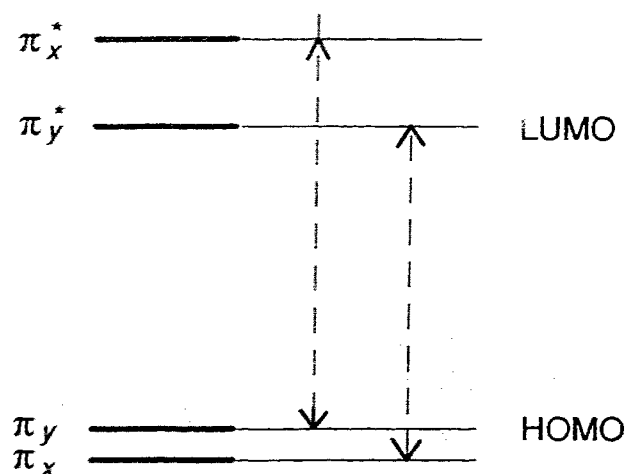


Figure 1.33 Charge rotations caused by the transitions, $\pi_x \leftrightarrow \pi_y^*$ and $\pi_y \leftrightarrow \pi_x^*$ at the NN group

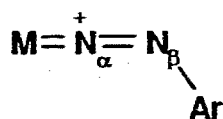
The energy difference between the two transitions, $\pi_x \leftrightarrow \pi_y^*$ and $\pi_y \leftrightarrow \pi_x^*$, is not significant. Interestingly, the electron density distributions on the N_α and N_β atoms in the filled frontier orbitals are largely different (refer to Figure 1.1). The near zero π_x and π_y electron densities at N_β in these orbitals indicate a small ΣQ term for this atom, which will lead to a small paramagnetic deshielding and, hence, a higher field chemical shift for the N_β nucleus. In fact, aryldiazonium ions N_2Ar^+ have been found with chemical shift range -65 ~ -15 ppm for N_α and -160 ~ -120 ppm for N_β .⁹⁷ Similarly, the compounds that belong to this group have always been found with higher field chemical shifts for the central nitrogens than for the terminal nitrogens.

The highest shielding has been observed for diazene and nitroso types of compounds. The common structural character for these compounds is that the nitrogen has a lone pair and also doubly bonds to an adjacent atom. The high-lying lone pair (HOMO) and low-lying π^* orbital make the $n \leftrightarrow \pi^*$ transition much

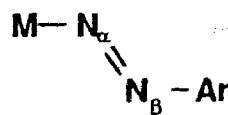
more facile than others. Moreover, higher charge density usually associated with such a π type of lone pair will also increase ΣQ and lead to increased paramagnetic deshielding.

1. 4. 4. 5. Application of ^{15}N NMR Spectroscopy to Aryldiazenido Complexes

The sensitivity of the nitrogen chemical shift and coupling constant have made nitrogen NMR spectroscopy a very important tool in determining the structures of diazenido and related diazene and hydrazido complexes. In mononuclear complexes, diazenido ligands, that can be either singly bent or doubly bent, show a large range of chemical shifts or shieldings. Especially, the chemical shift of N_α has been used commonly to diagnose the ligand geometry in complexes. A notable work has been published recently with a particular emphasis on this aspect.⁹⁷ Generally, the resonance of N_α spans from -90 to 160 ppm for the singly bent geometry, and over 200 ppm downfield for the doubly bent structure.



singly bent



doubly bent

The large spread of the nitrogen chemical shifts of diazenido ligands, even for the same type of compounds, strongly suggests that more structural and electronic information could be obtained from this NMR parameter. In other words, the nitrogen chemical shift may not only provide a criterion for

distinguishing the singly bent from the doubly bent diazenido ligand, but more importantly, it may also be used to probe the electron density distribution in the bonding structure. Surprisingly, this possibility has not been exploited yet. Therefore, attempts to do this will be the main interest of our discussion in this section. Chemical shifts and some measured $^1J(\text{N}, \text{N})$ s of the singly bent, doubly bent and bridging aryldiazenido complexes are listed in Tables 1.6, 1.7, and 1.8.

Singly Bent Aryldiazenido Complexes:

As shown in Table 1.6, for the singly bent diazenido complexes the four-coordinate compounds have the highest shieldings, at *ca.* -90 ppm for N_α . The lowest shieldings have been found for those compounds in a five-coordinate environment which range *ca.* 15 ~ 150 ppm for N_α . The N_α nitrogen shifts in the six-coordinate complexes fall in the middle and the seven-coordinate complex, $\text{W}(^{15}\text{N}_2\text{Ph})(\text{S}_2\text{CNMe}_2)_3$, also belongs to this group. Since in these compounds, the aryldiazenido ligands are all in the same geometry, *i.e.*, the singly bent geometry, an explanation for the cause of such widely spread chemical shifts for them in different compounds will focus on the coordination effect and the substituent effect. The effect of coordination on the chemical shift of a ligand is generally measured by the coordination shift, defined as the difference in shielding from the free to the coordinated ligand. The coordination shift appears to reflect the electronic properties of the metal centre, which is strongly related to the geometry of the molecule and to the coordination environment around the metal. The substituent effect may be attributed to the π -electron-donor or π -electron-acceptor substituents on the aryl ring.

Table 1.6. Nitrogen-15 Chemical Shifts and $^1J(N, N)$ values
of Singly Bent Aryldiazenido Complexes

Complex	$\delta(N_\alpha)$ ppm	$\delta(N_\beta)$ ppm	$ ^1J(N, N) $ Hz	ref.
<u>Seven-coordination</u>				
$W(^{15}N_2Ph)(S_2CNMe_2)_3$	-38.2	-138.0	16	a
<u>Six-coordination</u>				
$RuCl_3(p\text{-}^{15}NNC_6H_4NO_2)(PPh_3)_2$	-47.7	---	---	a
$RuCl_3(^{15}NNPh)(PPh_3)_2$	-46.8	---	---	a
$RuCl_3(N^{15}NPh)(PPh_3)_2$	---	-185	---	a
$RuCl_3(p\text{-}^{15}NNC_6H_4Me)(PPh_3)_2$	-46.4	---	---	a
$[Cp^*Re(p\text{-}^{15}NNC_6H_4OMe)(PMe_3)_2]^+$	-19.2	---	---	b
$[CpRe(p\text{-}^{15}NNC_6H_4OMe)(CO)_2]^+$	-8.2	---	---	b
$[CpRe(p\text{-}N^{15}NC_6H_4OMe)(CO)_2]^+$	---	-125.1	---	b
$[Cp^*Re(p\text{-}^{15}NNC_6H_4OMe)(CO)_2]^+$	-7.3	---	---	b
$[Cp^*Re(p\text{-}N^{15}NC_6H_4OMe)(CO)_2]^+$	---	-118.5	---	b
$[Cp^*Re(p\text{-}N_2C_6H_4OMe)(CO)_2]^+$	-6.7 ^a	-123 ^a	---	b
$ReBr_2(^{15}N_2Ph)(^{15}NHNPPh)(PPh_3)_2$	-3.7	-124.7	13	a
$[Cp^*Ir(p\text{-}^{15}NNC_6H_4OMe)(C_2H_4)]^+$	-2.3	---	---	c
<u>Five-coordination</u>				
$[Fe(CO)_2(^{15}N_2Ph)(PPh_3)_2]^+$	15.6	-104.2	15	a
$[Cp^*Ir(p\text{-}^{15}NNC_6H_4OMe)(PPh_3)]^+$	33.2	---	---	c
$[Ir(^{15}N_2Ph)(dppe)_2]^+$	46.4	-38.2	14	a
$[Os(CO)_2(^{15}N_2Ph)(PPh_3)_2]^+$	58.5	-21.8	15	a

(Continue Table 1.6)

$[\text{IrCl}(\text{}^{15}\text{N}_2\text{Ph})(\text{PPh}_3)_3]^+$	59.0	-22.9	14	a
$[\text{IrCl}(\text{}^{15}\text{N}_2\text{Ph})(\text{PMePh}_2)_3]^+$	64.0	-23.6	15	a
$\text{OsH}(\text{CO})(\text{}^{15}\text{N}_2\text{Ph})(\text{PPh}_3)_2$	98.9	-35.5	17	a
$[\text{RhCl}(\text{}^{15}\text{N}_2\text{Ph})(\text{PMePh}_2)_3]^+$	109.2	4.8	16	a
$[\text{Ru}(\text{CO})_2(\text{}^{15}\text{N}_2\text{Ph})(\text{PPh}_3)_2]^+$	116.8	-25.2	16	a
$[\text{RhCl}(\text{}^{15}\text{N}_2\text{Ph})(\text{PhP}\{(\text{CH}_2)_3\text{PPh}_2\}_2)]^+$	137.9	40.2	14	a
<u>Four-coordination</u>				
$[\textit{trans}\text{-IrCl}(\text{}^{15}\text{N}_2\text{Ph})(\text{PPh}_3)_2]^+$	-92.1	-239.0	8	a
$[\textit{trans}\text{-RhCl}(\text{}^{15}\text{N}_2\text{Ph})(\text{PPh}_3)_2]^+$	-89.8	-225.7	7	a

*: Nitrogen-14 NMR data.

a: Data source: reference 97.

b: D. Sutton, unpublished data.

c: This work.

Previously, the coordination shift of a ligand has been classified as small,¹³⁴ so that this important effect upon the chemical shift of a ligand has often been simply neglected, or touched on lightly in rationalizing the NMR behavior of the ligand in complexes. Unfortunately, this has also been assumed in previous discussions of nitrogen ligated complexes, such as the dinitrogen and diazenido complexes^{97, 107}. This simple generalization can not, obviously, explain the experimentally large range of chemical shifts of N_α for singly bent diazenido complexes (*ca.* 200 ppm), *e.g.*, from 137.9 ppm for $[\text{RhCl}(\text{}^{15}\text{N}_2\text{Ph})(\text{PhP}\{(\text{CH}_2)_3\text{PPh}_2\}_2)]^+$ to -92.1 ppm for $[\textit{trans}\text{-IrCl}(\text{}^{15}\text{N}_2\text{Ph})(\text{PPh}_3)_2]^+$, that covers about one third of the chemical shift range for all nitrogen ligands.

The large coordination shifts are not only true for the diazenides, but also occur in some dinitrogen and other related organonitrogen complexes.^{108,109,135}

In fact, small observed coordination shifts have been found only for specific cases, in which (1) the ligands have a degenerate π system, and (2) the metal fragment, correspondingly, engages in isotropic π back bonding with the ligand. In other words, only in those cases in which the ligands concerned have a cylinder-type π bonding system in either the free or coordinated state, such as in *trans*-(Me₂PhP)₄Re(N₂)Cl.^{118, 136} However, for those compounds, in which either of these two symmetry conditions is not fulfilled, this highly generalized conclusion¹³⁴ is often seen to fail, so that a rather larger coordination shift is normally observed.

In the discussion which follows, we will try to use the concepts of isotropy and anisotropy of the π electron distribution in the ligand and at the metal centre to analyze some typical examples in which the changes in *nitrogen chemical shifts* upon coordination, have not been understood before. Hopefully, through this kind of analysis, we can establish a qualitative relationship between the nitrogen coordination shifts of a ligand and the nature of its π bonding with the metal centre.

Molecular nitrogen, N₂, in free state, (D_{∞h}), has two degenerate sets of π and π^* orbitals. When it is in an external magnetic field, the most probable transitions that will induce paramagnetic charge circulations, are $\sigma \leftrightarrow \pi^*$ and $\pi \leftrightarrow \sigma^*$ (which includes $n \leftrightarrow \pi^*$, since the lone pair orbitals on nitrogens are part of the σ framework). Although the energy difference between the π (SOMO) and π^* (LUMO) orbitals of dinitrogen is small, the transitions between them, *i.e.*, $\pi \leftrightarrow \pi^*$, are magnetically disallowed. When N₂ coordinates terminally to a metal centre and is involved in isotropic π back bonding, a small coordination shift would be expected for the dinitrogen ligand. This is simply because upon coordination of N₂, the local symmetry around the nitrogen atoms remains the same, so that the

symmetry of the transitions in the free ligand is still strictly held in its complexes. In addition, the effective average exciting energy, ΔE , is relatively insensitive to the coordination. This can be exemplified by *trans*-(Me₂PhP)₄Re(N₂)Cl,¹³⁶ with $\delta(N_\alpha)$: -89.3 and $\delta(N_\beta)$: -67.6 ppm, respectively and *trans*-[FeH(N₂)(Ph₂PCH₂CH₂PPh₂)₂]⁺¹¹⁸, with a $\delta(N_\alpha)$: -65.4 and a $\delta(N_\beta)$: -41.3 ppm, respectively, which are not greatly different from the value of -71.3 ppm for free dinitrogen.⁹⁷ Obviously, it is this group of complexes that fits the conclusion generalized previously.

However, when dinitrogen is terminally coordinated to a metal centre with anisotropic π back bonding orbitals, a large coordination shift will be expected. This is because in addition to those $\sigma \leftrightarrow \pi^*$ and $\pi \leftrightarrow \sigma^*$ types of transitions, a virtual circulation results from the magnetically allowed $\pi \leftrightarrow \pi^*$ transitions and leads to marked changes in the paramagnetic shielding around the nitrogen nuclei. This kind of $\pi \leftrightarrow \pi^*$ transition is magnetically quenched by a cylindrical π electron distribution in free N₂ or in a highly symmetric molecule as just discussed above. The effect of coordination to a metal centre with anisotropic (or singly-faced) π back bonding ability on the nitrogen chemical shift is obvious. This effect can be demonstrated in CpRe(CO)₂(N₂),¹³⁵ with $\delta(N_\alpha)$: -121 and $\delta(N_\beta)$: -26 ppm, separately and [Cp⁺₂Ti(N₂)]₂(μ -¹⁵N₂),¹³⁷ with $\delta(N)$: +299 ppm for the bridging nitrogen.

It is also noteworthy that coordination shifts for the two nitrogen nuclei in the dinitrogen ligand are often in opposite directions. Generally, the nitrogen ligated to metal centre is shifted upfield and the terminal one shifts downfield by comparison with free N₂. This can be reasonably well understood in terms of the nodal plane character of the M-N-N bonding. The filled frontier orbitals always have their nodal planes near N _{α} , in both σ and π directions, which will largely

decrease the electron density at N_α and increase electron density at N_β . Consequently, the chemical shift of N_β is always located downfield relative to that of N_α . Interestingly, therefore, the difference of chemical shifts of N_α and N_β , $\Delta\delta$, in the terminally coordinated dinitrogen ligand, may also be used, in principle, to measure the relative position, in energy, of the corresponding metal d orbitals.

Through the above analyses of the coordination shifts of the dinitrogen ligand attached to different metal centres we have seen that the charge circulation in the direction perpendicular to the inter-nuclear axis, *i.e.*, $\sigma \leftrightarrow \pi^*$ and $\pi \leftrightarrow \sigma^*$ transitions, is relatively small in contributing to the chemical shift change, by comparison with that in the direction parallel to this axis, *i.e.*, $\pi \leftrightarrow \pi^*$ transitions, if they are allowed by the molecular symmetry. For the free aryldiazenido ligand, a substantial electron density difference in the two π bonding directions, as we have seen earlier, makes the charge circulation of the $\pi \leftrightarrow \pi^*$ transitions a significant component in the paramagnetic shielding tensors. Therefore, changes in the chemical shift of N_α and N_β of this ligand upon coordination will be expected to be largely related to the changes of this component in the π bonding interactions with the metal centres. Therefore, in order to understand the magnitude of the coordination shifts of the singly bent aryldiazenido ligand, the changes of the charge density in the ligand π orbitals upon the coordination must be taken into account.

The different geometries adopted by N_2Ar in its free and coordinated states make a direct comparison of the shieldings of this ligand meaningless, but, the large number of the widely spread chemical shifts of this ligand in complexes still allows us to analyze the trend of the coordination shifts.

As we know from the discussions in the earlier sections, the π bonding character for a singly bent diazenido ligand is such as to accept π back bonding

strongly from the metal centre in a single-faced fashion, that is, in the molecular plane, due to its low-lying LUMO in this direction (refer to Figure 1.2). So, coordination to a transition metal centre will cause an increase of the ligand's π electron density in this direction, and consequently, an increase of the ΣQ term in the Pople equation 1.13, which, in turn, will cause a deshielding for both nitrogen nuclei of the ligand, but especially for N_α .

In a four-coordinate compound, such as [*trans*-IrCl($^{15}\text{N}_2\text{Ph}$)(PPh $_3$) $_2$] $^+$ or [*trans*-RhCl($^{15}\text{N}_2\text{Ph}$)(PPh $_3$) $_2$] $^+$ listed in Table 1.6, the π type of LUMO of the singly bent aryldiazenido ligand is located in the plane perpendicular to the P-M-P axis. In other words, the π back bonding into the LUMO of the diazenido ligand is only enhanced by the *trans* chloro ligand. However, in a six-coordinate octahedral complex, the LUMO of the singly bent diazenido ligand always tends to be in the plane which contains the metal and more π basic ligands (including the *trans* π basic ligand), due to the inherent orientation selectivity of this ligand, which has been discussed in section 1.3.2.1). Therefore, in this case, the π back bonding between the metal and the LUMO of the diazenido ligand is such that it is enhanced not only by the *trans* π base ligand, but also by either or both of two *cis* π base ligands. In other words, more charge density is expected to have been pushed from the metal centre to the diazenido ligand in six coordinate compounds than in the comparable four coordinate ones. Consequently, in a six-coordinate complex, the paramagnetic deshildings at both nitrogen nuclei will be expected to increase and result in a downfield shift of the chemical shifts for both nitrogens of the singly bent diazenido ligand. This can be seen clearly from the experimental data listed in Table 1.6. It is also worthy to note that in both the six- and four-coordinate complexes, ligand field splittings, respective to the singly bent diazenido ligand, are approximately same, so that the contribution to the

paramagnetic deshieldings from the perpendicular circulations of $\sigma \leftrightarrow \pi^*$ and $\pi \leftrightarrow \sigma^*$ of the diazenido ligand would, in principle, be same for both cases.

From the discussion in section 1.3.2, we know that for the singly bent diazenido compounds, there is a substantial difference of π -back bonding strengths between octahedral geometry (including the related square planar geometry) and trigonal bipyramidal geometry. A trigonal bipyramidal complex with the singly bent diazenido ligand in the unique equatorial position has been found to have the strongest π back bonding strength. Correspondingly, these give the lowest field chemical shifts for the nitrogen nuclei among the singly bent aryldiazenido compounds, and the deshieldings observed for the nitrogen nuclei, especially N_{α} , in such trigonal bipyramidal complexes span a wide range, of ca. 120 ppm (see Table 1.6). Notably, the diazenido ligand in $[\text{RhCl}(\text{}^{15}\text{N}_2\text{Ph})(\text{PhP}((\text{CH}_2)_3\text{PPh}_2)_2)]^+$,⁹⁷ which has the highest deshielding among such compounds, in fact, has been characterized in the solid state to have a doubly bent geometry.^{138, 139} This could be understood in that the π back acceptance by the diazenido ligand in this compound is very strong, and a fairly weak interaction exists in its solid structure;¹³⁹ together these two effects have promoted a charge transfer from the metal centre to this ligand resulting a formal 16e metal centre.

For the three-legged piano stool type of compounds, although they have been often considered as having a six-coordinate environment, (so they are listed in the group of six-coordinate compounds in Table 1.6), the frontier orbital interaction pattern makes their chemical behavior more similar to that of the five-coordinate compounds. This is also reflected in their NMR behavior in that the deshieldings of the nitrogen nuclei in these compounds are higher than those of normal octahedral compounds, but lower than those of trigonal bipyramidal

compounds. The reason for the lower deshieldings than in trigonal bipyramidal compounds can be fairly well understood in terms of the insufficient overlap of the filled metal orbital and the LUMO of the ligand in such compounds by comparison with that in trigonal bipyramidal compounds.

The importance of such correlations between the nitrogen chemical shifts of the singly diazenido bent ligand and the π back bonding strength in the M-N-NAr linkage is that nitrogen NMR measurements may provide us with a useful criterion of the degree of π back bonding strength in the studied systems. In fact, such correlations show excellent agreement with $\nu(\text{NN})$ IR stretching frequencies, the usual criterion for determining the π back bonding in diazenido compounds. The IR frequency of $\nu(\text{NN})$ for a singly bent diazenido ligand in normal octahedral or square planar molecules is in the range of 1800 ~ 1900 cm^{-1} , but it shifts down to a range of 1700 ~ 1800 cm^{-1} with a Cp or Cp* ligand present in the system. The lowest IR stretching frequencies for this ligand have been found in the trigonal bipyramidal molecules, and range from 1500 cm^{-1} to 1700 cm^{-1} .

Finally, the effect of substituents attached to the phenyl ring appears to be small by comparison with the coordination effect. For example, in Table 1.6, the compounds, $\text{RuCl}_3(\text{N}_2\text{R})(\text{PPh}_3)_2$ ($\text{R} = p\text{-C}_6\text{H}_4\text{X}$; $\text{X} = \text{Me}, \text{H}$ or NO_2), show only a negligible difference in their N_α chemical shifts.

Doubly Bent Aryldiazenido Complexes:

As shown in Table 1.7, the doubly bent diazenido ligands show dramatic deshielding for both N_α and N_β . The large paramagnetic deshielding found for this type of compound arises from the smaller ΔE term between the HOMO (lone pair orbital) and the LUMO (π^* orbital), (refer to Figure 1.2), of this ligand.

Table 1.7 Nitrogen Chemical Shifts and $^1J(N, N)$ Values of Doubly Bent Aryldiazenido Complexes

Complex	$\delta(N_\alpha)$ ppm	$\delta(N_\beta)$ ppm	$ ^1J(N, N) $ Hz	ref.
$[trans-IrBr(^{15}N_2Ph)(dppe)_2]^+$	220.5	158.3	18	a
$Cp^*Ir(p-^{15}NNC_6H_4OMe)(CO)(OEt)$	223.5	---	---	b
$[trans-RhCl(^{15}N_2Ph)(dppe)_2]^+$	224.6	135.3	18	a
$IrCl_2(^{15}N_2Ph)(CO)(PPh_3)_2$	241.4	150.2	18	a
$RhCl_2(^{15}N_2Ph)(PEtPh_2)_2$	241.0	---	16	a
$Cp^*Ir(p-^{15}NNC_6H_4OMe)(PPh_3)(H)$	271.9	---	---	b
$PtCl(^{15}N_2Ph)(PEt_3)_2$	285.0	162.0	19	a
$RhCl_2(^{15}NNPh)(PPh_3)_2$	298.4	---	---	a
$RhCl_2(p-^{15}NNC_6H_4NO_2)(PPh_3)_2$	327.1	---	---	a

a: Data source: reference 97.

b: This work.

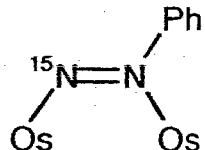
In fact, the δ -value for N_α is even greater than that of simple *trans*-RN=NR (R = Aryl) compounds, which generally resonate in the range 120 ~170 ppm.⁹⁷ This indicates that some coordination effect must also contribute to the observed chemical shifts. In fact, from the fragment orbital interactions built up in section 1.3.3, we know that, upon coordination to a non-Group VI metal centre in a low oxidation state, the energy gap between the HOMO and the LUMO of the doubly

bent diazenido ligand always tends to decrease, and this, in turn, will lead to a large deshielding for the nitrogens of this ligand.

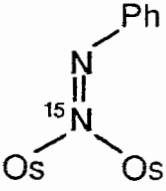
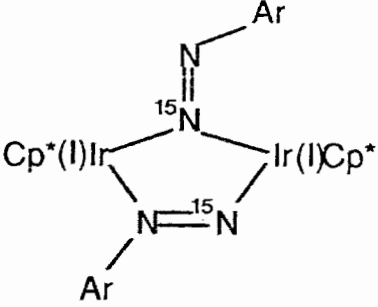
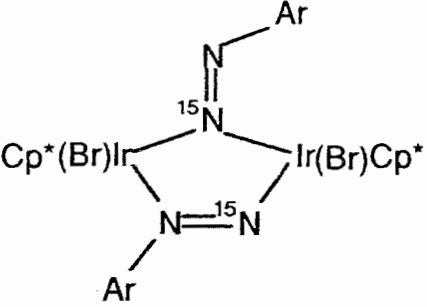
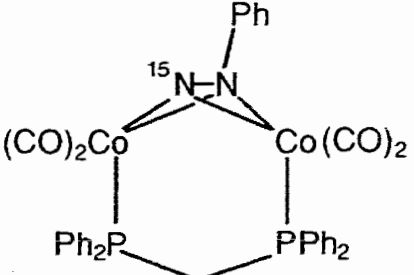
Bridging Aryldiazenido Complexes:

^{15}N NMR spectroscopy should be particularly suited to the study of complexes having two coordinated nitrogens such as in those in which the diazenido ligand bridges two metal centres. This is because the chemical shift is very sensitive to the inter-bond angle, especially when a nitrogen lone pair is involved. The versatility of the bridging types of the ligand is expected to cause a considerable range of chemical shifts. However, only a few such compounds have been made. The available chemical shifts are listed in Table 1.8, including compounds made in this research. Obviously, a systematization of these few chemical shift data in regard to structural character could be immature at this stage. However, a comparison on the chemical shifts of some bridging diazenido complexes will be discussed in Chapter III when we start to deal with those bridging diazenido compounds made in this work.

Table 1.8 Nitrogen Chemical Shifts of Bridging Aryldiazenido Complexes

Complex	$\delta(\text{N}_\alpha)$ ppm	Ref.
	313	140

(continue Table 1.8)

	68	140
	η^1 64.1 η^2 300.0	a
	η^1 69.8 η^2 303.4	a
	-165.0	141

a: This work

CHAPTER II

Syntheses, Dynamic NMR and X-ray Structures of $[\text{Cp}^*\text{Ir}(\text{C}_2\text{H}_4)\text{NO}]\text{BF}_4$ and $[\text{Cp}^*\text{Ir}(\text{C}_2\text{H}_4)(p\text{-N}_2\text{C}_6\text{H}_4\text{OMe})]\text{BF}_4$ — A comparison of the π acidity of ligands NO^+ and N_2Ar^+

2.1 Introduction

In transition metal nitrosyl and diazenido complexes, the analogous duality of the bonding modes of these two ligands characterized by linear and bent M-N-O and M-N-N structure skeletons has been recognized for many years.^{14, 34} This analogy, as we mentioned in Chapter I, facilitated the early development of transition metal diazenido and nitrosyl chemistry. However, it is also evident that there exist some differences between NO and N_2Ar in their complexes with regard to their syntheses and chemical reactivities.³⁴ For example, neutral $[\text{Mn}(\text{CO})_4\text{NO}]$ with a linear NO ligand can be readily formed by the reaction of *basic* $[\text{Mn}(\text{CO})_5]^-$ or $[\text{Mn}(\text{CO})_5\text{H}]$ precursors with nitrosonium ion, NO^+ .¹⁴² In contrast to this, no complex with a secured aryldiazenido ligand can be obtained even at -70°C by the similar reaction with N_2Ar^+ .¹⁴³ Protonation of the doubly bent aryldiazenido ligand at the N_α position is commonly observed,^{13, 34} and occurs also for the singly bent diazenido ligand in some five-coordinate complexes.⁸⁰ However, protonation of the linear nitrosyl ligand has not been seen.

In order to understand this diversity between NO and N_2Ar ligands, a knowledge of the electronic structure of the bonding between the metal and these two ligands is required. There have been several previous studies concerning this aspect, particularly emphasizing the relative importance of π -

bonding in analogous NO and N₂Ar compounds.^{16-17, 71, 144-149} However, the chemical and spectroscopic results advanced from these studies have shown an uncertainty in this aspect. Some of them suggest N₂Ar⁺ to be the stronger π -acceptor of the two,^{71, 144, 145} but others support the reverse.^{16, 17, 145-149} This ambiguity may well have generated a certain confusion in understanding the differential chemical behavior of these two species. This puzzling problem, together with others mentioned in section 1.1 of this Thesis, stimulated our interest in reassessing the bonding characteristics of a transition metal to NO⁺ and N₂Ar⁺ by using a suitable modeling system. The model based on the frontier fragment orbital interaction has been established and discussed in Chapter I. Within the framework of this model, the relative strength of the π bonding in analogous NO⁺ and N₂Ar⁺ compounds may be illustrated by using the concepts of "single-faced" and "cylinder-type" π -bonding ability for N₂Ar⁺ and NO⁺, respectively. For a highly symmetric molecule, such as octahedral, the metal centre has equal ability to donate its π electrons in all possible coordination directions due to its isotropically distributed $d\pi$ electrons. So, it would be expected that the NO⁺ ligand might accept π back-donation from the metal centre more effectively by using its doubly degenerate or the "cylinder-type" π^* orbitals than the N₂Ar⁺ ligand which only has its intrinsic "single-faced" π -accepting ability. This would possibly account for the observations that NO⁺ was the better π -acceptor of these two ligands. However, for a complex with low symmetry, the π back-bonding potential of the metal centre could well be anisotropic. So a π -acid ligand in this complex can get the efficient π back-donation from the metal centre only in one direction no matter whether the ligand has a "cylinder-type" or "single-faced" π^* orbitals. Since the N₂Ar⁺ ligand has

lower LUMO than NO^+ , (refer to Section 1.2.2.1 and 1.2.2.1), it will be expected that N_2Ar^+ ligand in this latter case becomes the better π -acceptor.

One of the challenges generally associated with modeling the electronic structure of a molecule is to design a new molecule strictly according to the model and to see whether the chemical behavior of this designed molecule is consistent with what the model anticipates. In order to test the relative importance of the π back-bonding for NO^+ and N_2Ar^+ ligands, a convincing target molecule, we believe, should have low symmetry, because the results obtained from the low symmetry molecule will be more straightforward in relating to its electronic structure.

The title compounds provide an excellent opportunity to compare the bonding of a linear nitrosyl and a singly bent aryldiazenido ligand in identical low symmetry chemical environments. Since both of the title compounds are new, the syntheses, together with their IR, NMR studies and X-ray structure determinations will be reported here.

2.2. Experimental Section

General

All solvents were dried and purified by the standard methods and freshly distilled under nitrogen immediately before use. All reactions and manipulations were carried out in standard Schlenk ware, connected to a switchable double manifold providing vacuum and nitrogen.

Infrared spectra were measured for solutions in CaF_2 cells by using a Bomem Michelson 120 FTIR instrument. Some of the routine ^1H NMR spectra were recorded at 100 MHz by using a Varian SY-100 Fourier Transform Spectrometer. Dynamic proton NMR and ^{13}C , ^{14}N , and ^{15}N NMR spectra were

obtained by Mrs. M. Tracey of the NMR service of Simon Fraser University on a Bruker AMX-400 Fourier Transform instrument at operating frequencies of 400.1, 100.6, 28.9 and 40.5 MHz for ^1H , ^{13}C , ^{14}N and ^{15}N respectively. Chemical shifts (δ) are reported in ppm, downfield positive, relative to tetramethylsilane (TMS) for ^1H and ^{13}C spectra, and relative to MeNO_2 and $\text{Me}^{15}\text{NO}_2$ for ^{14}N and ^{15}N spectra respectively.

Temperatures of the samples used in the dynamic NMR studies were obtained from the temperature controller of the AMX-400 spectrometer. The thermocouple of the temperature controller had been previously calibrated with an accuracy ± 0.2 °C in the temperature range concerned. Free energies of activation were calculated from the Eyring equation (Eqn.2.1)¹⁵⁰

$$\Delta G^\ddagger = -R T_c \ln \frac{\pi \Delta \nu h}{\sqrt{2} k T_c} \quad (\text{Eqn. 2.1})$$

$$= a T_c \left[9.972 + \log \left(\frac{T_c}{\Delta \nu} \right) \right]$$

where $\Delta \nu$ is the chemical shift difference of the coalescing resonances in the absence of exchange, T_c is the coalescence temperature, and R , h and k have their normal thermodynamic significance. The reduced parameter $a=1.914 \times 10^{-2}$ $\text{kJ.mol}^{-1}.\text{K}^{-1}$.

Mass spectra were obtained by Mr G. Owen on a Hewlett-Packard Model 5985 GC-MS spectrometer equipped with a fast atom bombardment (FAB) probe (xenon source, Phrasor Scientific, Inc., accessory), and utilized samples dispersed or dissolved in sulfolane. The pattern of the envelope of the fragment ions was matched with that simulated by computer for the species in question. The masses are quoted for the ^{193}Ir isotope. Microanalyses for elements C, H

and N were performed by Mr M-K. Yang of the Microanalytical Laboratory of Simon Fraser University.

Starting Materials

Bisethylene pentamethylcyclopentadienyl iridium was synthesized according to the method provided in reference [151]. *Para*-methoxyphenyl-diazonium tetrafluoroborate was prepared by the standard procedures from *para*-methoxyaniline (Aldrich) and sodium nitrite, and purified periodically by recrystallization from acetone and diethyl ether. The diazonium salt substituted with ^{15}N at the terminal nitrogen (N_α) was prepared by using $\text{Na}^{15}\text{NO}_2$ (95% ^{15}N , MSD Isotopes).

Preparation of $[\text{Cp}^*\text{Ir}(\text{C}_2\text{H}_4)(p\text{-N}_2\text{C}_6\text{H}_4\text{OMe})]\text{BF}_4$ (1)

$\text{Cp}^*\text{Ir}(\text{C}_2\text{H}_4)_2$ (100 mg, 0.26 mmol.) was dissolved into 5 mL acetone in a 100 mL Schlenk tube equipped with a magnetic stirring bar. The solution was cooled for 15 minutes at -78°C , (dry ice / ethanol bath), by immersing at least 2/3 length of the Schlenk tube into the bath, then $[(p\text{-N}_2\text{C}_6\text{H}_4\text{OMe})]\text{BF}_4$ (18 mg, 0.26 mmol) pre-dissolved in 5 mL acetone was added dropwise by pipette in such a way that the drops of the diazonium salt solution first touched the upper part of the Schlenk tube and then slowly flowed down the glass wall into the reaction mixture. Directly adding the diazonium salt solution into the reaction mixture without allowing it to cool in this way generally promoted other side reactions and resulted in an oily product. The reaction mixture was continuously stirred during and after addition of the diazonium salt solution for about one hour at -78°C . The colour of the reaction solution changed from colourless to yellow then to orange-red. When the reaction had finished (IR monitoring the disappearance of the band at 2253 cm^{-1} due to the NN vibration of the free

diazonium ion), hexane was added slowly until no more solid was precipitated. The supernatant solution was removed carefully by pipette and the remaining brown solid washed twice with *ca.* 20 mL of hexane affording the analytically pure product (1) almost quantitatively. Recrystallization of the product (1) from acetone / hexane at -10 °C (in the refrigerator) gave dark red crystals of compound (1) in greater than 90% yield. More product could be recovered as fine crystals by evaporation of the supernatant solution. M. P. 150 ~ 155 °C. IR $\nu(\text{NN})$ 1710 cm^{-1} (KBr), 1724 cm^{-1} (EtOH); ^1H NMR (400 MHz, CDCl_3): δ 2.25s (15H, C_5Me_5), 3.25s,b (4H, C_2H_4), 3.91s (3H, OMe), 7.23q (4H, C_6H_4); $^{13}\text{C}\{^1\text{H}\}$ NMR (CDCl_3): δ 9.61 (C_5Me_5), 49.32 (C_2H_4), 56.01 (OMe), 100.89 (C_5Me_5), 111.77, 117.08, 125.21 and 164.09 (C_6H_4); ^{14}N NMR ($\text{MeNO}_2\text{-}d_3$): δ -107s,b (N_β), -2.86s,b (N_α), FABMS (m/z): 491 (M^+), 463 ($\text{M}^+ - \text{C}_2\text{H}_4$), 433 ($\text{M}^+ - \text{C}_2\text{H}_4 - \text{OMe}$), 405 ($\text{M}^+ - \text{C}_2\text{H}_4 - \text{N}_2 - \text{OMe}$), 354 ($\text{M}^+ - \text{N}_2\text{C}_6\text{H}_4\text{OMe} - 2\text{H}$); Anal. (*Calcd.*): C, 39.52; H, 4.54; N, 4.85. (*Found*): C, 39.11; H, 4.53; N, 4.84.

Preparation of $[\text{Cp}^*\text{Ir}(\text{C}_2\text{H}_4)(p\text{-}^{15}\text{NNC}_6\text{H}_4\text{OMe})]\text{BF}_4$ (1a)*

The $^{15}\text{N}_\alpha$ isotope substituted complex (1a) was synthesized analogous to compound (1), by using $(p\text{-}^{15}\text{NNC}_6\text{H}_4\text{OMe})\text{BF}_4$. IR $\nu(^{15}\text{NN})$: 1675 cm^{-1} (KBr); ^{15}N NMR (acetone- d_6): -2.26s (N_α).

Preparation of $[\text{Cp}^*\text{Ir}(\text{C}_2\text{H}_4)(\text{NO})]\text{BF}_4$ (2)

To a solution of $\text{Cp}^*\text{Ir}(\text{C}_2\text{H}_4)_2$ (100 mg, 0.26 mmol.) in 10 mL acetone at a temperature < -10 °C was slowly added an equimolar amount of $[\text{NO}][\text{BF}_4]$

*: The number followed by a letter a denotes a $^{15}\text{N}_\alpha$ enriched sample. This convention will be used throughout this Thesis.

(freshly washed with CH_2Cl_2) and the reaction mixture was stirred for one hour at this temperature. The colour changed from colourless to grey-green in the first 5 minutes after the addition and remained the same until the reaction finished (monitored by IR). The solution was evaporated *in vacuo* to ca. 5 mL, and then diethyl ether was added slowly to precipitate the grey-green-coloured product (2). The supernatant solvent was removed carefully by pipette and the remaining solid product was washed twice with excess diethyl ether. Recrystallization of compound (2) from acetone/diethyl ether afforded the dark-brown crystalline product in ca. 90% yield. IR $\nu(\text{NO})$: 1822 cm^{-1} (acetone), 1820 cm^{-1} (EtOH); ^1H NMR (100 MHz, CDCl_3): δ 2.34s (15H, C_5Me_5), 3.47q (4H, C_2H_4); $^{13}\text{C}\{^1\text{H}\}$ NMR (100MHz, CDCl_3): δ 9.82 (C_5Me_5), 47.06 (C_2H_4) and 105.16 (C_5Me_5); FABMS (m/z): 386 (M^+), 358 ($\text{M}^+ - \text{C}_2\text{H}_4$), 356 ($\text{M}^+ - \text{NO}$); Anal. (*Calcd.*): C, 30.52; H, 4.05; N, 2.97. (*Found*): C, 30.79; H, 4.03; N, 2.91.

X-ray crystal structure determination of $[\text{Cp}^*\text{Ir}(\text{C}_2\text{H}_4)(p\text{-N}_2\text{C}_6\text{H}_4\text{OMe})]\text{BF}_4$ (1)

Crystals suitable for X-ray structure analysis were obtained by recrystallization of compound (1) from acetone and diethyl ether at $-10\text{ }^\circ\text{C}$. After examination by microscopy with polarized light, a large brown single crystal was slowly ground into a sphere and mounted into a capillary tube, the diameter of which was just a good-fit with that of the crystal to keep the crystal motionless. The crystal was then well centered in the X-ray beam of an Enraf Nonius CAD-4F diffractometer equipped with graphite monochromatized $\text{MoK}\alpha$ radiation.

Intensity data were collected at $-40 \pm 1\text{ }^\circ\text{C}$. A final unit cell was determined by least squares procedures from the setting angles of 25 well-centered reflections (with $9^\circ \leq \theta \leq 22^\circ$) chosen from a random variety of points in reciprocal space. A monoclinic unit cell was first assumed and then proven by

investigation of symmetry-related reflections from the intensity data file. Selected crystallographic and experimental parameters are given in Table 2.1.

A total of 3716 independent reflections were measured, of which 2611 reflections were classed as observed ($I_o \geq 2.5\sigma(I_o)$) and used in the structure calculation and refinement. Three intensity standards were measured every one and half hour of acquisition time, and showed no significant change in intensity during the data collection.

Lorentz, polarization and spherical absorption corrections^{152, 153} were applied to convert the 2611 intensity data into the relative structure factor amplitudes and their esds.

The structure was solved by Patterson and conventional Fourier methods and refined by using full matrix least-squares procedures. The assumption that the space group was centrosymmetric $P2_1/n$ * was confirmed by the successful solution and refinement of the structure. Anisotropic thermal parameters for Ir, F and O atoms and the C atoms in the methyl groups and ethylene ligand, and isotropic thermal parameters for other atoms were included in the final refinement. The refinement was considered complete when the maximum shift/esd was < 0.01 . The positions of hydrogen atoms were generated with $d(C-H) = 0.95 \text{ \AA}$ by the computer program.¹⁵⁴ A total of 54 atoms and 183 variables against 2611 observations were involved in the final refinement. The quantity minimized by the least-squares program was $\sum w(|F_o| - |F_c|)^2$, where w is the unit weight. The analytical forms of the scattering factors for neutral atoms were used.¹⁵⁵

*: The standard space group symbol of $P2_1/n$ is $P2_1/c$, which could be obtained by a rotation of a, c axes into the diagonal positions.

Inspection of the residuals ordered in the ranges of $\sin\theta/\lambda$, F_0 and the values of individual indexes showed no unusual features or trends in the unit weight scheme. The largest peak in the final difference Fourier map had an electron density $1.2 \text{ e}^-/\text{\AA}^3$ and was located at 0.94 \AA from the Ir atom. Positional parameters and thermal parameters of non-hydrogen atoms are listed in Table 2.2 and selected bond distances and angles are given in Table 2.3. The computing programs used for data reduction, structure solution and refinement were from *NRC.VAX Crystal Structure System*.¹⁵⁴ All computations were carried out on an in-house Micro VAX-II computer. A perspective view of the molecular cation of (1) is given in Figure 2.1.

X-ray Crystal Structure Determination of $[\text{Cp}^*\text{Ir}(\text{C}_2\text{H}_4)(\text{NO})]\text{BF}_4$ (2)

Dark brown crystals of (2) were obtained from acetone and diethyl ether. Most of the crystals were found to be perfectly twinned by examination under the polarizing microscope. A tetragonal-shaped crystal was carefully cut from a twinned crystal and mounted on a glass fibre. Intensity data were collected at $23 \pm 1 \text{ }^\circ\text{C}$ with an Enraf-Nonius CAD-4F diffractometer using graphite monochromatized $\text{Mo K}\alpha$ radiation. Lattice parameters were determined as above from 25 reflections ($14^\circ \leq \theta < 20^\circ$). A total of 2922 reflections were measured; 1923 of the 2706 unique reflections were classed as observed with $I_0 \leq 2\sigma(I_0)$. The scan range was $0.85 + 0.35\tan\theta$ and scan speed $0.72\text{-}2.75 \text{ deg./min}$. The intensities of two standards (0, 0, -2; 1, -4, 0) were measured every hour of acquisition time, showed no long term change and had a RMS deviation of 1.4%. The data reduction included Lorentz and polarization corrections and an analytical absorption correction^{152, 153} based on the psi-scan data of two reflections (with $\kappa > 82^\circ$); transmission was 0.355 - 0.648. The

structure was solved by Patterson synthesis and refined by full matrix least-squares and Fourier methods. The assumption that the space group is centric $P2_1/n$ was confirmed by the following successful refinement. Calculated hydrogen positions ($d(C-H) = 0.95 \text{ \AA}$) were used in the final model. Disc shaped thermal vibration ellipsoids of F atoms in the anion BF_4^- indicated a spherically disordered BF_4^- , which was successfully modelled by three BF_4^- s with a total occupancy equal to one. The F atoms, given the same anisotropic thermal parameter, were allowed to ride on the corresponding B atom in each BF_4^- . Final refinement included anisotropic thermal parameters for Ir, O, C and N and isotropic thermal parameters for other non-hydrogen atoms. Hydrogen atoms were included in fixed positions in structure factor calculations. Refinement was considered complete when the shift/error ratio was less than 0.002; 161 parameters against 30 atoms were varied. Counter weights w were used ($w = 1/(kF_o^2 + \sigma^2 F_o)$ and $k = 0.0003$). The largest positive peak in the final electron density map was $1.1(2) \text{ e\AA}^{-3}$ and was located 0.88 \AA from the Ir atom, and the largest negative peak was -0.87 e\AA^{-3} . The analytical form of scattering factors for the neutral atoms was used,¹⁵⁵ and all non-hydrogen scattering factors were corrected for real and imaginary components of anomalous dispersion. Inspection of $w\Delta^2$ as a function of $\sin\theta/\lambda$, F_o and values of h , k , l showed no unusual features or trends. Selected crystallographic and experimental parameters are given in Table 2.1. Positional thermal parameters are listed in Table 2.4., and bond distances and angles are listed in Table 2.5. Programs used for data reduction were from the *NRC VAX Crystal Structure System*¹⁵⁴ and for structure solution were from *Crystals*¹⁵⁶ and run on a micro VAX-II computer. The diagram was generated with the program ORTEP. A perspective view of the cation $[Cp^*Ir(C_2H_4)(NO)]^+$ is given in Figure 2.2.

Table 2.1. Crystallographic Data for the Structure Determinations of (1) and (2)

Formula	[Cp*Ir(C ₂ H ₄)(<i>p</i> -N ₂ C ₆ H ₄ OMe)]BF ₄ (1)	[Cp*Ir(C ₂ H ₄)(NO)]BF ₄ (2)
Crystal System	Monoclinic	Monoclinic
Space Group	P 2 ₁ /n (No.14) ^a	P 2 ₁ /n (No.14) ^a
a (Å)	8.5780(10)	7.4540(10)
b (Å)	20.5310(23)	24.381(3)
c (Å)	12.0310(15)	8.5360(10)
β (°)	93.500(10)	93.850(10)
Z	4	4
FW	577.22	472.31
ρ (g/cm ³)	1.814	2.027
μ (MoKα) (cm ⁻¹)	63.4	86.3
Crystal Size (mm)	0.30 (∅)	0.30 x 0.20 x 0.20
λ (Å)	0.71069	0.71069
Transmission	0.238 - 0.253	0.355 - 0.648
Min - Max 2θ (°)	0 - 50	2 - 50
Scan Type	ω - 2θ	ω - 2θ
Min h, k, l	-10, 0, 0	-8, 0, 0
Max h, k, l	10, 24, 14	8, 28, 10
R _f ^b	0.0281	0.0336
R _w ^c	0.0308	0.0412
GOF	1.10	1.50

a: See the footnote of page 126

b: $R_f = \frac{\sum (|F_o| - |F_c|)}{\sum |F_o|}$ for observed data

c: $R_w = \frac{[\sum w(|F_o| - |F_c|)^2 / \sum w|F_o|^2]^{1/2}}$ for observed data

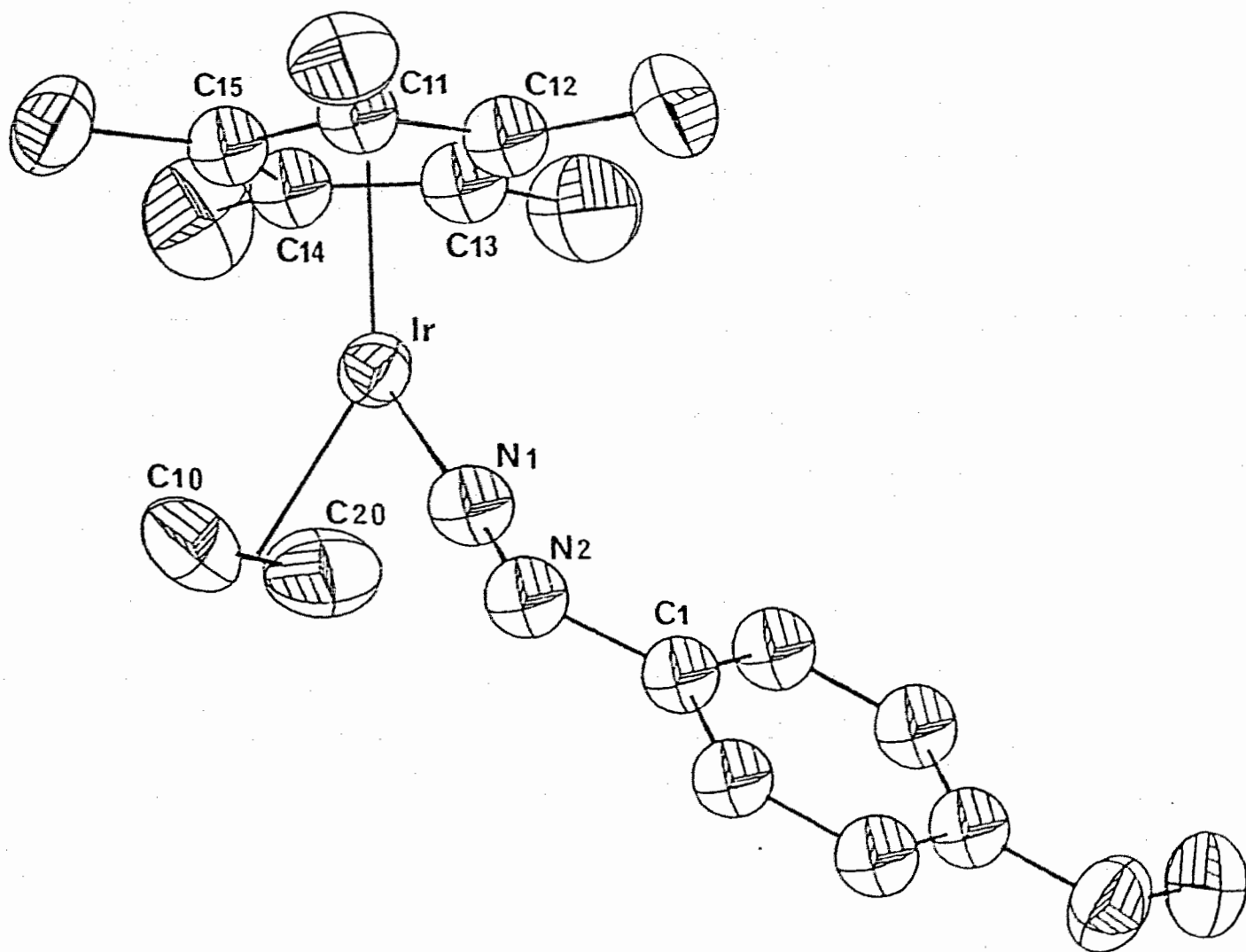


Figure 2.1 A perspective view of the cation $[\text{Cp}^*\text{Ir}(\text{C}_2\text{H}_4)(p\text{-N}_2\text{C}_6\text{H}_4\text{OMe})]^+$ of (1). (The thermal ellipsoids represent 50 % probability contours).

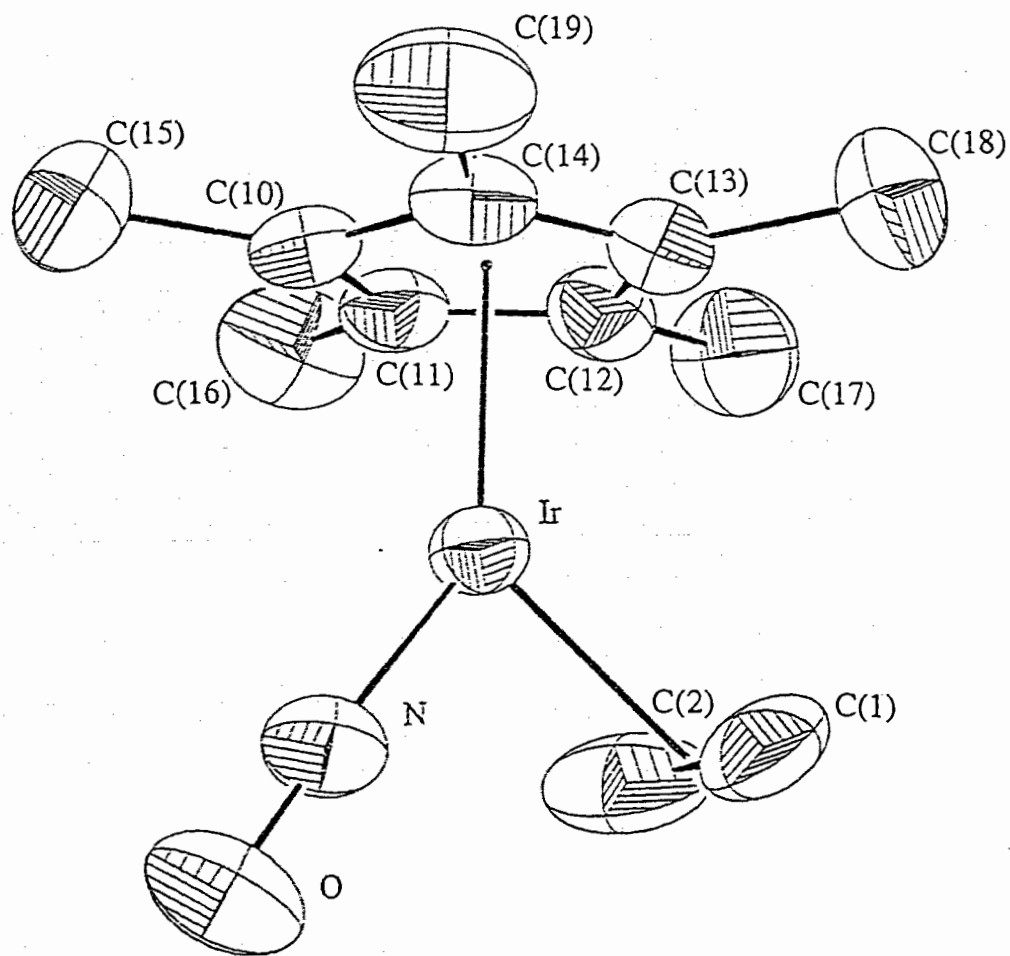


Figure 2.2 A perspective view of the cation $[\text{Cp}^*\text{Ir}(\text{C}_2\text{H}_4)(\text{NO})]^+$ of (2).
(The thermal ellipsoids represent 50 % probability contours).

Table 2.2 Positional and Thermal Parameters for Compound (1) ^a

Atom	x/a	y/b	z/c	Biso
Ir	0.21120(3)	0.11305(2)	0.09575(3)	
F1	0.1820(8)	0.2909(3)	0.6869(6)	
F2	0.2383(11)	0.2333(5)	0.5402(6)	
F3	0.3134(10)	0.201(4)	0.7052(8)	
F4	0.0674(10)	0.1970(4)	0.6485(9)	
O	0.8281(7)	0.0063(3)	0.5538(5)	
C	0.8732(11)	0.0666(5)	0.6072(7)	
C10	0.3385(12)	0.1037(5)	-0.0558(8)	
C20	0.4227(11)	0.1433(5)	0.0196(9)	
C21	-0.1459(11)	0.0543(5)	0.1378(8)	
C22	0.0302(13)	0.1366(5)	0.3333(8)	
C23	0.1984(13)	0.2575(5)	0.2220(10)	
C24	0.1206(14)	0.2498(5)	-0.0420(9)	
C25	-0.0923(11)	0.1237(5)	-0.0934(8)	
B	0.1948(14)	0.2312(6)	0.6445(10)	5.44(23)
N1	0.3172(7)	0.0451(3)	0.1597(5)	4.01(13)
N2	0.3875(8)	-0.0018(3)	0.1962(5)	3.98(13)
C11	-0.0444(8)	0.1124(4)	0.1235(6)	3.53(13)
C12	0.0345(9)	0.1498(4)	0.2096(6)	4.00(15)
C13	0.1094(9)	0.2036(4)	0.1593(7)	4.05(15)
C14	0.0760(9)	0.1999(4)	0.0415(6)	3.97(15)
C15	-0.0197(9)	0.1435(4)	0.0196(6)	3.87(15)
C1	0.5016(8)	0.0049(4)	0.2881(6)	3.49(14)

Continue Table 2.2

C2	0.5372(9)	0.0637(4)	0.3401(7)	4.07(15)
C3	0.6476(9)	0.0667(4)	0.4274(7)	4.28(16)
C4	0.7211(9)	0.0100(4)	0.4656(7)	4.00(15)
C5	0.6868(9)	-0.0490(4)	0.4124(7)	4.14(16)
C6	0.5757(9)	-0.0519(4)	0.3242(6)	3.73(14)

Atom	U ₁₁	U ₂₂	U ₃₃	U ₁₂	U ₁₃	U ₂₃
Ir	3.889(15)	4.150(15)	4.073(15)	0.075(17)	-0.257(10)	-0.250(17)
F1	13.3(6)	6.2(4)	12.4(5)	0.5(4)	-1.8(4)	-0.7(4)
F2	19.0(9)	21.3(10)	9.4(6)	-7.9(8)	4.3(6)	-3.1(6)
F3	16.8(8)	10.1(6)	18.0(8)	4.7(6)	-3.2(6)	1.5(6)
F4	12.1(6)	11.7(6)	29.3(12)	-6.8(5)	8.5(7)	-6.8(7)
O	6.9(4)	7.1(4)	6.2(4)	1.0(3)	-1.5(3)	0.3(3)
C	8.1(7)	7.0(6)	5.6(5)	-0.6(5)	-0.7(5)	-0.7(5)
C10	8.1(7)	7.6(7)	6.5(6)	0.7(6)	2.8(5)	0.0(5)
C20	5.2(5)	8.8(8)	9.9(8)	-0.9(5)	1.7(5)	0.7(6)
C21	6.1(6)	6.6(6)	8.9(7)	-1.0(5)	0.6(5)	0.6(5)
C22	9.2(7)	10.3(9)	5.2(5)	0.9(6)	1.2(5)	-0.3(5)
C23	8.4(7)	7.1(7)	10.4(8)	-0.6(6)	0.2(6)	-2.3(6)
C24	11.5(9)	6.3(6)	8.5(7)	0.0(6)	1.1(6)	2.6(6)
C25	6.9(6)	8.5(7)	6.4(6)	0.5(5)	-1.9(5)	-0.7(5)

a: Thermal parameters (x100).

Table 2.3. Selected Bond Lengths (Å) and Inter-Bond Angles (deg.) of (1)

(a) Bond Lengths

Ir-C(10)	2.190(8)	Ir-C(20)	2.172(9)
N(1)-N(2)	1.205(9)	Ir-N(1)	1.811(7)
N(2)-C(1)	1.438(10)	Ir-C(11)	2.238(7)
C(11)-C(12)	1.427(11)	Ir-C(12)	2.236(8)
C(11)-C(15)	1.430(11)	Ir-C(13)	2.211(8)
C(12)-C(13)	1.431(11)	Ir-C(14)	2.204(8)
C(13)-C(14)	1.431(11)	Ir-C(15)	2.220(8)
C(14)-C(15)	1.434(11)	O-C	1.436(11)
O-C(4)	1.362(10)	C(1)-C(2)	1.384(11)
C(1)-C(6)	1.385(11)	C(2)-C(3)	1.372(11)
C(3)-C(4)	1.389(12)	C(4)-C(5)	1.394(12)
C(5)-C(6)	1.384(11)	C(10)-C(20)	1.387(16)
C(21)-C(11)	1.494(12)	C(22)-C(12)	1.514(12)
C(23)-C(13)	1.518(13)	C(24)-C(14)	1.501(13)
C(25)-C(15)	1.517(11)		

(b) Inter-Bond Angles

C(10)-Ir-C(20)	37.1(4)	C(10)-Ir-N(1)	91.3(3)
C(20)-Ir-N(1)	89.3(3)	Ir-N(1)-N(2)	176.2(6)
N(1)-N(2)-C(1)	120.4(6)	Ir-C(11)-C(21)	127.3(6)
Ir-C(12)-C(22)	126.8(6)	Ir-C(13)-C(23)	126.0(6)
Ir-C(14)-C(24)	126.8(6)	Ir-C(15)-C(25)	127.0(6)
C(21)-C(11)-C(12)	126.9(7)	C(21)-C(11)-C(15)	125.2(7)

Continue Table 2.3

C(12)-C(11)-C(15)	107.8(7)	C(22)-C(12)-C(11)	125.3(8)
C(22)-C(12)-C(13)	126.3(8)	C(23)-C(13)-C(12)	125.2(8)
C(23)-C(13)-C(14)	126.6(8)	C(24)-C(14)-C(13)	125.6(8)
C(24)-C(14)-C(15)	126.5(8)	C(25)-C(15)-C(11)	126.1(7)
C(25)-C(15)-C(14)	125.5(7)	C-O-C(4)	116.8(7)
N(2)-C(1)-C(2)	123.5(7)	N(2)-C(1)-C(6)	116.0(7)
Ir-C(10)-C(20)	70.8(5)	Ir-C(20)-C(10)	72.2(5)
O-C(4)-C(3)	125.1(7)	O-C(4)-C(5)	115.0(7)

Table 2.4 Positional and Thermal Parameters for (2) *a, b*

Atom	x/a	y/b	z/c	Biso
Ir	0.24892(5)	0.39146(1)	0.43954(4)	
O	0.4601(14)	0.4664(4)	0.6423(10)	
N	0.3768(13)	0.4383(4)	0.5580(10)	
C(1)	0.3762(19)	0.3183(5)	0.5467(14)	
C(2)	0.2374(20)	0.3339(6)	0.6333(14)	
C(10)	0.0767(14)	0.4353(4)	0.2544(11)	
C(11)	-0.0313(13)	0.3956(4)	0.3230(11)	
C(12)	0.0464(15)	0.3442(4)	0.2935(12)	
C(13)	0.1979(15)	0.3522(4)	0.2033(12)	
C(14)	0.2204(14)	0.4081(4)	0.1773(12)	
C(15)	0.0408(19)	0.4960(4)	0.2470(15)	
C(16)	-0.1992(15)	0.4066(6)	0.4015(17)	

Continue Table 2.4

C(17)	-0.0376(20)	0.2896(5)	0.3355(16)		
C(18)	0.3033(21)	0.3066(6)	0.1294(16)		
C(19)	0.3484(18)	0.4351(6)	0.0790(13)		
B(1)	0.7971(16)	0.3561(5)	0.8830(14)	0.0715(42)	
F(1)	0.8225(23)	0.3149(6)	0.7680(19)	0.1162(27)	
F(2)	0.9564(21)	0.3856(7)	0.9103(23)	0.1162(27)	
F(3)	0.7419(26)	0.3315(7)	1.0189(17)	0.1162(27)	
F(4)	0.6596(22)	0.3914(7)	0.8185(22)	0.1162(27)	
B(2)	0.8070(27)	0.3482(8)	0.8819(23)	0.0715(42)	
F(11)	0.6575(35)	0.3273(13)	0.9560(36)	0.1162(27)	
F(12)	0.7656(43)	0.3526(13)	0.7197(24)	0.1162(27)	
F(13)	0.8556(46)	0.3996(9)	0.9460(38)	0.1162(27)	
F(14)	0.9519(34)	0.3108(12)	0.9088(37)	0.1162(27)	
B(3)	0.7983(23)	0.3599(6)	0.8951(20)	0.0715(42)	
F(21)	0.9668(28)	0.3722(11)	0.8368(31)	0.1162(27)	
F(22)	0.8073(38)	0.3090(7)	0.9726(29)	0.1162(27)	
F(23)	0.7598(35)	0.4017(9)	1.0049(29)	0.1162(27)	
F(24)	0.6630(33)	0.3595(11)	0.7738(27)	0.1162(27)	

Atom	U ₁₁	U ₂₂	U ₃₃	U ₁₂	U ₁₃	U ₂₃
Ir	389(2)	441(2)	359(2)	6(2)	-18(1)	17(2)
O	1194(80)	911(66)	855(65)	-299(50)	-427(58)	-100(56)
N	640(60)	632(58)	575(55)	-69(40)	-219(44)	-6(43)

Continue Table 2.4

C(1)	1010(93)	507(61)	737(79)	201(60)	-350(59)	8(60)
C(2)	1049(98)	1000(106)	551(72)	332(61)	-172(59)	-320(84)
C(10)	538(55)	574(50)	364(50)	51(40)	-122(38)	54(40)
C(11)	446(47)	615(49)	397(48)	-0(43)	-89(36)	12(40)
C(12)	602(60)	505(46)	456(53)	-59(43)	-74(41)	-76(41)
C(13)	716(66)	539(46)	372(51)	-37(42)	4(42)	125(46)
C(14)	496(55)	637(51)	356(47)	17(42)	-50(37)	-45(42)
C(15)	961(98)	575(55)	795(87)	88(65)	-94(76)	87(67)
C(16)	381(57)	1309(123)	878(91)	-137(84)	24(53)	1(67)
C(17)	1075(113)	566(67)	914(97)	-5(64)	-68(84)	-253(69)
C(18)	1266(130)	963(105)	766(91)	-267(76)	9(85)	515(90)
C(19)	786(86)	1089(108)	474(65)	102(62)	138(56)	-112(73)

=====
a: Disordered BF_4^- was modeled by three BF_4^- 's with the occupancies 0.4404, 0.2477 and 0.3119 respectively

b: Anisotropic temperature factors (U_{ij}) x1000

Table 2.5 Selected Bond Lengths (Å) and Inter-Bond Angles (°) for (2)

<u>Bond lengths</u>					
Ir-N	1.762(9)	Ir-C(1)	2.19(1)	Ir-C(2)	2.17(1)
Ir-Cp* centroid	1.89	Ir-C(10)	2.239(9)	Ir-C(11)	2.255(9)
Ir-C(12)	2.22(1)	Ir-C(13)	2.24(1)	Ir-C(14)	2.27(1)
O-N	1.15(1)	C(1)-C(2)	1.37(2)	C(10)-C(11)	1.41(1)
C(11)-C(12)	1.41(1)	C(12)-C(13)	1.42(1)	C(13)-C(14)	1.39(1)

Continue Table 2.5

C(14)-C(10)	1.45(1)	C(10)-C(15)	1.51(1)	C(11)-C(16)	1.48(2)
C(12)-C(17)	1.52(1)	C(13)-C(18)	1.52(1)	C(14)-C(19)	1.47(1)
B(1)-F(1)	1.4263(2)	B(1)-F(2)	1.3946(2)	B(1)-F(3)	1.3924(3)
B(1)-F(4)	1.4204(3)	B(2)-F(11)	1.4119(5)	B(2)-F(12)	1.4025(2)
B(2)-F(13)	1.4059(5)	B(2)-F(14)	1.4203(3)	B(3)-F(21)	1.4135(4)
B(3)-F(22)	1.4055(3)	B(3)-F(23)	1.4270(3)	B(3)-F(24)	1.3960(4)

Inter-Bond Angles

N-Ir-C(1)	94.9(4)	C(10)-C(11)-C(12)	106.4(9)
N-Ir-C(2)	91.6(5)	C(11)-C(12)-C(13)	109.0(9)
N-Ir-Cp* centroid	141.8	C(12)-C(13)-C(14)	109.2(9)
C(1)-Ir-C(2)	36.4(5)	C(13)-C(14)-C(10)	105.9(9)
C(1)-Ir-Cp* centroid	121.3	C(14)-C(10)-C(11)	109.5(9)
C(2)-Ir-Cp* centroid	124.2	F(1)-B(1)-F(2)	109.09(2)
Ir-N-O	175.8(9)	F(1)-B(1)-F(3)	109.26(1)
Ir-C(1)-C(2)	71.1(7)	F(1)-B(1)-F(4)	106.62(2)
Ir-C(2)-C(1)	72.5(7)	F(2)-B(1)-F(3)	112.28(2)
Ir-C(10)-C(15)	126.2(8)	F(2)-B(1)-F(4)	109.66(1)
Ir-C(11)-C(16)	126.4(8)	F(3)-B(1)-F(4)	109.76(2)
Ir-C(12)-C(17)	126.6(8)	F(11)-B(2)-F(12)	110.01(4)
Ir-C(13)-C(18)	128.6(8)	F(11)-B(2)-F(13)	109.72(4)
Ir-C(14)-C(19)	128.5(8)	F(11)-B(2)-F(14)	108.12(2)
C(15)-C(10)-C(11)	125.9(10)	F(12)-B(2)-F(13)	110.47(3)
C(15)-C(10)-C(14)	124.3(10)	F(12)-B(2)-F(14)	108.91(3)
C(16)-C(11)-C(10)	125.9(11)	F(13)-B(2)-F(14)	109.58(4)

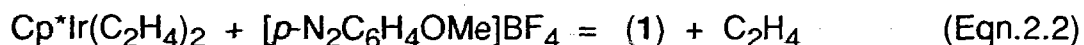
Continue Table 2.5

C(16)-C(11)-C(12)	127.6(10)	F(21)-B(3)-F(22)	109.70(4)
C(17)-C(12)-C(11)	123.6(11)	F(21)-B(3)-F(23)	107.59(3)
C(17)-C(12)-C(13)	126.9(10)	F(21)-B(3)-F(24)	110.81(3)
C(18)-C(13)-C(12)	125.0(10)	F(22)-B(3)-F(23)	109.09(2)
C(18)-C(13)-C(14)	125.3(11)	F(22)-B(3)-F(24)	110.65(3)
C(19)-C(14)-C(10)	125.5(10)	F(23)-B(3)-F(24)	108.92(3)
C(19)-C(14)-C(13)	128.3(11)		

2.3. Syntheses and Characterization

Synthesis and Characterization of $[\text{Cp}^*\text{Ir}(\text{C}_2\text{H}_4)(p\text{-N}_2\text{C}_6\text{H}_4\text{OMe})]\text{BF}_4$ (**1**)

The careful, slow addition of a solution of para-methoxyphenyldiazonium tetrafluoroborate in acetone to a colourless solution of $\text{Cp}^*\text{Ir}(\text{C}_2\text{H}_4)_2$ in acetone at $-78\text{ }^\circ\text{C}$ produced the corresponding mono-ethylene diazenido complex (**1**) in good isolated yield (typically $> 90\%$ after recrystallization)(Eqn.2.2)



As the reaction proceeds, the reaction mixture changes from a colourless to a transient yellow first, and then to an orange-red. The final dark-red crystals of complex (**1**) can be isolated by recrystallization from acetone/hexanes at $-10\text{ }^\circ\text{C}$.

Fast addition of the diazonium solution into the $\text{Cp}^*\text{Ir}(\text{C}_2\text{H}_4)_2$ solution, or a rise in the reaction temperature has been found often to lead to a dark-red colour for the reaction mixture. Upon addition of hexanes to this dark-red solution, a red oily species can be precipitated out. Recrystallization of the red oil with acetone/hexanes at $-10\text{ }^\circ\text{C}$ could only give (1) in low yield as crystals covered by the oily species. Repeating recrystallizations to attempt to obtain complex (1) free of the contamination always resulted in more red oily species. This indicated that the red oil could be an ionic decomposition product of compound (1). The IR spectrum of a thin film of this mixture on a KBr disc showed only the absorption at 1710 cm^{-1} due to complex (1) in the range of $1600 \sim 2300\text{ cm}^{-1}$. However, its ^1H NMR (in acetone- d_6) showed that beside resonances for compound (1), there were several other broad and featureless signals at δ ca. $1.2 \sim 1.8$ ppm.

Compound (1) is a relatively high melting solid. It is very soluble in most common polar solvents, such as acetone, CHCl_3 , CH_2Cl_2 , MeNO_2 and MeCN , but insoluble in non-polar solvents such as hexanes and diethyl ether. It is stable to air in the solid state. After exposure of the crystals of this compound in air at ambient temperatures for days, no obvious change in the IR spectrum was observed. However, in solution this compound exhibits only limited stability. There is no observable change in colour of the orange-yellow solution of compound (1) in non-halogenated solvents over a period of hours at room temperature, but it slowly changes to orange-red in days. In halogenated solvents, compound (1) decomposes rapidly; for instance in CHCl_3 solution, it reacts with the solvent to produce the corresponding dichloro dimer complex, $(\text{Cp}^*\text{IrCl}_2)_2$.

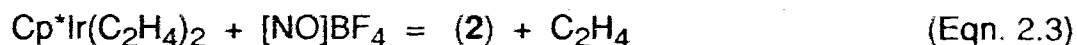
Compound (1) has been fully characterized by analysis and spectroscopy. Signals due to the parent ion, $[\text{Cp}^*\text{Ir}(\text{C}_2\text{H}_4)(\text{N}_2\text{C}_6\text{H}_4\text{OMe})]^+$, the fragments

formed by loss of the C_2H_4 ligand, $[Cp^*Ir(N_2C_6H_4OMe)]^+$, and the aryldiazenido ligand, $[Cp^*Ir(C_2H_4)]^+$, as well as others are observable in the FABMS spectrum of (1). Compound (1) displays a single $\nu(NN)$ absorption in its IR spectrum at 1724 cm^{-1} (EtOH) that falls within the range generally associated with the presence of a terminally coordinated aryldiazenido ligand. The assignment was confirmed by an isotopic shift of 35 cm^{-1} to lower wavenumber in a $^{15}N_\alpha$ -enriched sample. The 1H NMR spectrum of (1) shows clearly the presence of the aryl group, which occurs as a typical AA'BB' pattern in the aromatic region and a singlet at 3.91 ppm for the OMe protons of the *p*-methoxyphenyldiazenido group. A strong singlet was assigned to the methyl groups of the Cp^* ligand at 2.25 ppm (integral 15H), and a broad singlet at 3.25 ppm, (integral 4H) could be assigned to four equivalent protons in the C_2H_4 ligand. The feature of this peak merits some discussion in light of the dynamic molecular behavior of (1), which will be given in the next section. The ^{13}C NMR spectrum of (1) is consistent with its 1H NMR spectrum. It is worth mentioning that only a single C_2H_4 resonance was observed in the ^{13}C NMR spectrum. Two broad peaks at -2.86 and -107 ppm in the ^{14}N NMR spectrum of (1) clearly indicate the presence of a singly bent diazenido ligand in the complex, (refer to Table 1.6), the downfield one is assigned as the ligating nitrogen (N_α) which has been confirmed by ^{15}N NMR of the compound (1a). The molecular structure of (1) has been unequivocally established by a single crystal X-ray crystallographic analysis, which reveals that it possesses a two-legged piano-stool molecular structure in the solid state.

Synthesis and Characterization of $[Cp^*Ir(C_2H_4)(NO)]BF_4$ (2)

When the addition of solid $[NO]BF_4$ (freshly washed with CH_2Cl_2) to a solution of $Cp^*Ir(C_2H_4)_2$ in acetone was carried out at $-10\text{ }^\circ\text{C}$, a grey-greenish

product was obtained, which analysis indicated to be $[\text{Cp}^*\text{Ir}(\text{C}_2\text{H}_4)(\text{NO})]\text{BF}_4$ (**2**).
(Eqn. 2.3)



Compound (**2**) could also be obtained at an even lower temperature. But, at a higher temperature, such as room temperature, an orange-red oil was produced, from which no tractable organometallic complexes were isolable. Solid (**2**) can be recrystallized from acetone/diethyl ether. Its solubility properties are similar to compound (**1**), but (**2**) may be more stable than (**1**) in non-halogenated solvents for no decomposition of it in solutions at room temperature during a period of days was observed.

In its IR spectrum, compound (**2**) shows a very strong $\nu(\text{NO})$ absorption near 1820 cm^{-1} in solution indicating a linear terminal NO ligand. The FABMS clearly exhibits peaks due to the molecular ion, $[\text{Cp}^*\text{Ir}(\text{C}_2\text{H}_4)(\text{NO})]^+$, and fragments resulting from the loss of NO and C_2H_4 ligands. In its ^1H NMR spectrum, a strong singlet at 2.34 ppm is attributed to Cp^* protons, and a typical AA'XX' pattern at ca. 3.47 ppm is attributed to a rotation-free ethylene ligand that must be orientated with the C-C axis normal or parallel to the Cp^* plane. A singlet observed at 47.06 ppm for the ethylene ligand in a proton-decoupled ^{13}C NMR spectrum indicates two equivalent carbon atoms for this ligand in (**2**), and therefore, unequivocally establishes that the coordinated ethylene ligand is parallel to the Cp^* plane. Consistent with this spectroscopic evidence, a single-crystal X-ray diffraction study of compound (**2**) has unambiguously demonstrated the molecular structure of this monomeric complex in solid state.

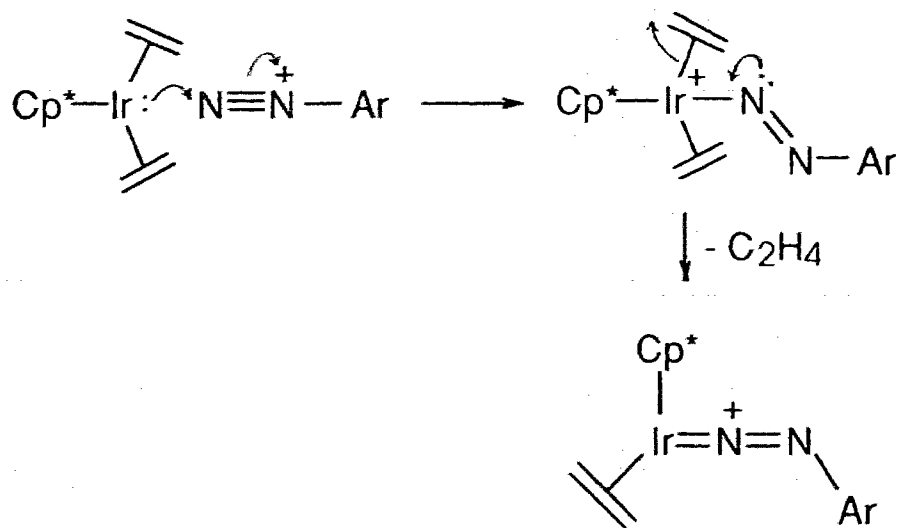
2.4. Discussion

Syntheses of $[\text{Cp}^*\text{Ir}(\text{C}_2\text{H}_4)(p\text{-N}_2\text{C}_6\text{H}_4\text{OMe})]\text{BF}_4$ (1) and $[\text{Cp}^*\text{Ir}(\text{C}_2\text{H}_4)(\text{NO})]\text{BF}_4$ (2)

The mono-ethylene aryldiazenido compound (1) and nitrosyl compound (2) can be readily obtained by the substitution of an ethylene ligand in $\text{Cp}^*\text{Ir}(\text{C}_2\text{H}_4)_2$ at low temperature either by aryldiazonium, N_2Ar^+ (Eqn. 2.2), or nitrosonium, NO^+ (Eqn. 2.3). The susceptibility of $\text{Cp}^*\text{Ir}(\text{C}_2\text{H}_4)_2$ to undergo these two ligand substitution reactions is apparently unusual. $\text{Cp}^*\text{Ir}(\text{C}_2\text{H}_4)_2$ has been recognized as the most inert to substitution among a series of compounds with similar structure,¹⁵⁷ *i.e.*, Cp^*ML_2 , ($\text{Cp}^* = \text{Cp}$ or Cp^* , $\text{M} = \text{Co}$, Rh or Ir , $\text{L} = \text{CO}$ or C_2H_4). So far, no direct substitution of an ethylene ligand in $\text{Cp}^*\text{Ir}(\text{C}_2\text{H}_4)_2$ to form $\text{Cp}^*\text{IrL}(\text{C}_2\text{H}_4)$ has been reported in the literature, although $\text{Cp}^*\text{Ir}(\text{PMe}_3)(\text{C}_2\text{H}_4)$ has been synthesized in an alternative way by Bergman.¹⁵⁸ Attempts to obtain $\text{Cp}^*\text{IrL}(\text{C}_2\text{H}_4)$ ($\text{L} = \text{CO}$ and PPh_3) in this research work by stirring a hexane solution of $\text{Cp}^*\text{Ir}(\text{C}_2\text{H}_4)_2$ saturated with CO gas, as well as by refluxing $\text{Cp}^*\text{Ir}(\text{C}_2\text{H}_4)_2$ with PPh_3 in ethanol for days have failed to result in any conversion of the $\text{Cp}^*\text{Ir}(\text{C}_2\text{H}_4)_2$. Obviously, the inertness of $\text{Cp}^*\text{Ir}(\text{C}_2\text{H}_4)_2$ toward nucleophilic ligand substitution reactions reflects the highly electron-rich metal centre of $\text{Cp}^*\text{Ir}(\text{C}_2\text{H}_4)_2$.

Clearly, the observed facile substitution of ethylene ligand by N_2Ar^+ and NO^+ in this work indicates that a different mechanism is likely to be involved in these reactions. In other words, diazonium N_2Ar^+ , and nitrosonium, NO^+ , in these reactions may act as Lewis acids instead of Lewis bases. In fact, this Lewis acid property of N_2Ar^+ was pointed out as early as 1975 by Sutton who states: "Generally, an 18-electron configuration is maintained by replacement of

a two electron donor such as CO or PR_3 by N_2Ar^+ . Such a process is favoured by attack at an electron-rich metal site" ¹³ Accordingly, a suggested mechanism involving an initial electrophilic attack by the N_2Ar^+ group at $\text{Cp}^*\text{Ir}(\text{C}_2\text{H}_4)_2$ is summarized in Scheme 2.1.



Scheme 2.1

A similar mechanism is also expected in the reaction of $\text{Cp}^*\text{Ir}(\text{C}_2\text{H}_4)_2$ with NO^+ .

To be involved in such *electrophilic* substitution, the incoming ligand should have a low-lying empty orbital largely located at the ligating atom, and the metal fragment should have a high-lying filled orbital pointing to the coordination direction. The low-lying LUMO of the aryldiazenido(+1) ligand has been well discussed in Chapter I (refer to Figure 1.2) and is shown on the right hand side of Figure 2.3. The metal fragment $\text{Cp}^*\text{Ir}(\text{C}_2\text{H}_4)_2$, has a ground state geometry

with the four carbon atoms of the two ethylene ligands located in a plane below the iridium atom and parallel to the Cp* plane.¹⁵⁹ The frontier orbitals of Cp*Ir(C₂H₄)₂ are shown on the left side of Figure 2.3. Obviously, the most likely approach of an incoming ligand is in the plane bisecting the two C₂H₄ ligands, *i.e.*, in the direction along the y axis of the coordinate system illustrated. Accordingly, the frontier orbital interactions between the fragments Cp*Ir(C₂H₄)₂ and N₂Ar⁺ are shown qualitatively in the centre of Figure 2.3. With the approach of the N₂Ar⁺ fragment toward to the metal centre, the HOMO of N₂Ar⁺ will push the 1a' and 2a' higher in energy, (shown in Figure 2.3 as dotted lines), which will enhance the antibonding character between iridium and the two ethylene ligands. Furthermore, the interaction between the LUMO of N₂Ar⁺ and the HOMO of Cp*Ir(C₂H₄)₂, (shown as the dashed line in Figure 2.3) will remove electron density from the HOMO of Cp*Ir(C₂H₄)₂, which will weaken the back-bonding of the metal to ethylene ligands. The total effect of these orbital interactions between the N₂Ar⁺ and the Cp*Ir(C₂H₄)₂ will significantly weaken the bond between the ethylene and the iridium and lead to a potential dissociation of an ethylene ligand from the metal centre. However, it should be emphasized that the interaction between the LUMO of N₂Ar⁺ and the HOMO of Cp*Ir(C₂H₄)₂ is the driving force for this process due to the relatively low-lying LUMO of N₂Ar⁺ and high-lying HOMO of Cp*Ir(C₂H₄)₂.

Another interesting feature is the critical temperatures used in the syntheses of high yield (1) and (2). Although the absence of any further investigation of the oily species obtained from the both reactions at high temperatures prevents a full understanding, the fact that the trend of

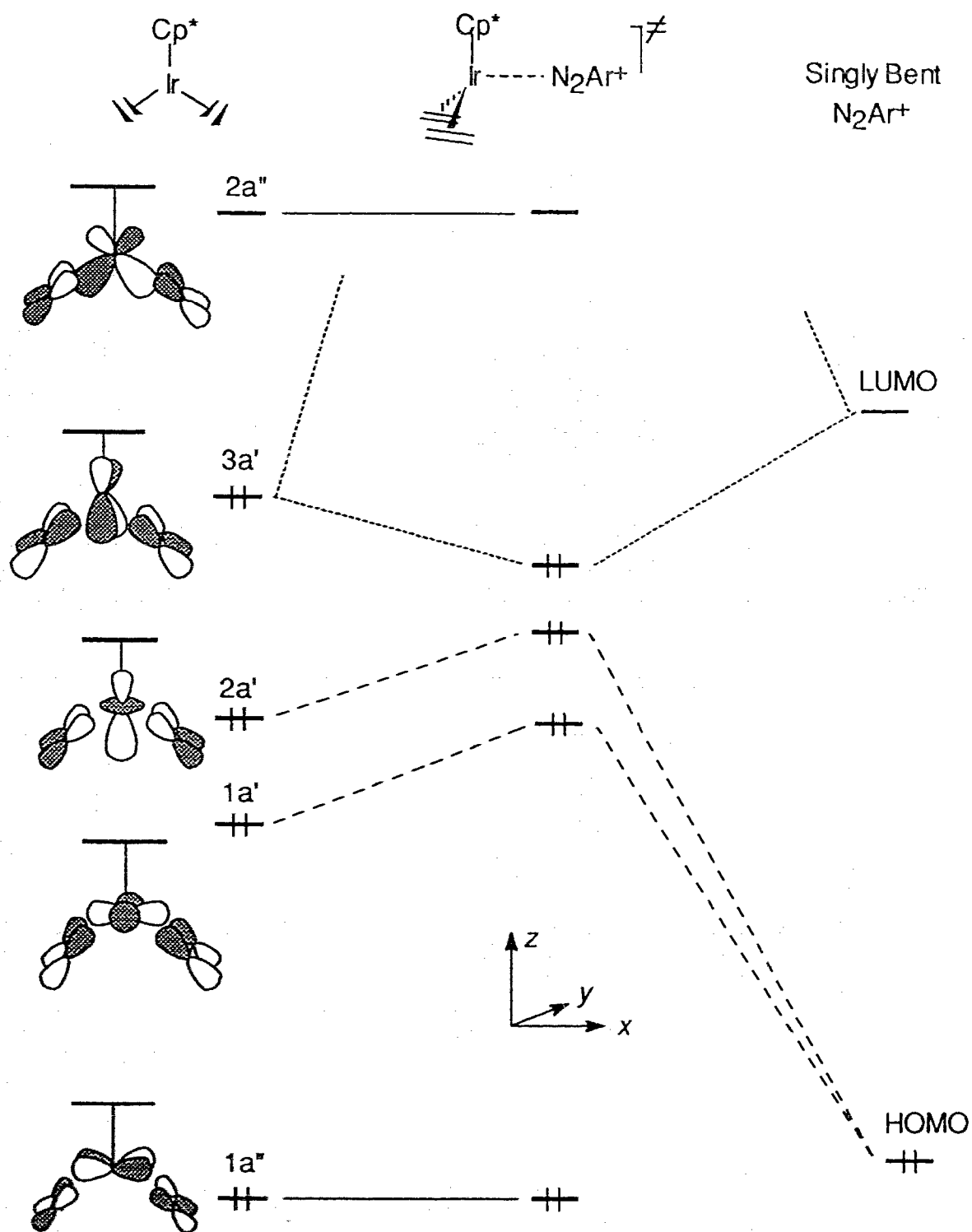
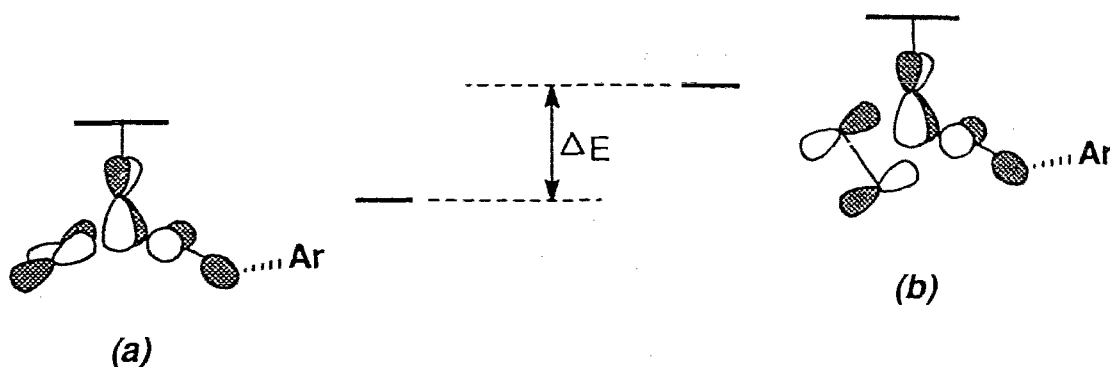


Figure 2.3 Qualitative orbital interactions of electrophilic attack of N_2Ar^+ at $\text{Cp}^*\text{Ir}(\text{C}_2\text{H}_4)_2$ (in a C_s symmetry)

these critical temperatures, ($< -78\text{ }^{\circ}\text{C}$ for (1) and $< -10\text{ }^{\circ}\text{C}$ for (2)) shows remarkable resemblance to the temperatures at which rotation of the ethylene ligands in these compounds is frozen out, (which will be discussed in detail in the next section), is perhaps indicative. Let us take compound (1) as example. At the low temperatures, the rigid ethylene ligand would be expected to lie in a position with its C-C bond parallel to Cp^+ plane. This could leave the HOMO of compound (1) at a low energy level, shown as **a** in Scheme 2.2. As the temperature increases, the ethylene ligand will start to rotate around the axis joining its centre to iridium. The stabilization energy of the HOMO of the iridium centre by the ethylene ligand through its π back-bonding would disappear completely at a 90° rotation of the ethylene ligand from its ground state position. Therefore, the HOMO of (1) will be expected now to occur at a higher energy, shown as **b** in Scheme 2.2. On the other hand, conformer **b** has also created a wider open position vulnerable a further attack by other nucleophilic species existed in the reaction system, such as the unreacted N_2Ar^+ , $\text{Cp}^+\text{Ir}(\text{C}_2\text{H}_4)_2$ or even a solvent molecule. Clearly, if such an attack occurred, even in a slight manner, a further increase of the energy of the HOMO would be expected. Consequently, this increase in energy of the HOMO would most probably cause a charge transfer from metal centre to the singly bent diazenido ligand forming a very unstable species which might, in turn, lead to decomposition. A similar argument could also apply to the corresponding nitrosyl compound (2), but the charge transfer would be expected to be much more difficult in this case, due to the rather high LUMO of NO^+ ligand. This could not only lay down an explanation for the critical temperatures to achieve better synthesis yields for (1) and (2), but it could also explain why (2) was experimentally observed to be more stable than (1).



Scheme 2.2

Variable-Temperature NMR Studies of the Hindered Rotation of the Ethylene Ligand in Complex (1)

The ambient-temperature ^1H NMR spectrum of the ethylene aryldiazenido complex (1) displays, in addition to the proton resonances due to the Cp^* ligand and the aryldiazenido ligand, a broad singlet for the four protons of the ethylene ligand at 3.25 ppm. For a two-legged piano stool compound (1), the broad singlet indicates that in solution the ethylene ligand is stereochemically non-rigid and undergoes a dynamic process. At room temperature, the rate of the fluxional process is intermediate on the NMR time scale, and so a time-averaged ^1H spectrum is obtained. Fluxional behavior of the coordinated ethylene ligand in half-sandwich complexes of this kind has been well documented as a hindered, or restrictive, rotation about the axis relating the metal to the midpoint of the double bond of the ethylene.^{151, 160 - 164} However, for a rapidly rotating ethylene ligand to give a limiting singlet absorption, the molecule (1) must have mirror symmetry in solution; that is, the molecule belongs to the point group C_s . In order for this to occur, the singly bent diazenido ligand has to be either located in the mirror plane or, if not, must be involved in a fast dynamic process which is

also related by this mirror symmetry. Since the Cp* ligand can be considered to be bisected by the mirror plane, the remaining task is to determine the relative orientation of the coordinated aryldiazenido ligand. Accordingly, a series of ^1H NMR spectra have been measured for compound (1) in acetone- d_6 solution from -64 to 22°C (Figure 2.4). As the solution is cooled to 0°C, the single absorption at 3.68 ppm for the ethylene protons broadens. At -20°C, the single peak diverges into a new asymmetric pattern. Finally, at -64°C, the spectrum is essentially that of the frozen limit, and shows rather complicated, but well resolved fine structure. An analysis of this frozen-out spectrum gave a set of chemical shifts and coupling constants for the ethylene protons in an ABCD spin system, which reproduced very well all the observed spectral line positions and their intensities. A computer simulated spectrum from these parameters, together with an enlargement of the experimentally observed one for comparison, is shown in Figure 2.5. Clearly, an ABCD spin system indicates that the ethylene ligand is in an orientation in an asymmetric environment in its ground, or frozen, state that makes all four protons inequivalent. Since it is well known that a non-rotating ethylene ligand in Cp or Cp* half-sandwich compounds of this type always adopts a position with its C-C axis parallel to the Cp or Cp* plane (simply because the π back-bonding is maximized in this position), the most probable molecular structure to account for this is one similar to the solid-state X-ray structure; *i.e.*, with a rigid, coordinated aryldiazenido ligand with the aryl group not in the plane defined by the centroid of the Cp*, Ir and the centre of the ethylene ligand. Interestingly, to account for a singlet C₂H₄ resonance at 22 °C exchange between the two orientations of the aryldiazenido

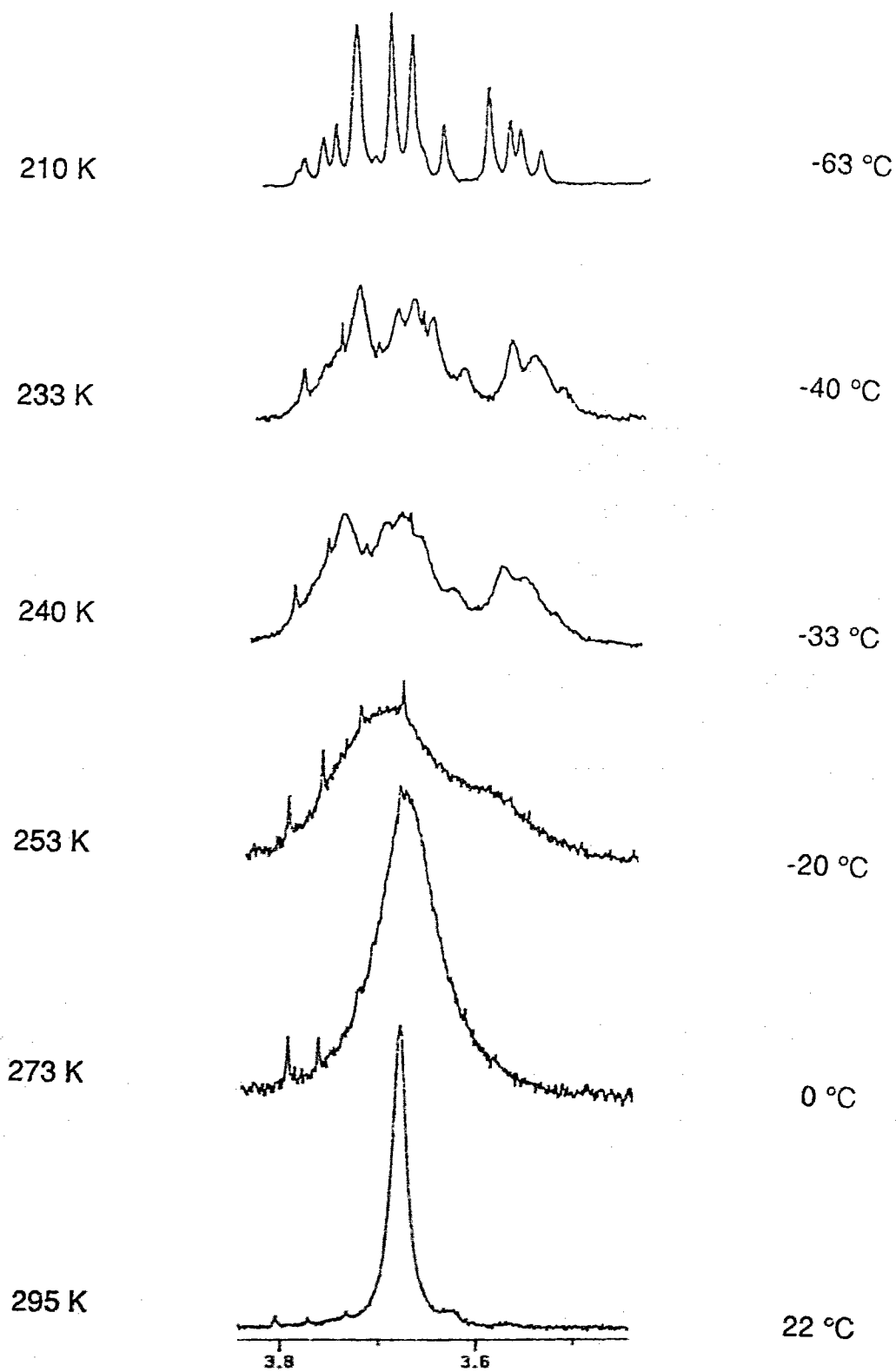


Figure 2.4 Variable-temperature ^1H NMR spectra for (1)

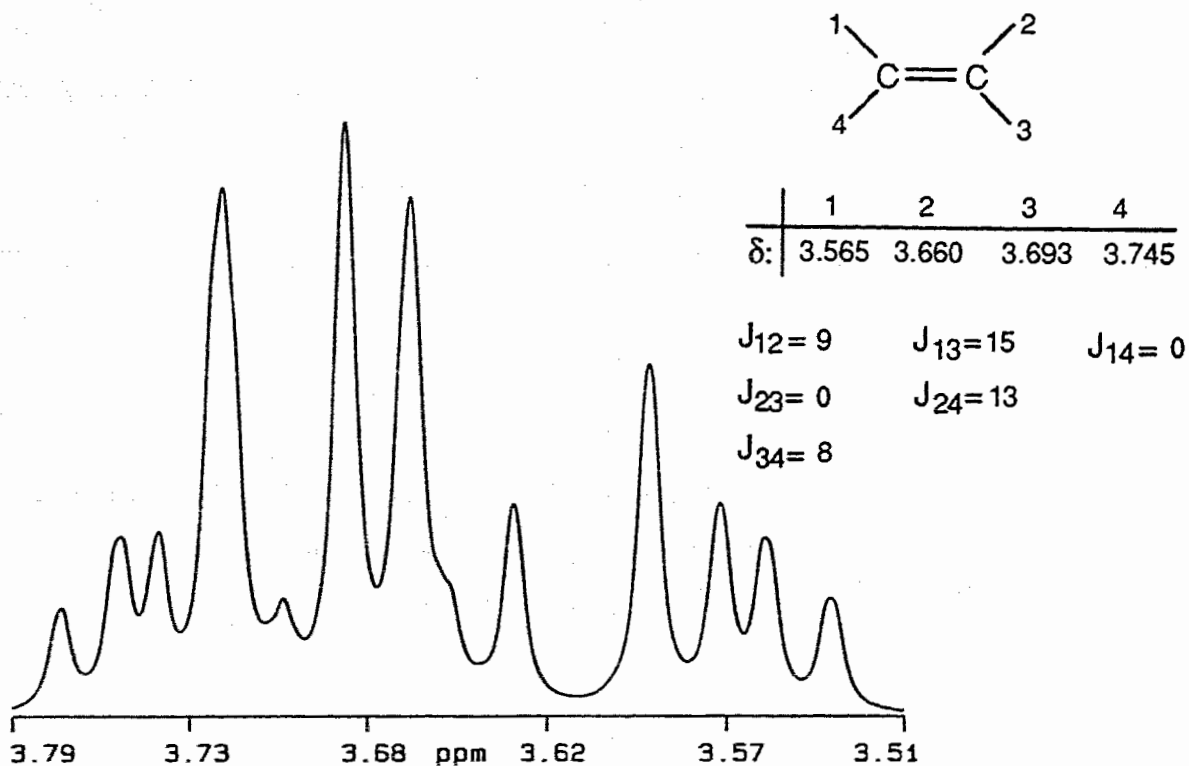
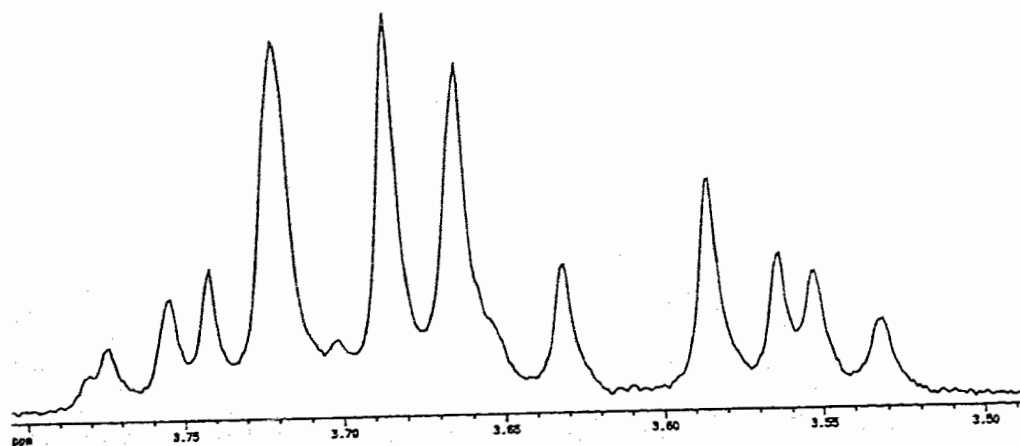
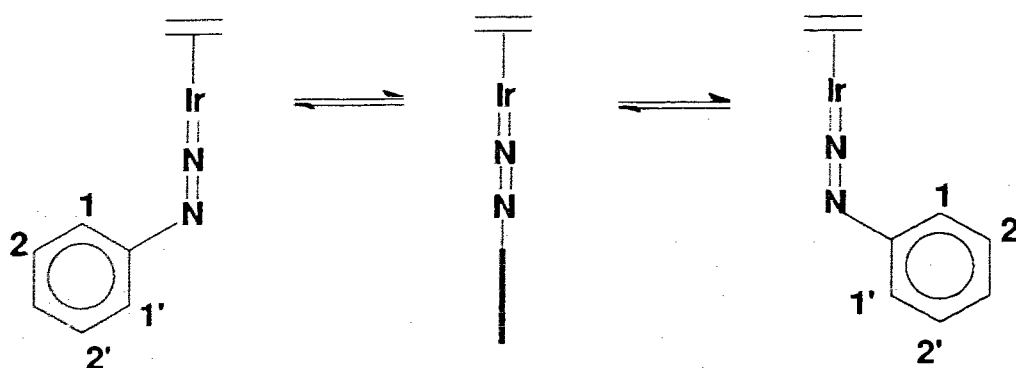


Figure 2.5 A comparison of the low-limit ¹H NMR spectrum of (1) (top) with the simulated spectrum (bottom)

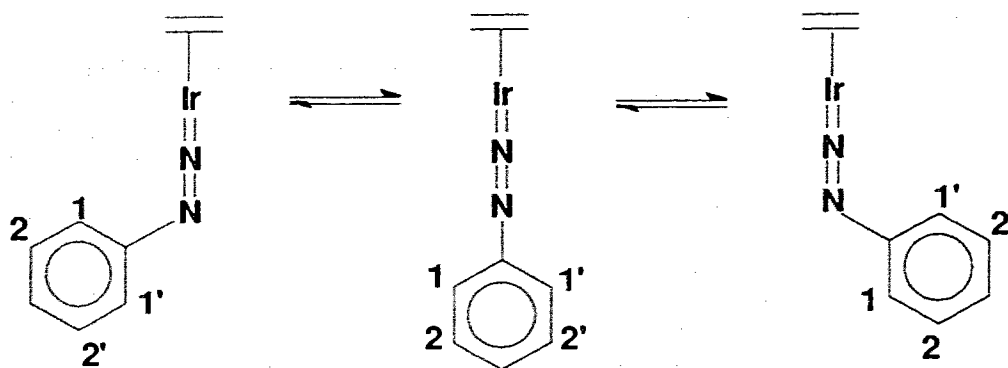
ligand (refer to Figure 2.6) must be fast; but the ABCD pattern observed at $-64\text{ }^{\circ}\text{C}$ requires that this exchange has been stopped on the NMR timescale. Surprisingly, to the best of our knowledge, observation of this fluxional behavior of the singly bent diazenido ligand has not been reported in the literature before. Further, this fluxional process could be accomplished by either a "flip" of the whole planar diazenido ligand from one side to another, by rotation about the metal-N-N axis, or by a "inversion" of the lone pair on N_{β} , which would involve a bent-linear-bent geometric change of the diazenido ligand. These two hypothetical mechanisms are shown in Figure 2.6 as (a) and (b), respectively, but may be equivalent to mechanism (a) if there were a free rotation about the C-N bond. Although, so far, no evidence has been found in this research to prefer one mechanism to another, the term "flip" will be used in this thesis to describe this fluxionality regardless of the detailed mechanism.

Furthermore, as we see from Figure 2.4, at about $-20\text{ }^{\circ}\text{C}$, the broadening singlet of the ethylene signal has diverged into a new asymmetric pattern. So, it appears to us that at least one of the two fluxional processes in compound (1) has slowed at this temperature range. Several possibilities may be considered for this: (1) The rotation of the ethylene may become slow at this temperature range, while the flipping of the diazenido ligand may still be fast. (2) The flipping process of the diazenido ligand may become slow, while the rotation process of the ethylene may still be fast. (3) Both fluxional processes may have been slowed down below the NMR time scale at this temperature range.

These mechanisms have been carefully assessed based on the experimental data, especially the spectrum at $-20\text{ }^{\circ}\text{C}$, and the first two are excluded. It appears to us both the ethylene rotation and the diazenido flipping are slowed at the temperature *ca.* $-20\text{ }^{\circ}\text{C}$ in the ^1H NMR spectra.



(a) "flip" mechanism ($1 \leftrightarrow 1'$ and $2 \leftrightarrow 2'$)



(b) "inversion" mechanism ($1 \leftrightarrow 1'$ and $2 \leftrightarrow 2'$)

Figure 2.6 Hypothetical mechanisms of the fluxional process of the singly bent aryl diazenido ligand (viewed down from the centroid of Cp*)

For the mechanism (1), if the ethylene rotation were slower than the NMR time scale while the flip of the diazenido was still in its rapid equilibrium, relative to the ethylene, the fragment $\text{Cp}^*\text{Ir}(\text{N}_2\text{Ar})$ would be in a time-averaged C_s symmetry and therefore a broad symmetric AA'BB' pattern, or a symmetric envelop of this pattern, should occur for the ethylene protons at the coalescence temperature. This has not been observed in the ^1H NMR spectra.

If it were true that flipping of the diazenido ligand slowed first at $-20\text{ }^\circ\text{C}$, while the rotation process of the ethylene were still fast, (mechanism (2)), relative to the rotating ethylene the fragment $\text{Cp}^*\text{Ir}(\text{N}_2\text{Ar})$ would be in a C_1 symmetry and consequently, the four protons of the ethylene ligand would be split to an AA'BB' pattern. Since this AA'BB' pattern should also be a symmetric one which has not been observed from the spectra, the mechanism (2) is ruled out.

These eliminations leave us with a mechanism that at the temperature ca. $-20\text{ }^\circ\text{C}$, *both* fluxional processes have been slowed down below the NMR time scale. In fact, this mechanism shows a good consistency with the experimentally observed ^1H NMR spectra. At room temperature, both of the fluxional processes are fast, however, at the coalescence temperature of ca. $-20\text{ }^\circ\text{C}$, both of them have been slowed down to *comparable* rates which are slower than the NMR time scale. That is, at any temperature lower than the coalescence temperature, the fragment $\text{Cp}^*\text{Ir}(\text{N}_2\text{Ar})$ is always in C_1 symmetry relative to the ethylene ligand. So the four protons of the ethylene are neither chemically nor magnetically identical to one another. Therefore, an ABCD pattern is observed. The resolution of this pattern is improved with decrease of temperature; and the low limit spectrum is obtained at $-63\text{ }^\circ\text{C}$. This trend is clear from the spectra

obtained in the temperature range -20 to -64 °C (see Figure 2.4).

Of a special interest in the hindered rotation of the ethylene ligand is to evaluate the activation energy for this rotation. Obviously, the mixing of the fluxional process of the singly bent diazenido ligand with this ethylene rotation in compound (1) complicates such an evaluation. However, from the above discussion, both fluxional processes decoalesced at *ca.* -20 °C and froze at -64 °C. So, in principle, an exchange barrier could be calculated from these data. Importantly, this calculated energy would be one of the upper-limits for the both exchange processes. That is, the activation energy for the rotation of the ethylene ligand or the inversion of the diazenido ligand must be smaller, or equal to this calculated energy. However, an ABCD pattern for a four spin system obtained for the ethylene protons in the low limit ¹H NMR spectrum also makes such a calculation not trivial. Therefore, in order to simplify this, a series of proton-decoupled variable-temperature ¹³C NMR spectra were measured for (1). The observed carbon resonances for the ethylene ligand in (1), compared with the signal for the OMe group, are shown in Figure 2.7.

At the ambient temperature, 22°C, a broad peak at *ca.* 50 ppm arises from the equivalent ethylene carbons of (1). When the solution is cooled down to 0 °C, this signal is collapsed into the base line. Finally, at -64 °C, the low limit spectrum is obtained, and further confirmed by the same half-height widths of these peaks obtained at -84 °C.

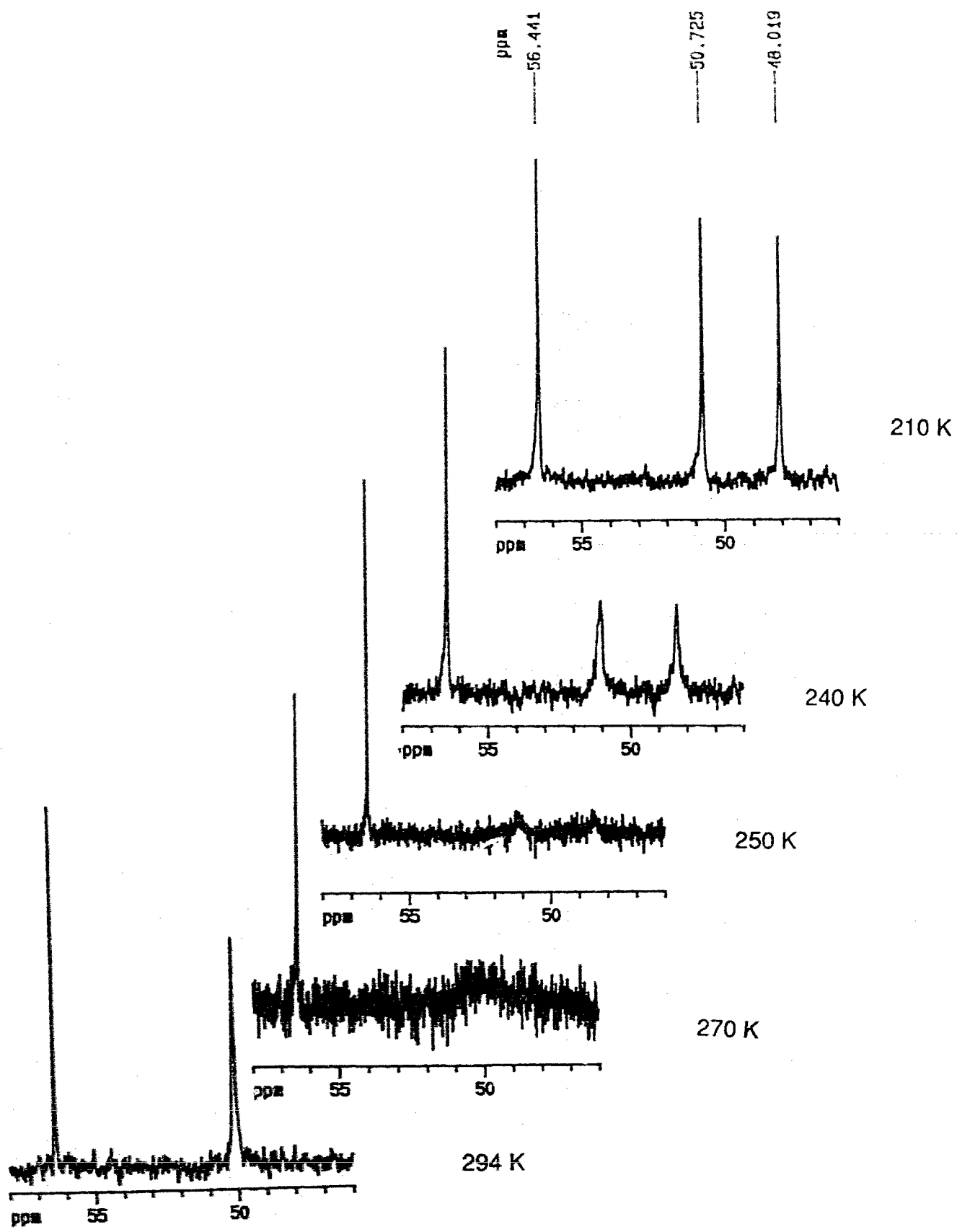


Figure 2.7 Variable-temperature ^{13}C NMR spectra for (1)

A free energy, ΔG^\ddagger can be calculated from the Eyring equation (Eqn. 2.1) by using the coalescence temperature T_c and $\Delta\nu$ obtained from the low limit ^{13}C NMR spectrum. Since from the variable temperature ^1H NMR study, we know that both ethylene and diazenido ligands undergo two different exchange processes within the same temperature range (22 ~ -64 °C), the barrier calculated from the Eyring equation may consist of contributions from both processes and it cannot be unambiguously assigned to the individual exchange process. This suspicion is supported by the observation that the weight-centre of the two peaks in the low limit ^{13}C NMR spectrum is not coincident with the chemical shift of the time-averaged singlet observed in the high temperature spectrum. So, the barrier calculated from the Eyring equation is, therefore, the upper-limit of the activation energy for either of the two exchange processes.

Variable-Temperature NMR Studies of the Hindered Rotation of the Ethylene Ligand in Complex (2)

As shown in Figure 2.8, at 21 °C, the ^1H NMR spectrum of the compound (2) in acetonitrile solution shows two pairs of symmetric broad absorptions in an essential AA'XX' pattern in the ethylene range, which corresponds to the slow exchange of the ethylene protons. When the solution of the complex is chilled to 0 °C, these two broad pairs are resolved into two sets of well defined multiplets related by mirror symmetry. This indicates that the exchange of the inequivalent ethylene protons has become slow compared with the NMR time scale. However, when the solution is heated, these absorptions broaden and finally, at 80 °C, they coalesce.

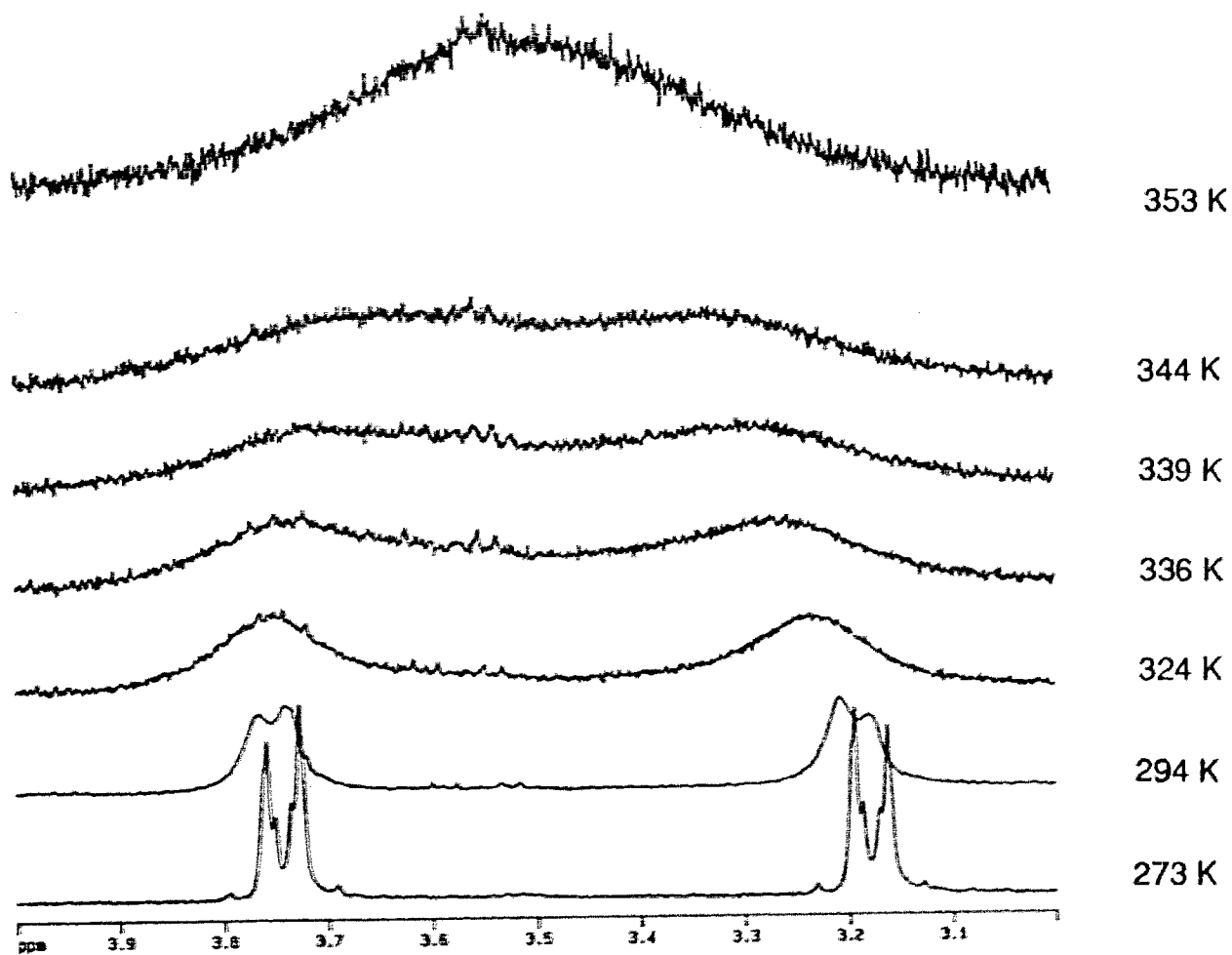


Figure 2.8 Variable-temperature ^1N NMR spectra for (2)

Energy Barrier of Ethylene Rotation as the Criterion of the π -Acidities of NO^+ and N_2Ar^+ Ligands

The free energies of activation (ΔG^\ddagger) for the ethylene rotation at coalescence for (1) and (2) were calculated by using the temperature of the coalescence (T_c) of the ethylene resonances and the chemical shift difference of these resonances ($\Delta\nu_0$) in the low-limit ^{13}C and ^1H NMR spectra respectively. The resulting values, listed in Table 2.6, show that the energy barriers of the ethylene rotation for the diazenido compound (1) is about 20 kJ/mol lower than for the nitrosyl compound (2). As we have mentioned in the last section, this ΔG^\ddagger derived from the T_c and $\Delta\nu_0$ of the ^{13}C NMR spectra of compound (1) is the *maximum possible* value for the energy barrier of the rotation of the ethylene ligand. Namely, the true value of the ΔG^\ddagger for compound (1) could be even smaller.

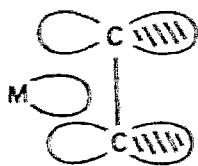
Table 2.6 Activation Parameters for Compounds (1) and (2)*

Complex	T_c (K)	$\Delta\nu_0$ (Hz)	ΔG^\ddagger (kJ/mol)
(1)	270 ± 1	272 ± 1	51.5 ± 0.1
(2)	353 ± 1	226 ± 1	68.7 ± 0.1

* (1) is $[\text{Cp}^*\text{Ir}(\text{C}_2\text{H}_4)(\text{N}_2\text{C}_6\text{H}_4\text{OMe})][\text{BF}_4]$; (2) is $[\text{Cp}^*\text{Ir}(\text{C}_2\text{H}_4)(\text{NO})][\text{BF}_4]$

The difference in the rotation barriers of the ethylene ligand in the analogous compounds (1) and (2) should directly reflect the binding difference of the ethylene ligand to the metal fragments $\text{Cp}^*\text{Ir}(\text{NO})^+$ and $\text{Cp}^*\text{Ir}(\text{N}_2\text{Ar})^+$. It has been customary to describe the binding of ethylene to a transition metal atom by the Dewar-Chat-Duncanson scheme,^{164, 165} consisting of two parts: (shown in

Figure 2.9.), (a) a σ -bond, corresponding to the classical coordination bond, formed by overlap of the filled π orbital of the olefin with a vacant metal orbital; and (b) a π -bond obtained through overlap of the vacant π^* orbital of the olefin with a filled d_{π} orbital of the metal.



Donation from
filled π orbital
to vacant metal
orbital

(a)



Back-bonding from
filled metal orbital
to acceptor π^*
orbital

(b)

Figure 2.9 The Dewar-Chatt-Duncanson scheme for bonding in a simple metal-olefin complex

The σ component would not be particularly restrictive of the rotation of the ethylene ligand about the metal-ethylene bond axis. However, the strength of the π component maximizes sharply for that orientation of the ethylene ligand in which its C-C axis lies in, or close to, the plane of the metal d_{π} orbital which overlaps with the π^* orbital of the ethylene. In the d^8 , 18-electron half-sandwich complexes, $\text{Cp}^*\text{IrL}(\text{C}_2\text{H}_4)$, one filled metal d_{π} orbital that has been raised in energy by repulsion with a low-lying π orbital of the Cp^* is energetically more

favorable than others for overlap with the empty π^* ethylene orbital. However, this favorable interaction can only occur when the C-C bond is parallel to the Cp* plane as in its ground state. This favorable interaction will decrease dramatically with a rotation of the ethylene ligand from this position, and it reaches its minimum upon a 90 °C rotation angle (the transition state), which brings the π^* orbital of the ethylene in the nodal plane of the filled metal $d\pi$ orbital. (refer to Scheme 2.2). Consequently this also indicates that the rotation barrier of the ethylene ligand in this type of two legged piano-stool complex is attributable to the electronic effect.

The ethylene rotation barriers for compounds (1) and (2) have been found as ≤ 51.1 and 68.7 kJ/mol., respectively. The greater restriction of the ethylene rotation in (2) than in (1) clearly indicates stronger $d\pi-\pi^*$ back-bonding in the metal-ethylene linkage of compound (2) than in (1). Similarly, in the ^1H NMR spectra, the observed chemical shifts of the Cp* ligand in (2) and (1) at 2.34 and 2.25 ppm also indicate more electron density located on the Ir(I) metal centre for (2) than for (1). Since the influence of the Cp* ligand on the metal's electronic configuration in both compounds should be similar, so, in seeking a reason behind the differential magnitudes of the rotation barrier for the ethylene ligand in these two compounds, it is reasonable to focus on the *ancillary* ligands, NO^+ and N_2Ar^+ .

These are well known to be π acids. In each case, a competition for the electrons in the metal $d\pi$ orbital will take place between the ethylene ligand and the ancillary ligand. The stronger the π acidity of this "trans" ligand, the more electron density will be pulled toward to this ligand from the metal centre and less electron density will be available for the back-bonding to the ethylene ligand. Correspondingly, this should result in a lower rotation barrier for the ethylene.

Thus, the different values of the ethylene rotation barriers in compounds (1) and (2) provide a measurement of the relative π acidities of NO^+ and N_2Ar^+ ligands. In other words, the lower ethylene rotation barrier found in compound (1) than in (2) is attributed to relatively stronger π acidity of the N_2Ar^+ ligand compared to NO^+ . Further, for $\text{Cp}^*\text{Ir}(\text{C}_2\text{H}_4)_2$ itself, there is no coalescence of the C_2H_4 proton resonances up to 110°C , indicating a much higher ethylene rotation barrier in this compound.¹⁵⁹ This can be attributed to the presence of the weak π acid ligand C_2H_4 in the position "trans" to the other.

These results, therefore, have provided us with experimental support of the theoretical prediction we have made in Chapter I, that the singly bent aryldiazenido ligand, on an absolute scale, is a better π acid than the nitrosyl ligand. It is also notable that in order for the singly bent aryldiazenido ligand to be a stronger π acid ligand in compound (1), it must bend its aryl tail away from the plane defined by Ir, the centroid of Cp^* and the centroid of the ethylene ligand (refer to Scheme 2.2). This has been unambiguously observed in solution from the low limit ^{13}C and ^1H NMR spectrum of (1), and in the solid state from the X-ray structure (Figure 2.1).

Crystal Structure of Compound (1)

The crystal structure consists of an assemblage of discrete cations, $[\text{Cp}^*\text{Ir}(\text{C}_2\text{H}_4)(\text{N}_2\text{C}_6\text{H}_4\text{OMe})]^+$, as equal number of *R* and *S* enantiomers, and anions, $[\text{BF}_4]^-$, related in the centrosymmetric space group $\text{P}2_1/n$. The asymmetric unit cell is an ion-pair $[\text{Cp}^*\text{Ir}(\text{C}_2\text{H}_4)(\text{N}_2\text{C}_6\text{H}_4\text{OMe})][\text{BF}_4]$. There are no abnormally short intermolecular contacts in the crystal. The cation,

$[\text{Cp}^*\text{Ir}(\text{C}_2\text{H}_4)(\text{N}_2\text{C}_6\text{H}_4\text{OMe})]^+$, has a five coordinated, pseudo two-legged piano-stool geometry. A perspective view of this cation together with the numbering scheme is given in Figure 2.2.

The Cp^* ligand is bonded to the iridium in a η^5 - coordination mode. The similar bond lengths from the five carbon atoms in the Cp^* ring to iridium, from 2.204(8) through 2.238(7) Å, indicate a regular C_{5v} symmetry for the $\eta^5\text{-C}_5\text{Ir}$ moiety. Thus, the two different ligands, C_2H_4 and $[\text{N}_2\text{C}_6\text{H}_4\text{OMe}]^+$, constituting the legs for this compound appears to have no measurable differential influence on the coordination geometry of the Cp^* ligand.

The similar distances of the two carbon atoms of the ethylene to the iridium of 2.190 (8) Å for Ir-C(10), and 2.172(9) Å for Ir-C(20), shows that the ethylene ligand is symmetrically coordinated to the iridium centre. The ethylene ligand has a carbon-carbon bond length of 1.387(16) Å which indicates this bond to be lengthened significantly relative to the typical uncoordinated C=C distances of 1.335(5) Å.¹⁶⁶ As expected, the ethylene ligand is found to be coordinated in an orientation parallel to the Cp^* plane.

The aryldiazenido ligand in this compound clearly has a singly bent geometry, with the Ir-N-N skeleton close to linear and the N-N-C angle about 120°. These values and other related parameters are compared in Table 2.7 with those of the only other iridium complex having a singly bent diazenido ligand, characterized by X-ray diffraction $[\text{IrCl}(\text{N}_2\text{Ph})(\text{PPh}_3)_2][\text{BF}_4]$.¹⁶⁷ The values of Ir-N and N-N bond lengths listed in Table 2.7 are indicative of significant multiple bonding between the iridium and the aryldiazenido ligand in both cases.

Table 2.7 Bond Angles ($^{\circ}$) and Distances (\AA) for Aryldiazenido Ligands

Parameters	(1)*	$[\text{IrCl}(\text{N}_2\text{Ph})(\text{PPh}_3)_2][\text{BF}_4]$
Ir-N(1)	1.811(7)	1.800(10)
N(1)-N(2)	1.205(9)	1.163(11)
Ir-N(1)-N(2)	176.2(6)	175.8(8)
N(1)-N(2)-C(1)	120.4(6)	126.9(10)

* (1) is $[\text{Cp}^*\text{Ir}(\text{C}_2\text{H}_4)(\text{N}_2\text{C}_6\text{H}_4\text{OMe})][\text{BF}_4]$

The most striking feature for the diazenido ligand is the orientation of the aryl ring in the complex. The aryl ring of the diazenido ligand indeed bends away from the plane containing Ir, the centroid of Cp^* and the centre of the ethylene which is, as described earlier, consistent with the ground-state molecular structure in solution.

Crystal Structure of Compound (2)

The single-crystal X-ray crystallographic analysis of compound (2) has established that the molecular structure of this complex consists of the crystallographically well-behaved cation and the disordered anion. The cation has two-legged piano-stool geometry. In addition to the regular $\eta^5\text{-Cp}^*$ ligand located on the top of the iridium centre, the cation also contains an essentially linear nitrosyl ligand (Ir-N-O angle of $175.8(9)^{\circ}$) and a $\eta^2\text{-C}_2\text{H}_4$ ligand. The nitrosyl and ethylene ligands constituting the legs of the piano-stool are bent down in the customary manner from the plane through Ir parallel to the Cp^* plane, i.e., $\text{Cp}^*(\text{centroid})\text{-Ir-N} = 141.8^{\circ}$, $\text{Cp}^*(\text{centroid})\text{-Ir-C}(1) = 121.3^{\circ}$ and $\text{Cp}^*(\text{centroid})\text{-Ir-C}(2) = 124.2^{\circ}$. The remarkably larger value of the angle

Cp*(centroid)-Ir-N, comparing with the angles of Cp*(centroid)-Ir-C(1) and Cp*(centroid)-Ir-C(2), may indicate that some degree of secondary π bonding could be exerted by the nitrosyl ligand. Since the nitrosyl ligand has "cylinder-type" π^* orbitals, in addition to the π^* orbital that primarily overlaps with the metal-centred HOMO resulting in the effective single-faced back-bonding, the remaining orthogonal π^* orbital could also overlap with the metal-centred SOMO giving additional partial back-bonding. These two π interactions are shown in Figure 2.10.



Figure 2.10 π back-bonding from Cp*Ir(C₂H₄) to NO⁺

Since the SOMO is largely located in the direction opposite to the Cp*, the larger Cp*(centroid)-Ir-N angle could be the result of the nitrosyl bending away from the Cp* to obtain a better overlap with the Ir SOMO. On the other hand, this secondary effect would not be expected to involve the η^2 -C₂H₄ ligand because it only has "single-faced" π bonding ability. The C₂H₄ ligand is coordinated to the iridium atom in a normal η^2 fashion similar to that in compound (1). The dimensions of the triangular cyclopropene-type skeletons of Ir and η^2 -C₂H₄ in (1) and (2) are similar: Ir-C(10) = 2.190(8) Å, Ir-C(20) = 2.172(9) Å and C(10)-C(20)

= 1.387(16) Å for (1) and Ir-C(1) = 2.19(1) Å, Ir-C(2) = 2.17(1) Å and C(1)-C(2) = 1.37(2) Å for (2).

The most striking features of the metrical details of the nitrosyl ligand in (2) are the unusually long Ir-N bond length at 1.762(9) Å, and the unusually short N-O bond length at 1.15(1) Å. These two distances are significantly different from the comparable distances in other iridium nitrosyl compounds.^{168, 169} A comparison of bond distances and angles of the nitrosyl ligand for these complexes, together with their IR data, are listed in Table 2.8. The shorter N-O and longer Ir-N distances observed for (2) are indicative that the characteristic "single-faced" π back-bonding feature dominates the primary bonding interaction of iridium atom and the nitrosyl. By contrast, the compounds $[\text{IrH}(\text{NO})(\text{PPh}_3)_3]^+$ and $\text{Ir}(\text{NO})(\text{PPh}_3)_3$ both have a metal centre with the "cylinder-type" of π back-bonding ability, and so, as the linear nitrosyl ligand coordinates to such metal centre, it will exert the π back-bonding from the both directions. The trend of IR absorptions $\nu(\text{NO})$ listed for these three compounds is also consistent with this rationalization.

Table 2.8 IR and Structural Data for Linear Monoiridium Nitrosyl Complexes

Complex	$\nu(\text{NO})(\text{cm}^{-1})$	Ir-N-O ($^\circ$)	Ir-N(Å)	N-O(Å)	Ref.
(2)	1820	175.8(9)	1.762(9)	1.15(1)	t.w. ^a
$[\text{IrH}(\text{NO})(\text{PPh}_3)_3]^+$	1780	175	1.68	1.21	168
$\text{Ir}(\text{NO})(\text{PPh}_3)_3$	1600	180	1.67	1.24	169

a: t.w.: this work

The anion BF_4^- was found to occur in a spherically disordered fashion in which the disc-shaped ellipsoids for the four fluorine atoms were satisfactorily modeled by three BF_4^- 's with the total occupancy equal to one.

2.5. Conclusion

The monoethylene pentamethylcyclopentadienyl iridium complexes, $[\text{Cp}^*\text{Ir}(\text{C}_2\text{H}_4)(\text{N}_2\text{C}_6\text{H}_4\text{OMe})][\text{BF}_4]$ (**1**) and $[\text{Cp}^*\text{Ir}(\text{C}_2\text{H}_4)(\text{NO})][\text{BF}_4]$ (**2**), have been synthesized in high yield (> 90%) by the reaction of $\text{Cp}^*\text{Ir}(\text{C}_2\text{H}_4)_2$ with $[\text{NO}][\text{BF}_4]$ and $[\text{p-N}_2\text{C}_6\text{H}_4\text{OMe}][\text{BF}_4]$ in acetone, respectively. A mechanism involving an initial electrophilic attack of the incoming ligand NO^+ , or N_2Ar^+ at the metal centre of the $\text{Cp}^*\text{Ir}(\text{C}_2\text{H}_4)_2$, followed by extrusion of C_2H_4 is postulated to account for the mild conditions the reactions required, which is in sharp contrast with the *normal* ligand substitution behavior of $\text{Cp}^*\text{Ir}(\text{C}_2\text{H}_4)_2$. The ^{15}N enriched compound (**1a**) has also been made, and its IR and nitrogen (both ^{14}N and ^{15}N) NMR data have unambiguously established that the aryldiazenido ligand is in a singly bent geometry. ^1H and $^{13}\text{C}\{^1\text{H}\}$ NMR spectra of both compounds show that they are stereochemically nonrigid in solutions at ambient temperatures, the principal fluxionalities involving the restricted rotation of the ethylene ligand in both compounds, but also a fast exchange of position of the aryl group in (**1**). This latter fluxional process of the singly bent diazenido ligand is the first to be observed and reported. The restricted rotation of the coordinated ethylene ligand in both (**1**) and (**2**) has been studied by the variable-temperature NMR technique, from which the free energies of activation for this process have been estimated to be $\leq 51.5 \pm 0.1$ kJ/mol for (**1**) and 68.7 ± 0.1 kJ/mol for (**2**). The X-ray crystal structures of (**1**) and (**2**) have been determined. Compound (**1**) crystallizes in the monoclinic space group $P2_1/n$, with $a = 5.5780(10)$ Å, $b =$

20.5310(23) Å, $c=12.0310(15)$ Å, $\beta=93.500(10)^\circ$ and $Z=4$; the structure was solved by conventional heavy-atom methods and was refined by full-matrix least-squares procedures to $R=0.028$ and $R_w=0.031$ for 2611 absorption-corrected reflections with $I > 2.5\sigma(I)$. Crystals of compound (2) are monoclinic, space group $P21/n$, with $a=7.4540(10)$ Å, $b=24.381(3)$ Å, $c=8.5360(10)$ Å, $\beta=93.850(10)^\circ$ and $Z=4$; $R=0.034$ and $R_w=0.041$ for 1923 absorption-corrected reflections with $I > 2.0\sigma(I)$. The most chemically interesting feature of these two compounds is that the different rotation barriers of their ethylene ligands provide us with a direct comparison of the π acidity of NO^+ and N_2Ar^+ on an absolute, or single-faced, scale. The singly bent N_2Ar^+ ligand is found to be a stronger π acid than NO^+ .

CHAPTER III

Pentamethylcyclopentadienyl Mono- and Di-iridium Aryldiazenido Complexes and Their Derivatives— Ancillary ligand effect on the geometrical preference of the diazenido ligand

3.1 Introduction

A wide range of coordination geometries adopted by the aryldiazenido ligands in their complexes (Figure 1.27) has stimulated great interest in the structural study of these complexes. Of key importance in this study is an understanding of the different electronic interactions involved in the various geometrically different diazenido complexes. Some effort has been devoted to obtaining a detailed description of the electronic structure of the bonding in transition metal aryldiazenido complexes.^{24, 26} However, little is known about the influence that the molecular geometry and the ancillary ligands have on the metal-diazenido bonding. We have been concerned with such questions, both in the experimental arena and in the theoretical domain. These concerns have been discussed rather extensively in Chapter I of this Thesis where an account of the different interactions involved in complexes with different coordinated aryldiazenido ligands has been given in terms of the fragment molecular orbital interaction analysis.

From the previous discussions (Chapter I) the ancillary ligands have been found important in setting the energy of the metal-centred orbitals and in tailoring them to specific shapes which may, or may not, be favorable for the metal centre in binding a diazenido ligand with a specific geometry. So the nature, the number and the geometrical disposition of the ancillary ligands could directly influence

the stability and the geometrical preference of a diazenido ligand in the complexes. In this chapter, a systematic study of the ligand effect on the metal-diazenido bonding will be described in the case of the $\text{Cp}^*\text{Ir}(\text{L})(\text{N}_2\text{Ar})$ system, where L is the ancillary ligand. This study is motivated by the hope that conversion of the singly bent diazenido ligand to other geometries can be observed in the rather simple $\text{Cp}^*\text{Ir}(\text{L})(\text{N}_2\text{Ar})$ system by changing the relative π acidity, or basicity, of the ancillary ligand L. In fact, we have observed that when L is a strong π -acid, such as CO, no stable aryldiazenido compounds could be isolated; when L is a weak π -acid, C_2H_4 or PR_3 , the singly bent aryldiazenido complexes are produced, and when L is a strong π -base (I^- , Br^- or the metal base $\text{Cp}^*\text{Ir}(\text{CO})_2$), complexes with the doubly bent aryldiazenido groups occurring as different bridging ligands are obtained. Further, the system $\text{Cp}^*\text{Ir}(\text{PPh}_3)(\text{L})(\text{N}_2\text{Ar})$ which has a doubly bent aryldiazenido ligand can only be observed for particular kinds of ancillary ligand L.

Syntheses, characterizations, spectroscopic studies and selected chemical reactions of the new pentamethylcyclopentadienyl iridium aryldiazenido complexes and their derivatives are also described.

Finally, despite numerous unsuccessful attempts to synthesize $[\text{Cp}^*\text{Ir}(\text{CO})(\text{N}_2\text{Ar})]\text{BF}_4$ these attempts have yielded results that are also important in understanding the chemistry of organometallic aryldiazenido complexes; important enough for a discussion their own right. This part of the study, involving CO as the ancillary ligand will, therefore, be presented in the next chapter. However, it should be noted that there is a close relationship between the material presented in this and the next chapters.

3. 2. Experimental Section

General Procedures

Solvents were dried prior to use and freshly distilled under nitrogen from sodium/benzophenone (diethyl ether), calcium hydride (dichloromethane), sodium (hexanes), predried anhydrous calcium sulfate (absolute ethanol). A small amount of CCl_4 was dried by passing through a column packed with predried neutral alumina. All preparations or reactions and manipulations were carried out in standard Schlenk ware, connected to a switchable double manifold providing vacuum and nitrogen, unless otherwise noted.

Infrared spectra for solutions were measured in CaF_2 cells, and solid samples were measured as either KBr pellets or thin film on a KBr disc by using a Bomem Michelson 120 FTIR instrument. Some of the routine ^1H NMR spectra were recorded at 100 MHz by using a Varian SY-100 Fourier Transform Spectrometer. The remaining ^1H NMR and ^{15}N NMR spectra were obtained in the NMR service of Simon Fraser University by Mrs. M. Tracey on a Bruker AMX-400 instrument at operating frequencies of 400.1 and 40.5 MHz for ^1H , and ^{15}N respectively. Chemical shifts (δ) are reported in ppm, downfield positive, relative to tetramethylsilane (TMS) for ^1H , and relative to external $\text{Me}^{15}\text{NO}_2$ for ^{15}N spectra separately. Coupling constants are reported in Hertz.

Mass spectra were obtained by Mr G. Owen on a Hewlett-Packard Model 5985 GC-MS spectrometer equipped with fast atom bombardment (FAB) probe (xenon source, Phrasor Scientific, Inc., accessory), and utilized samples dispersed or dissolved in thioglycerol, sulfolane or *m*-nitrobenzyl alcohol (NOBA). C.I. MS were obtained by using isobutane as the chemical ionization reagent. The pattern of the envelopes of the fragment ions were matched with that simulated by computer for the species in question and are referred to ^{193}Ir

for mono-iridium species, or the highest intensity peak ($^{193}\text{Ir} + ^{191}\text{Ir}$) for the di-iridium species. Microanalyses for elements C, H, N were performed by Mr. M-K, Yang of the Microanalytical Laboratory of Simon Fraser University.

The author is grateful to Dr. R. J. Batchelor for the X-ray crystallographic analysis of the single crystal structure of compound (7).

Starting Materials

Bisethylene pentamethylcyclopentadienyl iridium was synthesized according to the literature method.¹⁵¹ Pentamethylcyclopentadienyl iridium dicarbonyl was synthesized either by the Maitlis' method¹⁷⁰ or by the method developed by us, which will be discussed in Chapter IV. *Para*-methoxyphenyl-diazonium tetrafluoroborate was prepared by the standard procedure from *para*-methoxyaniline (Aldrich) and sodium nitrite, and purified periodically by recrystallization from acetone and diethyl ether. The diazonium salt substituted with ^{15}N at the terminal nitrogen (N_α) was prepared by using $\text{Na}^{15}\text{NO}_2$ (95% ^{15}N , MSD Isotopes).

Preparation of $[\text{Cp}^*\text{Ir}(\text{PPh}_3)(p\text{-N}_2\text{C}_6\text{H}_4\text{OMe})]\text{BF}_4$ (3) or (3a)

Method 1: To a 10 mL ethanol solution containing equimolar quantities of $\text{Cp}^*\text{Ir}(\text{C}_2\text{H}_4)_2$ (30 mg, 0.078 mmol) and PPh_3 (21 mg, 0.080 mmol) was added $[p\text{-N}_2\text{C}_6\text{H}_4\text{OMe}][\text{BF}_4]$ or $[p\text{-}^{15}\text{NNC}_6\text{H}_4\text{OMe}][\text{BF}_4]$ (17 mg, 0.077 mmol). Following the addition of the diazonium salt, the colorless solution immediately changed to orange red. After the solution was stirred for 1 hour, the solution was taken to dryness which gave compound (3) or (3a) quantitatively as an orange-red oil. IR $\nu(\text{NN})$: 1701 cm^{-1} (ethanol), 1710 cm^{-1} (CH_2Cl_2), $\nu(^{15}\text{NN})$ for (3a): 1676 cm^{-1} (ethanol), $^1\text{H NMR}$ (100 MHz): $\delta(\text{acetone-}d_6)$ 2.12d (15H, $J_{\text{P-Me}} = 2$,

Cp*), 3.85s (3H, OMe), 7.06q (4H, AA'BB' pattern, C₆H₄), 7.20 ~ 7.90m (15H, Ph); δ (CDCl₃) 1.97d (15H, J_{p-Me} = 2, Cp*), 3.87s (3H, OMe), 6.98d (4H, J_{H-H} = 1, C₆H₄), 7.40 ~ 7.52m (15H, Ph), ¹⁵N NMR for (3a): δ (acetone-*d*₆) 33.23d (¹⁵N α , J_{p-¹⁵N α} = 7), FABMS (NOBA, Xenon) (*m/z*): 725 (M⁺), 590 (M⁺-N₂C₆H₄OMe), Anal. (calcd): C, 51.79; H, 4.60; N, 3.45, (found): C, 52.18; H, 4.81; N, 3.62.

Method 2: To a solution of (1) or (1a) (30 mg, 0.052 mmol) in 10 mL ethanol was slowly added solid PPh₃ (14 mg, 0.053 mmol), and the reaction mixture was stirred at room temperature for about one hour. The color changed from yellow to orange red. The solution was then evaporated to dryness in vacuo, affording analytically pure product (3) or (3a) as an orange red oil.

Preparation of Cp*Ir(PPh₃)(H)(*p*-N₂C₆H₄OMe) (4) or (4a)

An excess of NaBH₄ was added to an acetone solution (5 mL) of [Cp*Ir(PPh₃)(*p*-N₂C₆H₄OMe)]BF₄ (3) or (3a) (42 mg, 0.052 mmol), and the mixture was stirred for 1 hour at -10 °C. The color of the reaction solution changed from orange red to peach red. The acetone solvent was removed in vacuo. To the solid residue was added excess hexanes (15 mL) and the mixture was stirred vigorously for 15 minutes. The peach red solution was filtered through a Celite filter to remove the insoluble salts (NaBF₄ and NaBH₄) and evaporated to dryness in vacuo to give a rose purple oily product (4) or (4a) in 89% yield. IR ν (Ir-H): 2133 *br.* cm⁻¹ (hexanes). ¹H NMR (100 MHz, acetone-*d*₆) δ : -15.9d, (1H, J_{p-H} = 33.5, Ir-H), 1.51dd (15H, J_{p-Me} = 1.8, J_{H-H} = 0.7, Cp*), 3.57s (3H, OMe), 6.58d (4H, J = 1.7, C₆H₄), 7.10 ~ 7.60m (15H, Ph), ¹⁵N NMR for (4a) (acetone-*d*₆) δ : 271.89s (¹⁵N α), CIMS, (*m/z*): 590 ([Cp*Ir(PPh₃)]⁺), 464

([Cp*Ir(H)(N₂C₆H₄OMe)]⁺), Anal. (calcd): C, 57.92; H, 5.28; N, 3.86, (found): C, 58.12, H, 5.43; N, 3.89.

Preparation of [Cp*Ir(PPh₃)(Cl)(*p*-NHNC₆H₄OMe)]BF₄ (**6**) or (**6a**)

Method 1: Freshly synthesized (**3**) or (**3a**) (42 mg, 0.052 mmol) in 5 mL ethanol solution was slowly purged by HCl gas for 5 minutes at room temperature. A cold water bath (~ 10 °C) was used to absorb the heat released from the solvation of the HCl gas in ethanol. The color of the reaction solution changed from orange red to dark green. After stirring for another 5 minutes, the volatiles were removed *in vacuo* leaving dark yellow solid residue. This solid was then re-dissolved in a minimum amount of acetone, and excess diethyl ether was added slowly with vigorous stirring until no further solid precipitated. The yellow supernatant solution was carefully removed by pipette and the remaining yellow solid was washed twice with 20 mL portions of diethyl ether. This gave (**6**) or (**6a**) as the diethyl ether solvated product, [Cp*Ir(PPh₃)(Cl)(*p*-NHNC₆H₄OMe)]BF₄(**6**)·1/2 Et₂O or (**6a**)·1/2 Et₂O, as a fine yellow powder, in 92% yield. More product can be recovered from the supernatant solution and the diethyl ether washing solution. IR ν(N-N): 1483 cm⁻¹ (KBr), and 1460 cm⁻¹ (KBr) for (**6a**), ¹H NMR (100 MHz): δ(acetone-*d*₆) 1.54*d*, (15H, J_{P-Me} = 2.2, Cp*), 3.93*s* (3H, OMe), 7.05*d* and 7.40*d* (4H, AA'BB' pattern, C₆H₄), 7.52*s* and 7.58*s* (15H, Ph) and 13.73*d* (1H, J_{15N-H} = 70 for (**6a**)); δ(CDCl₃) 1.52*d*, (15H, J_{P-Me} = 2.2, Cp*), 3.92*s* (3H, OMe), 6.92*d* and 7.19*d* (4H, AA'BB' pattern, C₆H₄), 7.45*s* and 7.50*s* (15H, Ph) and 13.01*d* (1H, J_{15N-H} = 69 for (**6a**)); ¹⁵N NMR for (**6a**): δ(acetone-*d*₆) -64.24*d* (J_{15N-H} = 70); FABMS (NOBA, Xenon) (*m/z*): 761 (M⁺), 625 (M⁺-NHNC₆H₄OMe), 589 (M⁺-N₂C₆H₄OMe - Cl), 511 (M⁺-NHNC₆H₄OMe - Cl -

Ph), Anal. for (6a)-1/2 Et₂O, (calcd): C, 50.20; H, 4.89; N, 3.16, (found): C, 50.21, H, 4.83; N, 3.09.

Method 2: Freshly synthesized (4) or (4a) (22 mg, 0.031 mmol) in 3 mL predried CCl₄ was stirred vigorously in the dark at -10 °C. After 20 minutes, still in the dark and at -10 °C, the solvent was removed *in vacuo*, resulting in a red solid product. Redissolving this solid into the minimum amount of acetone gave a red solution. To this solution was slowly added 2 drops of HBF₄/diethyl ether solution, which afforded an immediate brownish precipitate. The supernatant solution was then carefully removed by pipette and the remaining dark yellow solid was pumped *in vacuo* overnight. ¹H NMR spectroscopy of this solid indicated that (6) or (6a) was the major product, but was contaminated with variable amounts of the known compound, Cp*Ir(PPh₃)Cl₂¹⁵¹ (¹H NMR, δ:1.34d, J_{P-Me} = 2, (Cp*) and 7.35 ~ 7.75m (aromatic)).

Attempts to synthesize Cp*Ir(PPh₃)(Cl)(*p*-N₂C₆H₄OMe) (5)

1). By deprotonation of [Cp*Ir(PPh₃)(Cl)(*p*-NHNC₆H₄OMe)]BF₄ (6)

To a yellow solution of (6) (44 mg, 0.052 mmol) in 5 mL acetone was added 2 drops of NEt₃. The color of the reaction solution immediately changed to red. Diethyl ether (*ca.* 2 mL) was added carefully to precipitate pale gray NHEt₃-BF₄. After filtering, the filtrate was concentrated to 2 mL *in vacuo* and excess diethyl ether was added slowly until no further solid precipitated. The supernatant was removed by pipette and the solid remaining was washed twice with diethyl ether to yield the product as an orange powder. IR and proton NMR of this solid indicated that it was a mixture of the known compound,

$\text{Cp}^*\text{Ir}(\text{PPh}_3)\text{Cl}_2$, (< 5% based on the proton NMR integration) and another major species which had identical IR ($\nu(\text{NN})$: 1711 cm^{-1} in CH_2Cl_2 , 1699 cm^{-1} on KBr disc) and proton NMR features (δ : $2.12d$ (15H, $J_{\text{P-Me}} = 2$, Cp^*), $3.85s$ (3H, OMe), $7.06q$ (4H, AA'BB' pattern, C_6H_4), $7.20 \sim 7.90m$ (15H, Ph) in acetone- d_6) to the compound (3), $[\text{Cp}^*\text{Ir}(\text{PPh}_3)(p\text{-N}_2\text{C}_6\text{H}_4\text{OMe})]\text{BF}_4$. Consequently, this major species was assigned as $[\text{Cp}^*\text{Ir}(\text{PPh}_3)(p\text{-N}_2\text{C}_6\text{H}_4\text{OMe})]\text{Cl}$ (5').

2). By exchange of hydride ligand in (4) with chlorine

Freshly synthesized (4) (22 mg, 0.031 mmol) in 3mL predried CCl_4 was stirred in the dark at $-10\text{ }^\circ\text{C}$ for 20 minutes; longer reaction time resulted in the formation of $\text{Cp}^*\text{Ir}(\text{PPh}_3)\text{Cl}_2$ as a major product later. The solvent was removed *in vacuo* to give a red powder. The IR spectrum of this red solid in the range of $2300 \sim 1600\text{ cm}^{-1}$ showed only a band at 1711 cm^{-1} in CH_2Cl_2 , and 1717 cm^{-1} in CCl_4 . The ^1H NMR spectra of this solid in either CDCl_3 or acetone- d_6 clearly showed the expected resonances due to the protons of the Cp^* group, OMe group and the aromatic groups. However, no reproducible, or recognizable patterns could be assigned to each group of these resonances. The ^{15}N NMR spectrum (by using (4a)) in acetone- d_6 showed, in addition to a rather large peak at -73 ppm for free ^{15}NN , a medium intensity resonance at -89.20 ppm . No free $^{15}\text{NNAr}^+$, which generally occurs in the range of $-65 \sim -70\text{ ppm}$, was observed in the ^{15}N NMR spectrum. Microanalysis gave 2.77% nitrogen content in the red solid, which was lower than the calculated 3.68% of nitrogen for $\text{Cp}^*\text{Ir}(\text{PPh}_3)(\text{Cl})(p\text{-N}_2\text{C}_6\text{H}_4\text{OMe})$. Attempts to further purify this material failed due to its facile decomposition to give $\text{Cp}^*\text{Ir}(\text{PPh}_3)\text{Cl}_2$ as the main isolated product. However, a further protonation of this mixture in solution by

HBF₄/diethyl ether always yielded the compound [Cp*Ir(PPh₃)(Cl)(*p*-NHNC₆H₄OMe)]BF₄ (**6**) and Cp*Ir(PPh₃)Cl₂. The relative ratio of the products produced by the protonation was strongly dependent upon how long the hydrido-chloro exchange reaction proceeded and the time taken in manipulations to purify them.

Preparation of [Cp*Ir(I)]₂(μ²-η²-*p*-N₂C₆H₄OMe)(μ²-η¹-*p*-N₂C₆H₄OMe) (**7**) or (**7a**)

To a solution of [Cp*Ir(C₂H₄)(*p*-N₂C₆H₄OMe)]BF₄ (**1**) or (**1a**) (50 mg, 0.061 mmol) in 10 mL ethanol was added an equivalent of ground predried KI. The reaction mixture was vigorously stirred for ca. 2 h at room temperature. The colour of the solution changed from yellow to brown and a large amount of fine dark brown precipitate was produced. After removing the solvent *in vacuo* at room temperature, the solid residue was re-dissolved in ca. 10 mL CH₂Cl₂ giving a brownish green solution and some fine white precipitate (NaBF₄). Following filtration, the filtrate was evaporated to dryness affording analytically pure compound (**7**) or (**7a**) quantitatively. Recrystallization of (**7**) or (**7a**) from CH₂Cl₂/hexanes at -10 °C gave cuboid-shaped dark brown crystals in higher than 90% yield. M.P. 224 °C (decomposition), ¹H NMR (100 MHz): δ(CDCl₃) 1.29s (15H, C₅Me₅), 1.37s (15H, C₅Me₅), 3.84s (6H, 2OMe), 6.85d (2H, J = 9, aromatic), 6.96d (2H, J = 9, aromatic) and 7.74d (4H, J = 9, aromatic), (see Figure 3.1), ¹⁵N NMR for (**7a**): δ(CDCl₃) 64.12 (N_α) and 300.03 (N_β), EIMS (*m/z*): 590 (M⁺⁺), Anal. (calcd): C, 34.64; H, 3.76; N, 4.75, (found): C, 34.54; H, 3.77 N, 4.73.

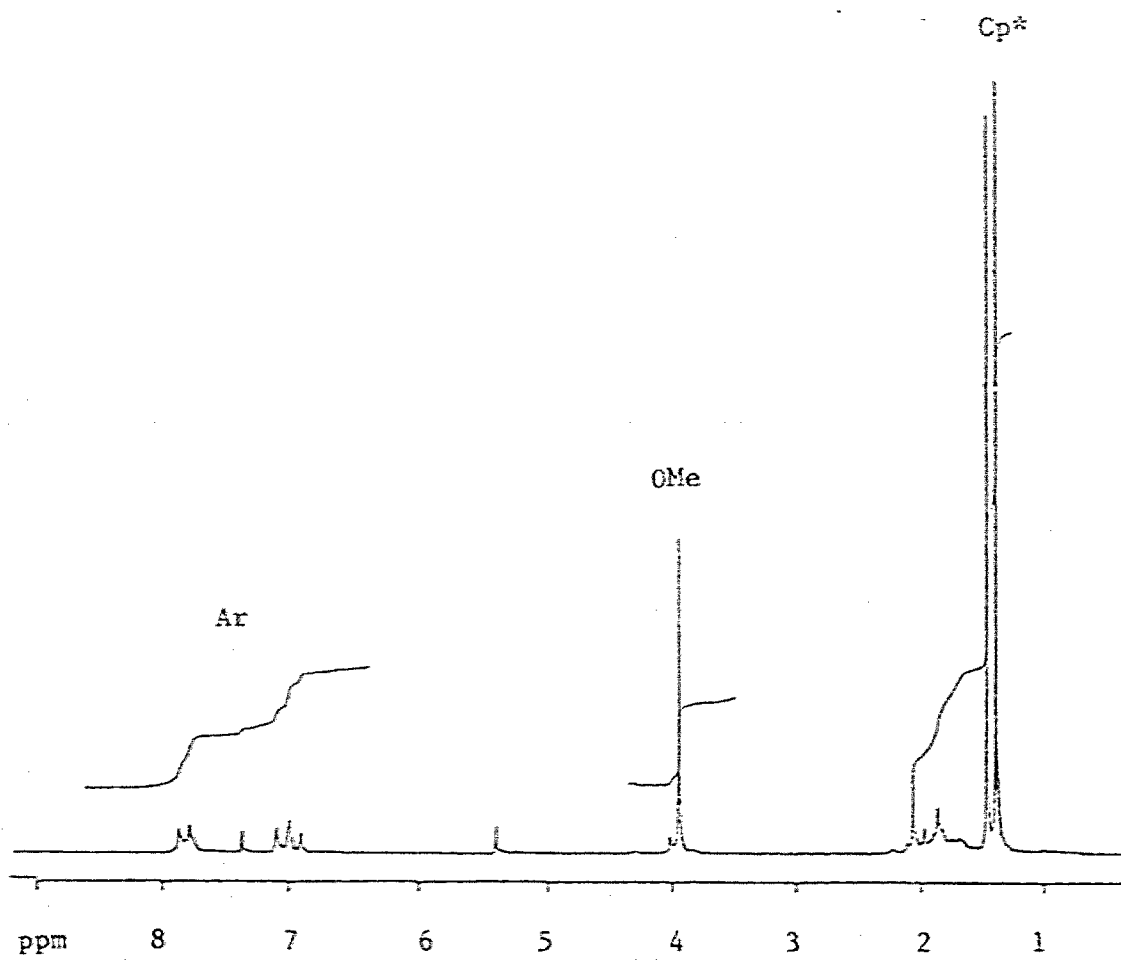


Figure 3.1 ^1H NMR spectrum of (7) in CDCl_3

Preparation of $[\text{Cp}^*\text{Ir}(\text{Br})]_2(\mu^2-\eta^2-p\text{-N}_2\text{C}_6\text{H}_4\text{OMe})(\mu^2-\eta^1-p\text{-N}_2\text{C}_6\text{H}_4\text{OMe})$ (8) or (8a)

A similar procedure to that used for (7) or (7a), but using predried KBr and a rather longer time (ca. 4 h), gave (8) and (8a) quantitatively as dark brown microcrystals. ^1H NMR (100 MHz): $\delta(\text{CDCl}_3)$ 1.22s (15H, C_5Me_5), 1.28s (15H, C_5Me_5), 3.86s (6H, 2OMe), 6.85d (2H, $J = 9$, aromatic), 6.95d (2H, $J = 9$, aromatic) and 7.79d (4H, $J = 9$, aromatic), ^{15}N NMR for (8a): $\delta(\text{CDCl}_3)$ 69.84 ($\text{N}\alpha$) and 303.44 ($\text{N}\alpha'$), MS (EI)(m/z): 542 (M^{++}), 463 ($\text{M}^{++}\text{-Br}$), 407 ($\text{M}^{++}\text{-N}_2\text{C}_6\text{H}_4\text{OMe}$), Anal. (calcd.): C, 37.64; H, 4.09; N, 5.16, (found): C, 38.08; H, 4.11; N, 5.09

Observation of $\{[\text{Cp}^*\text{Ir}(\text{I})]_2(\mu^2-\eta^2-p\text{-}^{15}\text{N}\alpha\text{HNC}_6\text{H}_4\text{OMe})(\mu^2-\eta^1-p\text{-}^{15}\text{NNC}_6\text{H}_4\text{OMe})\} [\text{BF}_4]$ (9a) by protonation of (7a)

To a solution of (7a) (30 mg, 0.025 mmol) in 1 mL CDCl_3 in a ϕ 2.5 mm NMR tube was added 0.1 mL (2 drops) $\text{HBF}_4/\text{Et}_2\text{O}$ at room temperature. The solution became slightly cloudy. A ^{15}N NMR measurement following by a ^1H NMR measurement were immediately carried out. ^1H NMR (100 MHz): $\delta(\text{CDCl}_3)$ 1.62s (15H, C_5Me_5), 2.00s (15H, C_5Me_5), 3.84s (6H, 2OMe), 7.06m (6H, aromatic), 8.20d (1H, $J = 9$, aromatic), 8.33d (1H, $J = 9$, aromatic) and 15.20d (1H, $J_{^{15}\text{N-H}} = 79$, $^{15}\text{N}\alpha\text{-H}$), ^{15}N NMR: $\delta(\text{CDCl}_3)$ 65.1s ($^{15}\text{N}\alpha$) and -110.7s, b ($^{15}\text{N}\alpha\text{-H}$).

Observation of $\{[\text{Cp}^*\text{Ir}(\text{Br})]_2(\mu^2-\eta^2-p\text{-}^{15}\text{N}\alpha\text{HNC}_6\text{H}_4\text{OMe})(\mu^2-\eta^1-p\text{-N}_2\text{C}_6\text{H}_4\text{OMe})\} [\text{BF}_4]$ (10a) by protonation of (8a)

To a solution of (8a) (30 mg, 0.028 mmol) in ca. 2 mL CDCl_3 was added 0.1 mL (2 drops) $\text{HBF}_4/\text{Et}_2\text{O}$ at room temperature. Some precipitate was formed

and filtered off. The filtrate was collected in a ϕ 2.5 mm NMR tube for NMR measurements. ^1H NMR (100 MHz): $\delta(\text{CDCl}_3)$ 1.51s (15H, C_5Me_5), 1.90s (15H, C_5Me_5), 3.84s (6H, 2OMe), 6.89~7.41m (6H, aromatic), 8.20d (1H, $J = 9$, aromatic), 8.43d (1H, $J = 9$, aromatic) and 15.32d (1H, $J_{15\text{N-H}} = 79$, $^{15}\text{N}\alpha\text{-H}$).

Preparation of $\{[\text{Cp}^*\text{Ir}(\text{CO})]_2(\mu^2\text{-}\eta^2\text{-}p\text{-N}_2\text{C}_6\text{H}_4\text{OMe})\}\text{BF}_4$ (**11**)

A yellow ethanol solution (10 mL) of $[\text{Cp}^*\text{Ir}(\text{C}_2\text{H}_4)(p\text{-N}_2\text{C}_6\text{H}_4\text{OMe})]\text{BF}_4$ (**1**) (20 mg, 0.035 mmol) and $\text{Cp}^*\text{Ir}(\text{CO})_2$ (13 mg, 0.035 mmol) in a 50 mL pear-shaped flask equipped with a condenser was refluxed under a nitrogen atmosphere. IR monitoring the reaction indicated that (**1**) was completely consumed in about 12 hours. The dark red solution was cooled to room temperature, transferred to a Schlenk tube and concentrated *in vacuo* to about 3 mL, then excess diethyl ether was added to precipitate the brownish product. Recrystallization of this product from acetone/diethyl ether gave ruby red crystals of compound (**11**) in less than 10% yield. IR $\nu(\text{CO})$: 1922, 1970 cm^{-1} (KBr); ^1H NMR (100 MHz): $\delta(\text{CDCl}_3)$ 2.13s (15H, Cp^*), 2.01s (15H, Cp^*), 3.89s (3H, OMe), 7.05q (4H, AA'BB' pattern, C_6H_4); FABMS (Thioglycerol, Xenon) (m/z): 847 (M^+), 817 ($\text{M}^+ - \text{CO}$ or $- \text{N}_2$), 789 ($\text{M}^+ - 2\text{CO}$ or $- \text{CO} - \text{N}_2$), 761 ($\text{M}^+ - 2\text{CO} - \text{N}_2$), 463 ($[\text{Cp}^*\text{IrN}_2\text{C}_6\text{H}_4\text{OMe}]^+$), Anal. (calcd): C, 37.34; H, 4.00; N, 3.00, (found): C, 37.46, H, 4.06; N, 3.24.

Single Crystal X-ray Crystallographic Analysis of $\{[\text{Cp}^*\text{Ir}(\text{CO})]_2(\mu^2\text{-}\eta^2\text{-}p\text{-N}_2\text{C}_6\text{H}_4\text{OMe})\}\text{BF}_4$ (**11**)

Data were collected at -40 $^\circ\text{C}$ on an Enraf-Nonius CAD4-F diffractometer with graphite monochromatized $\text{Mo-K}\alpha$ radiation. The final unit cell was determined by least squares from the setting angles of 25 carefully centred

reflections (with $26^\circ \leq 2\theta \leq 41^\circ$) chosen from a variety of well spaced points in reciprocal space. An orthorhombic unit cell was first assumed and then confirmed by investigation of the symmetry related reflections. Selected crystallographic and experimental parameters are given in Table 3.1.

A total of 3438 unique reflections were measured, of which 1661 reflections were classed as observed ($I_o \geq 2.5\sigma(I_o)$) and used in structure calculations and refinements. Two intensity standards were measured every one and half hour of acquisition time, and showed no significant change in intensity during the data collection process. An analytical absorption correction based upon the crystal shape was used and it was checked against the measured absorption of psi-scan data based on four high angle reflections with $\chi > 84^\circ$. Lorentz and polarization corrections¹⁵³ were applied to convert the 1817 data into the relative structure factors.

The Patterson method was used to solve the structure initially in the space group *Pcmb*. Refinement converged to *ca.* $R_f = 0.10$. Significantly, the thermal motion parameters and some inter-atomic distances were physically unreasonable in this model. The structure was then refined in the noncentric space group *Pc2₁b*. A simple isotropic model gave $R_f = 0.08$, but had 4 intense electron density peaks in an electron density difference map. Each of these peaks occurred near one of the Ir atoms. Careful examination of the near-origin region of the Patterson map showed short vectors consistent with these four peaks. The position of each peak was approximately related to one of the Ir atoms in the main structure by a pseudo-mirror normal to the *a* direction. Therefore, they are assigned to 4 disordered Ir atoms.

Refinement of this model commenced with one occupancy variable for the Ir atoms and resulted in 15% occupancy for the smaller Ir sites and 85% for the

larger and gave an improved agreement ($R_f = 0.048$). The light atoms in the larger component were, therefore, assigned to 85% occupancy; the light (non-hydrogen) atoms in the 15% disordered structure could not be seen in the electron density difference map due to their small contribution (comparable with normal hydrogen atoms) and, therefore, were created as an image of the corresponding main structure by the pseudo-mirror normal to the *a* direction.

The refinement of the disordered structure in space group $Pc2_1b$ was initially carried out in steps using the "Crystals Crystallographic Package"¹⁵⁴ with large block-matrix least squares. The first step involved only the refinement of the 85% component (with some restraints on the molecular geometry) and the four Ir atoms of the 15% component together with the light atoms of this component in fixed positions. This gave an agreement $R_f = 0.0451$. The second step involved fixing the refined 85% component and the four Ir atoms of the 15% component in the structure factor calculations and refining only the light atoms of the 15% component, which gave an agreement $R_f = 0.0440$.

The final refinement included both the 85% and 15% components. The light atoms of the 15% component were treated as rigid groups and appropriate angles and planes were used to maintain the reasonableness of this model throughout. The hydrogen atoms were included in the calculated positions (C-H = 0.96 Å) in the structure factor calculations but were not refined. Only isotropic thermal motion was allowed, and chemically similar atoms were constrained to have similar motions.* The refinement was considered complete when $\text{shift/esd} \leq 0.01$. In the final refinement, 305 atoms and 259 variables were included against 1661 observed independent reflections and gave final values of $R_f = 0.0438$, $R_w = 0.0492$. The largest peak in the final electron density difference map was $1.2 \text{ e}\text{\AA}^{-3}$ at 0.96 \AA from Ir(1). The BF_4^- ion was also disordered, and

was treated by a simple model in which three of the F atoms were assigned two sites with 0.5 occupancy. Unit weights were employed.

: The isotropic thermal motion of the following similar atoms were treated equivalently: O atoms of carbonyls, C atoms of the carbonyls, N atoms in the diazenides, C atoms of the ring members in each Cp group, C atoms of methyl groups in each Cp*, C atoms of the ring in each phenyl group, H atoms of the methyl groups in Cp* groups, H atoms in the phenyl groups, F atoms in BF₄⁻, B atoms in BF₄⁻ and Ir atoms in 85% occupancy with their pseudo-image partners in 15% occupancy.

Table 3.1. Crystallographic Data for the Structure Determination of
 $[(\text{Cp}^*\text{Ir}(\text{CO}))_2(\mu^2\text{-}\eta^2\text{-}p\text{-N}_2\text{C}_6\text{H}_4\text{OMe})]\text{BF}_4$ (**11**)

Formula	$\text{Ir}_2\text{F}_4\text{O}_3\text{N}_2\text{C}_{29}\text{BH}_{37}$
Crystal System	Orthorhombic
Space Group	$Pc2_1b$
a (Å)	8.821(1)
b (Å)	20.237(2)
c (Å)	34.808(5)
Z	8
T (K)	233
FW	932.3
ρ (g/cm ³)	1.995
μ (MoK α) (cm ⁻¹)	85.85
Crystal Size (mm)	0.34 x 0.26 x 0.11
λ (Å)	0.71069
Transmission	0.2191 - 0.3759
Min - Max 2θ (°)	0 - 50
Scan Type	ω - 2θ
Min. h, k, l	0, 0, 0
Max. h, k, l	8, 19, 34
R_1^a	0.0438
R_w^b	0.0492
GOF ^c	1.093

a: $R_1 = \sum(|F_o| - |F_c|) / \sum |F_o|$ for observed data

b: $R_w = [\sum w(|F_o| - |F_c|)^2 / \sum w|F_o|^2]^{1/2}$ for observed data

c: $\text{GOF} = [\sum w(|F_o| - |F_c|)^2 / \text{degrees of freedom}]^{1/2}$

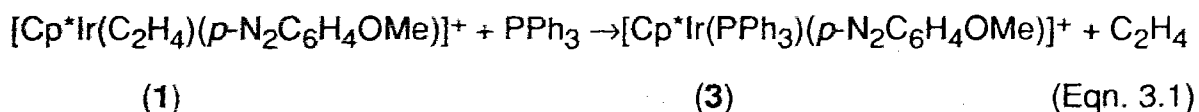
3.3 Results

3.3.1 Syntheses and Characterizations

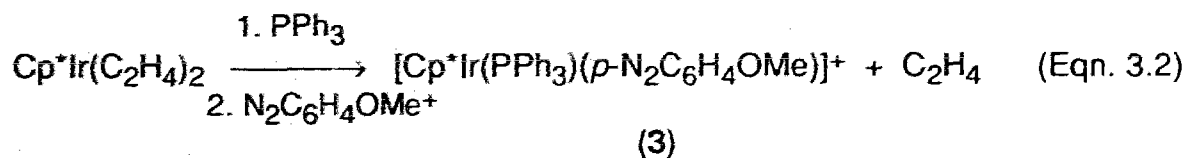
3.3.1.1 The Singly and Doubly Bent Aryldiazenido and Diazene

Complexes Containing the Cp*Ir(PPh₃) Core

As mentioned in the previous chapter, in the complex [Cp*Ir(C₂H₄)(*p*-N₂C₆H₄OMe)]BF₄ (1), the singly bent aryldiazenido ligand, as a strong π acid, weakens the bonding between the ethylene ligand and the iridium centre. This should also influence the reactivity of the compound; it will be expected that the singly bent aryldiazenido ligand may induce lability of the ethylene ligand in regard to ligand exchange reactions. In agreement with this, treatment of (1) with an equimolar amount of PPh₃ in ethanol solution at room temperature affords quantitatively the corresponding triphenylphosphine aryldiazenido complex, [Cp*Ir(PPh₃)(*p*-N₂C₆H₄OMe)]BF₄ (3), (Equation 3.1)



Alternatively, a direct reaction of the bisethylene compound Cp*Ir(C₂H₄)₂, *in situ*, with equimolar amounts of PPh₃ and [*p*-N₂C₆H₄OMe)]BF₄ also gives quantitatively the target compound (3). (Equation 3.2)



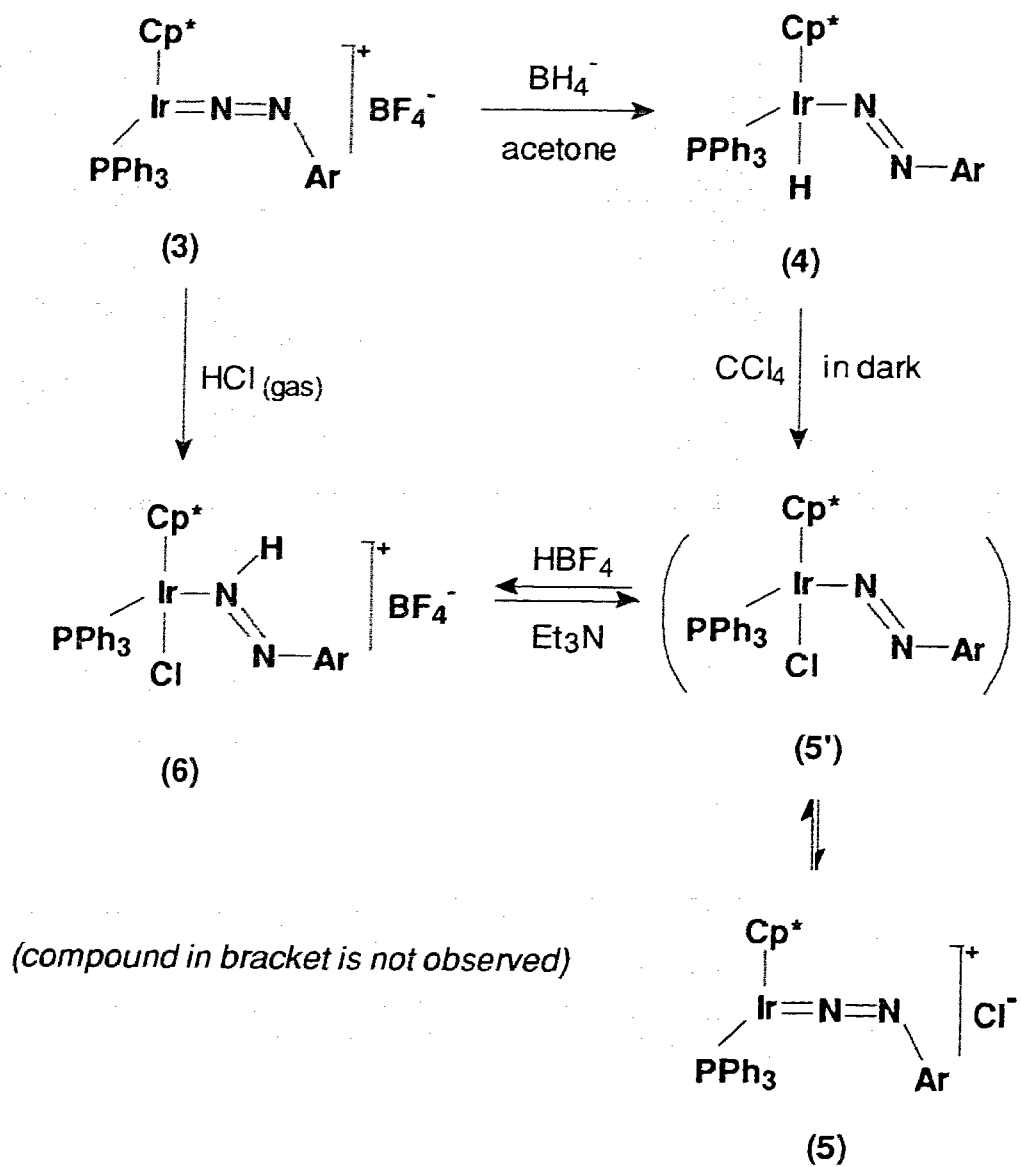
Compound (3) is stable under a nitrogen atmosphere either as the pure oil or as solutions in non-halogenated solvents. It decomposes slowly in halogenated solvents, for example CDCl_3 .

The analytical and spectroscopic data for compound (3) have been given in the experimental section, and suggest the monomeric nature of this compound. The chemically interesting feature of the IR spectrum of $[\text{Cp}^*\text{Ir}(\text{PPh}_3)(p\text{-N}_2\text{C}_6\text{H}_4\text{OMe})]\text{BF}_4$ (3) is that $\nu(\text{NN})$ at 1710 cm^{-1} in EtOH, occurs at a lower wavenumber than that exhibited by its analogue, $[\text{Cp}^*\text{Ir}(\text{C}_2\text{H}_4)(p\text{-N}_2\text{C}_6\text{H}_4\text{OMe})]\text{BF}_4$ (1), which has $\nu(\text{NN})$ at 1724 cm^{-1} in EtOH. This indicates that the π interaction is the dominant component in causing the different NN bonding strengths in the two analogous compounds. Considering only σ type of interactions, PPh_3 is generally expected to be a better σ donor than C_2H_4 due to its higher-lying HOMO, so the trans influence of PPh_3 on the weakening of the $\text{Ir-N}\alpha$ σ bond would be expected to be larger than that of ethylene. This, in turn, would cause a weakening of the $\text{Ir-N}\alpha$ bonding and a strengthening of the NN bonding of the aryldiazenido ligand in the phosphine compound, $[\text{Cp}^*\text{Ir}(\text{PPh}_3)(p\text{-N}_2\text{C}_6\text{H}_4\text{OMe})]\text{BF}_4$ (3), by comparison with the corresponding ethylene compound (1). Obviously, this is contrary to what we have observed experimentally. However, considering now the π interaction, C_2H_4 ligand is generally considered as a better π acid than PPh_3 ligand, so there should be more electron density at the metal centre available for π -back-bonding to the antibonding π orbitals of the aryldiazenido ligand in $[\text{Cp}^*\text{Ir}(\text{PPh}_3)(p\text{-N}_2\text{C}_6\text{H}_4\text{OMe})]\text{BF}_4$ (3), than in $[\text{Cp}^*\text{Ir}(\text{C}_2\text{H}_4)(p\text{-N}_2\text{C}_6\text{H}_4\text{OMe})]\text{BF}_4$ (1) and this accounts for the lower $\nu(\text{NN})$ value for (3). The lower field ^{15}N NMR chemical shift for $\text{N}\alpha$ in (3) than in (1) also indicates greater anisotropy of the π electron density at the $\text{N}\alpha$

position in (3) than in (1), which is also consistent with the view that greater π electron density is back-bonded to the aryldiazenido ligand from the metal centre in (3).

It is also interesting to note that the ^1H NMR spectrum of compound (3) in CDCl_3 shows a doublet resonance ($J = 1$ Hz) for the aromatic protons in the *para*-methoxyphenyl group, but in acetone- d_6 , it shows the familiar AA'BB' pattern. This difference suggests to us that the acetone solvent may be weakly involved in the coordination sphere of the coordinatively unsaturated metal centre, which may induce a slight distortion of the the molecular geometry, and hence a change of the electron distribution in the molecule.

The reaction of compound (3) with BH_4^- in acetone solution at -10 °C gives the corresponding hydrido complex, $\text{Cp}^*\text{Ir}(\text{PPh}_3)(\text{H})(\rho\text{-N}_2\text{C}_6\text{H}_4\text{OMe})$ (4), in good yield (Scheme 3.1). This type of complex, in which a hydrido ligand coexists with a doubly bent aryldiazenido ligand, is not common.^{13, 34} The only other examples were reported by Haymore and Ibers.⁸⁰ These are the complexes $\text{M}(\text{H})(\text{CO})_2(\text{PPh}_3)_2(\text{N}_2\text{Ph})$ ($\text{M} = \text{Os}, \text{Ru}$), which were prepared by the deprotonation of the corresponding diazene complexes $[\text{M}(\text{H})(\text{CO})_2(\text{PPh}_3)_2(\text{NHNPh})]^+$. Haymore and Ibers also attempted, without success, to obtain these compounds through a reaction of the corresponding five-coordinated singly bent diazenido compounds $[\text{M}(\text{CO})_2(\text{PPh}_3)_2(\text{N}_2\text{Ph})]^+$ with H^- , apparently because the reducing conditions destroyed the aryldiazenido ligand. Therefore, it is significant that we have been able to achieve a similar reaction in high yield in our system. Conveniently, this hydrido (doubly bent diazenido) complex is relatively stable either in the solvent-free state or in halogen-free solvents, so it has been fully characterized. Compound (4) gives peach red coloured solutions in acetone or hexane and is a beautiful rose-purple colour in the solvent-free state.



Scheme 3.1

No IR band due $\nu(\text{NN})$ of the doubly bent aryldiazenido ligand could be assigned, even with the aid of a ^{15}N -enriched sample. A broad medium intensity band at 2133 cm^{-1} was observed in both the ^{14}N sample and the ^{15}N -enriched sample, and is assigned as $\nu(\text{Ir-H})$. The proton NMR spectrum in acetone- d_6 shows, in addition to the resonances for the aromatic and the methoxy protons, a sharp doublet, integrating for one hydrogen, in the hydride range (δ : -15.9 ppm with $^2J_{\text{P-H}} = 33.5\text{ Hz}$) and a well resolved doublet of doublets, integrating for 15 hydrogens, in the Cp^* methyl region (δ : 1.51 ppm with $J_{\text{P-Me}} = 1.8\text{ Hz}$ and $J_{\text{H-Me}} = 0.7\text{ Hz}$) (Figure 3.2). Therefore, presence of the hydride ligand in (4) has been confirmed by both IR and proton NMR spectroscopy.

The evidence for a doubly bent aryldiazenido ligand in (4) has been unambiguously provided by the ^{15}N NMR spectrum of (4a). The only resonance is a singlet at δ : 271.9 ppm, assigned to $^{15}\text{N}\alpha$, and this falls within the typical chemical shift range for a doubly bent aryldiazenido ligand, δ : 200 ~ 350 ppm.^{34, 97, 171} Compared with the ^{15}N NMR chemical shift values for the corresponding singly bent aryldiazenido ligand in complexes (1a) and (3a), (δ : -2.26 ppm for (1a), and 33.2 ppm for (3a)), this shift indicates that there is a consistent, but dramatic increase of the deshielding for the $\text{N}\alpha$ nucleus in complex (4). This obviously results from the presence of a lone pair of electrons on the $\text{N}\alpha$ atom in (4). Another interesting feature exhibited by compound (4a) is that no ^{15}N coupling to the hydridic proton or to the ^{31}P of the phosphine could be observed in the ^1H or ^{15}N NMR spectrum of (4a). Since ^{31}P - ^{15}N coupling was easily recognized in the ^{15}N NMR spectrum of compound (3a), where the phosphine ligand and the diazenido ligand are trans to each other in a two-legged piano-stool structure, it seems that the molecular geometry and the

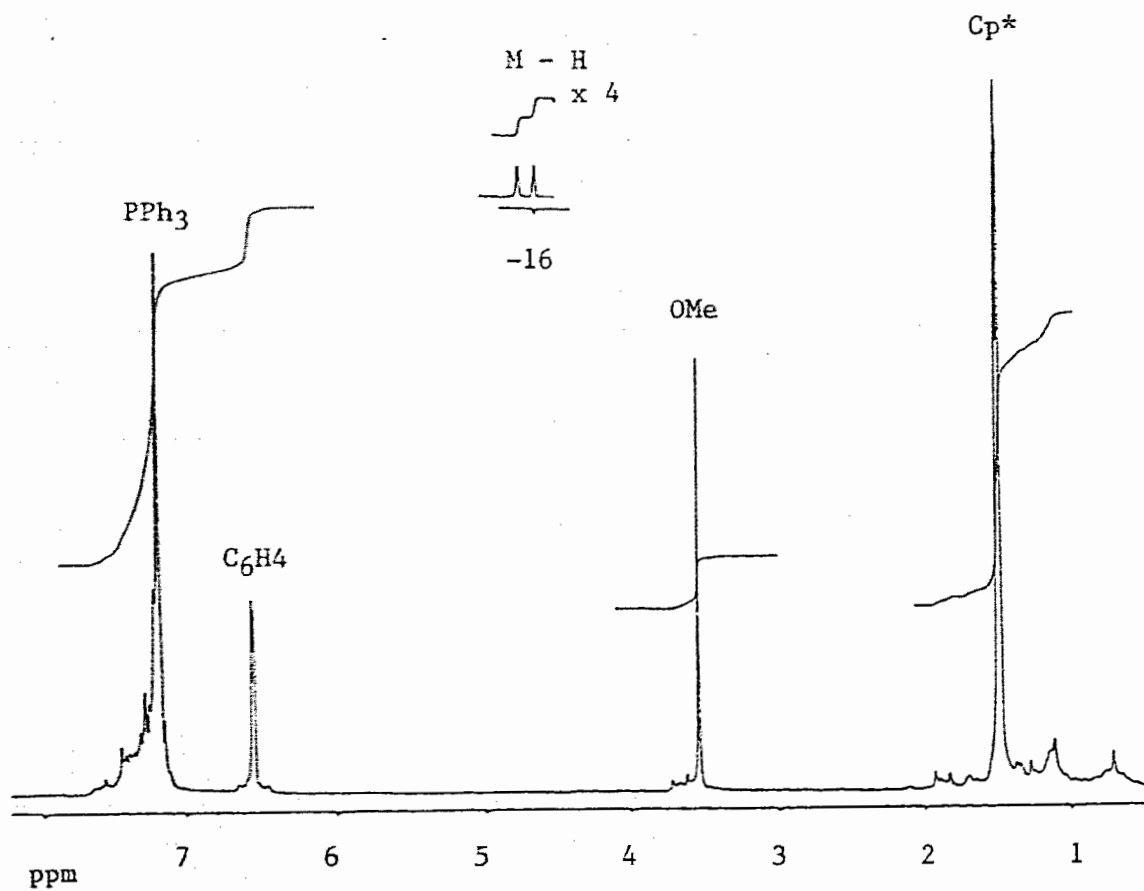
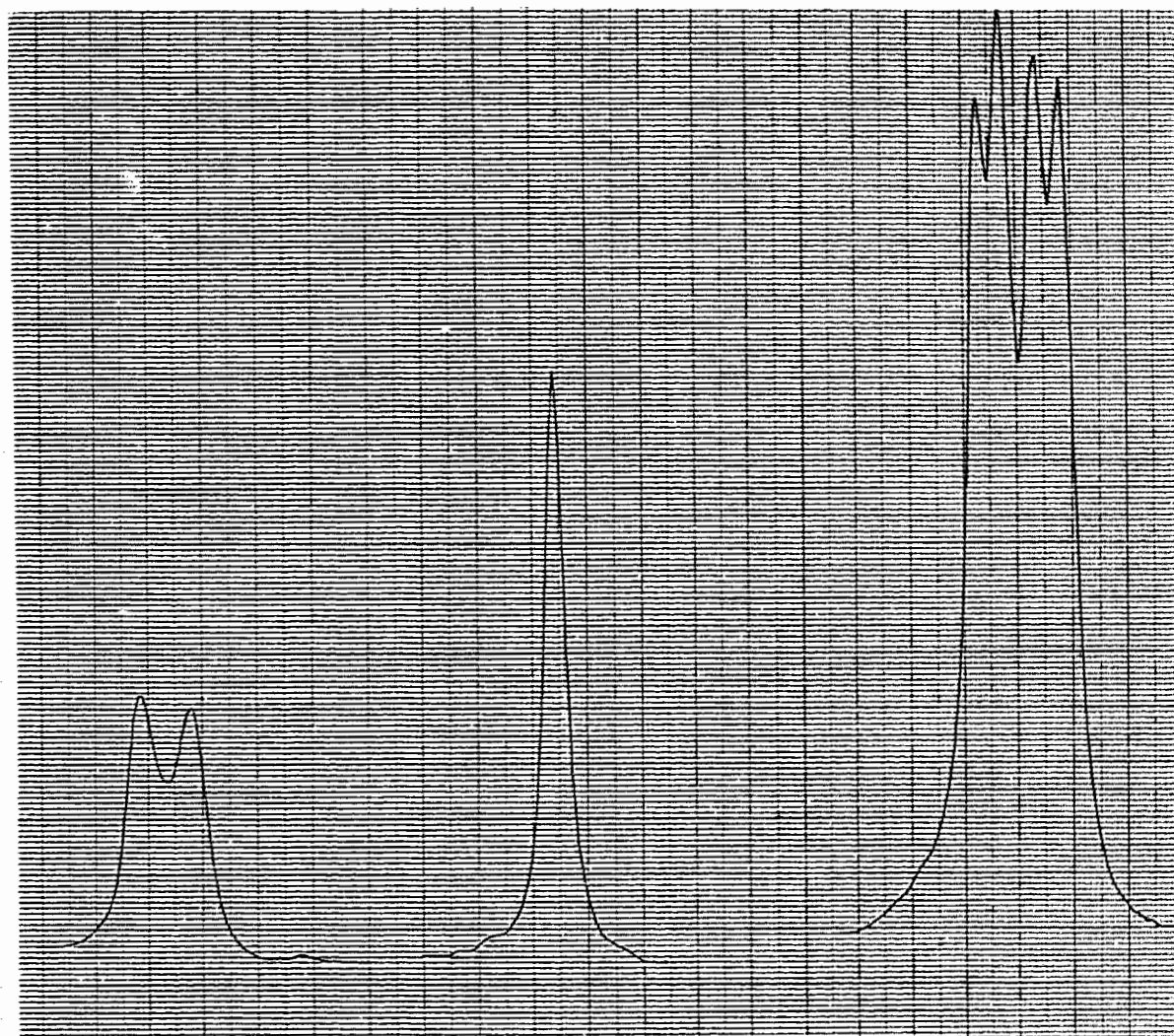


Figure 3.2 ^1H NMR spectrum of (4) in acetone- d_6 , in a wide window
(more in next page)



$p\text{-C}_6\text{H}_4$

OMe

$\eta^5\text{-C}_5\text{Me}_5$

Figure 3.2 ^1H NMR spectrum of (4) in acetone- d_6 , (expansion of Cp^+ , OMe and C_6H_4 resonances)

relative positions of related ligands are responsible for this difference here, but it is not immediately apparent how this is so. Note that the absence of $^{15}\text{N}\alpha\text{-H}$ coupling was also reported by Haymore and Ibers for their complexes.⁸⁰

An attempt to synthesize $\text{Cp}^*\text{Ir}(\text{PPh}_3)(\text{Cl})(p\text{-N}_2\text{C}_6\text{H}_4\text{OMe})$ (**5**), the chloro analogue of compound (**4**), by a direct hydrido-chloro exchange reaction of (**4**) with excess CCl_4 in the dark at $-10\text{ }^\circ\text{C}$ was not successful. However, a related compound, the salt $[\text{Cp}^*\text{Ir}(\text{PPh}_3)(p\text{-N}_2\text{C}_6\text{H}_4\text{OMe})]\text{Cl}$ (**5'**), together with a variable amount of the known complex $\text{Cp}^*\text{Ir}(\text{PPh}_3)\text{Cl}_2$,¹⁷⁰ is believed to be produced. However *in situ* protonation of the products of this exchange with $\text{HBF}_4/\text{OEt}_2$ results in the diazene complex $[\text{Cp}^*\text{Ir}(\text{PPh}_3)(\text{Cl})(p\text{-NHNC}_6\text{H}_4\text{OMe})]\text{BF}_4$ (**6**) and $\text{Cp}^*\text{Ir}(\text{PPh}_3)\text{Cl}_2$.¹⁷⁰ This diazene complex $[\text{Cp}^*\text{Ir}(\text{PPh}_3)(\text{Cl})(p\text{-NHNC}_6\text{H}_4\text{OMe})]\text{BF}_4$ (**6**), can be synthesized by an alternative way discussed in the next paragraph, and deprotonation of it gives only $[\text{Cp}^*\text{Ir}(\text{PPh}_3)(p\text{-N}_2\text{C}_6\text{H}_4\text{OMe})]\text{Cl}$ (**5'**), instead of $\text{Cp}^*\text{Ir}(\text{PPh}_3)(\text{Cl})(p\text{-N}_2\text{C}_6\text{H}_4\text{OMe})$ (**5**), plus a trace of $\text{Cp}^*\text{Ir}(\text{PPh}_3)\text{Cl}_2$ (see Scheme 3.1). Further, the $\nu(\text{NN})$ value, (1711 cm^{-1} in CH_2Cl_2 and 1717 cm^{-1} in CCl_4), undoubtedly indicates a singly bent, and not a doubly bent aryldiazenido ligand as required for (**5'**) and not (**5**).

The aryldiazene complex $[\text{Cp}^*\text{Ir}(\text{PPh}_3)(\text{Cl})(p\text{-NHNC}_6\text{H}_4\text{OMe})]\text{BF}_4$ (**6**), or (**6a**) can be conveniently prepared in high yield (92%) in one synthetic step from the reaction of $[\text{Cp}^*\text{Ir}(\text{PPh}_3)(p\text{-N}_2\text{C}_6\text{H}_4\text{OMe})]\text{BF}_4$ (**3**), or (**3a**) directly with HCl gas in ethanol solution. The lower $\nu(\text{NN})$ in the IR spectrum at 1483 cm^{-1} , $\nu(^{15}\text{NN})$ at 1460 cm^{-1} for (**6a**), is consistent with the presence of a diazene ligand. This has been further substantiated by the ^1H and ^{15}N NMR spectra for (**6a**). A characteristic doublet (δ : 13.73 ppm with $J_{\text{H-}^{15}\text{N}} = 70\text{ Hz}$ in acetone- d_6) observed in the ^1H NMR spectrum (Figure 3.3), together with a high field doublet (δ : -64.24

ppm with $J_{^{15}\text{N-H}} = 70$ ppm in acetone- d_6) observed in the ^{15}N NMR spectrum (Figure 3.4) of (6a) unambiguously establish the presence of a η^1 -coordinated diazene, $-\text{NHNC}_6\text{H}_4\text{OMe}$, ligand in complex (6), or (6a). Both the chemical shift and coupling constant are consistent with analogous data previously established for the aryldiazene ligand in mono-nuclear complexes.^{172, 173, 174} Another spectral feature exhibited by (6a) in its ^1H NMR spectrum is that the chemical shift of the NH observed in acetone- d_6 is ca. 0.7 ppm downfield compared with that in CDCl_3 . This suggests that weak hydrogen bonds could be formed between the oxygen atom of the solvent (acetone) and hydrogen of the diazene; this would decrease the shielding at the proton of the diazene and cause its chemical shift to move downfield. This could also explain why compound (6) is isolated as the diethyl ether solvated form $[\text{Cp}^*\text{Ir}(\text{PPh}_3)(\text{Cl})(p\text{-NHNC}_6\text{H}_4\text{OMe})]\text{BF}_4 \cdot 1/2(\text{Et})_2\text{O}$. Each solvent molecule may be hydrogen-bonded to two molecules of (6) through the lone pairs on its oxygen.

As mentioned above, deprotonation of (6) by triethylamine gives an orange yellow compound that is (5'), instead of the desired compound $\text{Cp}^*\text{Ir}(\text{PPh}_3)(\text{Cl})(p\text{-N}_2\text{C}_6\text{H}_4\text{OMe})$ (5). This compound shows identical IR and ^1H NMR spectra to compound (3). Therefore, it is believed that (5') contains the same cation as that in (3), namely, $[\text{Cp}^*\text{Ir}(\text{PPh}_3)(p\text{-N}_2\text{C}_6\text{H}_4\text{OMe})]^+$, but a different anion. So, it is assigned as $[\text{Cp}^*\text{Ir}(\text{PPh}_3)(p\text{-N}_2\text{C}_6\text{H}_4\text{OMe})]\text{Cl}$ (5'). However, the reprotonation of this compound with $\text{HBF}_4/\text{Et}_2\text{O}$ results in the corresponding diazene complex $[\text{Cp}^*\text{Ir}(\text{PPh}_3)(\text{Cl})(p\text{-NHNC}_6\text{H}_4\text{OMe})]\text{BF}_4$ (6) where now the Cl group is coordinated. A mechanism involving a direct protonation of (5'), and then immediately followed by the coordination of the Cl^- counter ion is less plausible, because the protonation of the positively

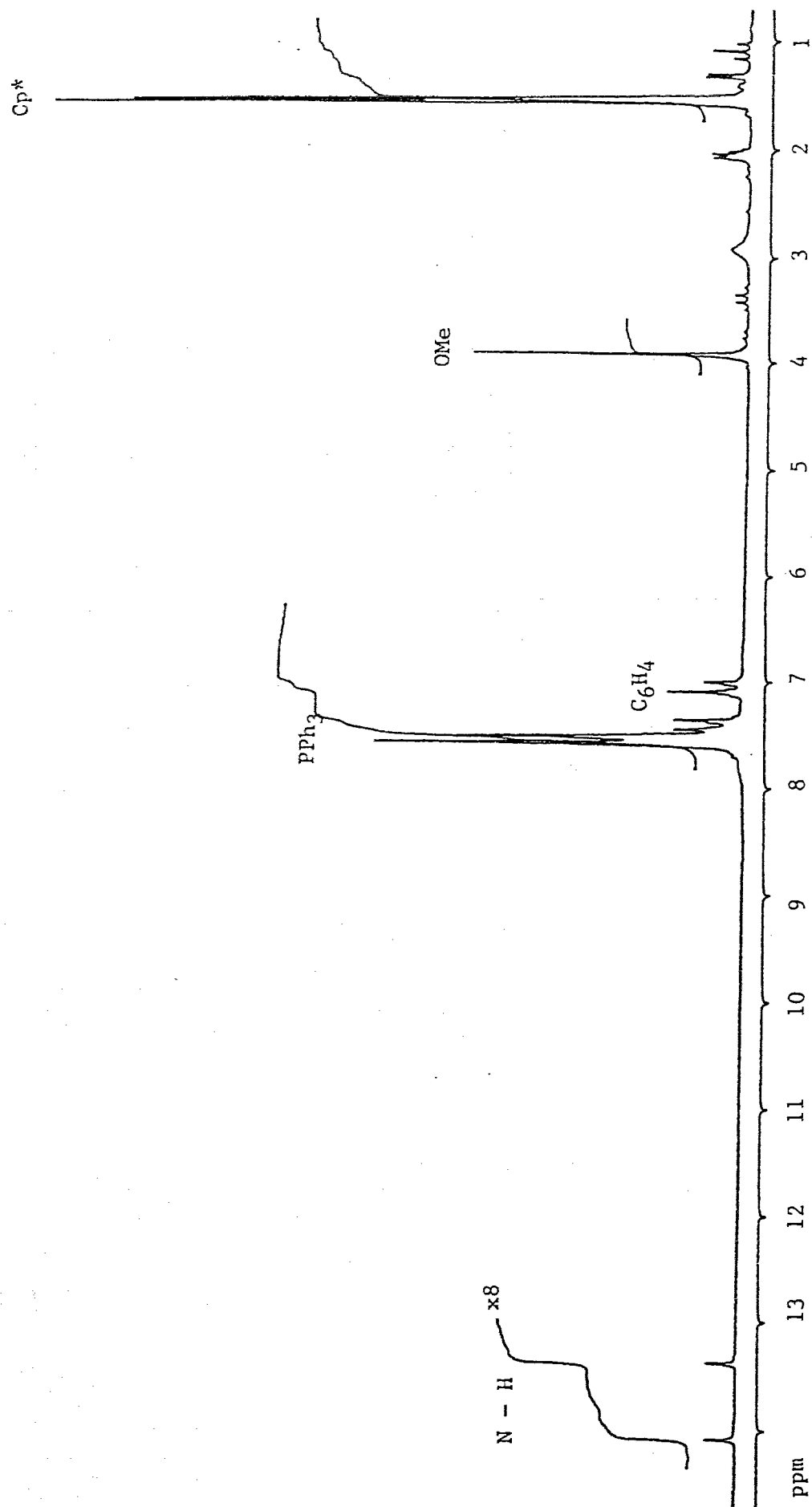


Figure 3.3 ^1H NMR spectrum of **(6a)** in acetone- d_6

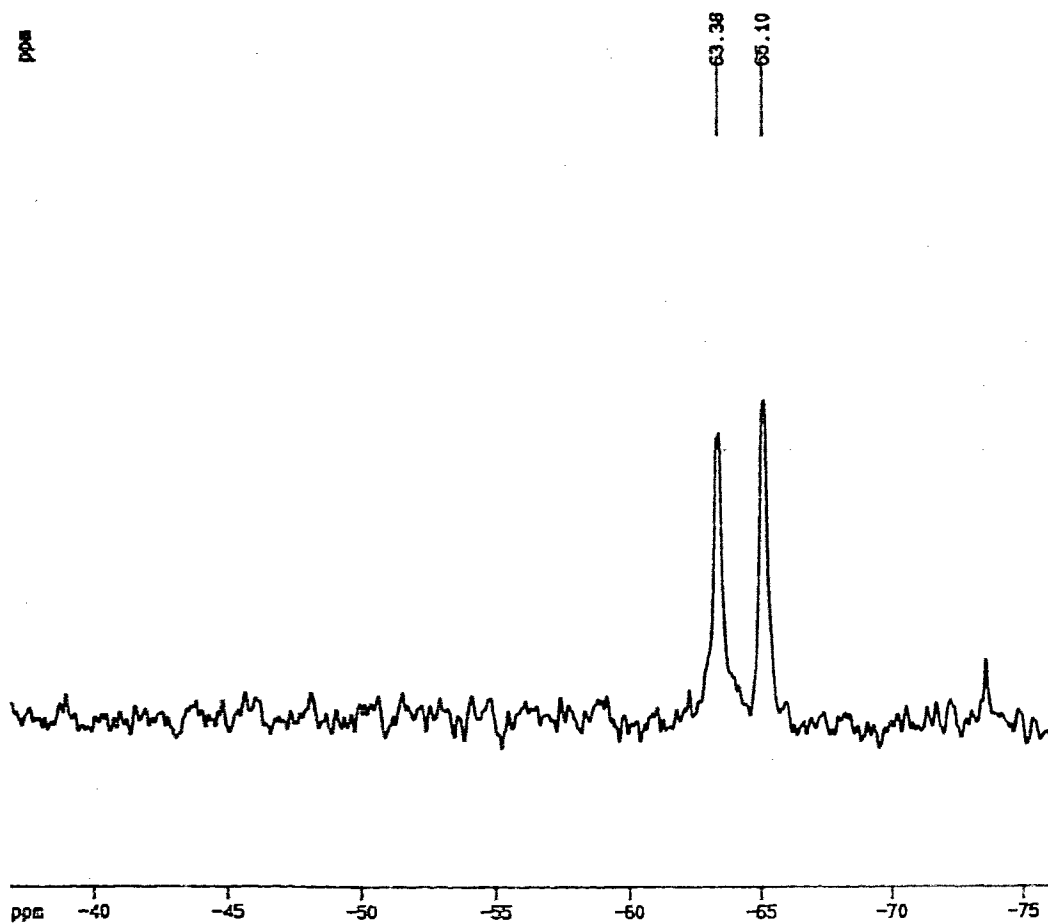
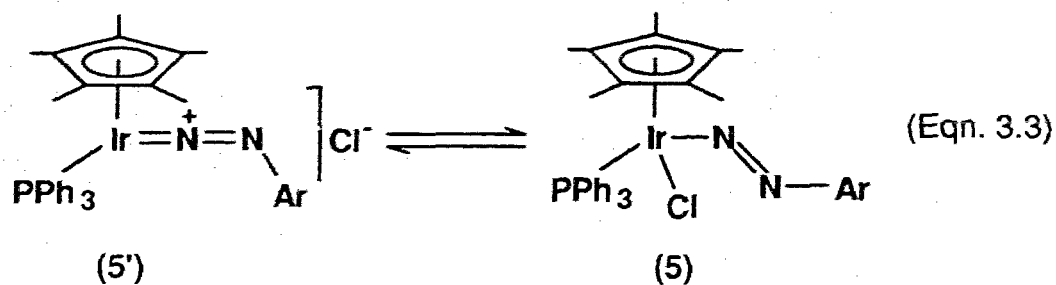


Figure 3.4 ^{15}N NMR spectrum of (6a) in acetone- d_6

charged N_{α} of the singly bent aryldiazenido ligand to result in a di-cation is expected to be difficult. Therefore, we postulate an equilibrium between (5') and corresponding neutral species, $Cp^*Ir(PPh_3)(Cl)(p-N_2C_6H_4OMe)$ (5) (Equation 3.3)



It is possible that the by-product $Cp^*Ir(PPh_3)Cl_2$ formed during the purification of (5), or (5') is further evidence for this. This can result if the doubly bent aryldiazenido ligand in $Cp^*Ir(PPh_3)(Cl)(p-N_2C_6H_4OMe)$ (5) is readily replaced by a Cl^- ion, the counter ion of (5').

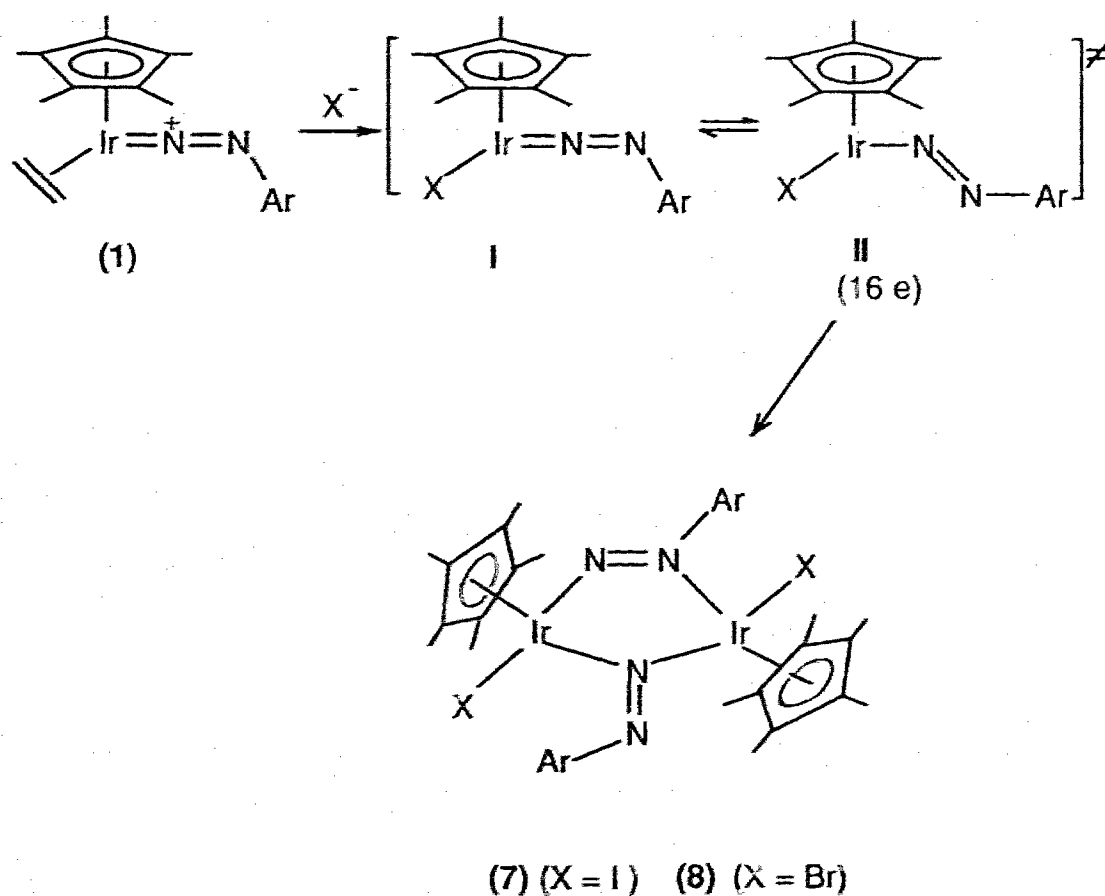
3.3.1.2 Complexes Containing Bridging Aryldiazenido and Aryldiazene Ligands

1). Halides (I^- or Br^-) as the Ancillary Ligands

Substitution of ethylene by I^- in the reaction of (1) with an equimolar amount of KI in ethanol quantitatively gives the di-iridium complex $[Cp^*Ir(I)]_2(\mu^2-\eta^2-p-N_2C_6H_4OMe)(\mu^2-\eta^1-p-N_2C_6H_4OMe)$ (7), [or (7a) when (1a) is used]. The corresponding bromo complex (8), [or (8a)] has also been synthesized in a similar way, but required a slightly longer reaction time (four hours). The use of KX ($X=I$ or Br), instead of other more soluble sources of X^- , in these reactions is to avoid creating a high initial concentration of the X^- ion in the reaction solution

because this may cause a further substitution of the aryldiazenido ligand to form $(Cp^*IrX_2)_2$.

Formation of (7), or (8) from the corresponding singly bent aryldiazenido complex (1) is less straightforward than what we have seen in the synthesis of $[Cp^*Ir(PPh_3)(p-N_2C_6H_4OMe)]BF_4$ (3) from the same starting material, where the singly bent geometry of the diazenido ligand is retained in both the reactant (1) and the product (3). Substitution of the ethylene of (1) by the strong π bases I^- or Br^- should first give a singly bent aryldiazenido species such as the intermediate I, (Scheme 3.2). This is because the ethylene ligand of (1) is quite labile and we



Scheme 3.2

have seen that it can be readily replaced by PR_3 . Dimerization of this singly bent aryldiazenido intermediate to give products (7) or (8) is unlikely in view of the absence of a lone pair on N_α and the presence of a low energy lone pair of electrons on N_β . On the other hand, however, there is expected to be a strong destabilization of the π interaction between the mutually *trans* X^- and N_2Ar^+ ligands in this intermediate (a further discussion of this upon the molecular orbital interactions will be given later in section 3.4.2). Thus it would be expected that a rearrangement of this intermediate through a MLCT (Metal to Ligand Charge Transfer) could occur readily to form a neutral 16-electron intermediate II with a doubly bent aryldiazenido ligand. It is this intermediate, (in which the doubly bent diazenido ligand has a high-lying HOMO distributed almost equally between its N_α and N_β positions, and the iridium centre is in a d^6 electronic configuration) that most likely leads to the dimerization reaction to form (7) or (8).

For both compounds (7) and (8) crystals suitable for X-ray diffraction study were obtained by crystallization from CH_2Cl_2 /hexanes. Compounds (7) and (8) are very soluble in CH_2Cl_2 , CHCl_3 and acetone, and are slightly soluble in EtOH, Et₂O and even hexanes. They are stable as either solid or as solutions even in the halogenated solvents.

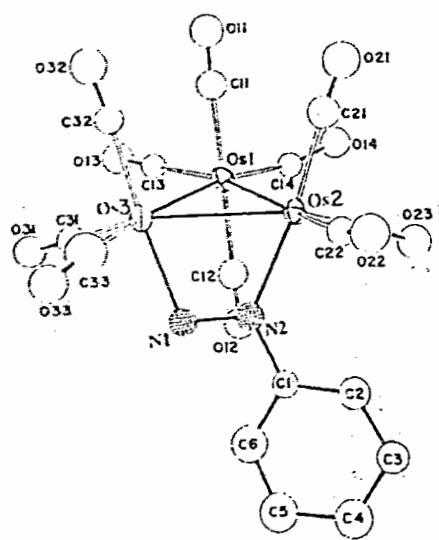
Both of these compounds have been fully characterized by analysis and spectroscopy. Infrared spectra of (7) and (8) show no bands assignable to $\nu(\text{NN})$ either in the 1600 ~ 2500 cm^{-1} range, indicating the absence of a singly bent aryldiazenido ligand, or in the finger-print region, even by comparing with the ¹⁵N-enriched samples, (7a) and (8a). Therefore no assignment of $\nu(\text{NN})$ can be made.

The proton NMR spectrum of (7) in CDCl_3 shows two sharp singlets in the methyl group region (δ : 1.29 and 1.37 ppm), and two significantly different

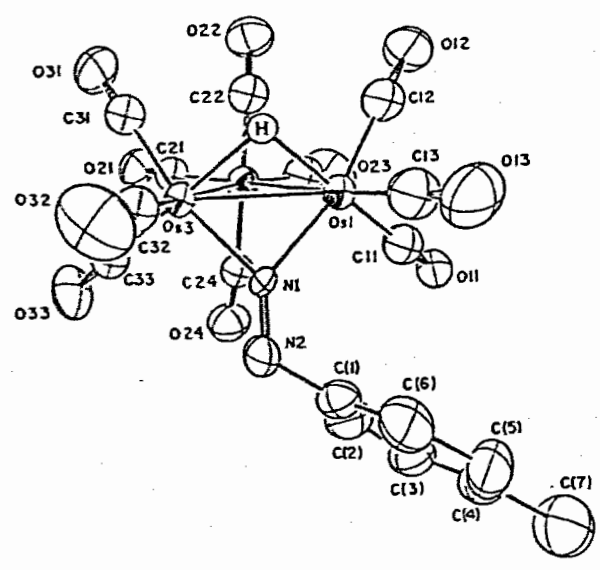
AA'BB' patterns in the aromatic proton range, (see Figure 3.1), indicative of two inequivalent Cp* groups, and two inequivalent -C₆H₄OMe groups. Significantly, the ¹⁵N NMR spectra of (7a) and (8a) unequivocally show the presence of two coordinatively distinct aryldiazenido ligands, one of which gives a resonance at δ: 64.12 ppm for (7a), (δ: 69.84 ppm for (8a)), and the other at δ: 300.03 ppm for (7a), (δ: 303.44 ppm for (8a)). The downfield signal at δ ~ 300 ppm indicates an anomalous deshielding at this nitrogen nucleus, which can only be caused by presence of a high-lying, in energy, lone pair. Consequently, this nitrogen has been assigned as the N α of an η^2 - coordinated aryldiazenido ligand. The signal occurring at the relative high field with δ ~ 60 ppm clearly falls into the chemical shift range for an η^1 - coordinated aryldiazenido ligand. Since an η^1 - terminal singly bent aryldiazenido ligand is chemically impossible in our system, an η^1 - bridging aryldiazenido is therefore concluded.

Very few ¹⁵N chemical shift data are known for bridging aryldiazenido complexes (see Table 1.8 in section 1.4.4.5). Samkoff and Shapley have reported ¹⁵N α chemical shifts for (μ -H)Os₃(CO)₁₀(μ^2 - η^2 -*p*-N₂C₆H₄Me) and (μ -H)Os₃(CO)₁₀(μ^2 - η^1 -*p*-N₂C₆H₄Me)¹⁴⁰ (see Figure 3.5). They found that the ¹⁵N α chemical shifts were 68 ppm and 313 ppm for the μ^2 - η^1 - and the μ^2 - η^2 - bridging aryldiazenido ligands, respectively. The two different ¹⁵N α chemical shifts observed in both (7a) and (8a) are closely parallel these data, clearly indicating their structural similarity.

So far, based on only the analysis and the spectroscopic data, the molecular structures of the compounds (7) and (8) have been reasoned to be dimeric with two different Cp*Ir(X) cores. This requires that they are linked by two different bridged (*i.e.*, η^1 - and η^2 -) aryldiazenido ligands. This molecular



(a)



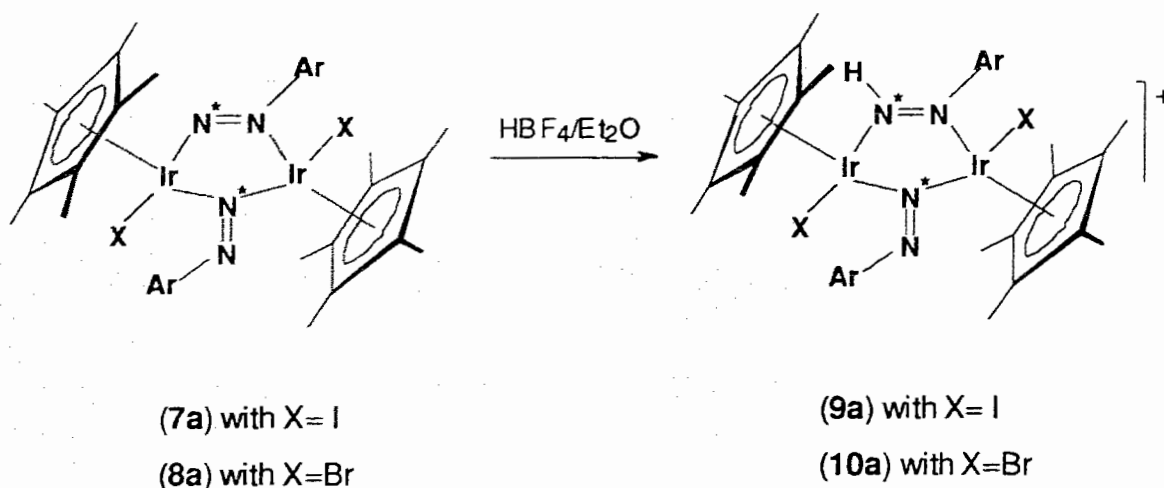
(b)

Figure 3.5 Molecular structures of (a) $(\mu\text{-H})\text{Os}_3(\text{CO})_{10}(\mu^2\text{-}\eta^2\text{-}p\text{-N}_2\text{C}_6\text{H}_4\text{Me})$ and (b) $(\mu\text{-H})\text{Os}_3(\text{CO})_{10}(\mu^2\text{-}\eta^1\text{-}p\text{-N}_2\text{C}_6\text{H}_4\text{Me})$.

structure was confirmed later by an X-ray crystal structure of (7) (see section 3.3.2.1). Further, since (8) has similar spectroscopic properties to (7), we believe that compounds (7) and (8) have similar structures.

Protonation of (7a) in CDCl_3 with a slight excess of $\text{HBF}_4/\text{Et}_2\text{O}$ changes the colour of the solution immediately to dark brown, accompanied by the formation of a precipitate. The ^{15}N NMR spectrum of this protonated species observed *in situ* shows a sharp singlet at δ : 65.1 ppm, which is in a position almost identical to that for (7a) (at δ : 64.1 ppm), plus a broad resonance occurs at δ : -110.7 ppm. No resonance near δ : 300 ppm as was seen for the precursor (7a) was observed in this spectrum. The ^1H NMR spectrum of the same sample showed, in addition to the resonances for the Cp^* and $-\text{C}_6\text{H}_4\text{OMe}$ groups, a sharp doublet at δ : 15.2 ppm with $J_{\text{H}-^{15}\text{N}} = 79$ Hz, which is undoubtedly assigned to $\text{H}-^{15}\text{N}\alpha$. This NMR evidence clearly demonstrates that protonation of (7a) occurred only at the α nitrogen of the η^2 -coordinated aryldiazenido ligand, as shown in Eqn. 3.3. A similar ^1H NMR spectrum was observed for the formation of (10a) by protonating (8a), with resonances occurring at δ : 15.3 ppm and $J_{\text{H}-^{15}\text{N}} = 79$ Hz. The pronounced upfield shift of the $^{15}\text{N}\alpha$ resonance upon protonation of the μ^2 - η^2 -coordinated aryldiazenido ligand clearly shows the sensitivity of the ^{15}N chemical shift to the presence of lone pair of electrons on the nucleus in question. The same feature was also observed for the corresponding osmium compounds, where, upon a protonation of $\text{N}\alpha$ in $(\mu\text{-H})\text{Os}_3(\text{CO})_{10}(\mu^2\text{-}\eta^2\text{-}p\text{-N}_2\text{C}_6\text{H}_4\text{Me})$, the $^{15}\text{N}\alpha$ chemical shift moved upfield to -61 ppm, with $J_{^{15}\text{N}\alpha\text{-H}} = 81$ Hz.¹⁴⁰

(Eqn. 3.3)

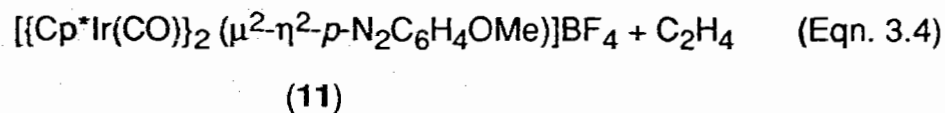
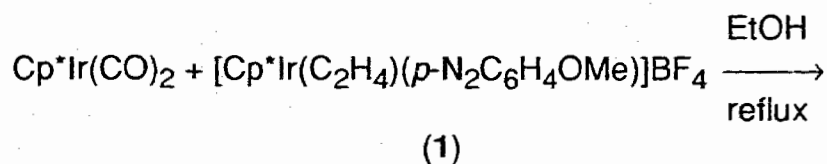


(N*: ¹⁵N labelled)

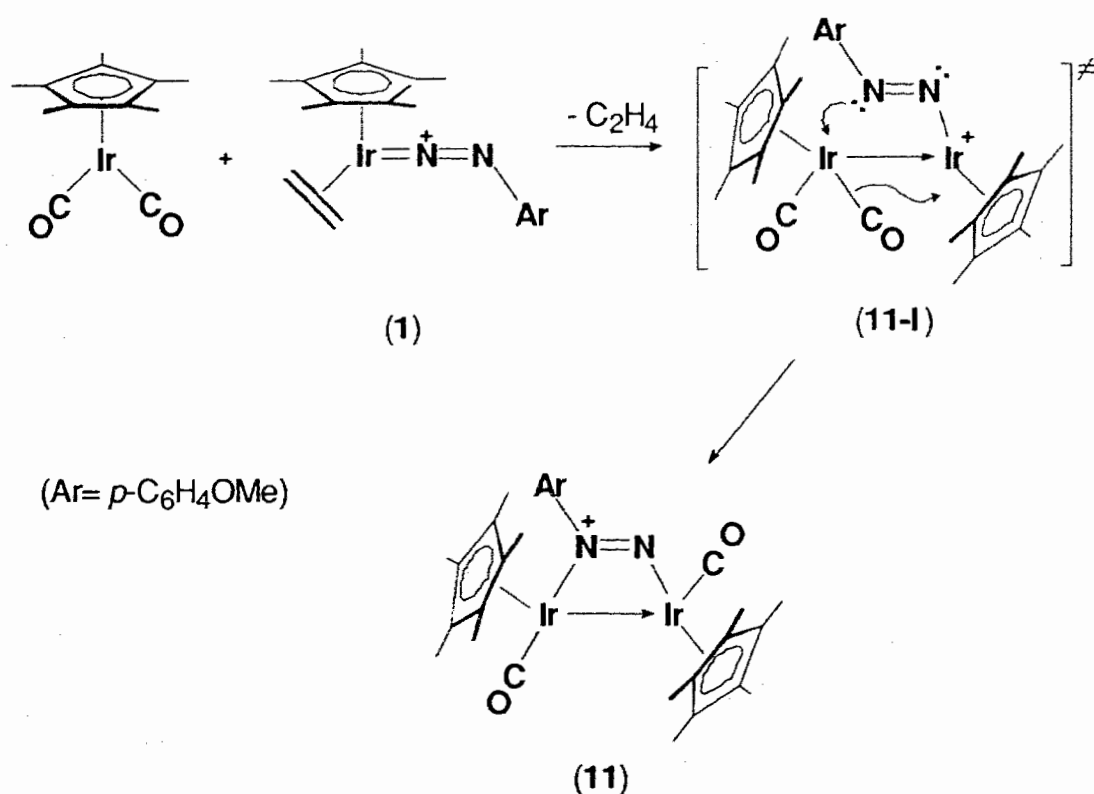
3. 3. 1. 3 Metal Base, ¹⁶ Cp*Ir(CO)₂, as the Ancillary Ligand

Various electron-rich transition metal complexes have been often used in the preparation of dinuclear complexes. Since Cp*Ir(CO)₂ is a convenient metal base, its reaction with compound (1) was carried out in expectation of forming a dinuclear aryldiazenido complex. Treatment of equimolar amounts of Cp*Ir(CO)₂ and compound (1) in EtOH under reflux afforded the desired complex (11).

(Equation 3.4).



In this reaction, we believe that the metal base $\text{Cp}^*\text{Ir}(\text{CO})_2$ first coordinates to the iridium centre in (1) by replacing ethylene to give an unobserved intermediate (11-I), (Scheme 3.3). This intermediate is proposed to contain an Ir(III) metal centre and a terminally coordinated doubly bent



Scheme 3.3

aryldiazenido ligand. This intermediate then rearranges rapidly by a pathway involving a terminal-bridging-terminal transfer of a CO group assisted by bridging of the N_2Ar^- ligand to give the product (11). Support for this suggestion can be found in the related compound $[\text{Cp}^*(\text{CO})_2\text{Ir} \rightarrow \text{Ir}(\text{CO})(\text{Cl})\text{Cp}^*]\text{BF}_4$,¹⁷⁶ which is

synthesized by Ag^+ mediated displacement of one Cl ligand from $\text{Cp}^*\text{Ir}(\text{CO})\text{Cl}_2$ by the base $\text{Cp}^*\text{Ir}(\text{CO})_2$. The iridium of the $\text{Cp}^*\text{Ir}(\text{CO})\text{Cl}$ fragment in $[\text{Cp}^*(\text{CO})_2\text{Ir} \rightarrow \text{Ir}(\text{CO})(\text{Cl})\text{Cp}^*]\text{BF}_4$ is also in an Ir(III) oxidation state. Furthermore, the CO groups in $[\text{Cp}^*(\text{CO})_2\text{Ir} \rightarrow \text{Ir}(\text{CO})(\text{Cl})\text{Cp}^*]\text{BF}_4$ undergo exchange at room temperature, presumably by a terminal-bridging interchange mechanism. This closely parallels the mechanism that we have suggested for the formation of (11). Notably, this reaction is very similar to what we have seen in the syntheses of (7) and (8). This parallelism clearly demonstrates the influence of these π base ligands on the trans aryldiazenido ligand in our system.

Compound (11) can be crystallized from acetone/hexanes. Unlike the other bridging aryldiazenido complexes (7) and (8), compound (11) is air-sensitive both in solution and in the solid state.

The infrared spectrum of (11) exhibits the expected two $\nu(\text{CO})$ bands at 1922 and 1970 cm^{-1} , respectively, for the two terminal CO ligands. However, the $\nu(\text{NN})$ band could not be unambiguously assigned due to its lower wavenumber in the finger-print region. The ambient temperature ^1H NMR spectrum of (11) in CDCl_3 shows the expected resonances for *one* $-\text{C}_6\text{H}_4\text{OMe}$ group in the normal region and with the normal pattern, and *two* different Cp^* resonances at δ : 2.13 and 2.01 ppm respectively. This indicates that in solution the aryldiazenido ligand is either coordinated to only one iridium, or is asymmetrically coordinated to two iridium centres in the molecule. The single crystal X-ray crystallographic analysis of (11) has unequivocally established the latter case for the solid state (Figure 3.6).

3. 3. 2 X-ray Crystallographic Analyses

3. 3. 2. 1 Complex $[[\text{Cp}^*\text{Ir}(\text{CO})]_2(\mu^2-\eta^2-p\text{-N}_2\text{C}_6\text{H}_4\text{OMe})]\text{BF}_4$ (**11**)

General Features

The single crystal X-ray crystallographic analysis of $[[\text{Cp}^*\text{Ir}(\text{CO})]_2(\mu^2-\eta^2-p\text{-N}_2\text{C}_6\text{H}_4\text{OMe})]\text{BF}_4$ (**11**), the essential details of which are summarized in Table 3.1, has established the dimeric nature of this complex. The crystal structure consists of eight discrete molecules per unit cell. The molecular structure and numbering scheme are shown in Figure 3.6. The positional coordinates and the thermal parameters of the non-hydrogen atoms are listed in Table 3. 2. The pertinent intramolecular dimensions for a molecule of (**11**) are contained in Table 3.3.

The molecule of $[[\text{Cp}^*\text{Ir}(\text{CO})]_2(\mu^2-\eta^2-p\text{-N}_2\text{C}_6\text{H}_4\text{OMe})]\text{BF}_4$ (**11**) contains two iridium atoms and each of these is also linked to a terminal carbonyl and a η^5 -pentamethylcyclopentadienyl ligand. So each of the iridium atoms is approximately in a distorted three-legged piano stool coordination environment, with the legs separated at angles: $\text{Ir}(2)\text{-Ir}(1)\text{-N}(1) = 68.0(10)^\circ$; $\text{Ir}(2)\text{-Ir}(1)\text{-C}(1) = 84.8(19)^\circ$ and $\text{C}(1)\text{-Ir}(1)\text{-N}(1) = 94.0(16)^\circ$ for the Ir(1) atom, and $\text{Ir}(1)\text{-Ir}(2)\text{-N}(2) = 70.7(10)^\circ$; $\text{Ir}(1)\text{-Ir}(2)\text{-C}(2) = 91.4(24)^\circ$ and $\text{C}(2)\text{-Ir}(2)\text{-N}(2) = 94.2(22)^\circ$ for the Ir(2) atom. The significantly smaller Ir-Ir-N angles, by comparison with other angles at the both iridium atoms, may reflect the highly strained four-member ring formed by the two iridium atoms and the two nitrogen atoms. These values are similar to those found in the related $(\mu\text{-H})\text{Os}_3(\text{CO})_{10}(\mu^2-\eta^2\text{-N}_2\text{Ph})$, in which the corresponding angles are $64.4(7)^\circ$ and $68.6(7)^\circ$.¹⁴⁰

The Ir(1)-Ir(2) distance of 2.723 (4) Å is significantly shorter than the

Ir...Ir distance of 3.5829(7) Å found in the related bridging aryldiazenido complex (7), in which the two iridium atoms are considered as non-bonding (molecular structure of compound (7) will be discussed in the following section). This indicates that two iridium atoms in (11) are directly bonded to each other by a single bond. Interestingly, this Ir-Ir bond distance is also significantly shorter (by ca. 0.11 Å) than those found in other di-iridium complexes without any supporting bridging ligand, *e.g.*, Ir-Ir single bond distance = 2.8266(6) Å for [Cp*(CO)₂Ir-Ir(CO)(Cl)Cp*] BF₄,¹⁷⁶ and 2.8394(12) Å for [Cp*(CO)₂Ir-Ir(CO)₂Cp*] [BF₄]₂,¹⁷⁷ which clearly shows the shortening effect of the bridging aryldiazenido ligand on the Ir-Ir bond length. However, notably, this seems contrary to what is observed in (μ-H)Os₃(CO)₁₀(μ²-η²-N₂Ph),¹⁴⁰ where the distance (2.895(2) Å) between the two osmium atoms bearing the μ²-η²-N₂Ph ligand is lengthened relative to the other two non-bridged Os-Os distances (2.868(2) and 2.862(3) Å), and to the value of 2.877(3) Å found in Os₃(CO)₁₂.¹⁷⁸

The carbon frameworks of the pentamethylcyclopentadienyl ligands in (11) contain no peculiarities in the bond lengths and bond angles. Likewise, there are no significant differences in the ring carbon to iridium bond lengths, indicating the pentamethylcyclopentadienyl ligands are symmetrically coordinated to the iridium atoms.

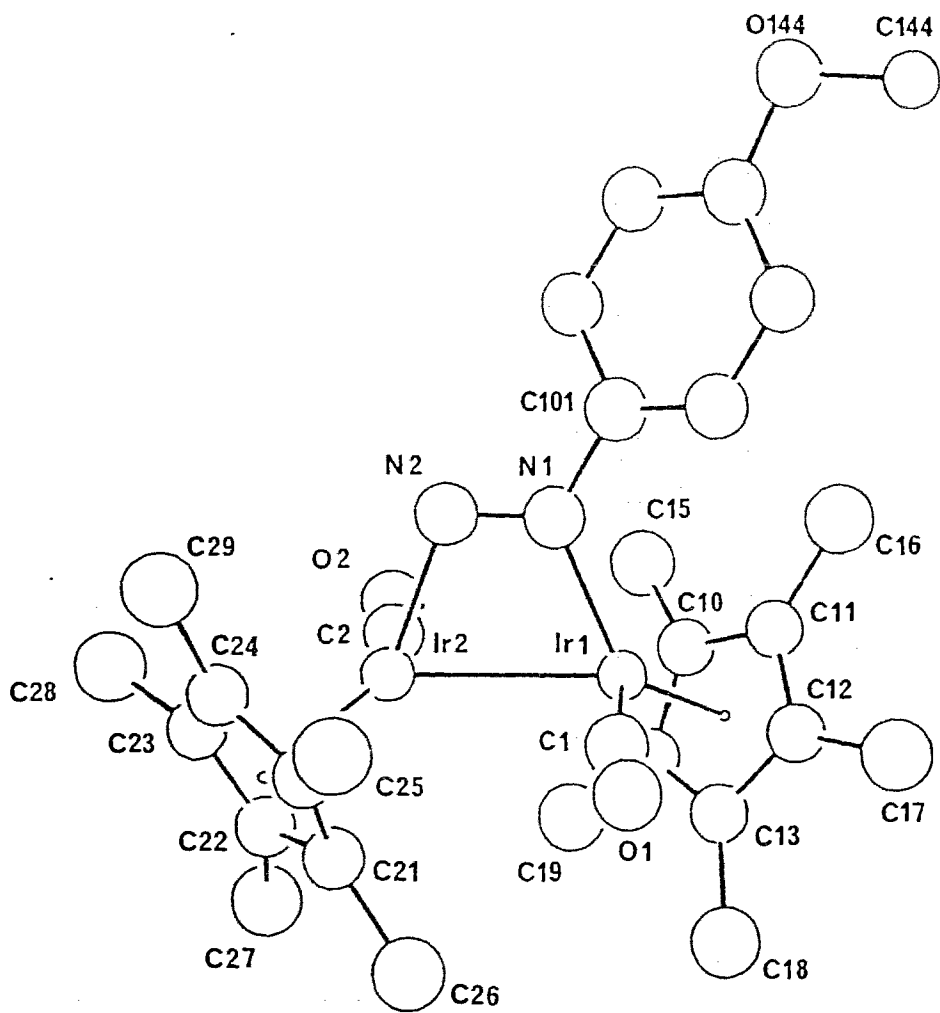
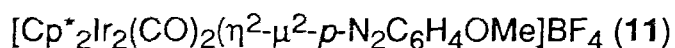


Figure 3.6 Perspective view of the cation of compound (11). (The thermal ellipsoids represent 50 % probability contours).

Table 3.2 The Positional Parameters of Non-hydrogen Atoms for

Atom	x/a	y/b	z/c	U(iso) *
Ir(1)	0.0506(3)	0.2048(2)	0.22854(7)	0.0356(7)
N(1)	-0.170(2)	0.183(1)	0.2376(8)	0.051(6)
O(1)	-0.000(4)	0.320(2)	0.176(1)	0.060(6)
C(1)	0.009(6)	0.279(2)	0.202(1)	0.049(6)
C(10)	0.181(3)	0.115(1)	0.249(1)	0.049(3)
C(11)	0.155(2)	0.107(1)	0.210(1)	0.049(3)
C(12)	0.232(3)	0.158(2)	0.1921(9)	0.049(3)
C(13)	0.303(2)	0.198(1)	0.219(1)	0.049(3)
C(14)	0.272(2)	0.171(2)	0.255(1)	0.049(3)
C(15)	0.127(4)	0.067(2)	0.280(2)	0.069(4)
C(16)	0.065(3)	0.051(2)	0.192(2)	0.069(4)
C(17)	0.237(5)	0.166(3)	0.149(1)	0.069(4)
C(18)	0.407(3)	0.254(2)	0.208(2)	0.069(4)
C(19)	0.345(4)	0.195(2)	0.292(1)	0.069(4)
Ir(2)	-0.0661(3)	0.2724(2)	0.28937(8)	0.0388(7)
N(2)	-0.233(3)	0.214(1)	0.2657(8)	0.051(6)
O(2)	0.018(5)	0.166(2)	0.345(1)	0.060(6)
C(2)	-0.002(6)	0.210(3)	0.322(2)	0.049(6)
C(20)	0.040(4)	0.3567(6)	0.323(1)	0.049(3)
C(21)	0.039(4)	0.3745(6)	0.284(1)	0.049(3)
C(22)	-0.111(4)	0.3786(6)	0.273(1)	0.049(3)
C(23)	-0.206(4)	0.3639(7)	0.303(1)	0.049(3)

(Continue Table 3.2)

Atom	x/a	y/b	z/c	U(iso) *
C(24)	-0.111(4)	0.3506(7)	0.3340(9)	0.049(3)
C(25)	0.186(5)	0.354(1)	0.346(2)	0.069(4)
C(26)	0.179(5)	0.3965(9)	0.262(2)	0.069(4)
C(27)	-0.202(7)	0.4002(9)	0.238(1)	0.069(4)
C(28)	-0.379(4)	0.364(1)	0.301(2)	0.069(4)
C(29)	-0.172(7)	0.3324(7)	0.374(1)	0.069(4)
C(101)	-0.267(4)	0.139(1)	0.2175(8)	0.053(8)
C(102)	-0.266(5)	0.133(2)	0.178(1)	0.053(8)
C(103)	-0.355(4)	0.091(2)	0.156(2)	0.053(8)
C(104)	-0.453(4)	0.053(2)	0.177(1)	0.053(8)
C(105)	-0.456(5)	0.058(2)	0.217(1)	0.053(8)
C(106)	-0.364(3)	0.099(2)	0.239(1)	0.053(8)
O(144)	-0.555(4)	0.009(2)	0.160(1)	0.055(7)
C(144)	-0.515(6)	-0.007(3)	0.122(2)	0.04(1)
Ir(3)	0.5739(3)	0.2822(2)	0.02320(7)	0.0289(6)
N(3)	0.353(2)	0.307(1)	0.0139(8)	0.051(6)
O(3)	0.488(5)	0.179(2)	0.081(1)	0.060(6)
C(3)	0.517(6)	0.220(2)	0.058(1)	0.049(6)
C(30)	0.676(2)	0.380(1)	0.041(1)	0.049(3)
C(31)	0.710(3)	0.370(1)	0.002(1)	0.049(3)
C(32)	0.801(2)	0.314(2)	-0.000(1)	0.049(3)
C(33)	0.824(2)	0.289(1)	0.037(1)	0.049(3)

(Continue Table 3.2)

Atom	x/a	y/b	z/c	U(iso) *
C(34)	0.746(3)	0.330(2)	0.0622(9)	0.049(3)
C(35)	0.590(3)	0.441(2)	0.056(2)	0.069(4)
C(36)	0.663(4)	0.417(2)	-0.031(2)	0.069(4)
C(37)	0.870(4)	0.285(2)	-0.037(1)	0.069(4)
C(38)	0.924(3)	0.229(2)	0.044(2)	0.069(4)
C(39)	0.750(5)	0.324(3)	0.106(1)	0.069(4)
Ir(4)	0.4546(4)	0.2108(2)	-0.03564(8)	0.0351(7)
N(4)	0.289(3)	0.273(1)	-0.0139(7)	0.051(6)
O(4)	0.553(5)	0.309(2)	-0.0952(9)	0.060(6)
C(4)	0.508(6)	0.274(3)	-0.070(2)	0.049(6)
C(40)	0.371(4)	0.1108(6)	-0.016(1)	0.049(3)
C(41)	0.525(4)	0.1062(5)	-0.024(1)	0.049(3)
C(42)	0.551(4)	0.1189(6)	-0.063(1)	0.049(3)
C(43)	0.411(5)	0.1311(6)	-0.0798(9)	0.049(3)
C(44)	0.301(4)	0.1260(6)	-0.051(1)	0.049(3)
C(45)	0.299(7)	0.0985(9)	0.024(1)	0.069(4)
C(46)	0.630(6)	0.0819(6)	0.009(1)	0.069(4)
C(47)	0.702(5)	0.1096(9)	-0.084(2)	0.069(4)
C(48)	0.386(7)	0.1435(7)	-0.123(1)	0.069(4)
C(49)	0.133(4)	0.1389(7)	-0.061(2)	0.069(4)
C(201)	0.260(3)	0.352(1)	0.0324(7)	0.038(6)
C(202)	0.159(3)	0.393(1)	0.013(1)	0.038(6)
C(203)	0.063(4)	0.438(2)	0.030(1)	0.038(6)

(Continue Table 3.2)

Atom	x/a	y/b	z/c	U(iso) *
C(204)	0.079(4)	0.438(2)	0.070(1)	0.038(6)
C(205)	0.175(4)	0.400(2)	0.092(1)	0.038(6)
C(206)	0.267(4)	0.357(2)	0.0718(9)	0.038(6)
O(244)	-0.019(4)	0.482(2)	0.089(1)	0.055(7)
C(244)	-0.036(6)	0.483(3)	0.132(2)	0.04(1)
Ir(501)	-0.075(2)	0.2145(6)	0.2293(3)	0.0356(7)
N(501)	0.135(2)	0.172(1)	0.2335(8)	0.051(6)
O(501)	-0.070(6)	0.343(1)	0.1859(7)	0.060(6)
C(501)	-0.058(4)	0.284(1)	0.1959(4)	0.049(6)
C(510)	-0.197(4)	0.121(1)	0.2461(8)	0.049(3)
C(511)	-0.175(3)	0.118(1)	0.2065(8)	0.049(3)
C(512)	-0.260(3)	0.171(1)	0.1924(7)	0.049(3)
C(513)	-0.330(2)	0.206(2)	0.2219(9)	0.049(3)
C(514)	-0.290(2)	0.174(2)	0.2560(8)	0.049(3)
C(515)	-0.134(6)	0.069(1)	0.274(1)	0.069(4)
C(516)	-0.080(4)	0.065(1)	0.185(1)	0.069(4)
C(517)	-0.266(4)	0.185(2)	0.1492(7)	0.069(4)
C(518)	-0.436(3)	0.263(2)	0.212(1)	0.069(4)
C(519)	-0.358(3)	0.192(2)	0.295(1)	0.069(4)
Ir(502)	0.048(2)	0.2820(8)	0.2846(4)	0.0388(7)
N(502)	0.179(1)	0.222(1)	0.2507(7)	0.051(6)
O(502)	-0.048(6)	0.199(2)	0.3536(4)	0.060(6)
C(502)	-0.031(4)	0.225(1)	0.3199(3)	0.049(6)

(Continue Table 3.2)

Atom	x/a	y/b	z/c	U(iso) *
C(520)	-0.040(3)	0.382(1)	0.3051(9)	0.049(3)
C(521)	0.000(4)	0.3862(6)	0.2650(9)	0.049(3)
C(522)	0.160(4)	0.373(1)	0.2597(8)	0.049(3)
C(523)	0.227(3)	0.360(1)	0.2964(8)	0.049(3)
C(524)	0.103(3)	0.366(1)	0.3237(7)	0.049(3)
C(525)	-0.207(4)	0.401(2)	0.320(1)	0.069(4)
C(526)	-0.112(6)	0.4107(7)	0.233(1)	0.069(4)
C(527)	0.277(5)	0.373(2)	0.225(1)	0.069(4)
C(528)	0.404(3)	0.343(2)	0.301(1)	0.069(4)
C(529)	0.147(4)	0.354(2)	0.3676(7)	0.069(4)
C(601)	0.247(3)	0.123(2)	0.222(1)	0.053(8)
C(602)	0.244(3)	0.119(2)	0.182(1)	0.053(8)
C(603)	0.340(4)	0.079(3)	0.159(2)	0.053(8)
C(604)	0.447(5)	0.035(3)	0.174(2)	0.053(8)
C(605)	0.470(5)	0.032(3)	0.213(2)	0.053(8)
C(606)	0.373(5)	0.070(2)	0.236(2)	0.053(8)
O(644)	0.528(6)	-0.001(4)	0.149(3)	0.055(7)
C(644)	0.385(5)	0.043(3)	0.185(2)	0.04(1)
Ir(503)	-0.572(2)	0.2935(6)	0.0241(3)	0.0289(6)
N(503)	-0.344(2)	0.309(1)	0.0168(7)	0.051(6)
O(503)	-0.441(6)	0.197(2)	0.0809(4)	0.060(6)
C(503)	-0.511(4)	0.228(1)	0.0568(3)	0.049(6)
C(530)	-0.693(3)	0.389(1)	0.0392(7)	0.049(3)

(Continue Table 3.2)

Atom	x/a	y/b	z/c	U(iso) *
C(531)	-0.728(3)	0.373(1)	0.0011(7)	0.049(3)
C(532)	-0.808(2)	0.313(2)	0.0005(8)	0.049(3)
C(533)	-0.821(2)	0.293(2)	0.0386(9)	0.049(3)
C(534)	-0.751(3)	0.339(1)	0.0627(7)	0.049(3)
C(535)	-0.608(5)	0.4517(9)	0.053(1)	0.069(4)
C(536)	-0.678(6)	0.417(1)	-0.0330(8)	0.069(4)
C(537)	-0.870(2)	0.277(2)	-0.035(1)	0.069(4)
C(538)	-0.915(3)	0.229(2)	0.044(1)	0.069(4)
C(539)	-0.754(4)	0.335(2)	0.1070(7)	0.069(4)
Ir(504)	-0.446(2)	0.2216(7)	-0.0400(3)	0.0351(7)
N(504)	-0.288(1)	0.268(1)	-0.0066(7)	0.051(6)
O(504)	-0.588(5)	0.347(1)	-0.0721(5)	0.060(6)
C(504)	-0.540(3)	0.300(1)	-0.0522(3)	0.049(6)
C(540)	-0.359(4)	0.1192(9)	-0.0253(7)	0.049(3)
C(541)	-0.517(4)	0.1165(6)	-0.0275(8)	0.049(3)
C(542)	-0.562(3)	0.132(1)	-0.0653(8)	0.049(3)
C(543)	-0.429(3)	0.144(1)	-0.0865(6)	0.049(3)
C(544)	-0.307(3)	0.136(1)	-0.0617(7)	0.049(3)
C(545)	-0.265(6)	0.105(2)	0.0108(9)	0.069(4)
C(546)	-0.637(6)	0.0925(9)	0.002(1)	0.069(4)
C(547)	-0.720(4)	0.127(2)	-0.084(1)	0.069(4)
C(548)	-0.400(4)	0.160(2)	-0.1286(6)	0.069(4)
C(549)	-0.141(3)	0.146(2)	-0.072(1)	0.069(4)

(Continue Table 3.2)

Atom	x/a	y/b	z/c	U(iso) *
C(701)	-0.251(3)	0.361(2)	0.032(1)	0.038(6)
C(702)	-0.156(4)	0.400(2)	0.009(1)	0.038(6)
C(703)	-0.084(5)	0.450(3)	0.030(2)	0.038(6)
C(704)	-0.098(5)	0.457(3)	0.070(2)	0.038(6)
C(705)	-0.202(4)	0.417(3)	0.090(1)	0.038(6)
C(706)	-0.265(3)	0.369(2)	0.066(1)	0.038(6)
O(744)	-0.011(6)	0.506(4)	0.085(2)	0.055(7)
C(744)	0.064(6)	0.475(5)	0.140(2)	0.04(1)
F(11)	0.379(4)	-0.007(2)	0.344(1)	0.161(7)
F(12)	0.504(5)	-0.102(1)	0.343(1)	0.160(7)
F(13)	0.440(5)	-0.052(2)	0.2892(8)	0.168(7)
F(14)	0.618(4)	-0.009(2)	0.326(1)	0.183(7)
F(21)	-0.181(5)	-0.021(3)	0.080(2)	0.151(7)
F(22)	0.054(6)	-0.012(2)	0.100(1)	0.158(7)
F(23)	-0.087(7)	0.077(1)	0.090(2)	0.134(7)
F(24)	-0.008(5)	0.018(2)	0.0407(9)	0.173(7)
F(41)	0.003(6)	-0.041(1)	0.064(1)	0.163(7)
F(42)	-0.089(7)	-0.011(2)	0.112(1)	0.166(7)
F(43)	0.074(5)	0.040(2)	0.093(1)	0.160(7)
B(1)	0.485(3)	-0.043(1)	0.3256(8)	0.17(3)
B(2)	-0.056(4)	0.0155(7)	0.078(1)	0.17(3)

* Isotropic thermal motion were restrained for C, N and O atoms.

Table 3.3 Selected Bond Lengths (Å) and Inter-Bond Angles (°)of $[\text{Cp}^*_2\text{Ir}_2(\text{CO})_2(\eta^2\text{-}\mu^2\text{-}p\text{-N}_2\text{C}_6\text{H}_4\text{OMe})\text{BF}_4]$ (**11**)

(a) Bond Lengths

Ir(1) - Ir(2)	2.723(4)	Ir(1) - N(1)	2.02(2)	Ir(1) - C(1)	1.81(2)
Ir(1) - C(10)	2.26(2)	Ir(1) - C(11)	2.27(2)	Ir(1) - C(12)	2.24(2)
Ir(1) - C(13)	2.26(2)	Ir(1) - C(14)	2.26(2)	Ir(2) - N(2)	2.06(2)
Ir(2) - C(2)	1.79(2)	Ir(2) - C(20)	2.26(2)	Ir(2) - C(21)	2.27(2)
Ir(2) - C(22)	2.26(2)	Ir(2) - C(23)	2.28(2)	Ir(2) - C(24)	2.25(2)
N(1) - N(2)	1.29(2)	N(1) - C(101)	1.41(3)	C(1) - O(1)	1.21(2)
C(2) - O(2)	1.20(2)	O(144) - C(104)	1.41(4)	O(144) - C(144)	1.41(6)
Ir(3) - Ir(4)	2.719(4)	Ir(3) - N(3)	2.04(2)	Ir(3) - C(3)	1.80(2)
Ir(3) - C(30)	2.27(2)	Ir(3) - C(31)	2.27(2)	Ir(3) - C(32)	2.25(2)
Ir(3) - C(33)	2.26(2)	Ir(3) - C(34)	2.26(2)	N(3) - N(4)	1.30(2)
N(3) - C(201)	1.39(3)	C(3) - O(3)	1.20(2)	Ir(4) - N(4)	2.08(2)
Ir(4) - C(4)	1.81(2)	Ir(4) - C(40)	2.26(2)	Ir(4) - C(41)	2.25(2)
Ir(4) - C(42)	2.25(2)	Ir(4) - C(43)	2.26(2)	Ir(4) - C(44)	2.25(2)
C(4) - O(4)	1.20(2)	O(244) - C(204)	1.40(4)	O(244) - C(244)	1.50(7)

(b) Inter-Bond Angles

Ir(2) - Ir(1) - N(1)	68.0(10)	Ir(4) - Ir(3) - N(3)	68.8(10)
Ir(2) - Ir(1) - C(1)	84.8(19)	Ir(4) - Ir(3) - C(3)	91.4(19)
N(1) - Ir(1) - C(1)	94.0(16)	N(3) - Ir(3) - C(3)	90.4(18)
Ir(1) - N(1) - N(2)	115.1(25)	Ir(3) - N(3) - N(4)	114.0(23)
Ir(1) - N(1) - C(101)	130.0(20)	Ir(3) - N(3) - C(201)	130.7(23)
N(2) - N(1) - C(101)	114.9(24)	N(4) - N(3) - C(201)	115.3(23)

(Continue Table 3.3)

Ir(1) - C(1) - O(1)	162.9(51)	Ir(3) - C(3) - O(3)	176.0(53)
Ir(1) - Ir(2) - N(2)	70.7(10)	Ir(3) - Ir(4) - N(4)	70.9(10)
Ir(1) - Ir(2) - C(2)	91.4(24)	Ir(3) - Ir(4) - C(4)	91.0(24)
N(2) - Ir(2) - C(2)	94.2(22)	N(4) - Ir(4) - C(4)	89.6(21)
Ir(2) - N(2) - N(1)	106.2(24)	Ir(4) - N(4) - N(3)	106.3(23)
Ir(2) - C(2) - O(2)	170.3(49)	Ir(4) - C(4) - O(4)	171.1(62)
C(144) - O(144) - C(104)	112.9(41)		
C(244) - O(244) - C(204)	122.0(41)		

Features of the Aryldiazenido Ligand

The nitrogen-nitrogen bond of the aryldiazenido ligand is essentially coplanar with the iridium-iridium bond, and it exhibits an η^2 -bridging mode with Ir(1)-N(1)= 2.02(2) Å and Ir(2)-N(2)= 2.06(2) Å. The N(1)-N(2) bond length (1.29(2) Å) has the expected value for an N=N double bond distance, but is perhaps slightly longer than found in other bridged aryldiazenido complexes. For example, N=N double bond lengths of 1.20(4) Å and 1.24(2) Å were found for $\mu^{2-\eta^2}$ - and $\mu^{2-\eta^1}$ -aryldiazenido ligands, separately, in $(\mu\text{-H})\text{Os}_3(\text{CO})_{10}(\mu^{2-\eta^2}\text{-N}_2\text{Ph})$ ¹⁵ and $(\mu\text{-H})\text{Os}_3(\text{CO})_{10}(\mu^{2-\eta^1}\text{-N}_2\text{C}_6\text{H}_4\text{Me})$,¹⁷⁹ (see Figure 3.5), and values of 1.23(1) Å and 1.19(1) Å were found for $\mu^{2-\eta^2}$ - and $\mu^{2-\eta^1-p}$ - $\text{N}_2\text{C}_6\text{H}_4\text{OMe}$, separately, in compound (7) (see section 3.3.2.2). However, we have to note that the disordered structure may contribute to the rather large esds on the NN distance, and undoubtedly affects the accuracy of this value.

Another structural feature is that the NN group is not coplanar with the

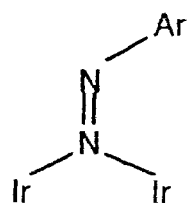
aromatic ring. This is not very common for terminally coordinated aryldiazenido ligands in either the singly bent or the doubly bent geometry. A rather crowded arrangement of the aryl ring and the Cp* ligand located in the same region could be responsible for this. Evidence for this is the relatively large value (130.0(2)°) for Ir(1)-N(1)-C(101), and the small values for the other two angles at the N(1) atom, i.e. N(2)-N(1)-C(101)= 114.9(24)° and N(2)-N(1)-Ir(1)= 115.1(25)°.

3.3.2.2 Complex [Cp*Ir(I)]₂(μ²-η²-p-N₂C₆H₄OMe) (μ²-η¹-p-N₂C₆H₄OMe) (**7**)

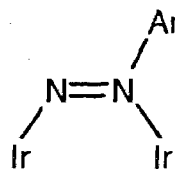
General features

Compound (**7**) crystallized in a triclinic lattice, ($a = 8.937(2)$ Å, $b = 10.036(2)$ Å, $c = 10.893(2)$ Å, $\alpha = 79.98(1)^\circ$, $\beta = 79.52(1)^\circ$, $\gamma = 70.36(1)^\circ$ and $Z = 1$). The crystal structure analysis, (performed by Dr. R. J. Batchelor), has revealed that each unit cell contains one disordered molecule lying on the inversion centre of the centrosymmetric space group $P\bar{1}$ at (1/2, 1/2, 1/2). An ordered model in the non-centric space group P_1 was also carefully considered, but it did not provide a more satisfactory solution. Therefore, the disordered model in the space group of $P\bar{1}$ was retained in the structure refinement process, and gave final values of $R_f = 0.021$, $R_w = 0.029$ and GOF = 1.74.

Interestingly, the disorder is clearly visible only in the region of the nitrogen atoms and is consistent with the superposition of two different bonding modes with nearly equal occupancies for the bridging aryldiazenido ligands. These two bonding modes are shown as **A** and **B** in Figure 3.7. There is no observable disorder in the Cp*, Ir and iodine regions. This is confirmed by the well behaved thermal motion for these group in the final model, which contains only disordered diazenido ligands.



A ($\mu^2\text{-}\eta^1\text{-bridging}$)



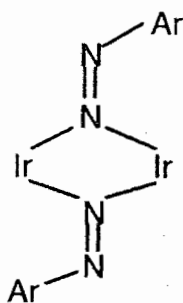
B ($\mu^2\text{-}\eta^2\text{-bridging}$)

Figure 3.7 Two coordination modes of the bridging aryldiazenido ligand found in complex (7)

The spectroscopic data, as well as the "electron-precise" nature of the complex,¹⁸⁰ with each Ir(III) atom obeying the 18-electron (EAN) rule, support the likelihood of two bridging aryldiazenido ligands in (7). The disordered structure of (7) could possibly be explained in two ways (see Figure 3.8). Combination I accounts for the disorder in terms of equal populations of two *different* molecules in which only **A** and **B** modes occur respectively. Combination II postulates only one kind of molecule, but superimposed orientations as shown.

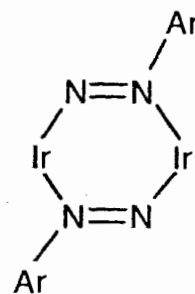
Combination I is immediately ruled out because to account for the observed $N\alpha$ position, the non-bonding $N\alpha\cdots N\alpha$ distance in **AA**, (50% occupancy in combination I) would be only ca. 1.9 Å, significantly shorter than the sum of nitrogen van der Waals radii (ca. 3.0 Å). Therefore, it was concluded that the disorder was best described by combination II. That is, each molecule contains two coordinatively different bridging aryldiazenido ligands ($\mu^2\text{-}\eta^1\text{-}$ and $\mu^2\text{-}\eta^2\text{-}$ fashions). Furthermore, in the combination II, the superimposed **AB** and

Combination I



AA

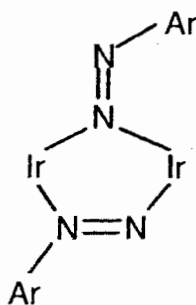
(50% occupancy)



BB

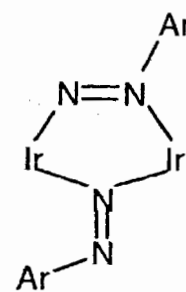
(50% occupancy)

Combination II



AB

(50% occupancy)



BA

(50% occupancy)

Figure 3.8 Two possible modes of the doubly bridging aryldiazenido complex (7)

BA structures are related by an inversion centre, therefore, it is concluded that molecule (7) exists in the solid state in two superimposed enantiomers.

It is also worthy to note that although both modes (combinations **I** and **II**) here for (7) are consistent with the previously described spectroscopic observations for this complex, we believe that the molecular structure of (7) in solution is similar to that in the solid, because it is unreasonable to expect a significant change in the short $N\alpha \cdots N\alpha$ distance in **AA** simply by solvation.

The molecular structure and selected numbering scheme are shown in Figure 3.9, while the pertinent intramolecular bond lengths and angles are listed in Table 3.4. There are no unusual intermolecular distances in the crystal structure. Each iridium atom has a distorted three-legged piano-stool coordination environment, provided by the centroid of an η^5 -Cp* ligand, an iodide ligand and two different coordinated aryldiazenido ligands. The pronounced lengthening of the iridium-iridium separation of 3.5829(7) Å, relative to $[\{Cp^*Ir(CO)\}_2(\mu^2-\eta^2-p-N_2C_6H_4OMe)]BF_4$ (11) and $[Cp^*(CO)_2Ir-Ir(CO)(Cl)Cp^*]BF_4$ ¹⁷⁶ where the Ir-Ir single bond distances are 2.723(4) Å and 2.8266(6) Å respectively, clearly indicates the absence of a direct metal-metal bond in (7). Notably, even longer non-bonding Ir...Ir distances have been found in $(Cp^*IrX_2)_2$ (X=Cl, 3.7169(1) Å; X=Br, 3.902(13) Å and X=I, 4.072(1) Å).^{181, 182} The distance from iridium to the centroid of the Cp* ring is 1.820 Å for (7), which is shorter than that found in the Ir(I) compound $[Cp^*Ir(CO)]_2$ (Ir-Cp* centroid = 1.901 Å),¹⁸³ but longer than those in the Ir(III) compounds $(Cp^*IrX_2)_2$ (X=Cl, 1.756 Å; X=Br, 1.771 Å and X=I, 1.801 Å).^{181, 182} This distance is sensitive to the electron population in the LUMO of a Cp*Ir(III) fragment, because this orbital is metal-ring anti-bonding. (In $[Cp^*Ir(CO)]_2$, *i.e.*, Cp*Ir(I), this orbital is the HOMO

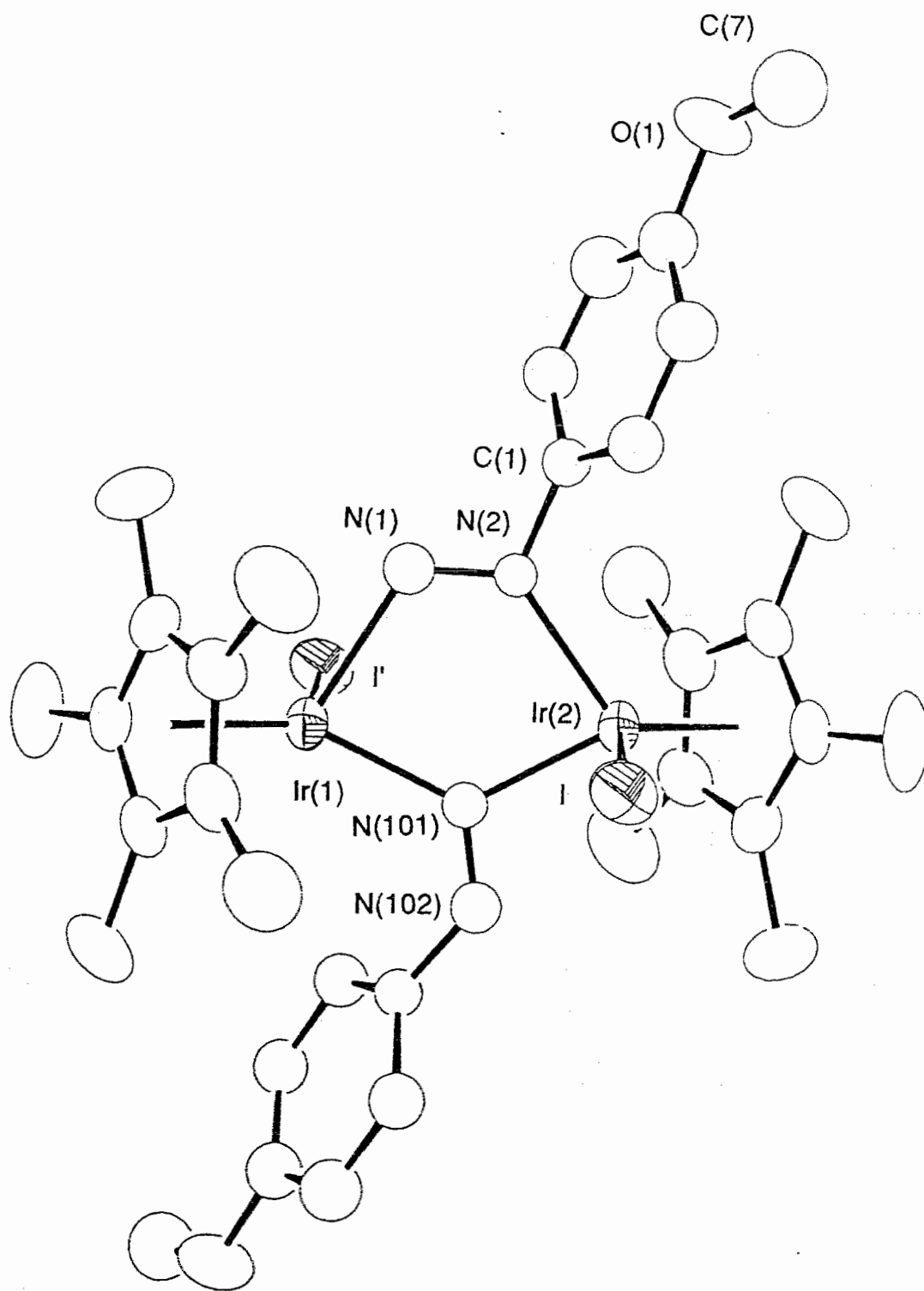


Figure 3.9 Perspective view of the molecular structure of compound (7). (The thermal ellipsoids represent 50 % probability contours).

Table 3.4. Selected Intramolecular Distances (Å) and Angles (°) for

(a) Bond Lengths			
Ir(1) ^a - N(1)	2.143(9)	Ir(1) - N(101)	2.000(7)
Ir(2) - N(2)	2.147(6)	Ir(2) - N(101)	2.030(7)
Ir(2) - C(10)	2.177(5)	Ir(2) - C(20)	2.154(5)
Ir(2) - C(30)	2.161(5)	Ir(2) - C(40)	2.237(5)
Ir(2) - C(50)	2.249(5)	Ir(2) - Cp ^b	1.820
Ir(2) - I	2.6913(8)	N(1) - N(2)	1.23(1)
N(101) - N(102)	1.19(1)	N(2) - C(1)	1.411
N(102) - C(101)	1.417	O(1) - C(4)	1.380
O(1) - C(7)	1.395	O(101) - C(104)	1.376
O(101) - C(107)	1.399		
(b) Bond Angles			
N(2) - Ir(2) - I	89.4(2)	N(101) - Ir(2) - I	90.5(2)
N(1) - Ir(1) - I ^a	85.6(2)	N(101) - Ir(1) - I'	87.0(2)
N(1) - Ir(1) - Cp'	124.1	N(2) - Ir(2) - Cp	125.1
N(101) - Ir(1) - Cp'	133.5	N(101) - Ir(2) - Cp	141.4
N(1) - Ir(1) - N(101)'	85.0(3)	N(2) - Ir(2) - N(101)'	83.5(3)
N(2) - N(1) - Ir(1)	120.3(6)	N(1) - N(2) - Ir(2)	125.5(6)
N(102) - N(101) - Ir(2)	123.8(6)	N(102) - N(101) - Ir(1)	110.9(6)
C(1) - N(2) - Ir(2)	122.4(5)	Ir(2) - N(101) - Ir(1)	124.9(4)
C(1) - N(2) - N(1)	111.7(7)	C(101) - N(102) - N(101)	131.7(8)
C(2) - C(1) - N(2)	119.0(7)	C(6) - C(1) - N(2)	120.9(7)

(continue Table 3.4)

C(102) - C(101) - N(102)	123.6(7)	C(106) - C(101) - N(102)	117.2(7)
C(7) - O(1) - C(4)	118.8	C(107) - O(101) - C(104)	118.7

a: Ir(1) related to Ir(2) by (1-x, -y, -z), and the same relation between the primed atoms and their primary atoms.

b: Cp denotes the centre of mass of the five Cp* ring carbon atoms.

because it is now completely occupied). The variation of this distance in the above compounds indicates that the LUMO of the Cp*Ir(III) fragment in (7) has been largely populated, and suggests that the N₂Ar⁻ ligand has a stronger electron donating ability than the halides. The Ir-I bond length of 2.6913(8) Å is comparable to the value of 2.694(1) Å found for the terminal Ir-I bond in (Cp*IrI₂)₂.¹⁸²

An interesting feature of (7) is that the molecular core, consisting of the two iridium atoms, the three metal-bonded nitrogens atoms and the two *ipso* carbons of the aryl rings, is essentially planar, with only small deviations from the best least-squares plane defined by the planar Ir-N(1)-N(2)-Ir-N(101)' ring, e.g., C(1), 0.085(12); N(102)', 0.191(11) and C(101)', -0.003(13) Å. This planarity suggests a degree of π electron delocalization in the five-member ring and including also the nitrogen atom N(102)'.

The Aryldiazenido Ligands

The disorder in the structure limits the accuracy obtained for the positions of the aryldiazenido nitrogen atoms, although the model shows a flat region in

the final electron density difference map at the nitrogen group area and is therefore considered satisfactory.

For the $\mu^2\text{-}\eta^2$ - bridging aryldiazenido ligand, the N(1)-N(2) bond length is 1.23(1) Å, consistent with a N=N double bond. This value is comparable to that found in $(\mu\text{-H})\text{Os}_3(\text{CO})_{10}(\mu^2\text{-}\eta^2\text{-N}_2\text{Ph})$ (N-N = 1.233(2) Å)¹⁴⁰ and is slightly smaller than that found in $\{[\text{Cp}^*\text{Ir}(\text{CO})]_2(\mu^2\text{-}\eta^2\text{-}p\text{-N}_2\text{C}_6\text{H}_4\text{OMe})\}\text{BF}_4$ (**11**) (N-N = 1.29(2) Å) (see section 3.3.2.1). The N=N group is symmetrically bridging the two iridium centres with Ir(1)-N(1)=2.143(9) Å and Ir(2)-N(2)= 2.147(6) Å. These distances are longer than those found in $\{[\text{Cp}^*\text{Ir}(\text{CO})]_2(\mu^2\text{-}\eta^2\text{-}p\text{-N}_2\text{-C}_6\text{H}_4\text{OMe})\}\text{BF}_4$ (**11**) (Ir(1)-N(1)= 2.02(2) Å and Ir(2)-N(2)= 2.06(2) Å).

For the $\mu^2\text{-}\eta^1$ - bridging aryldiazenido ligand, the N(101)-N(102) distance of 1.19(1) Å is comparable with those found in similarly coordinated aryldiazenido complexes.^{140, 184, 185, 186} This bridge is also essentially symmetric between the two iridium atoms (Ir(1)-N(101)= 2.030(7) Å, Ir(2)-N(101)= 2.000(7) Å and Ir-N(average)= 2.015(10) Å) and involves an angle of Ir(1)-N(101)-Ir(2)= 124.9(4)°. This angle, however, is significantly larger than that in a similar coordinated aryldiazenido compound $\{[\text{Ir}(\text{NO})(\text{PPh}_3)]_2(\mu^2\text{-O})(\mu^2\text{-}\eta^1\text{-}o\text{-N}_2\text{C}_6\text{H}_4\text{-NO}_2)\}\text{PF}_6$ (Ir-N-Ir'= 94(4)°).¹⁸⁴

Another interesting feature of the bridging aryldiazenido ligands is that the planes of the aromatic rings of the *p*-methoxyphenyl groups each make an angle ca. 120° with the molecular core plane. This feature indicates non-conjugation of the π electrons between the N=N group and its aromatic ring in both of the bridging aryldiazenido ligands. A similar phenomenon has also been observed in other bridging aryldiazenido complexes.^{140, 179, 184, 186}

3.4 Discussion

From the experimental results for these species with a generalized formula $[\text{Cp}^*\text{Ir}(\text{L})(p\text{-N}_2\text{C}_6\text{H}_4\text{OMe})]^{0 \text{ or } +}$, we can see an important influence of the ancillary ligand L on the geometrical preference of the aryldiazenido ligand. When L is a weak π -acid, the aryldiazenido ligand prefers the singly bent geometry, but when L is a strong π -base, the aryldiazenido ligand prefers to adopt a doubly bent geometry. This interrelationship between the nature of the ancillary ligand and the conformational preference of the aryldiazenido ligand can be fairly well understood in terms of a fragment molecular orbital analysis.^{21, 22}

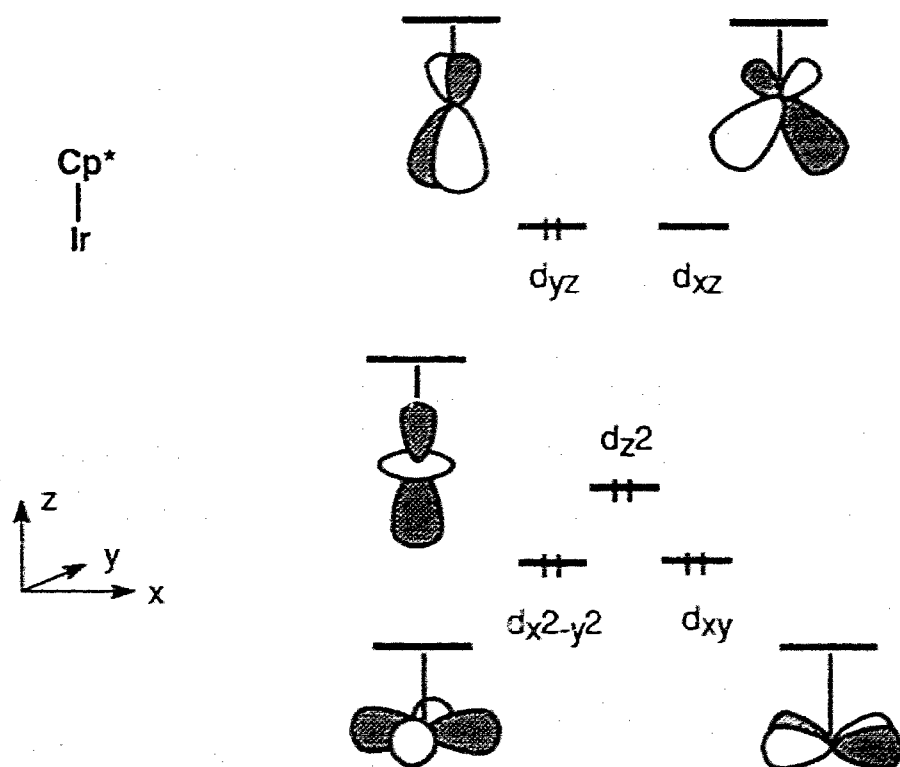


Figure 3.10 The frontier orbitals of the Cp^*Ir fragment

Before we start to analyze the ligand effect, let us first construct the frontier orbitals for the $\text{Cp}^*\text{Ir}(=\text{N}^+=\text{NAr})$ fragment. Detailed discussion of the frontier orbitals of the Cp^*Ir fragment have been given elsewhere.^{28, 29} Here we shall describe only their salient features, emphasizing those π orbitals which eventually control the conformation of the aryldiazenido ligand. The frontier orbitals for Cp^*Ir are shown in figure 3.10. For the Ir(I) , d^8 metal centre, assuming a doubly-occupied singlet ground state, the HOMO of this fragment can be assigned as the d_{yz} orbital in the chosen coordinate system. It is this d_{yz} orbital that is mainly involved in the π -back-bonding interaction with a singly bent aryldiazenido ligand, which is presumed to coordinate to the metal centre in the xz plane, but with its aryl ring tail out of the xz plane. (see figure 3.11). It is worth mentioning that the energies of the HOMO of the Cp^*Ir fragment and the LUMO of the singly bent aryldiazenido ligand are fairly close. This is because the HOMO of the metal fragment is anti-bonding between iridium and the Cp^* ligand (refer to Figure 3.10), and the LUMO of the aryldiazenido ligand is a low-lying empty orbital, even lower than that of the NO^+ ligand (as we saw in Chapter II). Although it should be noted that a lower π -type of metal-centred orbital, d_{xy} , can also interact with the LUMO of the N_2Ar^+ ligand, it will participate in this type of π bonding to a lesser extent due to its low energy, and hence its effect will be neglected here, where we only consider the primary π interaction (Figure 3.11).

The principal issue now remaining is the influence of the different ancillary ligands, L, on the primary π interaction between the Cp^*Ir fragment and the N_2Ar^+ ligand. Each case is considered separately, as follows.

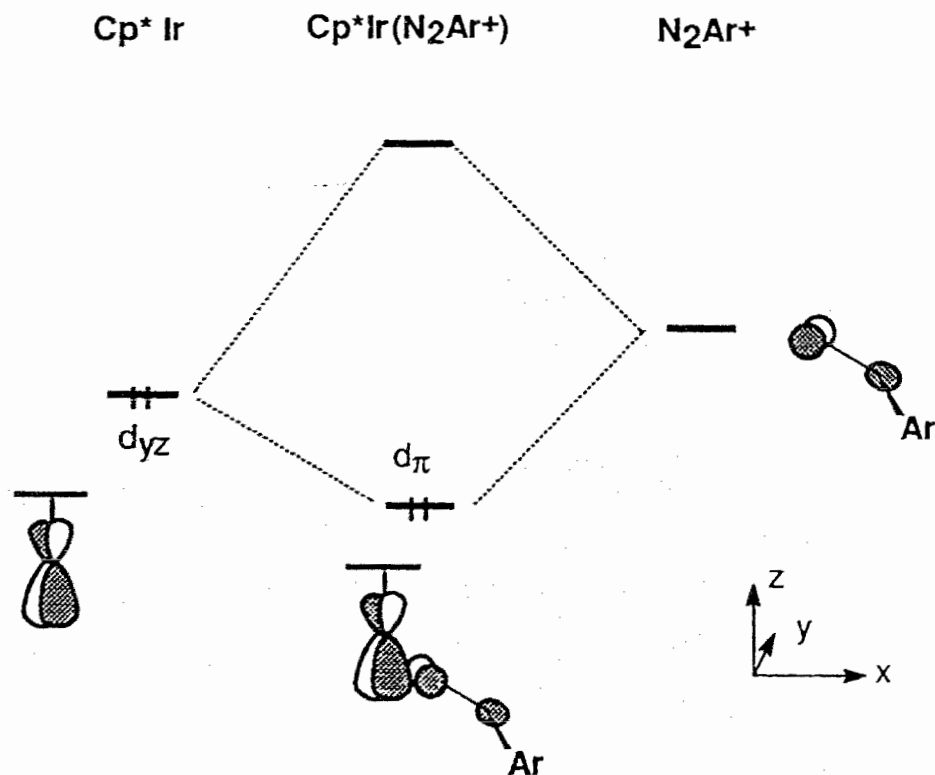


Figure 3.11 The primary π interaction between Cp^*Ir fragment and singly bent N_2Ar^+ ligand

3. 4. 1 The Ancillary Ligand, L, Is a π -Acid

A weak π acid, *e.g.* C_2H_4 or PR_3 , generally has an empty π orbital at a rather high energy. When it coordinates to the $\text{Cp}^*\text{IrN}_2\text{Ar}^+$ fragment in the direction "trans" to the diazenido ligand, its empty π orbital will match in symmetry the d_{yz} orbital of the $\text{Cp}^*\text{IrN}_2\text{Ar}^+$ fragment (as shown in Figure 3.12) or can be brought into the matching position by a rotation about the M-L σ bond. Due to this d_{yz} orbital's involvement, the primary π interaction between the Cp^*Ir and N_2Ar^+ fragments will now be certainly affected. Since the empty π orbital of the ancillary ligand is located at a much higher energy level (*i.e.*, it is a weak π acid) the participation of this orbital in the primary interaction will be expected to

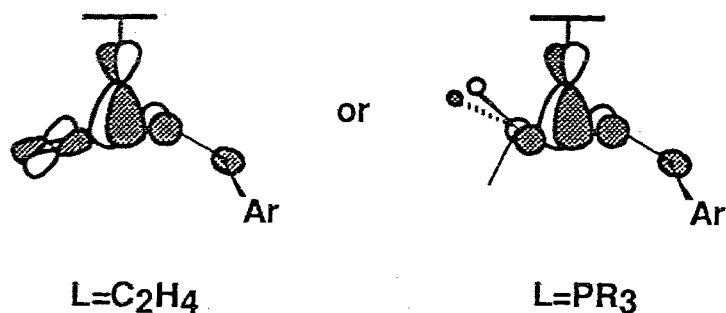


Figure 3.12 π interaction between the $Cp^*IrN_2Ar^+$ fragment and the ancillary ligand L

be small. Consequently, the coordination of a weak π acid ligand, L, to the $Cp^*IrN_2Ar^+$ fragment will only be expected to cause a slight additional stabilization of the metal centred orbital, $d\pi$, which is schematically shown by the dotted line in Figure 3.13.

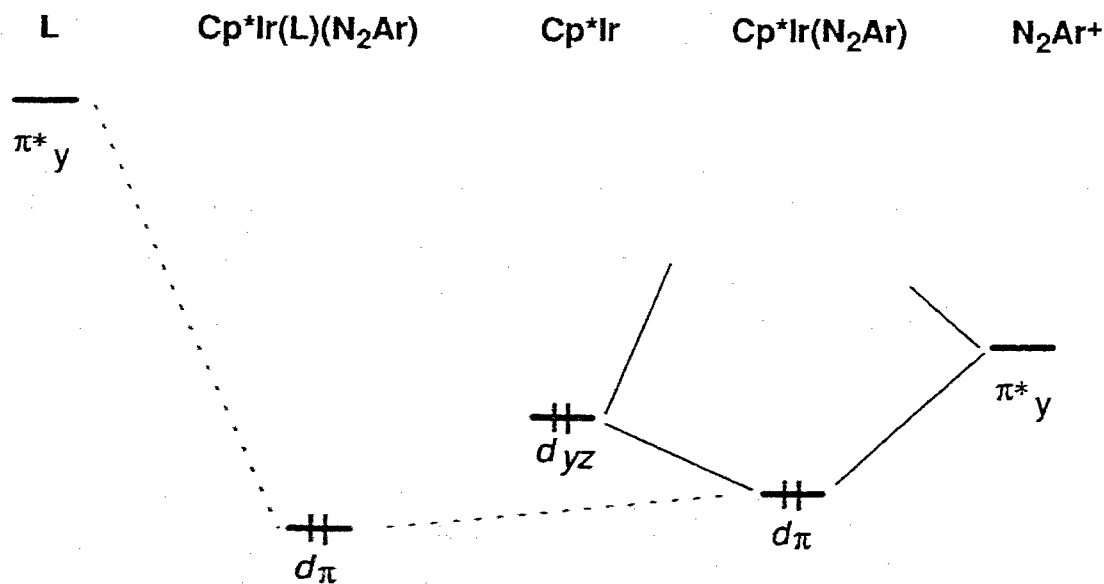


Figure 3.13 The influence of the weak π acid ligand, L, on the primary π interaction between Cp^*Ir and N_2Ar^+ fragments

Obviously, an increase of the relative π acidity, corresponding to a decrease of the energy level of the empty π orbital of the ligand L will stabilize the metal centred $d\pi$ orbital further. However any further stabilization of the metal $d\pi$ orbital caused by the presence of ligand L will also cause a decrease of the N_2Ar^+ ligand's participation in the $d\pi$ orbital. In other words, coordination of a π acid ligand L to the $Cp^*IrN_2Ar^+$ fragment always, more or less, weakens the π -back-bonding between the metal centre and the N_2Ar^+ group. The stronger the π acidity of the L ligand, the more is the stabilization of the $d\pi$ orbital, and consequently, the less is the participation of the π^*_y component of N_2Ar^+ in the $d\pi$ orbital and the weaker is the expected π -back-bonding between the metal centre and N_2Ar^+ .

Although both ethylene and triphenylphosphine ligands are weak π acids, the π acidity of ethylene ligand is believed to be slightly higher than that of the phosphine ligand. Thus, based on the above discussion, when ethylene, as the ancillary ligand L, coordinates to the $Cp^*IrN_2Ar^+$ fragment, it will be expected to weaken the iridium-aryldiazenido π -back-bonding more than that when L is triphenylphosphine. That is, the Ir-N α bond in $[Cp^*Ir(C_2H_4)(N_2Ar)]^+$ (**1**) would be expected to be weaker than in $[Cp^*Ir(PPh_3)(N_2Ar)]^+$ (**3**), and consequently, the N=N bond strength would be expected to be stronger for L= C_2H_4 than for L= PPh_3 . The experimental results show exactly this same trend as we have anticipated.

There are two further points. First, in principle, the singly bent geometry of the aryldiazenido ligand in such compounds will be retained, no matter how strong or how weak the π acidity of the ancillary ligand L is. Secondly, because the stronger the π acidity of L, the weaker is the metal-aryldiazenido bonding, a very strong π acid ligand would be expected to dramatically weaken the Ir-N α

bond. Conversely, the bonding between the L ligand and the Cp*Ir fragment would also be expected to be weakened by the presence of the singly bent aryldiazenido ligand, because this ligand is itself also a strong π acid. So, in this situation, the total effect would be a very unstable species in which both of the ligands, L and N_2Ar^+ are mutually incompatible. This latter point explains our lack of success in synthesizing $[Cp^*Ir(CO)(N_2Ar)]^+$ in this work. The actual results obtained will be given in Chapter IV.

3.4.2 The Ancillary Ligand L is a π -Base

In this section, we will see how the primary π interaction, shown in Figure 3.11, changes when the ancillary ligand is a π base.

A π base ligand should have at least one filled orbital of π symmetry, *i.e.*, in the direction perpendicular to the coordination direction. This kind of orbital is usually of low energy, lower than the metal-centred ones. When this π base ligand coordinates to the $Cp^*IrN_2Ar^+$ fragment in the direction "trans" to the aryldiazenido ligand, the filled π orbital will directly interact with metal d_{yz} orbital. Since this is a two-orbital-four-electron interaction, it can be formally considered that the filled metal-centred orbital, d_{yz} , has been raised in energy by the effect of the filled π orbital of L, toward the energy level of the π accepting orbital of the diazenido ligand (interaction (1) in Figure 3.14). Obviously, a further interaction between this metal d_{yz} orbital and the empty π^*_y orbital of the aryldiazenido ligand, shown as interaction (3) in Figure 3.14, becomes more favorable due to the proximity in energy.

However, we have to emphasize that this situation may be true only for those ligands that have a weak or medium π basicity strength. For a strong π

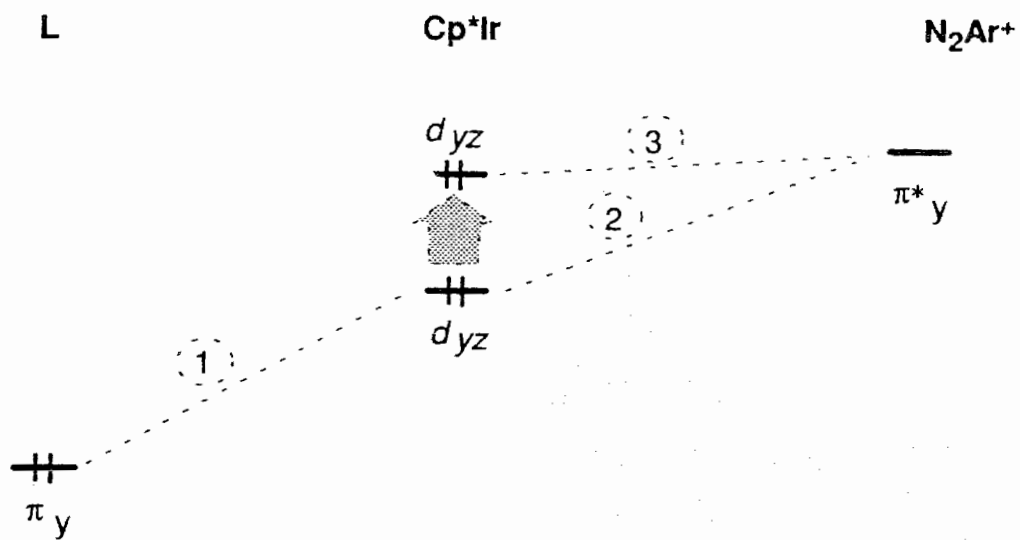


Figure 3.14 The influence of a π base ancillary ligand on the metal d_{yz} orbital

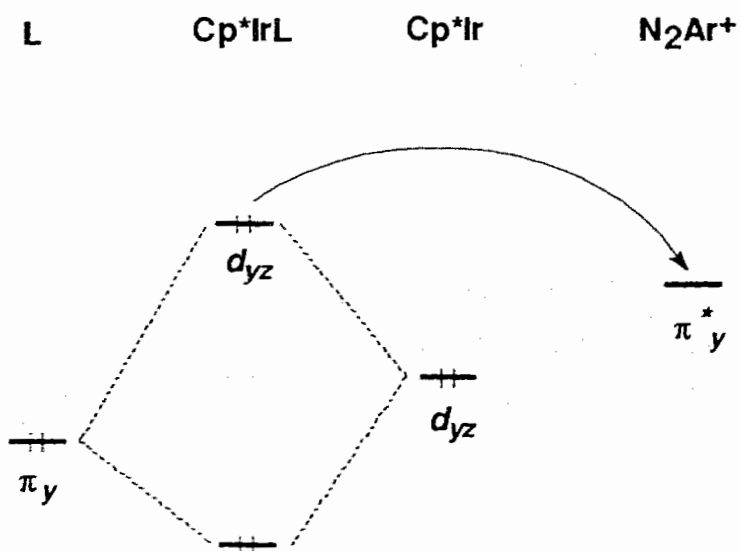
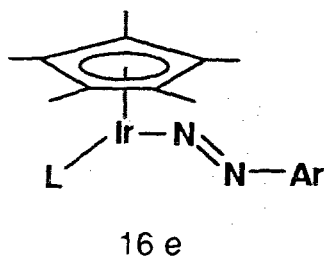


Figure 3.15 An iridium-diazenido MLCT caused by the trans strong π base ligand

base, the situation could be different. Then the interaction between the d_{yz} orbital of the Cp^*Ir fragment and the filled π orbital of L could be very strong; strong enough to push the filled metal centre orbital d_{yz} higher, in energy, than the π^*_y orbital of the singly bent aryldiazenido ligand. If this were to happen, a metal to ligand charge transfer would most likely occur (see Figure 3.15). This would leave a species with a 16-electron metal centre and a doubly bent aryldiazenido ligand, *i.e.*



Since this species would be expected to be very reactive, it could either dimerize itself, as we saw in the case of $\text{L} = \text{X}^-$, or rearrange itself, as we saw in the case where $\text{L} = \text{Cp}^*\text{Ir}(\text{CO})_2$, to form a more stable product.

The qualitative pictures drawn here lay out a clear explanation of the experimental facts we have accumulated in this chapter in the ligand exchange reaction of the ethylene ligand in $[\text{Cp}^*\text{Ir}(\text{C}_2\text{H}_4)(\text{N}_2\text{Ar})]^+$ by strong π base ligands, I^- , Br^- and the metal base $\text{Cp}^*\text{Ir}(\text{CO})_2$.

Finally, it might be worth mentioning that once this 16-e doubly bent aryldiazenido complex were to form, as mentioned in Chapter I, this ligand would most likely reorientate itself by a rotation of 90° to avoid an antibonding interaction between the lone pair of N_α and another filled metal π orbital, d_{xy} , and to construct a bonding interaction between the d_{xy} and the perpendicular π^* orbital of the doubly bent diazenido ligand. Were the ancillary ligand L not a

chiral one (*i.e.*, X^- and $Cp^*Ir(CO)_2$ as we used), this rotation should have the same probability toward either side of the plane containing the Ir, the centroid of the Cp^* and the ancillary ligand. Therefore, it would be expected to result in equal amount of two enantiomers, and a further dimerization or rearrangement of these two enantiomers in a non-chiral environment would most likely produce equal amounts of enantiomeric products. Equal amounts of enantiomers have been observed in both solid state structures of (7) and (11). Furthermore, as a logical extension, a future reaction in which the ancillary ligand L is a strong chiral π base would certainly be interesting.

3.5 Conclusion

The π effect of the ancillary ligands on the geometric preference of the aryldiazenido ligand in complexes with a general formula, $[Cp^*Ir(L)(p-N_2C_6H_4OMe)]^0$ or $+$ has been demonstrated in this chapter.

Replacement of the labile ligand C_2H_4 in (1) by PPh_3 results in $[Cp^*Ir(PPh_3)(p-N_2C_6H_4OMe)]BF_4$ (3) in high yield. Like compound (1), (3) also contains a singly bent aryldiazenido ligand, and both of them contain the weak π -acid, C_2H_4 or PPh_3 , as the ancillary ligand L. An understanding of this in terms of the molecular orbital interaction analysis has led to a conclusion that *a π -acid ligand "trans" to the aryldiazenido ligand will weaken the iridium-diazenido bond, and the stronger is the acidity of the ancillary ligand, the weaker is the iridium-diazenido bond, but the geometry of the singly bent diazenido ligand is retained.*

Addition of hydride to $[Cp^*Ir(PPh_3)(p-N_2C_6H_4OMe)]BF_4$ yields the corresponding hydrido complex $Cp^*Ir(PPh_3)(H)(p-N_2C_6H_4OMe)$ (4) with a doubly bent diazenido ligand. The chloro analogue, $Cp^*Ir(PPh_3)(Cl)(p-N_2C_6H_4OMe)$ (5), is unstable; it may change rapidly to $[Cp^*Ir(PPh_3)(p-N_2C_6H_4OMe)]Cl$ (5'), a

singly bent diazenido complex. However, protonation at $N\alpha$, forming the diazene complex $[\text{Cp}^*\text{Ir}(\text{PPh}_3)(\text{Cl})(p\text{-NHNC}_6\text{H}_4\text{OMe})]\text{BF}_4$ (**6**), can stabilize the chloro ligand in the coordination sphere.

Replacement of the labile ligand C_2H_4 from (**1**) by X , $\text{X} = \text{I}^-$ or Br^- , results in the complexes $[\text{Cp}^*\text{Ir}(\text{X})]_2(\mu^2\text{-}\eta^2\text{-}p\text{-N}_2\text{C}_6\text{H}_4\text{OMe})(\mu^2\text{-}\eta^1\text{-}p\text{-N}_2\text{C}_6\text{H}_4\text{OMe})$, (where $\text{X} = \text{I}$ for (**7**) or $\text{X} = \text{Br}$ for (**8**)). The possible pathway from the singly bent aryldiazenido complex (**1**) leading to such novel di-iridium compounds with two different bridging aryldiazenido ligands has been discussed. It is concluded that *in the compound with a general formula, $[\text{Cp}^*\text{Ir}(\text{L})(p\text{-N}_2\text{C}_6\text{H}_4\text{OMe})]$, when L is a strong π -base, the aryldiazenido ligand prefers a doubly bent geometry and this may be accomplished through a MLCT process.* Protonation of compounds (**7**) or (**8**) occurs only at the $N\alpha$ position of the $\mu^2\text{-}\eta^2$ - bridged aryldiazenido ligand. Similarly, replacement of the ethylene in (**1**) by a metal base, $\text{Cp}^*\text{Ir}(\text{CO})_2$, results in another di-iridium complex, $\{[\text{Cp}^*\text{Ir}(\text{CO})]_2(\mu^2\text{-}\eta^2\text{-}p\text{-N}_2\text{C}_6\text{H}_4\text{OMe})\}\text{BF}_4$ (**11**).

The X-ray crystal structures of (**7**) and (**11**) have been determined. Compound (**7**) crystallizes in the triclinic space group $P1$, with $a = 8.937(2)$ Å, $b = 10.036(2)$ Å, $c = 10.893(2)$ Å, $\alpha = 79.98(1)^\circ$, $\beta = 79.52(1)^\circ$, $\gamma = 70.36(1)^\circ$ and $Z = 1$; $R_F = 0.021$ and $R_w = 0.029$. Crystals of compound (**11**) are orthorhombic, space group $Pc21b$, with $a = 8.821(1)$ Å, $b = 20.237(2)$ Å, $c = 34.808(5)$ Å and $Z = 8$; $R_F = 0.044$ and $R_w = 0.049$ for 1661 absorption-corrected independent reflections with $I > 2.5\sigma$.

Finally, to the best of our knowledge, compounds (**7**) and (**8**) synthesized in this work are the first two examples of the dinuclear compound with two different bridging aryldiazenido ligands, and compound (**11**) is the only second example of a similar bridging coordinated aryldiazenido complex.

CHAPTER IV

Syntheses and Characterization of Mono- and Diiridium Carbonyl Complexes Formed from the Attempted Syntheses of $[\text{Cp}^*\text{Ir}(\text{CO})(p\text{-N}_2\text{C}_6\text{H}_4\text{OMe})]\text{BF}_4$; X-ray Crystal Structures of $[\text{Cp}^*_2\text{Ir}_2(\text{CO})_3\text{Cl}]\text{BF}_4$ and $[\text{Cp}^*_2\text{Ir}_2(\text{CO})_2(\eta^1\text{-}\mu^2, \eta^2\text{-}\mu^1\text{-}p\text{-C}_6\text{H}_4\text{OMe})]\text{BF}_4$

4.1 Introduction

In the previous discussion of the electronic influence of the ancillary ligand on the geometrical preference of the aryldiazenido ligand in the system $\text{Cp}^*\text{Ir}(\text{L})(p\text{-N}_2\text{C}_6\text{H}_4\text{OMe})$, we have pointed out that in the case of the ancillary ligand L being a strong π -acid, the π bonding strength between the M and N_2Ar could be dramatically weakened. In order to examine this, the synthesis of the unknown compound $[\text{Cp}^*\text{Ir}(\text{CO})(p\text{-N}_2\text{C}_6\text{H}_4\text{OMe})]\text{BF}_4$ (**12**), where the ancillary ligand is a carbonyl, has been attempted. As possible synthetic routes to the target complex (**12**), we have examined (1) reactions of $\text{Cp}^*\text{Ir}(\text{CO})_2$ (**14**) directly with $[p\text{-N}_2\text{C}_6\text{H}_4\text{OMe}][\text{BF}_4]$ under different reaction conditions, (2) reactions of $[\text{Cp}^*\text{Ir}(\text{C}_2\text{H}_4)(p\text{-N}_2\text{C}_6\text{H}_4\text{OMe})]\text{BF}_4$ (**1**) with carbon monoxide under varying reaction conditions, and (3) reactions of $[\text{Cp}^*\text{Ir}(\text{CO})]_2$ (**15**) with different stoichiometric amounts of $[p\text{-N}_2\text{C}_6\text{H}_4\text{OMe}][\text{BF}_4]$.

Unlike the previously described situations where the ancillary ligand was either a weak π -acid or a strong π -base, all of the results obtained from this latter study point to instability of $[\text{Cp}^*\text{Ir}(\text{CO})(p\text{-N}_2\text{C}_6\text{H}_4\text{OMe})]^+$ indicating that CO and aryldiazenido ligands are mutually destabilizing in this system. This feature is consistent with the theoretical analysis of the electronic relationship between the

aryldiazenido ligand and the ancillary ligand L in the system $\text{Cp}^*\text{Ir}(\text{L})(p\text{-N}_2\text{-C}_6\text{H}_4\text{OMe})$ that has been developed in this Thesis. Therefore, we believe that these failures to obtain $[\text{Cp}^*\text{Ir}(\text{CO})(p\text{-N}_2\text{C}_6\text{H}_4\text{OMe})]\text{BF}_4$ (**12**), in fact, reflect the realities of the electronic situation required for stability in this type of complexes.

On the other hand, although the synthesis of $[\text{Cp}^*\text{Ir}(\text{CO})(p\text{-N}_2\text{C}_6\text{H}_4\text{OMe})]\text{BF}_4$ (**12**) itself has not been successful, the chemistry that has emerged from these attempts is still interesting. While the aryldiazenido ligand seemingly can not be stabilized in the chosen two-legged piano-stool structure, it has been found to be stabilized in a related three-legged piano-stool carbonyl complex $\text{Cp}^*\text{Ir}(\text{CO})(\text{OEt})(p\text{-N}_2\text{C}_6\text{H}_4\text{OMe})$ (**19**). Some of the reactions yield interesting products of nitrogen extrusion.

Finally, we report some new facile synthetic routes to a variety of useful carbonyl compounds, some of which have been previously synthesized by different methods.

4.2 Experimental Section

The general experimental manipulations, solvent purifications and spectroscopic measurements are the same as described in the previous chapters.

The author is grateful to Dr. R. J. Batchelor for the X-ray crystallographic analysis of the single crystal structure of compound (**20**).

4. 2. 1. Preparations of the Precursor Materials

Preparation of $\text{Cp}^*\text{Ir}(\text{CO})\text{H}_2$ (**13**)^{187, 188}

A suspension of partially soluble $\text{Cp}^*\text{Ir}(\text{CO})\text{Cl}_2$ ¹⁸⁹ (30 mg, 0.07 mmol) and an excess of Zn dust (ca. 200 mg) in 10 mL absolute ethanol in a 50 mL

two-neck round bottom flask, equipped with a condenser and a nitrogen gas inlet, was purged with nitrogen gas for 20 minutes. With vigorous stirring, the reaction solution was heated slowly to 50 °C, and then 0.5 mL glacial acetic acid was slowly added into the reaction mixture from the top of the condenser (also the outlet of the nitrogen stream). After the yellow suspension of the $\text{Cp}^*\text{Ir}(\text{CO})\text{Cl}_2$ completely disappeared, the reaction mixture was stirred for another 20 minutes at 50 °C. The solvent was then removed *in vacuo*, and the dark-grey muddy residue was extracted with hexanes (3 X 5 mL). The combined extraction solution was evaporated to dryness affording a very pale yellow oil in good yield (>85%). IR, $\nu(\text{Ir-H})$, 2137 w cm^{-1} and $\nu(\text{CO})$, 1996 s cm^{-1} (hexanes); $^1\text{H NMR}$: $\delta(\text{acetone-}d_6)$ 2.10 s (15H, Cp^*), -16.58 s (2H, Ir-H); MS (EI, m/z): 358 (M^+), 356 (M^+-2H), 354 (M^+-4H), 352 (M^+-6H), 328 ($\text{M}^+-\text{CO}-2\text{H}$), 326 ($\text{M}^+-\text{CO}-4\text{H}$), 324 ($\text{M}^+-\text{CO}-6\text{H}$).

Preparation of $\text{Cp}^*\text{Ir}(\text{CO})_2$ (14) ^{190, 191}

The synthetic equipment setup was similar to that described above in the preparation of (13), but the nitrogen gas was replaced by carbon monoxide gas.

A suspension of partially soluble $[\text{Cp}^*\text{Ir}(\text{Cl})_2]_2$ (100mg, 0.125 mmol), excess Zn dust (*ca.* 500 mg) and 4 ~ 5 drops (*ca.* 0.2 mL) glacial acetic acid in 15 mL absolute ethanol was bubbled with CO gas for one hour at 50 °C. After the reaction finished, (monitored by IR), the reaction solution was cooled to room temperature and the solvent was removed *in vacuo*. To the residue was added 10 mL H_2O and 10 mL CH_2Cl_2 and the mixture was vigorously stirred for 0.5 hour. The CH_2Cl_2 layer was then pipetted out, and the residue was repeatedly extracted with CH_2Cl_2 (2 x 10 mL). The combined CH_2Cl_2 extract was dried over anhydrous Na_2CO_3 , filtered and rotary evaporated to dryness leaving the

product nearly quantitatively as yellow crystals. The product could be further purified by sublimation at 70 °C. IR, $\nu(\text{CO})$, 1939 and 2009 cm^{-1} (in acetone or CH_2Cl_2), 1945 and 2015 cm^{-1} (in hexanes or ethanol); $^1\text{H NMR}$: $\delta(\text{CDCl}_3)$ 2.15 s (Cp^*).

Preparations of $[\text{Cp}^*\text{Ir}(\text{CO})]_2$ (15) ¹⁹¹

Method 1. $\text{Cp}^*\text{Ir}(\text{CO})\text{Cl}_2$ ¹⁸⁹ (100 mg, 0.234 mmol) and excess predried anhydrous Na_2CO_3 (\approx 500 mg) in 10 mL ethanol were refluxed for about two hours with vigorous stirring. During the reaction, the orange yellow suspension of $\text{Cp}^*\text{Ir}(\text{CO})\text{Cl}_2$ slowly disappeared, and a brownish slurry was gradually produced. After the reaction mixture was cooled to room temperature, the solvent was removed under reduced pressure, the residue was extracted with CH_2Cl_2 (ca. 20 mL) and filtered through a Celite filter. Evaporating the dark green CH_2Cl_2 extraction solution to dryness afforded the desired product quantitatively as a brownish powder. The product can be recrystallized in CH_2Cl_2 / hexanes. Typical yield > 80%. IR $\nu(\text{CO})$, 1676 cm^{-1} (CH_2Cl_2); $^1\text{H NMR}$: $\delta(\text{CDCl}_3)$ 1.79 s (Cp^*); MS (EI, m/z): 710, (M^+); 680 ($\text{M}^+ - \text{CO} - 2\text{H}$); 648, ($\text{M}^+ - 2\text{CO} - 6\text{H}$); 463, ($[\text{Cp}^*\text{IrCp}^*]^+$).

Method 2. A reaction similar to method 1, but using 1 : 2 molar ratio of $\text{Cp}^*\text{Ir}(\text{CO})_2$ and $[\text{Cp}^*\text{IrCl}_2]_2$ under reflux condition for three hours, gave the desired product in 92% yield.

Method 3. To a Schlenk tube containing a solution of $\text{Cp}^*\text{Ir}(\text{CO})\text{Cl}_2$ (100 mg, 0.234 mmol) in anhydrous ethanol (20 mL) was added excess zinc dust (\approx 500 mg). This mixture was degassed twice and then stirring vigorously overnight (ca. 14 hours) at room temperature. When the starting material

$\text{Cp}^*\text{Ir}(\text{CO})\text{Cl}_2$ had completely disappeared (monitored by IR), the solution was pumped to dryness, and the residue was extracted with CH_2Cl_2 (3 x 5 mL). Removal of the solvent CH_2Cl_2 from the combined extraction solution *in vacuo* gave the desired product, generally in a yield > 90%.

Method 4. A reaction similar with method 3, but using 1:2 molar ratio of $\text{Cp}^*\text{Ir}(\text{CO})_2$ and $[\text{Cp}^*\text{IrCl}_2]_2$ as the starting materials, also gave the desired product in high yield.

4. 2. 2. Attempts to Synthesize $[\text{Cp}^*\text{Ir}(\text{CO})(p\text{-N}_2\text{C}_6\text{H}_4\text{OMe})]\text{BF}_4$ (12) through the Reactions of $\text{Cp}^*\text{Ir}(\text{CO})_2$ (14) with $[p\text{-N}_2\text{C}_6\text{H}_4\text{OMe}][\text{BF}_4]$

1). Reaction in *Acetone* Solvent – Formation of $[\text{Cp}^*\text{Ir}(\text{CO})_2(p\text{-C}_6\text{H}_4\text{OMe})]\text{BF}_4$ (16)

To a vigorously stirring, yellow solution of $\text{Cp}^*\text{Ir}(\text{CO})_2$ (14) (20 mg, 0.052 mmol) in acetone (3 mL) at $-78\text{ }^\circ\text{C}$ was added dropwise 1 mL acetone solution containing 12 mg $[p\text{-N}_2\text{C}_6\text{H}_4\text{OMe}][\text{BF}_4]$ salt (0.052 mmol) along the glass wall of the Schlenk tube. The addition of the aryldiazonium salt solution should be slow enough to allow the temperature of this solution to cool to ca. $-78\text{ }^\circ\text{C}$ on reaching the the bulk reaction solution. The colour of the reaction solution first changed from yellow to bright red, and then to dark brown as the addition proceeded. After the addition of the solution of $[p\text{-N}_2\text{C}_6\text{H}_4\text{OMe}][\text{BF}_4]$ was completed, the reaction mixture was stirring for another hour, and then 10 mL diethyl ether was slowly added into the reaction mixture with vigorous stirring. A dark brown precipitate was formed upon the addition of the diethyl ether. After the precipitate settled, the supernatant solution was removed carefully by a pipette and the

residue was washed three times with cold ether. Still at $-78\text{ }^{\circ}\text{C}$, the dark brown precipitate was dried *in vacuo* leaving $[\text{Cp}^*\text{Ir}(\text{CO})_2(\textit{p}\text{-C}_6\text{H}_4\text{OMe})]\text{BF}_4$ (**16**) as the product in good yield (80%). IR: $\nu(\text{CO})$ 2074 s, 2114 s cm^{-1} (acetone); ^1H NMR: $\delta(\text{CDCl}_3)$ 2.19 s (15H, Cp^*), 3.80 s (3H, OMe), 6.69 d and 7.11 d (4H, AA'BB' pattern, C_6H_4); FABMS (Sulfolane, Xenon) (m/z): 491 (M^+), 463 ($\text{M}^+ - \text{CO}$), 433 ($\text{M}^+ - \text{CO} - \text{OCH}_2$), 405 ($\text{M}^+ - 2\text{CO} - \text{OCH}_2$); Anal. (calcd.) C, 39.52; H, 3.84, (found) C, 39.81; H, 3.85; N, 0.40.

2). Reaction in CH_2Cl_2 solvent – Formation of $[(\text{Cp}^*\text{Ir})_2(\text{CO})_3\text{Cl}]\text{BF}_4$ (**17**)

To a solution of $\text{Cp}^*\text{Ir}(\text{CO})_2$ (**14**) (100 mg, 0.26 mmol) in 3 mL CH_2Cl_2 at room temperature was directly added solid $[\textit{p}\text{-N}_2\text{C}_6\text{H}_4\text{OMe}][\text{BF}_4]$ (60 mg, 0.26 mmol) and the reaction mixture was stirred vigorously. The colour of the reaction mixture changed from yellow to green. To completely dissolve $[\textit{p}\text{-N}_2\text{C}_6\text{H}_4\text{OMe}][\text{BF}_4]$ salt would take a period of about one hour. The effervescence was obvious initially, but gradually diminished after one hour as all diazonium salt dissolved. After another 3 to 4 hours stirring, a large amount of fine yellow powder was formed. As the IR spectrum of the solution showed that the $\text{Cp}^*\text{Ir}(\text{CO})_2$ (**14**) was completely consumed (ca. 6 hours), the solution was concentrated under reduced pressure to about 1.5 mL and an excess of hexanes was added to precipitate the yellow powder. The supernatant solution was carefully pipetted out and the yellow solid residue was washed twice with diethyl ether affording the analytically pure product $[(\text{Cp}^*\text{Ir})_2(\text{CO})_3\text{Cl}]\text{BF}_4$ (**17**) (85%). IR $\nu(\text{CO})$ 2017 s,b, 2058 m cm^{-1} (CH_2Cl_2); ^1H NMR: $\delta(\text{CDCl}_3)$ 1.94s (15H, Cp^*), 2.23s (15H, Cp^*), $^{13}\text{C}\{^1\text{H}\}$ NMR: $\delta(\text{CDCl}_3)$ 10.17, 10.39 and 103.05, 106.67 (C_5Me_5), 171.37 (carbonyls); FABMS (Thioglycerol, Xenon) (m/z): 775 (M^+), 745 ($\text{M}^+ - \text{CO} - 2\text{H}$), 717 ($\text{M}^+ - 2\text{CO} - 2\text{H}$); Anal. (calcd), C, 31.98; H, 3.50, (found), C, 32.08, H, 3.51.

3). Reaction in *ethanol* solvent -- Formation of [Cp*Ir(CO)(OEt)(*p*-NHN-C₆H₄OMe)]BF₄ (18), or (18a)

To a solution of Cp*Ir(CO)₂ (14) (20 mg, 0.052 mmol) in 10 mL of ethanol was added [*p*-N₂C₆H₄OMe]BF₄ (11.5 mg, 0.052 mmol), or [*p*-¹⁵NNC₆H₄OMe][BF₄] for (18a), at room temperature. To completely dissolve the diazonium salt took a period of *ca.* 10 minutes. The colour of the solution changed from yellow to orange. IR spectra showed that absorptions (2015 and 1945 cm⁻¹) due to Cp*Ir(CO)₂ (14) slowly decreased and a new band at 2058 cm⁻¹ increased. After one hour, the solvent was removed *in vacuo* affording an orange coloured oily product quantitatively. A complete characterization of this compound was unsuccessful due to its very poor stability in other solvents. IR: ν(CO) 2058 cm⁻¹ (ethanol), ¹H NMR (100 MHz, measured in less than 5 minutes after dissolving in acetone-*d*₆) δ: 1.12*t* (3H, J_{H-H} = 7, MeCH₂O), 1.96*s* (15H, Cp*), 3.85*s* (3H, OMe), 3.97*m* (2H, MeCH₂O), 7.10*d* and 7.81*d* (4H, AA'BB' pattern, C₆H₄); ¹⁵N NMR for (18a): δ(ethanol) -154*d* (J_{¹⁵N-H} = 88, ¹⁵Nα-H), FABMS (NOBA, Xenon) (*m/z*): 491 (M⁺ - EtOH), 463 (M⁺ - EtOH - CO).

Preparation of Cp*Ir(CO)(OEt)(*p*-N₂C₆H₄OMe) (19), or (19a)

To an orange solution of freshly synthesized (18), or (18a) *in situ* in 5 mL ethanol was added *ca.* 0.2 mL (3 drops) Et₃N. The color of the reaction solution changed immediately to red. The solvent was removed *in vacuo*, and an excess of hexanes was added to extract the neutral product. After removing the insoluble [Et₃NH]BF₄ through a Celite filter, the hexane filtrate was then evaporated to dryness resulting in a red oily product (19) or (19a) in ~ 80% yield (based on the amount of (14) used in the preparation). IR: ν(CO) 2025 cm⁻¹

(ethanol); 2029 cm^{-1} (hexanes); ^1H NMR (100 MHz, benzene- d_6) δ : 1.15 t (3H, $J_{\text{H-H}}=7$, MeCH_2O), 1.68 s (15H, Cp^*), 3.28 s (3H, OMe), 4.17 d , q (1H, $^2J_{\text{H-H}}=10$, $^3J_{\text{H-Me}}=7$, MeCH_2O), 4.35 d , q (1H, $^2J_{\text{H-H}}=10$, $^3J_{\text{H-Me}}=7$, MeCH_2O), 6.83 d and 7.74 d (4H, AA'BB' pattern, C_6H_4), ^{15}N NMR for (19a): δ (benzene- d_6) 223.5 s ($^{15}\text{N}\alpha$), MS (EI, m/z): 536 (M^+), 508 (M^+-CO), 491 (M^+-OEt), 463 ($\text{M}^+-\text{CO}-\text{OEt}$), 433 ($\text{M}^+-\text{OEt}-\text{CO}-\text{OCH}_2$), Anal. (calcd): C, 44.85; H, 5.08; N, 5.23, (found): C, 45.01, H, 5.12; N, 5.41.

Single Crystal X-ray Crystallographic Analysis of $[\text{Cp}^*(\text{CO})_2\text{Ir}-\text{Ir}(\text{CO})(\text{Cl})\text{Cp}^*]\text{BF}_4$ (17)

Data Collection

The crystallization of $[\text{Cp}^*_2\text{Ir}_2(\text{CO})_3\text{Cl}]\text{BF}_4$ (17) was conducted with the slow diffusion of large amount of diethyl ether into a saturated CH_2Cl_2 solution of the complex. A suitable yellow single crystal, pre-examined by microscopy under polarized light, was mounted on a glass fibre and well centred in the X-ray beam of an Enraf-Nonius CAD4-F diffractometer with graphite monochromatized $\text{Mo-K}\alpha$ radiation. The unit cell parameters were first obtained from the setting angles of 25 well-centred reflections, from which a monoclinic unit cell was indicated and then confirmed by the investigation of selected symmetry related reflections. The final, more accurate, unit cell was determined from the setting angles of 25 well-centred reflections, widely spread throughout reciprocal space, in the range $28^\circ < 2\theta < 50^\circ$. See Table 4.1 for pertinent crystal and data collection details.

All intensity data were collected at $20 \pm 1^\circ \text{C}$ and with $1.9^\circ < 2\theta < 50^\circ$. The bisecting mode and the coupled ω - 2θ scan mode were used in the data collection. Backgrounds were scanned for 25% of the peak width on either side

of the peak scan. An analytical absorption curve, based on the measurement of the crystal shape and contents in the crystal, showed a good fit ($R < 5\%$) to that based on 3 high χ angle reflections ($\chi > 82^\circ$), so it was applied to the intensity data. The intensity of 2 standard reflections were measured every 1 hour and 20 minutes of the acquisition time to assess possible changes in the crystal or X-ray beam. No appreciable variation in the intensity of these standards was observed over the course of the data collection, (RMS deviation from the mean $< 1.3\%$ and the long term experiment instability $< 0.95\%$), so a five-point smoothing curve based on these standard reflections was used to scale the data in the data reduction process. Lorentz and polarization corrections¹⁵³ were also applied. Of the 4427 unique reflections, 3299 reflections were classed as observed ($I_o \geq 2.5\sigma(I_o)$).

Structure Solution and Refinement

The structure was solved in the space group $P2_1/c$ by using a Patterson map to locate the heavy atoms. Subsequent refinements and difference Fourier syntheses led to location of all remaining non-hydrogen atoms. Scattering factors for neutral atoms were used in the calculation of the structure factors, including anomalous dispersion terms for all non-hydrogen atoms.¹⁵⁵ Anisotropic thermal motion, based on indications from the electron density difference Fourier maps, was refined for Ir, Cl, O and F atoms in the structure, to yield physically reasonable values. Some of the hydrogen atoms in the Cp* methyl groups had been revealed directly by using a low angle difference Fourier map, with $\sin\theta/\lambda$ cutoff value of 0.30 \AA^{-1} , phased on all non-hydrogen

Table 4.1. Crystallographic and Experimental Data^a for the Complex
 $[\text{Cp}^*_2\text{Ir}_2(\text{CO})_3\text{Cl}]\text{BF}_4$ (17)

Formula	$\text{Ir}_2\text{F}_4\text{O}_3\text{ClC}_{23}\text{BH}_{30}$
Formula weight	861.2
Crystal system	Monoclinic
Space group	P21/c
a (Å)	10.583(2)
b (Å)	14.256(3)
c (Å)	16.818(4)
β (deg.)	95.91(2)
V (Å ³)	2523.9(8)
Z	4
D_{calcd} (mg/mm ³)	2.266
$F(000)$	1615.51
μ (Mo-K α)(mm ⁻¹)	10.66
T (K)	293
Crystal dimensions (mm ³)	0.30 x 0.17 x 0.17
λ (Å)	0.71069
Transmission factors	0.169 - 0.300
Scan type	coupled $\omega - 2\theta$
Scan range (deg.)	1.00 + 0.35 tan θ
Scan speed (deg./min.)	0.82-5.49
2θ limits (deg.)	3.8 < 2θ < 50
Intensity standards	(-5, 2, 0); (2, -5, -3).
Oriental standards	(2, 5, -3); (-2, -7, 3); (3, -3, -3).

(Continue Table 4.1)

The <i>h, k, l</i> ranges	-12, 12; 0, 16; 0, 19
Reflections measured	5064
Unique reflections	4427
Reflections with $I > 2.5\sigma(I)$	3299
No. of variables	187
R_f^b	0.027
R_w^c	0.033 ^d
G_o^e	2.57

a: Enraf-Nonius CAD4-F diffractometer, Mo-K α radiation, graphite monochromator.

$$b: R_f = \frac{\sum (|F_o| - |F_c|)}{\sum |F_o|}$$

$$c: R_w = \frac{\sum w (|F_o| - |F_c|)^2}{\sum F_o^2}^{1/2}$$

$$d: w = [(\sigma(F))^2 + 0.00035F^2]^{-1}$$

$$e: G.o.f. = \frac{\sum w (|F_o| - |F_c|)^2}{(\text{No. of degrees of freedom})}^{1/2}$$

atoms. However, all hydrogen atoms were assigned by calculation and were input as fixed contributions in the following calculations; their idealized positions were repeatedly calculated after cycles of refinement from the geometries of their attached carbon atoms using a C-H distance of 0.96 Å. Isotropic thermal parameters were assigned to these hydrogen atoms, based on those of their attached carbon atoms.

A final full matrix least-square refinement of 187 parameters, for 64 atoms, converged to $R_f=0.027$ and $R_w=0.033$ with a maximum shift less than 0.05σ . A weighting scheme based on counting-statistics was used in the

final refinement, where the weight w was calculated from $w=[(\sigma(F_o))^2 + 0.00035F_o^2]^{-1}$. In the final difference Fourier map, the highest peak had an electron density $1.2(2) e/\text{\AA}^3$, located in the anion region at a distance 0.38 \AA from one F atom.

All calculations were performed on a micro VAX-II computer by using the NRC VAX Crystal Structure System. ¹⁵⁴

4. 2. 3. Attempts to Synthesize $[\text{Cp}^*\text{Ir}(\text{CO})(p\text{-N}_2\text{C}_6\text{H}_4\text{OMe})]\text{BF}_4$ (12**) through the Reactions of $[\text{Cp}^*\text{Ir}(\text{C}_2\text{H}_4)(p\text{-N}_2\text{C}_6\text{H}_4\text{OMe})]\text{BF}_4$ (**1**) with Carbon Monoxide**

1). Reaction in Acetone with Excess of Carbon Monoxide

In a typical reaction, CO gas was bubbled through an acetone solution of $[\text{Cp}^*\text{Ir}(\text{C}_2\text{H}_4)(p\text{-N}_2\text{C}_6\text{H}_4\text{OMe})]\text{BF}_4$ (**1**) (50 mg, 0.09 mmol.) at room temperature. The IR spectrum of the reaction solution showed that $\text{Cp}^*\text{Ir}(\text{CO})_2$ (**14**) ($\nu(\text{CO})$ 1939 and 2009 cm^{-1}) was immediately formed as the major product.

2). Reaction in acetone with equimolar amount of carbon monoxide

To an acetone solution of $[\text{Cp}^*\text{Ir}(\text{C}_2\text{H}_4)(p\text{-N}_2\text{C}_6\text{H}_4\text{OMe})]\text{BF}_4$ (**1**) in a Schlenk tube equipped with a rubber serum stopper was injected an equimolar amount of carbon monoxide gas. After stirring overnight (*ca.* 10 hours), the IR spectrum of the solution showed that $\text{Cp}^*\text{Ir}(\text{CO})_2$ (**14**) ($\nu(\text{CO})$ 1939 and 2009 cm^{-1}) was the only observed product. After evaporating the solution to dryness, the ^1H NMR spectrum of the residue showed $\text{Cp}^*\text{Ir}(\text{CO})_2$ (**14**) and unreacted compound (**1**) as the major components.

3). Reaction in ethanol with carbon monoxide

Carbon monoxide gas was slowly bubbled through an ethanol solution of $[\text{Cp}^*\text{Ir}(\text{C}_2\text{H}_4)(p\text{-N}_2\text{C}_6\text{H}_4\text{OMe})]\text{BF}_4$ (1) for ca. 5 minutes. The colour of the reaction solution changed rapidly from yellow to orange-yellow. The IR spectrum of this orange yellow solution showed a strong band at 2058 cm^{-1} due to compound (18) and two weak, but equal intensity, peaks at $1945, 2015\text{ cm}^{-1}$ due to $\text{Cp}^*\text{Ir}(\text{CO})_2$ (14). After removing the solvent *in vacuo*, the ^1H NMR spectrum of the residue confirmed the presence of (14) and (18), but showed no signals due to the starting material (1).

4. 2. 4. Attempts to Synthesize $\{[\text{Cp}^*\text{Ir}(\text{CO})]_2(\mu^2\text{-}\eta^2\text{-}(p\text{-N}_2\text{C}_6\text{H}_4\text{OMe}))\}\text{BF}_4$ (11) and $[\text{Cp}^*\text{Ir}(\text{CO})(p\text{-N}_2\text{C}_6\text{H}_4\text{OMe})]\text{BF}_4$ (12) through the Reactions of $[\text{Cp}^*\text{Ir}(\text{CO})]_2$ (15) with $[p\text{-N}_2\text{C}_6\text{H}_4\text{OMe}][\text{BF}_4]$

1). Formation of $\{[\text{Cp}^*\text{Ir}(\text{CO})]_2(1\text{-}\eta^1\text{-}1,2\text{-}\eta^2\text{-}\mu^2\text{-}p\text{-C}_6\text{H}_4\text{OMe})\}\text{BF}_4$ (20)

$[p\text{-N}_2\text{C}_6\text{H}_4\text{OMe}][\text{BF}_4]$ (16 mg, 0.07 mmol) in solution in ca. 2 mL acetone was added dropwise to a solution of $[\text{Cp}^*\text{Ir}(\text{CO})]_2$ (15) (50 mg, 0.07 mmol) in 5 mL acetone at $-78\text{ }^\circ\text{C}$. The colour of the reaction solution changed immediately from deep green-yellow to dark red. After stirring for 30 minutes, the IR spectrum of the solution showed only one broad absorption at 1964 cm^{-1} . The solvent was then removed under reduced pressure leaving a dark red foam. Recrystallization of this dark red residue from $\text{CH}_2\text{Cl}_2/\text{hexanes}$ at $-10\text{ }^\circ\text{C}$ yielded dark red crystals, (< 10 % yield), suitable for X-ray crystallographic analysis, covered by the dark red oil. ^1H NMR spectra of the crystals and the oil showed identical spectral features. This indicates that they are the same compound. IR: $\nu(\text{CO})$ $1964s, 1990w,sh.,\text{ cm}^{-1}$ (acetone); $1964s, 1995w,sh.,\text{ cm}^{-1}$ (ethanol); and $1968s,$

1993w, cm^{-1} (CH_2Cl_2); $^1\text{H NMR}$: $\delta(\text{CDCl}_3)$, 1.98s, (30H, Cp^*), 3.85s (3H, OMe), 6.52d and 6.92d (4H, AA'BB' pattern, C_6H_4); FABMS (NOBA, Xenon) (m/z): 819 (M^+), 789 ($\text{M}^+ - \text{CO}$), 763 ($\text{M}^+ - 2\text{CO}$); Anal. (calcd.) C, 38.50; H, 4.12, (found) C, 38.30; H, 4.00.

X-ray crystallographic analysis of the single crystal structure of this compound was kindly carried out by Dr. R. J. Batchelor.

2). Reaction of $[\text{Cp}^*\text{Ir}(\text{CO})]_2$ (15) with two equivalents of $[\text{p-N}_2\text{C}_6\text{H}_4\text{OMe}]\text{BF}_4$

In a similar reaction to that described above, but using two equivalents of $[\text{p-N}_2\text{C}_6\text{H}_4\text{OMe}][\text{BF}_4]$, only compound (19) and some unreacted aryldiazonium salt were formed, as indicated by the IR and $^1\text{H NMR}$ spectra of the final dark tar residue.

4. 3. Results and Discussion

4. 3. 1. Syntheses, Properties and Characterization of the Precursor

Compounds

$\text{Cp}^*\text{Ir}(\text{CO})\text{H}_2$ (13)

Compound (13) has been mentioned several times in the literature since 1982, mainly by two research groups.^{187, 188} However, to date, the $\nu(\text{CO})$ absorption (at 1996 cm^{-1} in cyclohexane) is the only published spectroscopic datum for this compound.¹⁸⁸ Our interest in this compound was that it might be an immediate precursor for the compound $[\text{Cp}^*\text{Ir}(\text{CO})(\text{p-N}_2\text{C}_6\text{H}_4\text{OMe})]\text{BF}_4$ (12). Because of the lack of published information, we report here some additional information about this compound.

In a slightly modified procedure to that which Shapley used to make $\text{CpIr}(\text{CO})\text{H}_2$,¹⁸⁷ $\text{Cp}^*\text{Ir}(\text{CO})\text{H}_2$ (13) can be readily made from the corresponding

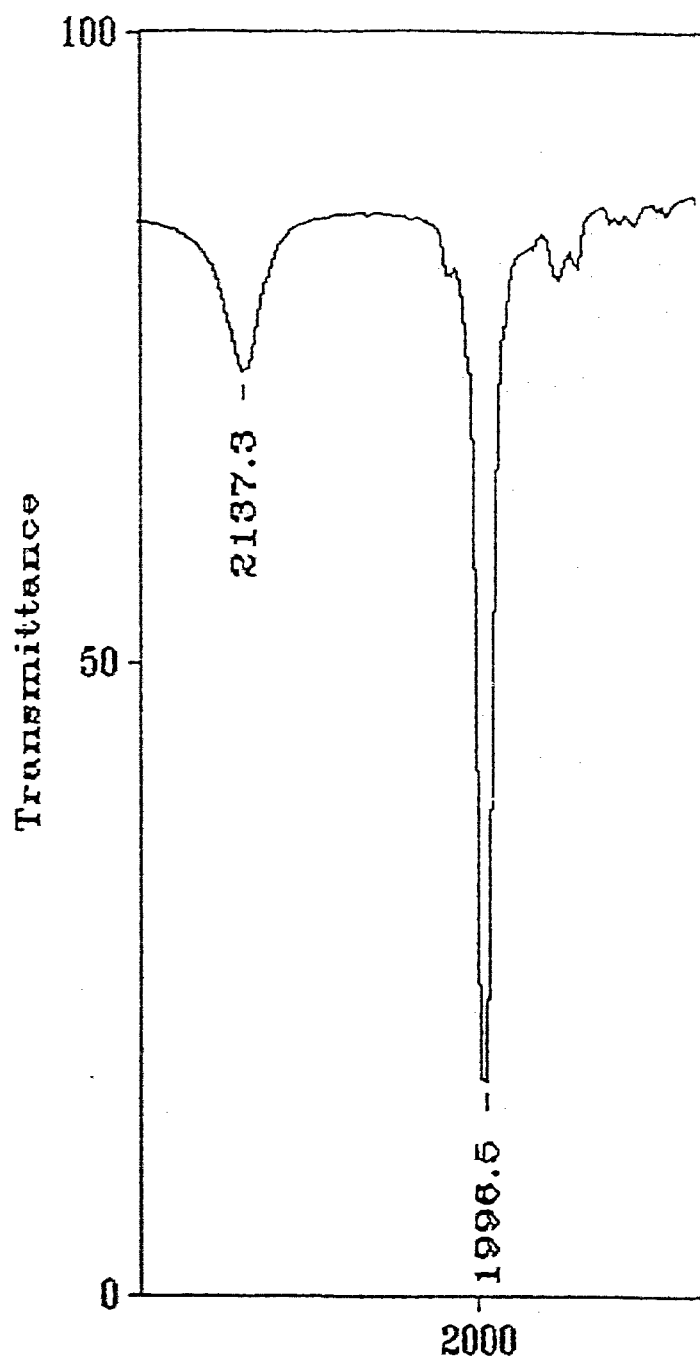


Figure 4.1. The infrared spectrum of (13) in hexanes

$\text{Cp}^*\text{Ir}(\text{CO})\text{Cl}_2$ ¹⁸⁹ in a good yield.

Similar to its analogue $\text{CpIr}(\text{CO})\text{H}_2$ ($\nu(\text{CO})= 2002 \text{ cm}^{-1}$ and $\nu(\text{Ir-H})= 2156 \text{ cm}^{-1}$ in CH_2Cl_2),¹⁸⁷ the infrared spectrum of (13) in hexanes exhibits one strong absorption at 1997 cm^{-1} and a weak band at 2137 cm^{-1} attributable to $\nu(\text{CO})$ and $\nu(\text{Ir-H})$, respectively (Figure 4.1). Notably, the $\nu(\text{CO})$ absorption of (13) is significantly lower than those of the corresponding halide analogues $\text{Cp}^*\text{Ir}(\text{CO})\text{X}_2$,¹⁸⁹ e.g., $\nu(\text{CO})$ are at 2035 cm^{-1} for $\text{X}=\text{Cl}$ and 2034 cm^{-1} for $\text{X}=\text{I}$. The ^1H NMR spectrum of (13) shows no unusual features; the hydrido resonance occurs at $\delta -16.58 \text{ ppm}$ as a singlet, comparable with the singlet observed for $\text{CpIr}(\text{CO})\text{H}_2$ at $\delta -16.47 \text{ ppm}$.¹⁸⁷ The most notable spectroscopic feature of (13) is the complicated fragmentation pattern observed in its EI mass spectrum (see Figure 4.2). The particular pattern due to the molecular ion is not

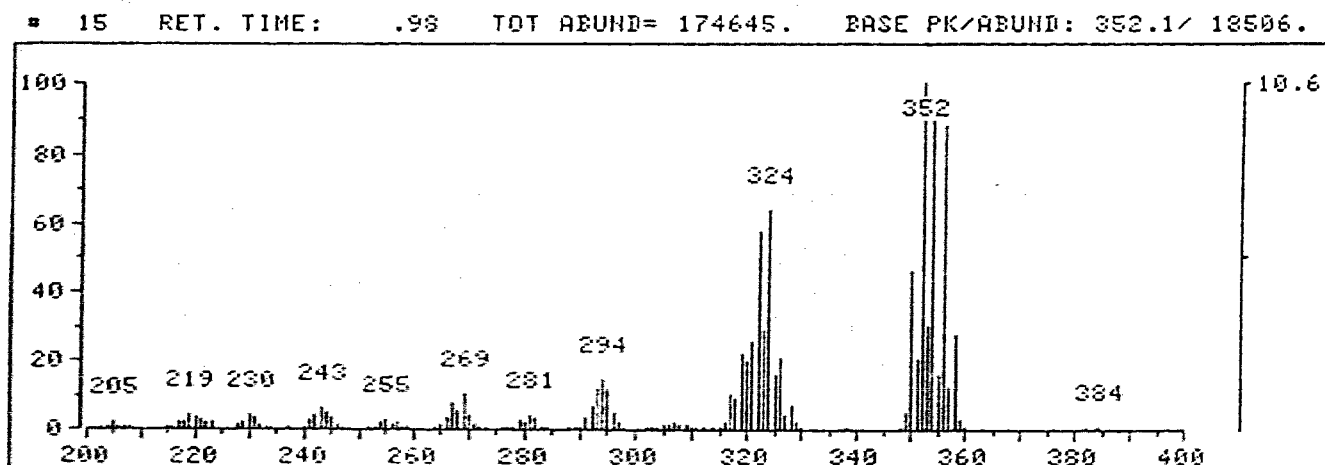
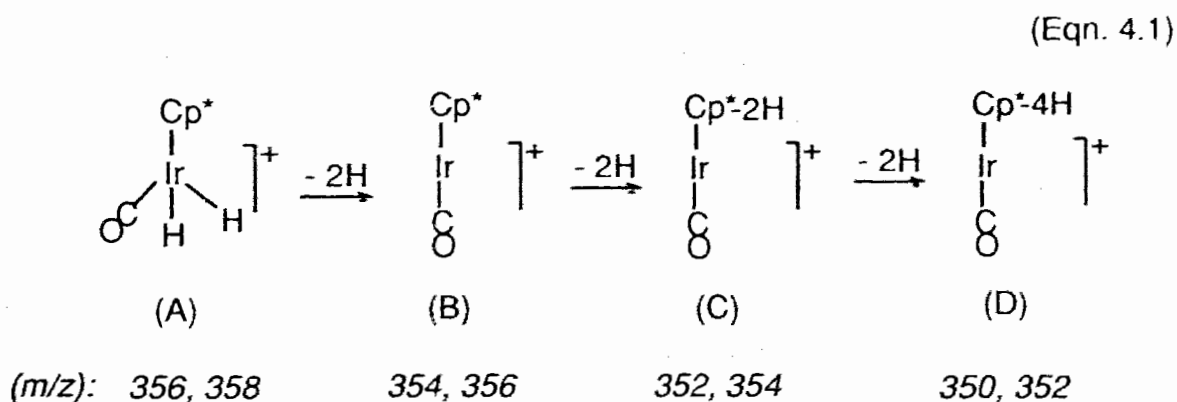


Figure 4.2. The EI mass spectrum of (13)

clear in the mass range $m/z = 350 \sim 360$, instead it seems to overlap with a series of other fragment ions. A careful examination of the highest group of peaks reveals that it mainly consists of four mono-iridium, mono-carbonyl fragment ions which are separated at intervals of 2, 4 and 6 in m/z unit, including the molecular ion $[\text{Cp}^*\text{Ir}(\text{CO})\text{H}_2]^+$ as the base peak. This situation can only be accounted for if the M^+ ion undergoes successive eliminations of three H_2 before its carbonyl ligand is eliminated. Since the complex under study contains only two chemically labile hydrido ligands, further dehydrogenation can take place only at the methyl groups of the Cp^* ligand. Consequently, a possible primary fragmentation pathway of the molecular ion $[\text{Cp}^*\text{Ir}(\text{CO})\text{H}_2]^+$ can be formulated as (Eqn. 4.1)



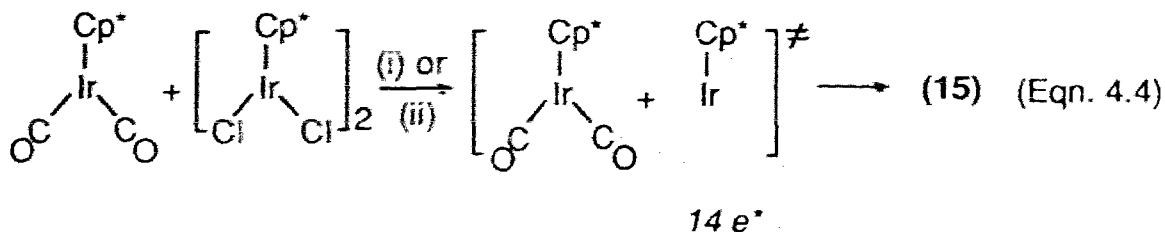
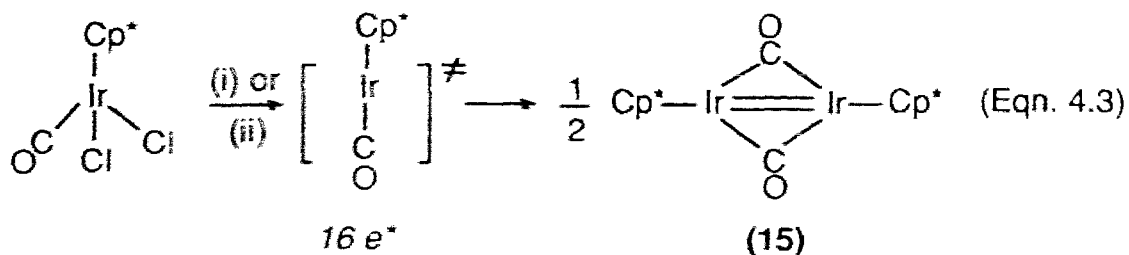
The relative intensities of the individual ions within this envelop have been calculated and are listed in Table 4.2; they produce a good fit to the experimental data. The lowest abundance for M^+ ($m/z = 356, 358$) in this group indicates that the molecular ion $[\text{Cp}^*\text{Ir}(\text{CO})\text{H}_2]^+$ is less stable than the other major ions. This could be attributed to the two chemically labile hydridos in the molecular ion. Experimentally, the relatively high intensity observed for fragment (B) could indicate a facile elimination of these two hydride ligands from (A).

However, for fragment ion (D), generated by elimination of four hydrogens from the Cp* ligand, the cyclometallation mechanism seems too farfetched. Therefore, we tend to support the ring expansion mechanism. That is, elimination of two hydrogens from the Cp* ligand of (B) would result in a ring expansion product (C) with a trimethyltropylium type of ligand, and elimination of four hydrogens would result in a further ring expansion product (D) with a monomethylcyclononatetraenyl ligand. Interestingly, like the pentamethylcyclopentadienyl ligand, both the tropylium and the cyclononatetraenyl ligands are aromatic rings. The common aromaticity feature of the three ligands could be directly related to the relative stability of the fragments (B), (C) and (D) observed here. Furthermore, it may be the reason why a successive two hydrogen elimination was observed here, instead of a one-hydrogen elimination.

In addition, the mass spectrum of (13) may also include some double-charged diiridium ions, which may attribute to the observed low intensity envelopes which consist of the peaks separated by an interval of one mass number.

Cp*Ir(CO)₂ (14)

CpIr(CO)H₂, the Cp analogue of (13), is reported to undergo facile ligand substitution to form CpIr(CO)L, where L is PPh₃, PPhMe₂ and CN-*t*-Bu,¹⁸⁷ respectively. Although the analogous reaction for Cp*Ir(CO)H₂ has not been reported in the literature, we have shown that this complex can undergo ligand exchange in presence of CO. That is, under *in situ* reaction conditions, carbon monoxide has been observed to facilitate H₂ loss from (13) and to form Cp*Ir(CO)₂ (14), (Eqn. 4.2)



(i) At room temperature, stirring with excess Zn dust for 12 hours.

(ii) Reflux with Na_2CO_3 in EtOH for 3 ~ 4 hours.

* Formal electron counting (in solution they may exist as solvated species).

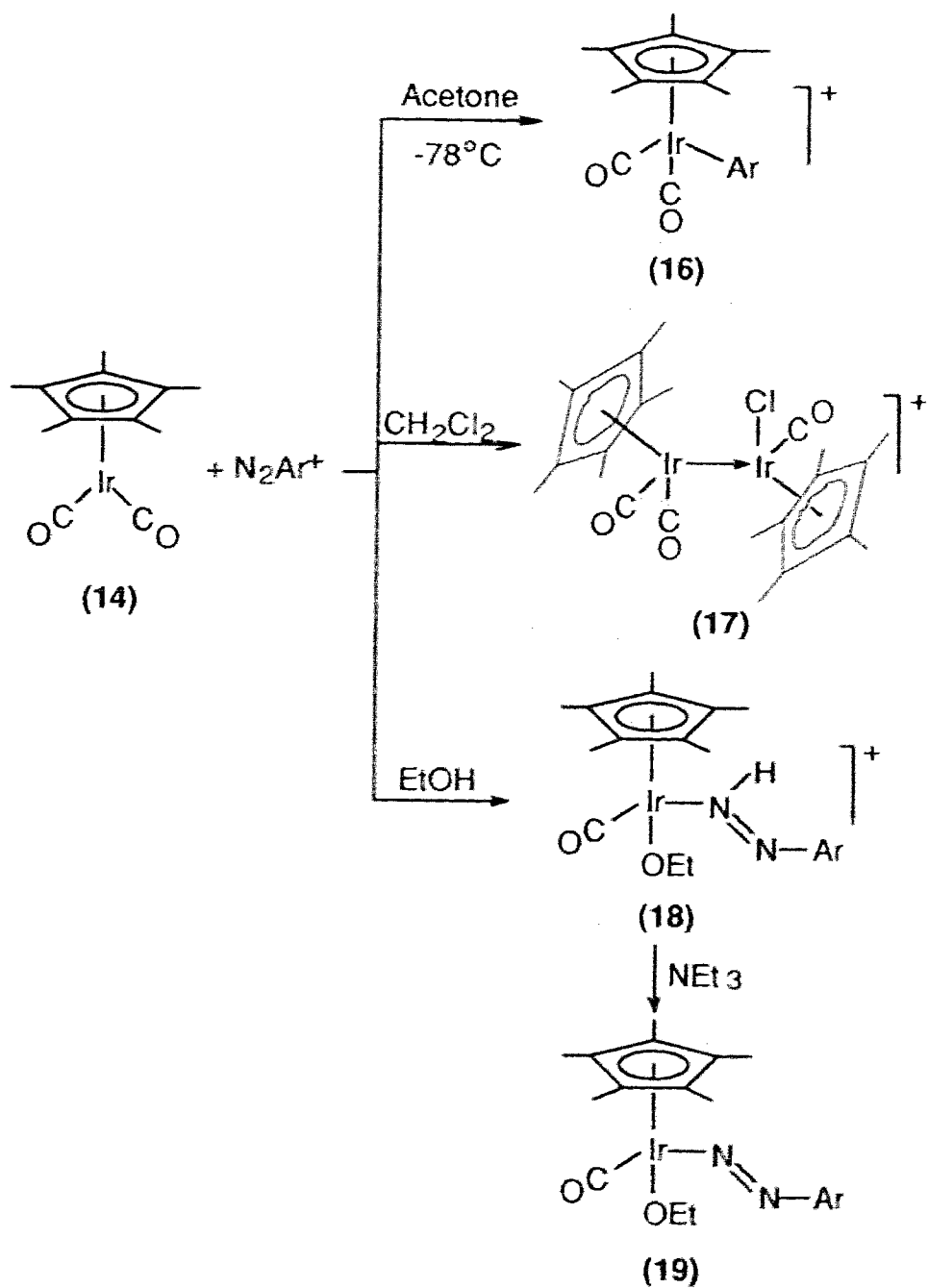
As documented in the literature, preparations of these type of dinuclear complexes for Co, Rh or Ir usually involve vigorous reaction conditions, such as photolysis or thermolysis. For example, $\text{Cp}^*_2\text{Co}_2(\mu^2\text{-CO})_2$ has been made by thermolysis of $\text{Cp}^*\text{Co}(\text{CO})_2$ in toluene for 24 hours,¹⁹⁵ or by photolysis of the same precursor in THF for 4 days with a continual N_2 purge.¹⁹⁵ $\text{Cp}^*_2\text{Rh}_2(\mu^2\text{-CO})_2$ has been synthesized by sublimation of $\text{Cp}^*\text{Rh}(\text{CO})_2$ at high pressure,¹⁹⁶ and $\text{Cp}^*_2\text{Ir}_2(\mu^2\text{-CO})_2$ was previously made by thermolysis of $\text{Cp}^*\text{Ir}(\text{CO})_2$ at 180 °C for one week.¹⁹¹ However, the reduction process used in the current method to generate the reactive intermediate can be carried out under rather mild conditions (even possibly at low temperature) and the assembly step is much more facile. It is then believed that this particular kind of coupled reduction-assembly procedure can provide a new synthetic approach to dinuclear complexes, both known and unknown.

Furthermore, since the synthetic procedure described in equation 4.4 involves two different precursor compounds, an extensive series of asymmetric dimeric complexes may be produced by interchanging the ligands or the metal centre on either or both precursors. In fact, preliminary attempts using this procedure have resulted in the synthesis of the asymmetric compound $\text{Cp}^*_2\text{IrRh}(\mu^2\text{-CO})_2$ ¹⁹⁷ from $[\text{Cp}^*\text{RhCl}_2]_2$ and $\text{Cp}^*\text{Ir}(\text{CO})_2$ quantitatively.¹⁹⁸ The asymmetric complex $\text{Cp}^*\text{CpIr}_2(\mu^2\text{-CO})_2$ was also prepared quantitatively from $[\text{Cp}^*\text{IrCl}_2]_2$ and $\text{CpIr}(\text{CO})_2$.¹⁹⁹ But, the complex $\text{Cp}^*\text{IrCpCo}(\mu^2\text{-CO})_2$ could not successfully be made from $[\text{Cp}^*\text{IrCl}_2]_2$ and $\text{CpCo}(\text{CO})_2$. Instead, a quantitative carbonyl transfer from the cobalt compound to the iridium centre forming $\text{Cp}^*\text{Ir}(\text{CO})_2$ was observed. Since an extensive study of these reactions is still underway and the chemistry of this aspect seems slightly out of the topic of this Thesis, the details of this study will not be given here.

4.3.2. Attempts to Synthesize $[\text{Cp}^*\text{Ir}(\text{CO})(p\text{-N}_2\text{C}_6\text{H}_4\text{OMe})]\text{BF}_4$ (12)

Reactions of $\text{Cp}^*\text{Ir}(\text{CO})_2$ with $[p\text{-N}_2\text{C}_6\text{H}_4\text{OMe}]\text{BF}_4$

As discussed in Chapter II, $\text{Cp}^*\text{Ir}(\text{C}_2\text{H}_4)_2$ reacts readily with the aryldiazonium salt, $[p\text{-N}_2\text{C}_6\text{H}_4\text{OMe}]\text{BF}_4$, to produce the corresponding aryldiazenido complex (1). Hence, the identical reaction with the isostructural analogue $\text{Cp}^*\text{Ir}(\text{CO})_2$ (14) was thought to be a valid route to $[\text{Cp}^*\text{Ir}(\text{CO})(p\text{-N}_2\text{C}_6\text{H}_4\text{OMe})]\text{BF}_4$. After numerous attempts using different reaction conditions and with different stoichiometries of the starting materials, no $[\text{Cp}^*\text{Ir}(\text{CO})(p\text{-N}_2\text{C}_6\text{H}_4\text{OMe})]\text{BF}_4$ was obtained, or even observed. Instead, these attempts led to the isolation, or observation of compounds (16), (17), (18) and (19) (see Scheme 4.1).



Scheme 4.1

Reactions Yielding Nitrogen Extrusion Products (16) and (17)

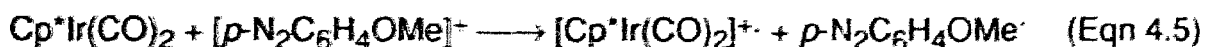
Mixing equimolar quantities of (14) and $[\rho\text{-N}_2\text{C}_6\text{H}_4\text{OMe}]\text{BF}_4$ in *acetone* at room temperature produced a dark red solution. From this solution, a dark tar was precipitated out upon addition of hexane, from which no aryldiazenido derivatives could be isolated.

At $-78\text{ }^\circ\text{C}$, the same reaction gave a bright red solution, which might be indicative of the formation of some aryldiazenido derivative.¹⁶ However, this highly coloured species did not survive long and the solution underwent a rapid colour change from the bright red to dark brown. From the resulting solution, a dark brown precipitate was isolated and in turn was characterized by spectroscopy and elemental analysis as $[\text{Cp}^*\text{Ir}(\text{CO})_2(\rho\text{-C}_6\text{H}_4\text{OMe})]\text{BF}_4$ (16), a nitrogen extrusion product. The higher $\nu(\text{CO})$'s observed for (16), at 2074 and 2114 cm^{-1} in *acetone*, compared to those observed for $\text{Cp}^*\text{Ir}(\text{CO})_2$ (14) ($\nu(\text{CO})=1939, 2009\text{ cm}^{-1}$ in *acetone*) are indicative of less electron density at the iridium centre for (16), which is consistent with the higher oxidation state of the iridium in (16). Similar shifts to higher wavenumbers for carbonyl ligands have also been observed in the IR spectrum for other Ir(III) derivatives.¹⁷⁷

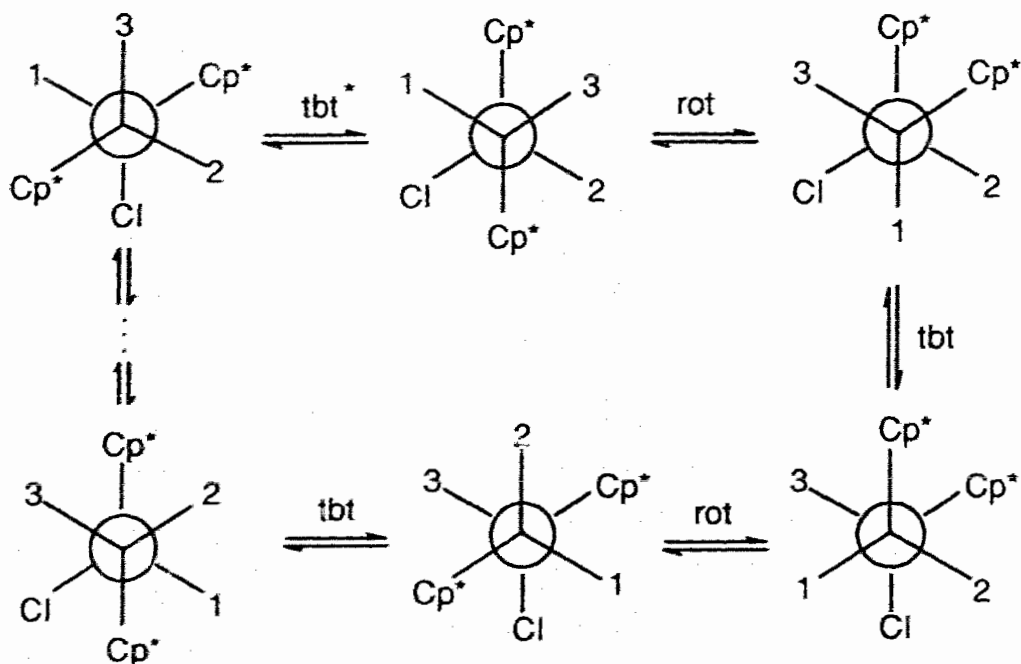
However, reaction of (14) with 0.5 equivalent of $[\rho\text{-N}_2\text{C}_6\text{H}_4\text{OMe}]\text{BF}_4$ in CH_2Cl_2 produces the diiridium complex $[\text{Cp}^*_2\text{Ir}_2(\text{CO})_3\text{Cl}]\text{BF}_4$ (17) in high yield. The solid state structure of complex (17) has been unequivocally established by single crystal X-ray crystallographic analysis (see Figure 4.4). The infrared spectral features exhibited by this compound in solution were also consistent with the molecular structure in the solid state. The observed $\nu(\text{CO})$ bands in CH_2Cl_2 fall within the terminal carbonyl range. The absorption at 2058 cm^{-1} shows no unusual feature, but the strong band at 2017 cm^{-1} is broad and asymmetric, likely indicative of a superposition of two near-coincident peaks at

around 2017 cm⁻¹. The most structurally interesting feature for this compound in solution is that its ambient ¹³C NMR spectrum shows only one signal, at δ: 171.4 ppm, in the carbonyl range. This observation indicates that compound (17) is possibly non-rigid in solution at room temperature, and the carbonyl ligands may undergo a fast exchange process on the NMR time scale, so that only a time-averaged ¹³C NMR spectrum is observed. This has been further confirmed by low temperature ¹³C NMR spectroscopy. At lower temperature (-86 °C), the singlet at δ: 171.4 ppm has been observed to decoalesce to two signals at δ 173.0 and 168.2 ppm with an intensity ratio of 2:1. Since two chemically different Cp* groups can be clearly identified in both ambient ¹H and ¹³C NMR spectra, it has been concluded that the chloro ligand is not likely involved in the fluxional process. Consequently, this fluxional process could be attributed to the exchange of the carbonyl ligands of (17) in a terminal-bridging-terminal fashion and an alternate rotation of the metal-metal bond. This is illustrated in Newman projections in Scheme 4.2. Interestingly, accompanying with each time of this exchange, the chiral metal centre, which is bonded to the chloro ligand, changes the sign of its chirality.

To account for the reaction product (16) obtained in acetone solution, it seems reasonable to assume that the reaction was initiated by a simple oxidation of Cp*Ir(CO)₂ by the diazonium ion.²⁰⁰ (Eqn. 4.5)



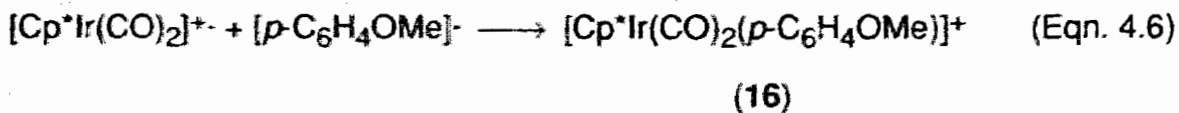
The neutral radical, *p*-N₂C₆H₄OMe[·], so generated would be very unstable and



*: tbt = terminal-bridging-terminal transfer of the trans related carbonyls
 rot = rotation of the metal-metal bond 120 degrees

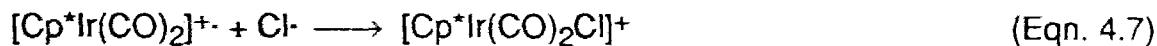
Scheme 4.2

immediately decompose to dinitrogen and the radical $[\rho\text{-C}_6\text{H}_4\text{OMe}]^\cdot$, which may then recombine with the cationic radical $[\text{Cp}^*\text{Ir}(\text{CO})_2]^{+\cdot}$ to yield the product (16) (Eqn. 4.6)

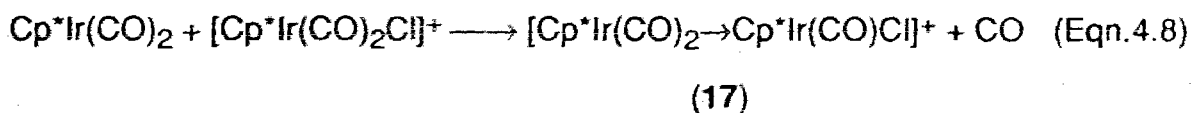


A similar reaction mechanism is believed to be operative when CH_2Cl_2 is used as the solvent. In this reaction system, the only chlorine source is solvent, CH_2Cl_2 . So a similar oxidation, like Eqn. 4.5, could occur first and then a chlorine radical Cl^\cdot could be generated from the solvent through a radical reaction, which

in turn could then combine with $[\text{Cp}^*\text{Ir}(\text{CO})_2]^+$ to form an 18e cationic species, $[\text{Cp}^*\text{Ir}(\text{CO})_2\text{Cl}]^+$ (Eqn. 4.7)



With excess nucleophile (or electron-rich metal base) $\text{Cp}^*\text{Ir}(\text{CO})_2$ ¹⁷⁵ present in the reaction system, a substitution reaction may then occur to give complex (17). (Eqn. 4.8)

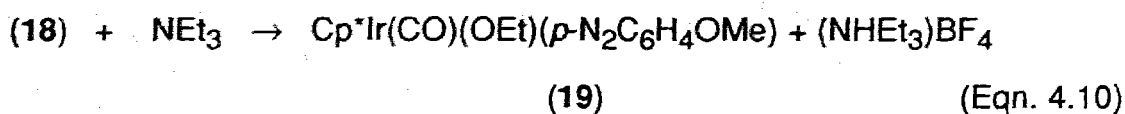
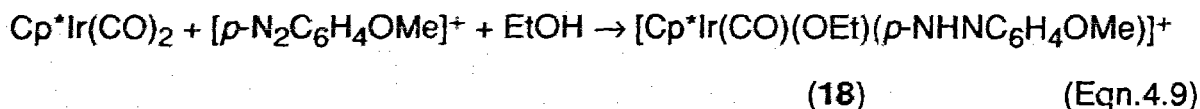


So in compound (17), the non bridged metal-metal bond could be formally considered as a donor-acceptor dative bond between Ir(I) and Ir(III). For a better comparison, compound (17) has also been subsequently synthesized from $\text{Cp}^*\text{Ir}(\text{CO})_2$ and $\text{Cp}^*\text{Ir}(\text{CO})\text{Cl}_2$ in the presence of AgBF_4 ¹⁷⁷. This independent synthesis may simply be viewed as proceeding by the formation of the unsaturated (or solvated) 16-electron intermediate $[\text{Cp}^*\text{Ir}(\text{CO})\text{Cl}]^+$ which is then attacked by the base $\text{Cp}^*\text{Ir}(\text{CO})_2$.

Reaction Yielding a Nitrogen-Retained Product

$\text{Cp}^*\text{Ir}(\text{CO})_2$ reacted rapidly with an equimolar quantity of $[\rho\text{-N}_2\text{C}_6\text{H}_4\text{OMe}] \text{BF}_4$ at room temperature in *ethanol* to produce an orange-yellow solution, from which an oily product could be obtained upon removal of the solvent. This orange oil was identified on the basis of IR, ¹H NMR and ¹⁵N NMR spectroscopy as the aryldiazene complex, $[\text{Cp}^*\text{Ir}(\text{CO})(\text{OEt})(\rho\text{-NHNC}_6\text{H}_4\text{OMe})]\text{BF}_4$ (18). This

compound was further verified by the deprotonation of it to yield a much more stable neutral aryldiazenido complex, $\text{Cp}^*\text{Ir}(\text{CO})(\text{OEt})(p\text{-N}_2\text{C}_6\text{H}_4\text{OMe})$ (**19**), containing a doubly bent aryldiazenido ligand. (see Eqn. 4.9 and Eqn. 4.10).



Since complex (**18**) can be stabilized only in ethanol solution, it is difficult to characterize it completely. However, compound (**19**) has been fully characterized by elemental analysis and spectroscopy. The IR spectrum of (**18**) in EtOH shows a strong absorption at 2058 cm^{-1} for $\nu(\text{CO})$. However, no $\nu(\text{NN})$ band could be assigned, even when the ^{15}N enriched sample was used. The ^1H NMR spectrum of this compound was measured immediately after it was dissolved into acetone- d_6 . Except for the proton directly bonded to $\text{N}\alpha$, all other proton signals were observed in the appropriate resonance range and with the correct integration. The ^{15}N NMR spectrum of the isotope enriched sample of (**18**) showed a doublet with a chemical shift at -154 ppm and a coupling constant of 88 Hz . Both the position of the resonance and the coupling constant indicated the existence of a terminally coordinated diazene ligand in (**18**).⁹⁷ Notably, the highest mass values (m/z : 489, 491) observed in the FABMS spectrum of (**18**) were not those of the parent, but the fragment from loss of EtOH, *i.e.*, $[\text{Cp}^*\text{Ir}(\text{CO})(p\text{-N}_2\text{C}_6\text{H}_4\text{OMe})]^+$ (ironically, the species we have been trying to obtain by synthesis).

As a matter of contrast, the deprotonation product, $\text{Cp}^*\text{Ir}(\text{CO})(\text{OEt})(p\text{-N}_2\text{C}_6\text{H}_4\text{OMe})$ (**20**), showed a much higher stability either in solutions or in the solvent-free state. The infrared spectrum of (**20**) exhibited a $\nu(\text{CO})$ absorption at 2025 cm^{-1} in ethanol, which is 23 wavenumbers lower than the corresponding $\nu(\text{CO})$ observed in its parent compound (**18**). This decrease in wavenumber, upon removal of the N_α proton clearly indicates the sensitivity of the $\nu(\text{CO})$ position to the N_α lone pair electrons of the diazenido ligand in this three-legged piano-stool structure. The ^1H NMR spectrum of (**19**) was recorded in C_6D_6 . In addition to those resonances corresponding to the protons in the Cp^* and $p\text{-N}_2\text{C}_6\text{H}_4\text{OMe}$ ligands, two well resolved multiplets due to the two diastereotopic methylene protons of the OEt group were also observed. Notably, this ^1H NMR feature of the OEt ligand in (**20**) was not observed in the ^1H NMR spectrum of the corresponding aryldiazenido compound (**18**), which might be attributable to a rather labile ethoxy group in (**18**). Furthermore, a far downfield singlet (δ 224 ppm, in comparison with δ -154 ppm for **18a**) observed in the ^{15}N NMR spectrum of (**19a**) confirmed the presence of a doubly bent aryldiazenido ligand in (**19**).

Reactions of $[\text{Cp}^*\text{Ir}(\text{C}_2\text{H}_4)(p\text{-N}_2\text{C}_6\text{H}_4\text{OMe})]\text{BF}_4$ (1**) with carbon monoxide**

Considering the lability of the ethylene in compound (**1**), we thought that a carbonyl ligand might be introduced to the iridium centre through a ligand substitution reaction which in turn would lead us to the target complex (**12**). Hence, (**1**) was reacted first with carbon monoxide gas (in excess) in acetone solution. This reaction resulted in $\text{Cp}^*\text{Ir}(\text{CO})_2$ as the only isolable organometallic species. The failure to obtain any aryldiazenido derivatives was thought to be due to excess CO in the reaction system. Subsequently, a stoichiometrically controlled reaction was carried out, in which equimolar amounts of (**1**) and

carbon monoxide were used. After a much longer reaction time, the IR and ^1H NMR spectra revealed that only the starting material (1) and product, $\text{Cp}^*\text{Ir}(\text{CO})_2$, existed in the final reaction mixture. Hence, it is unlikely that the expected complex $[\text{Cp}^*\text{Ir}(\text{CO})(p\text{-N}_2\text{C}_6\text{H}_4\text{OMe})]\text{BF}_4$ can be formed as a stable compound using this particular reaction.

A similar reaction was also carried out in ethanol solution with bubbling CO gas. The final products, $[\text{Cp}^*\text{Ir}(\text{CO})(\text{OEt})(p\text{-NHNC}_6\text{H}_4\text{OMe})]\text{BF}_4$ (18) and $\text{Cp}^*\text{Ir}(\text{CO})_2$, generated from this reaction indicates that the aryldiazenido ligand can be stabilized as a diazene in the three-legged piano-stool structure, but not in $[\text{Cp}^*\text{Ir}(\text{CO})(p\text{-N}_2\text{C}_6\text{H}_4\text{OMe})]\text{BF}_4$.

Reaction of $[\text{Cp}^*\text{Ir}(\text{CO})]_2$ with $[(p\text{-N}_2\text{C}_6\text{H}_4\text{OMe})]\text{BF}_4$

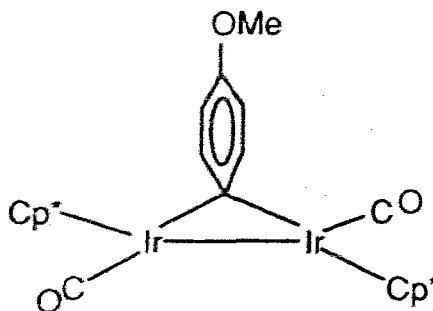
Reaction of $[\text{Cp}^*\text{Ir}(\text{CO})]_2$ with $[(p\text{-N}_2\text{C}_6\text{H}_4\text{OMe})]\text{BF}_4$ was first designed as an alternative synthetic route to compound $[\text{Cp}^*_2\text{Ir}_2(\text{CO})_2(\eta^2\text{-}\mu^2\text{-}p\text{-N}_2\text{C}_6\text{H}_4\text{OMe})]\text{BF}_4$ (11), which was produced from the reaction of $[\text{Cp}^*\text{Ir}(\text{CO})_2(p\text{-N}_2\text{C}_6\text{H}_4\text{OMe})]\text{BF}_4$ with $\text{Cp}^*\text{Ir}(\text{CO})_2$ in ethanol. (see Chapter III)

Treatment of a dark green acetone solution of $[\text{Cp}^*\text{Ir}(\text{CO})]_2$ with $[(p\text{-N}_2\text{C}_6\text{H}_4\text{OMe})]\text{BF}_4$ at $-78\text{ }^\circ\text{C}$ resulted in a dark red solution, from which compound $[\text{Cp}^*_2\text{Ir}_2(\text{CO})_2(1\text{-}\eta^1\text{-}1,2\text{-}\eta^2\text{-}\mu^2\text{-}p\text{-C}_6\text{H}_4\text{OMe})]\text{BF}_4$ (20), a nitrogen elimination product was isolated in a fairly good yield. Compound (20) is very soluble in chloroform, dichloromethane, acetone and ethanol. However, it is not very stable in solution at room temperature. It slowly decomposes to $[\text{Cp}^*\text{Ir}(\text{CO})]_2$, $\text{Cp}^*\text{Ir}(\text{CO})_2$ and other unidentified products.

The fast atom bombardment mass spectrum of (20) exhibits the appropriate molecular ion, as well as the ions corresponding to a sequential loss of two groups with $m/z = 28$, which could be either CO or N_2 in this case.

However, the elemental analysis for (20) immediately negated the possibility of the presence of N₂ in this compound. The IR spectrum of complex (20) in CH₂Cl₂ solution exhibited two bands at 1968 and 1993 cm⁻¹ (at 1964 and 1990 cm⁻¹ in ethanol), with the band at higher frequency much weaker than the lower one. Consequently, these two bands were assigned as two terminal carbonyls. The relative intensities and positions of the two absorption bands indicated that the two carbonyls were, most likely, separated with a large 2θ angle.²⁰¹ The most chemically interesting feature for (20) was found from its rather simple ¹H NMR spectrum. At room temperature the 100 MHz ¹H NMR spectrum showed a singlet at δ: 1.95 ppm attributed to Cp*, also a singlet at δ: 3.85 ppm and an AA'BB' pattern in the aromatic proton range corresponding to the *p*-C₆H₄OMe group. Integration of the signals indicated a relationship of two Cp*'s and one *p*-C₆H₄OMe ligand, which was in agreement with the molecular formula of [Cp*₂Ir₂(CO)₂(C₆H₄OMe)]BF₄. A singlet signal observed for the two Cp* ligands indicated that they must be located either in a similar, or more likely the rigorously same chemical environment. To distinguish these two possibilities, a low temperature (-90 °C) ¹H NMR spectrum of this compound in a different solvent (CD₂Cl₂) was recorded on a higher field (400 MHz) spectrometer. However, the features displayed by the low-temperature ¹H NMR spectrum were identical to that observed at ambient temperature in CDCl₃, except for a slight broadening of the line width and slightly different chemical shifts. So it is most likely that these two Cp* ligands rigorously have the same chemical environment. This could only occur if the two Cp* ligands are related to each other by symmetry. Consequently, the *p*-C₆H₄OMe group has to coordinate to two iridium centres in a symmetric-bridging fashion. To cause this, the aryl ligand *p*-C₆H₄OMe could coordinate to metal centres either in an electron

deficient μ - (or α , α -) bonding mode,^{202, 203} through its carbon atom which is para to the methoxyl in the phenyl ring, as shown below:



or in some mode involving a dynamic process which gives a time-averaged symmetric bridging p -C₆H₄OMe on the NMR time scale. It was then obvious that a single-crystal X-ray diffraction study would be helpful to establish the molecular structure of (20). Fortunately, after many failures, crystals suitable for a X-ray crystallographic study were successfully obtained from CH₂Cl₂/hexane solutions.

The formation of compound (20) is presumably initiated by an addition of diazonium ion to the unsaturated metal-metal bond, followed by a nitrogen extrusion from the adduct to give the bridging aryl complex as the final product. A bridge-terminal transfer of carbonyl ligands must also be involved in this process.

Chemistry closely related to this has been seen in the reactions of binuclear complexes containing unsaturated metal-metal bonds with diazoalkanes, in which bridging carbene complexes are often generated.^{204 - 206} However, to the best of our knowledge, compound (20) is the first instance where the bridging aryl group has been introduced from an aryldiazonium ion.

4.3.3. X-ray Single Crystal Structures of Compounds (17) and (20)

Molecular Structure of Complex (17)

Although the molecular structure of complex (17) in solution is fluxional on the NMR time scale, the molecular structure revealed in the solid state by X-ray diffraction is consistent with that deduced from the spectroscopic data for this compound.

In the solid state, the crystal structure of compound (17) consists of discrete cations $[\text{Cp}^*_2\text{Ir}_2(\text{CO})_3\text{Cl}]^+$ and the counter ions BF_4^- , separated by the normal van der Waals distances. There are no unusually short inter-ionic contacts.

The structure of the cation from compound (17) is shown in Figure 4.4, (H-atoms are excluded). Table 4.3 shows the selected interatomic distances and angles. Tables 4.4, 4.5 and 4.6 provide the positional and thermal motional parameters.

The two iridium atoms in the cation $[\text{Cp}^*_2\text{Ir}_2(\text{CO})_3\text{Cl}]^+$ are both in the typical three-legged piano-stool coordination environment, and share a common leg as a metal-metal bond. The Ir(1)-Ir(2) distance of 2.827(1) Å in complex (17) is the second longest Ir-Ir distance to be found in similar bis-pentamethylcyclopentadienyl diiridium complexes. Complex $[\text{Cp}^*\text{Ir}(\text{CO})_2]_2[\text{BF}_4]_2$ synthesized in this laboratory has the longest Ir-Ir bond length of 2.839(2) Å.¹⁷⁷ Since (17) and $[\text{Cp}^*\text{Ir}(\text{CO})_2]_2[\text{BF}_4]_2$ are the only two known examples containing an Ir-Ir single bond without any supportive bridging ligand, the long Ir-Ir single bonds observed in these two compounds are likely due to the lack of the bridging ligands. The M-C and C-O distances in this compound are comparable with those of the dication complex.¹⁷⁷

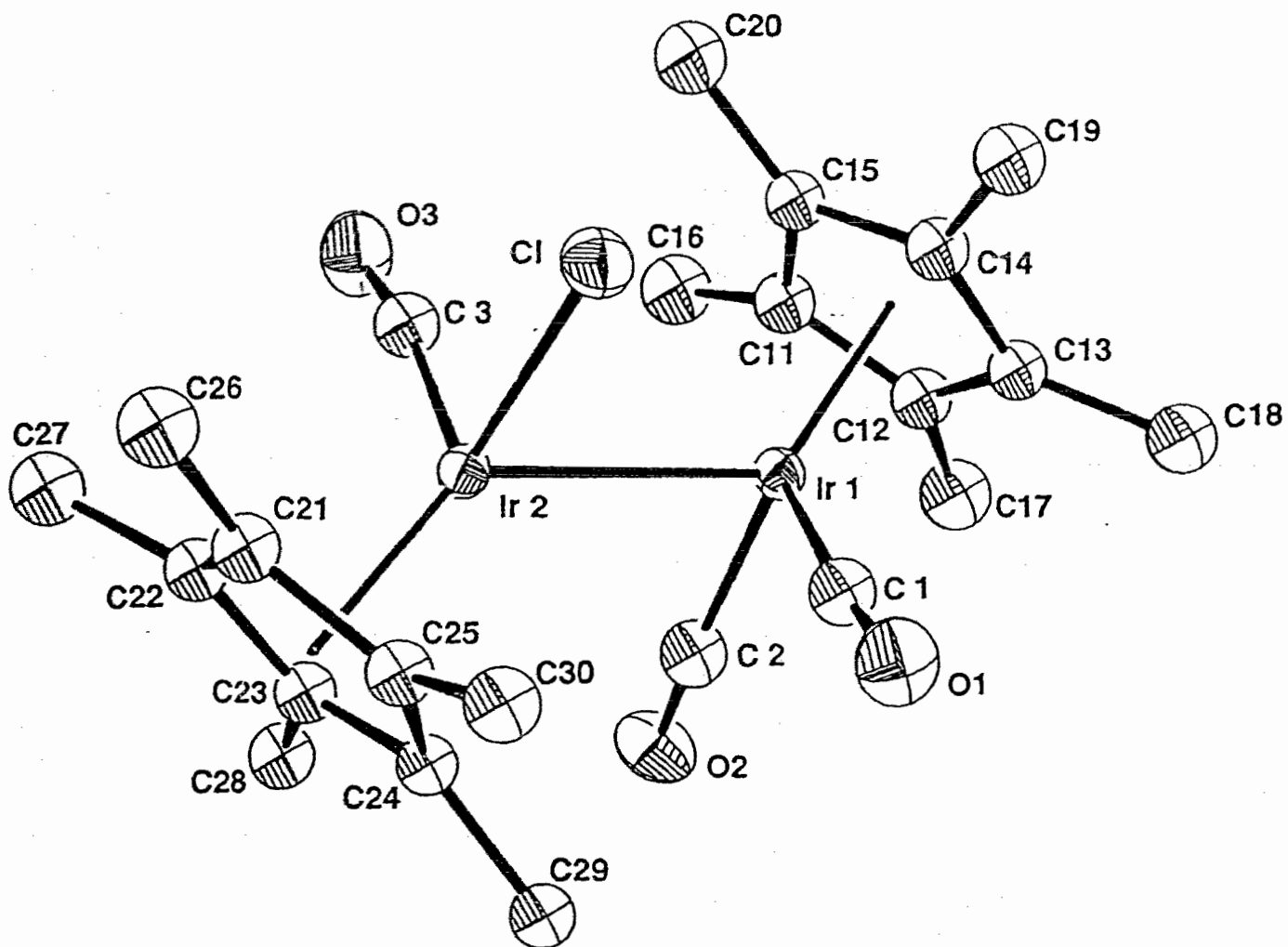


Figure 4.4 Molecular structure of the cation of (17). (The thermal ellipsoids represent 50 % probability contours).

Table 4.3. Selected Bond lengths (Å) and Inter-bond Angles (deg.)
for [Cp*₂Ir₂(CO)₃Cl]BF₄ (17)

(a) Bond Lengths

Ir(1)-Ir(2)	2.8266(6)	*Ir(1)-Ir(2)	2.855
Ir(1)-C(1)	1.907(10)	Ir(2)-Cl(1)	2.3939(24)
Ir(1)-C(2)	1.901(11)	Ir(2)-C(3)	1.849(10)
Ir(1)-C(11)	2.239(10)	Ir(2)-C(21)	2.221(10)
Ir(1)-C(12)	2.235(10)	Ir(2)-C(22)	2.206(10)
Ir(1)-C(13)	2.257(9)	Ir(2)-C(23)	2.198(9)
Ir(1)-C(14)	2.241(10)	Ir(2)-C(24)	2.301(9)
Ir(1)-C(15)	2.323(10)	Ir(2)-C(25)	2.262(10)
Ir(1)-Cp*(1) centroid	1.904	Ir(2)-Cp*(2) centroid	1.879
O(1)-C(1)	1.129(13)	O(3)-C(3)	1.152(13)
O(2)-C(2)	1.119(13)		
C(11)-C(12)	1.456(14)	C(21)-C(22)	1.386(14)
C(11)-C(15)	1.438(14)	C(21)-C(25)	1.475(14)
C(11)-C(16)	1.510(15)	C(21)-C(26)	1.500(15)
C(12)-C(13)	1.401(14)	C(22)-C(23)	1.455(14)
C(12)-C(17)	1.528(16)	C(22)-C(27)	1.503(15)
C(13)-C(14)	1.448(14)	C(23)-C(24)	1.475(13)
C(13)-C(18)	1.494(14)	C(23)-C(28)	1.492(14)
C(14)-C(15)	1.452(14)	C(24)-C(25)	1.409(13)
C(14)-C(19)	1.495(15)	C(24)-C(29)	1.482(14)
C(15)-C(20)	1.487(15)	C(25)-C(30)	1.496(14)

(continue Table 4.3)

F(1)-B(1)	1.329(20)	** F(1)-B(1)	1.374
F(2)-B(1)	1.378(19)	** F(2)-B(1)	1.409
F(3)-B(1)	1.314(20)	** F(3)-B(1)	1.421
F(4)-B(1)	1.398(22)	** F(4)-B(1)	1.474

(b) Inter-Bond Angles

Ir(2)-Ir(1)-C(1)	79.2(3)	Ir(1)-Ir(2)-C(3)	85.3(3)
Ir(2)-Ir(1)-C(2)	85.3(3)	Ir(1)-Ir(2)-Cl(1)	85.10(6)
Ir(2)-Ir(1)-Cp*(1) centroid	130.5	Ir(1)-Ir(2)-Cp*(2) centroid	133.2
C(1)-Ir(1)-Cp*(1) centroid	126.6	C(3)-Ir(2)-Cp*(2) centroid	124.2
C(2)-Ir(1)-Cp*(1) centroid	124.4	Cl-Ir(2)-Cp*(2) centroid	118.6
C(1)-Ir(1)-C(2)	96.7(4)	Cl(1)-Ir(2)-C(3)	99.0(3)
Ir(1)-C(11)-C(16)	129.1(7)	Ir(2)-C(21)-C(26)	126.6(7)
Ir(1)-C(12)-C(17)	125.9(9)	Ir(2)-C(22)-C(27)	125.5(7)
Ir(1)-C(13)-C(18)	126.1(7)	Ir(2)-C(23)-C(28)	129.6(7)
Ir(1)-C(14)-C(19)	128.9(7)	Ir(2)-C(24)-C(29)	133.4(7)
Ir(1)-C(15)-C(20)	132.0(7)	Ir(2)-C(25)-C(30)	127.3(7)
Ir(1)-C(1)-O(1)	174.7(9)	Ir(2)-C(3)-O(3)	170.3(9)
Ir(1)-C(2)-O(2)	173.2(9)		
F(1)-B(1)-F(2)	116.0(14)	F(2)-B(1)-F(3)	110.6(14)
F(1)-B(1)-F(3)	110.9(14)	F(2)-B(1)-F(4)	103.9(13)
F(1)-B(1)-F(4)	104.2(13)	F(3)-B(1)-F(4)	110.8(16)

* Upperlimit value corrected for thermal motion.

** Values corrected for thermal motion, based on F atoms riding on B atom.

Table 4.4 Positional Parameters and Biso's of Non-hydrogen Atoms
for $[\text{Cp}^*_2\text{Ir}_2(\text{CO})_3\text{Cl}]\text{BF}_4$ (17)

Atom	x/a	y/b	z/c	Biso (Å ²)
Ir(1)	0.29920(4)	0.22293(3)	0.36152 (3)	
Ir(2)	0.07961(4)	0.30616(3)	0.41347 (3)	
Cl(1)	0.2197 (3)	0.35979(18)	0.52534 (16)	
F(1)	0.4145 (9)	0.9392 (6)	0.4198 (5)	
F(2)	0.2126 (8)	0.9523 (6)	0.3544 (6)	
F(3)	0.3206 (11)	0.8198 (6)	0.3580 (8)	
F(4)	0.3823 (10)	0.9436 (11)	0.2910 (7)	
O(1)	0.2727 (8)	0.1032 (5)	0.5090 (5)	
O(2)	0.1236 (8)	0.1182 (6)	0.2380 (5)	
O(3)	0.1031 (8)	0.4574 (6)	0.2927 (5)	
B(1)	0.3279 (18)	0.9103 (12)	0.3594 (12)	4.6 (4)
C(1)	0.2759 (10)	0.1480 (7)	0.4520 (7)	2.70 (21)
C(3)	0.1044 (10)	0.4001 (7)	0.3425 (7)	2.28 (20)
C(11)	0.3942 (10)	0.3139 (7)	0.2779 (7)	2.39 (20)
C(12)	0.4558 (10)	0.2221 (7)	0.2826 (7)	2.36 (20)
C(13)	0.5123 (10)	0.2073 (7)	0.3602 (6)	2.08 (19)
C(14)	0.4867 (10)	0.2891 (7)	0.4072 (6)	2.20 (19)
C(15)	0.4216 (10)	0.3577 (7)	0.3539 (6)	2.10 (19)
C(16)	0.3367 (12)	0.3602 (8)	0.1998 (8)	3.36 (24)
C(17)	0.4642 (12)	0.1594 (8)	0.2084 (7)	3.40 (25)

(continue Table 4.4)

C(18)	0.5913 (11)	0.1258 (8)	0.3912 (7)	2.75 (22)
C(19)	0.5399 (11)	0.3079 (8)	0.4908 (7)	2.65 (21)
C(20)	0.3972 (11)	0.4577 (8)	0.3748 (7)	2.99 (23)
C(21)	-0.0878 (10)	0.3197 (7)	0.4812 (6)	2.19 (19)
C(22)	-0.1280 (10)	0.3294 (7)	0.4022 (6)	1.94 (18)
C(23)	-0.1006 (9)	0.2441 (7)	0.3598 (6)	1.96 (18)
C(24)	-0.0493 (9)	0.1768 (7)	0.4216 (6)	1.77 (18)
C(25)	-0.0368 (10)	0.2248 (7)	0.4952 (6)	1.97 (18)
C(26)	-0.1005 (11)	0.3867 (8)	0.5495 (7)	2.64 (21)
C(27)	-0.1956 (11)	0.4112 (8)	0.3620 (7)	2.79 (21)
C(28)	-0.1414 (10)	0.2218 (7)	0.2754 (7)	2.46 (20)
C(29)	-0.0304 (10)	0.0754 (7)	0.4087 (6)	2.03 (19)
C(30)	0.0085 (10)	0.1854 (7)	0.5764 (6)	2.31 (19)

Table 4.5 $U_{i,j}$ (x100) for Anisotropic motion of Atoms of $[\text{Cp}^*_2\text{Ir}_2(\text{CO})_3\text{Cl}]\text{BF}_4$ (17)

	U_{11}	U_{22}	U_{33}	U_{12}	U_{13}	U_{23}
Ir(1)	1.792(21)	2.066(21)	1.932(20)	-0.026(15)	0.298(16)	-0.042(16)
Ir(2)	1.852(21)	1.791(20)	2.129(22)	0.122(16)	0.275(16)	0.127(17)
Cl(1)	2.82 (14)	3.20 (14)	2.88 (15)	0.00 (11)	-0.07 (12)	-0.69 (11)
F(1)	9.5 (7)	8.8 (7)	5.5 (6)	-4.0 (5)	-0.7 (5)	-1.1 (5)

(continue Table 4.5)

F(2)	5.8 (6)	6.0 (6)	13.9 (9)	1.7 (4)	3.5 (6)	2.3 (6)
F(3)	13.6 (9)	4.0 (5)	23.2 (14)	2.8 (6)	-12.9 (10)	-4.7 (7)
F(4)	5.6 (7)	31.2 (19)	8.9 (9)	3.0 (9)	0.9 (7)	2.3 (11)
O(1)	4.3 (5)	4.7 (5)	3.3 (5)	0.1 (4)	0.6 (4)	1.0 (4)
O(2)	4.2 (5)	5.3 (5)	3.0 (5)	-1.1 (4)	-1.2 (4)	-1.4 (4)
O(3)	4.0 (5)	4.4 (5)	5.5 (6)	0.5 (4)	1.4 (5)	2.5 (4)

Anisotropic Temperature Factors are of the form

$$\text{Temp} = -2 \times \text{Pi}^2 (h^2 \times U_{11} \times a^{*2} + \dots + 2hk \times U_{12} \times a^* \times b^* + \dots)$$

Table 4.6 Positional Parameters and Biso's of Hydrogen Atoms
for $[\text{Cp}^*_2\text{Ir}_2(\text{CO})_3\text{Cl}]\text{BF}_4$ (17)

Atom	x/a	y/b	z/c	Biso (\AA^2)
H(111)	0.401	0.395	0.177	3.9
H(113)	0.272	0.403	0.212	3.9
H(121)	0.539	0.171	0.185	4.2
H(122)	0.463	0.094	0.225	4.2
H(123)	0.392	0.169	0.171	4.2
H(131)	0.676	0.134	0.383	3.5
H(132)	0.582	0.115	0.446	3.5
H(133)	0.560	0.069	0.362	3.5

(continue Table 4.6)

Atom	x/a	y/b	z/c	Biso (Å ²)
H(141)	0.620	0.337	0.491	3.6
H(142)	0.483	0.349	0.516	3.6
H(143)	0.548	0.251	0.520	3.6
H(151)	0.467	0.496	0.364	3.8
H(152)	0.322	0.480	0.345	3.8
H(153)	0.386	0.462	0.430	3.8
H(211)	-0.181	0.380	0.570	3.5
H(212)	-0.035	0.377	0.593	3.5
H(213)	-0.094	0.451	0.532	3.5
H(221)	-0.285	0.406	0.364	3.5
H(222)	-0.167	0.469	0.387	3.5
H(223)	-0.180	0.415	0.307	3.5
H(231)	-0.225	0.194	0.271	3.3
H(232)	-0.144	0.277	0.243	3.3
H(233)	-0.085	0.177	0.255	3.3
H(241)	-0.104	0.041	0.418	2.9
H(242)	-0.010	0.063	0.356	2.9
H(243)	0.040	0.052	0.445	2.9
H(251)	-0.059	0.154	0.598	3.2
H(252)	0.076	0.141	0.572	3.2
H(253)	0.039	0.234	0.612	3.2

Molecular Structure of Complex (20)

The X-ray single crystal structure of complex (20) was analyzed by Dr. R. J. Batchelor, and found in a monoclinic space group $P2_1/n$, ($a= 11.695(2)$, $b= 19.911(3)$, $c= 12.539(2)$ Å, $\beta= 96.541(8)$, $V=2900.8$ Å³, and $Z=4$). The structure (excluding H-atoms) of the cation of (20) in the crystal is shown in Figure 4.5. The molecule consists of a dimeric bis(pentamethyl-cyclopentadienyl)(Ir-Ir) structural frame, with two terminal carbonyls bonded to two iridium centres separately, and a *para*-methoxyphenyl ($p\text{-C}_6\text{H}_4\text{OMe}$) as a bridging ligand between the two iridiums. There are no unusual inter-ionic distances in the crystal structure. The selected bond distances and bond angles for compound (19) are listed in Table 4.7.

The iridium-iridium bond distance of 2.7294(5) Å is comparable to 2.723(4) Å found in the $\mu^2\text{-}\eta^2$ bridging aryldiazenido analogue, $[\text{Cp}_2(\text{CO})_2\text{Ir}_2(\mu^2\text{-}\eta^2\text{-N}_2\text{C}_6\text{H}_4)]\text{BF}_4$ (11), and 2.7166(2) Å found in $[\text{Cp}_2(\text{CO})_2\text{Ir}_2](\mu^2\text{-}\eta^2\text{-C}_6\text{H}_4)$.²⁰⁷ The bridging *para*-methoxyphenyl ligand in (20) coordinates to Ir(2) atom by an apparent η^1 -, (or σ -), linkage from C(1) of the phenyl ring, and to Ir(1) by η^2 -, (or π -), binding from C(1) and C(2) of the aromatic ring. The C₆-ring is planar (see Table 4.8) and the Ir(2) atom is approximately co-planar with the C₆-ring, with only a slight deviation of 0.050(11) Å from the least-squares plane through the six ring atoms. Further, the bond angle C(2)-C(1)-Ir(2) (122.5(5)°) is very close to the angle C(6)-C(1)-Ir(2) (123.8(5)°). It is then clear that the ligand $p\text{-C}_6\text{H}_4\text{OMe}$ is σ -bonded to Ir(2) apparently through a sp^2 hybridized atom C(1). The Ir(2)-C(1) distance of 2.054(7) Å is similar to the previously reported σ bond lengths between iridium and phenyl carbon. For example, Ir-C(phenyl) is 2.070(15) Å in $\text{Ir}(\text{C}_2\text{H}_4)_2(\text{PPh}_3)\text{PPh}_2\text{C}_6\text{H}_4$.²⁰⁸ and Ir-C(phenylene) 2.045(3) Å in $[\text{Cp}_2(\text{CO})_2\text{Ir}_2](\mu^2\text{-}\eta^2\text{-C}_6\text{H}_4)$.²⁰⁷ It should be also noted that as a result of the σ :

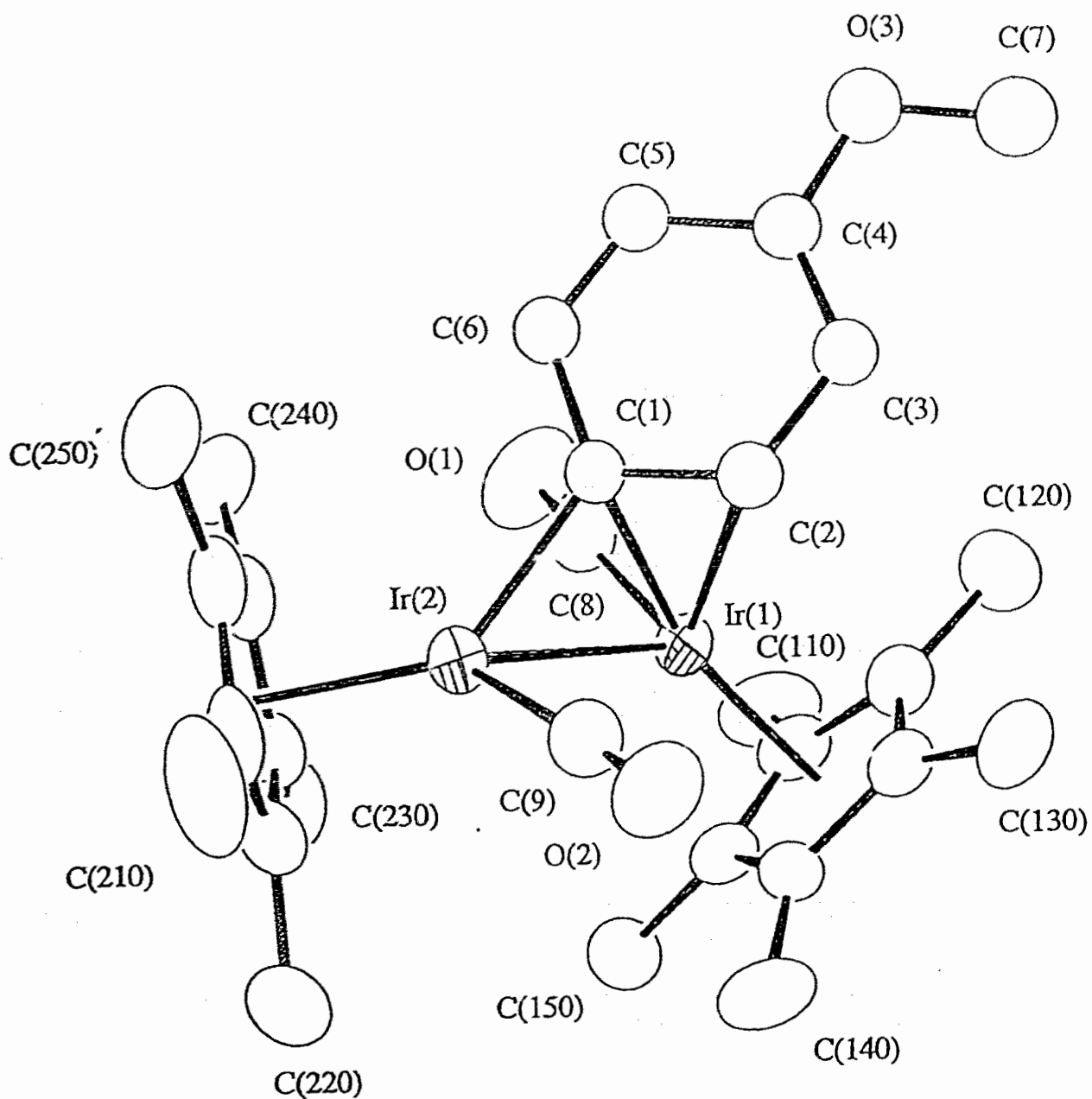


Figure 4.5 Molecular structure of the cation of (20). (The thermal ellipsoids represent 50 % probability contours).

π coordination of the bridging p -C₆H₄OMe, this π bond is slightly distorted. The Ir(1)-C(2) distance of 2.394(7) Å is slightly longer than Ir(1)-C(1) of 2.324(7) Å, and the internal dihedral angle between plane C(1)-C(2)-Ir(1) and the C₆-ring is not 90° but 116.2(3)°. The bonds of Ir(1)-Ir(2) and C(1)-C(2) are not co-planar but there is a torsional angle of -62.4(4)° for Ir(1)-Ir(2)-C(1)-C(2). The bond angle C(2)-C(1)-C(6) (113.7(7)°), compared to C(1)-C(2)-C(3) (123.3(7)°), presumably reflects a larger stereochemical influence of the sigma-bound iridium atom at C(1) relative to that of the hydrogen atom at C(2). In the phenyl ring, the bond lengths of C(3)-C(4) and C(5)-C(6), both 1.35(1) Å, are significantly shorter than the other intra-ring C-C bond distances, 1.40(1)-1.43(1) Å. Surprisingly, the bond lengths of 1.35(1) Å are not only much shorter than that of the carbon-carbon bonds in regular benzene (1.39 Å)²⁰⁹ but are even close to the bond length of an isolated C=C bond in ethene (1.34 Å).²¹⁰ So it is clearly indicated that, as a consequence of the π -bonding to iridium from C(1) and C(2), the aromaticity of the phenyl ring is disrupted and a localized, alternating multiple bond character is produced in the ring. Furthermore, the difference of the bond orders between C(3)-C(4) and C(4)-C(5) would be expected to have some effect on the -OMe group at C(4). Notably, the bond angle C(3)-C(4)-O(3) (125.4(7)°) is unusually much more obtuse than C(5)-C(4)-O(3) (115.2(7)°).

Interestingly, inspection of the molecular structure without considering the multiply coordinated aryl ligand reveals that the framework of Cp*Ir(CO)-Cp*Ir(CO) possesses approximate C₂ symmetry. In other words, the unusual asymmetric coordination of the aryl ring through simultaneous σ and π bondings to the two different iridium atoms does not cause significant difference in the configurations of two Cp*Ir(CO)- fragments. Thus, the asymmetric coordination

of the aryl shows much the same effect as a symmetric bridging aryl (see structure **B** in Figure 4.6) on the remaining molecular structure. This indicates that in solutions flipping of the aryl ligand from structure **A**, through **B**, to **C** (refer to Figure 4.6) and the reverse could occur without involving a significant change of the energy of the system.

Thus, although the structure of the molecular cation in the solid state is undoubtedly in a C_1 symmetry, in solution two possibilities for the molecular structure still can not be distinguished on the present evidence. One possibility is structure **B** being the only isomer present in solution. The other would be a fast fluxional exchange of the bridging aryl ligand in a process described in Figure 4.6.

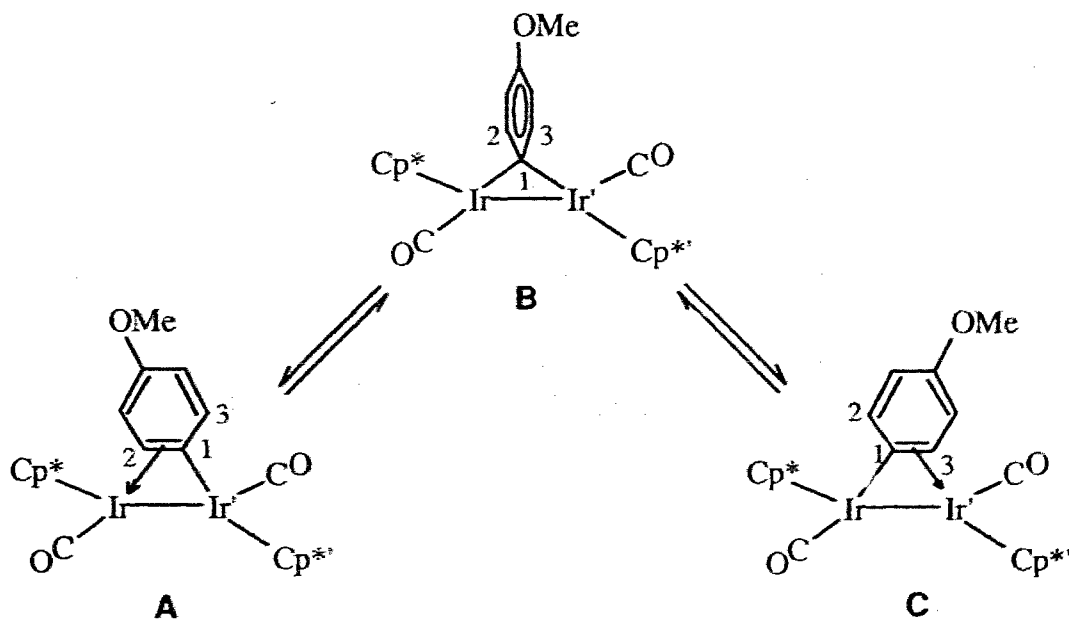


Figure 4.6 Possible fluxional process for the molecule (20) in solution

Table 4.7. Selected bond distances (Å) and angles (°) for
 $[\text{Cp}^*_2\text{Ir}_2(\text{CO})_2(1-\eta^1-1,2-\eta^2-\mu^2-p\text{-C}_6\text{H}_4\text{OMe})]\text{BF}_4$ (20)

(a) Bond Lengths

Ir(1) - C(1)	2.324(7)	Ir(2) - Ir(1)	2.7294(5)
Ir(1) - C(2)	2.394(7)	Ir(2) - C(1)	2.054(7)
Ir(1) - C(8)	1.857(9)	Ir(2) - C(9)	1.858(9)
Ir(1) - Cp1 ^a	1.902	Ir(2) - Cp2 ^b	1.898
Ir(1) - C(11)	2.192(7)	Ir(2) - C(21)	2.207(7)
Ir(1) - C(12)	2.242(8)	Ir(2) - C(22)	2.251(8)
Ir(1) - C(13)	2.331(8)	Ir(2) - C(23)	2.293(7)
Ir(1) - C(14)	2.335(8)	Ir(2) - C(24)	2.272(8)
Ir(1) - C(15)	2.197(7)	Ir(2) - C(25)	2.237(8)
O(1) - C(8)	1.13(1)	O(2) - C(9)	1.127(9)
O(3) - C(4)	1.367(9)	O(3) - C(7)	1.41(1)
C(1) - C(2)	1.43(1)	C(1) - C(6)	1.43(1)
C(2) - C(3)	1.40(1)	C(3) - C(4)	1.35(1)
C(4) - C(5)	1.41(1)	C(5) - C(6)	1.35(1)

(b) Interbond Angles

C(1) - Ir(1) - Ir(2)	47.1(2)	C(1) - Ir(2) - Ir(1)	56.0(2)
C(2) - Ir(1) - C(1)	35.2(2)	C(9) - Ir(2) - C(1)	88.8(3)
C(8) - Ir(1) - Ir(2)	91.2(3)	C(9) - Ir(2) - Ir(1)	89.4(3)
Cp1 - Ir(1) - Ir(2)	130.6	Cp2 - Ir(2) - Ir(1)	134.4
Cp1 - Ir(1) - C(8)	127.2	Cp2 - Ir(2) - C(9)	127.5

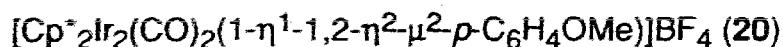
(continue Table 4.7)

Cp1 - Ir(1) - C(2)	115.8	Cp2 - Ir(2) - C(1)	136.1
C(2) - Ir(1) - Ir(2)	73.2(2)	C(2) - C(1) - Ir(1)	75.1(4)
C(8) - Ir(1) - C(1)	81.9(3)	Ir(2) - C(1) - Ir(1)	76.8(2)
C(8) - Ir(1) - C(2)	105.2(3)	C(2) - C(1) - Ir(2)	122.5(5)
Cp1 - Ir(1) - C(1)	148.7	C(6) - C(1) - Ir(1)	120.8(5)
C(3) - C(2) - Ir(1)	120.9(5)	C(6) - C(1) - Ir(2)	123.8(5)
C(1) - C(2) - Ir(1)	69.7(4)	O(1) - C(8) - Ir(1)	174.2(8)
C(6) - C(1) - C(2)	113.7(7)	O(2) - C(9) - Ir(2)	174.3(8)
C(3) - C(2) - C(1)	123.3(7)	C(3) - C(4) - O(3)	125.4(7)
C(4) - C(3) - C(2)	119.6(7)	C(5) - C(4) - O(3)	115.2(7)
C(5) - C(4) - C(3)	119.4(7)	C(7) - O(3) - C(4)	114.6(7)
C(6) - C(5) - C(4)	121.5(8)	C(5) - C(6) - C(1)	122.4(7)

a: Centroid of Cp* 1

b: Centroid of Cp* 2

Table 4.8. Least-squares plane for the aryl group of



Equation of the plane : $3.80(4)X + 7.45(6)Y + 10.356(23)Z = 6.818(18)$

Distances(Å) to the plane from the atoms in the plane.

C(1)	-0.013(9)	C(2)	0.016(9)
C(3)	-0.006(9)	C(4)	-0.007(10)
C(5)	0.007(10)	C(6)	0.004(10)

Chi squared for this plane 6.887

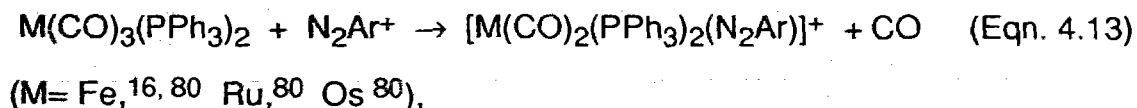
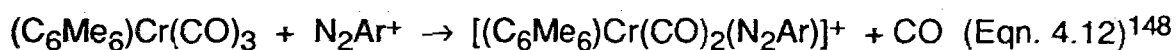
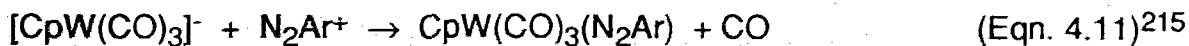
Distances(Å) to the plane from the atoms out of the plane.

Ir(1)	-2.015(8)	Ir(2)	-0.050(11)
O(3)	0.015(11)	C(7)	-0.020(15)

4.4 Conclusion

The numerous failures to synthesize $[\text{Cp}^* \text{Ir}(\text{CO})(\text{N}_2\text{Ar})]^+$ most probably reflect an unfavorable electronic arrangement in this system, *i.e.*, the sharing of one pair of metal d_{π} -electrons between two trans-arranged, different strong π -acid ligands. In fact, supportively, there has been no documented example of such a compound in the literature thus far in which a singly bent aryldiazenido ligand is geometrically or/and electronically trans to a carbonyl ligand. Instead, there are many instances in which attempts to synthesize such a compound by direct reaction of aryldiazonium ions and metal carbonyl or carbonyl derivatives have failed. For example, no stable aryldiazenido derivatives were obtained by reactions of aryldiazonium ions with $[\text{Mn}(\text{CO})_5]^-$,^{16, 211} $[\text{Co}(\text{CO})_4]^-$,^{16, 211} $[\text{V}(\text{CO})_6]^-$,^{16, 211} $\text{Fe}(\text{CO})_5$,²¹² $\text{Ni}(\text{CO})_4$,²¹³ $\text{Cr}(\text{CO})_6$,²¹³ $\text{Mo}(\text{CO})_6$,²¹³

$[\text{CpFe}(\text{CO})_2]^-$,^{16, 211, 214} $[\text{CpNi}(\text{CO})]^-$,¹⁶ $\text{CpMn}(\text{CO})(\text{PPh}_3)_2$,³⁴
 $(\text{C}_6\text{Me}_6)\text{Cr}(\text{CO})_2(\text{PPh}_3)$,¹⁴⁸ or $[\text{PPh}_3\text{SnFe}(\text{CO})_4]^-$.¹⁶ However, there are several
 examples where the aryldiazenido ligand occurs in metal carbonyl derivatives.
 For example, (Eqn. 4.11-4.13)



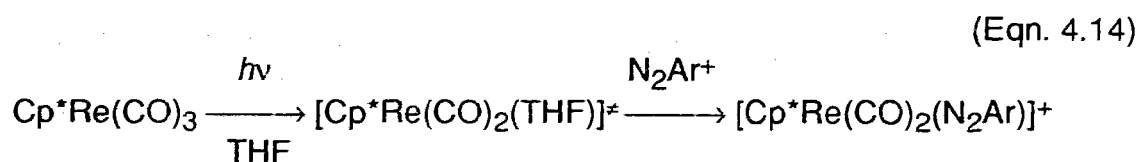
as well as $\text{Fe}(\text{CO})(\text{NO})(\text{N}_2\text{Ar})(\text{PPh}_3)$ ¹⁶ and $\text{Co}(\text{CO})_2(\text{N}_2\text{Ar})(\text{PPh}_3)$.¹⁶ In all these
 stable aryldiazenido carbonyl compounds, the singly bent aryldiazenido ligand
 is exclusively related to the carbonyls in a trigonal manner. Such an
 arrangement, unlike the trans one we mentioned above, creates an electronically
 favorable interaction between CO and N_2Ar^+ , as was discussed in section
 1.3.2.2.

Thus, it seems clear at this point that there exists a criterion for securing a
 stable N_2Ar^+ ligand in carbonyl derivatives. This criterion may be stated as

*In order to secure a singly bent aryldiazenido ligand in a metal carbonyl
 derivative, the diazenido ligand and a carbonyl should avoid sharing the same
 pair of metal $d\pi$ electrons in π bonding to the metal.*

It should also be mentioned that there are many aryldiazenido (carbonyl)
 compounds which, although they do not violate this principle, nevertheless have

not successfully been prepared from direct reactions of the diazonium ions with carbonyl precursors. In this case, the failures could be mainly due to two synthetic reasons; (1) poor lability of the CO leaving groups in the precursors, and (2) the oxidative ability of the aryldiazonium ions. To overcome these problems, it is thus sometimes necessary to carefully choose the leaving groups on the metal and the substituents on the diazonium salt. For example, a direct substitution of a carbonyl by diazonium ion in $\text{Cp}^*\text{Re}(\text{CO})_3$ was unsuccessful;²¹⁶ however, by a photolysis of $\text{Cp}^*\text{Re}(\text{CO})_3$ in THF solution, followed immediately by addition of an aryldiazonium salt, the target diazenido compound was obtained as a very stable species, largely due to the formation of the more labile THF complex as an intermediate, (Eqn. 4.14)



Finally, despite the failures experienced in the syntheses of $[\text{Cp}^*\text{Ir}(\text{CO})(\text{N}_2\text{Ar})]^+$, the results that have emerged from this study are nevertheless interesting. Several different products have been isolated from the same reaction of $\text{Cp}^*\text{Ir}(\text{CO})_2$ and N_2Ar^+ only by changing the reaction media, *i.e.*, formation of $[\text{Cp}^*\text{Ir}(\text{CO})_2(\text{Ar})]^+$ in acetone, $[\text{Cp}^*\text{Ir}(\text{CO})_2 \rightarrow \text{Ir}(\text{CO})(\text{Cl})\text{Cp}^*]^+$ in CH_2Cl_2 and $[\text{Cp}^*\text{Ir}(\text{CO})(\text{OEt})(\text{NHNAr})]^+$ in EtOH. Also the compound $[\text{Cp}^*_2\text{Ir}_2(\text{CO})_2(1-\eta^1-1,2-\eta^2-\mu^2-p\text{-C}_6\text{H}_4\text{OMe})]\text{BF}_4$ (**20**) with a novel bridging aryl ligand has been isolated from the reaction of $[\text{Cp}^*\text{Ir}(\text{CO})]_2$ and N_2Ar^+ , and provides the first example of a bridging aryl group generated from a diazonium ion. More importantly, the results obtained have actually broadened our

understanding of the chemistry involved in the reactions of aryldiazonium ions and metal carbonyls and carbonyl derivatives, and are in accord with the theoretical arguments that have formed the background for the experimental work that is presented in this Thesis.

Appendix I

Extended Hückel Molecular Orbital Theory (EHMO)

Extended Hückel Theory was developed by R. Hoffmann.^{23, 217} In order to determine the MO coefficients in the matrix eigenvalue problem

$$H C_i = \epsilon_i S C_i$$

where C_i denotes the vector of LCAO coefficients for the i -th MO of energy ϵ_i and S is the overlap matrix, following approximations were introduced

- (1). The AO basis consists of only valence-shell atomic orbitals, frequently Slater-type orbitals with orbital exponents determined by Slater's rule,^{218, 219}
- (2). The diagonal Hamiltonian H_{ii} is approximated by empirical valence shell orbital ionization potentials (VOIP or VSIP), *i.e.*

$$H_{ii} = -\text{VOIP}$$

- (3) The off-diagonal Hamiltonian H_{ij} is obtained from the Wolfsberg-Helmholtz arithmetic formula

$$H_{ij} = 0.5 K S_{ij} (H_{ii} + H_{jj})$$

where S_{ij} is the corresponding overlap integral, and is defined as $S_{ij} = \langle i | j \rangle$ and K is usually assigned a value of 1.7 to 2.0

The exponents of Slater's orbital used in this Thesis were already installed in the EHMO calculation program,²²⁰ and they are also available from standard sources.^{221 - 224} The H_{ij} used for transition metals were obtained from the literature where Self-Consistent Charge Calculations have always been used for metal carbonyls or typical organometallic molecules with ligands like Cp, R, CO, etc, and they are listed in the Appendix II. The K value of 1.75 has been used for the calculation of H_{ij} .

Appendix II

Table of standard H_{ii} 's

Atom	Orbital	H_{ii} (eV)	ref.
Br	4s	-22.07	225
	4p	-13.10	
C	2s	-21.4	23
	2p	-11.4	
Cl	3s	-26.3	226
	3p	-14.2	
Co	4s	-9.21	226
	4p	-5.26	
	3d	-13.18	
Cr	4s	-8.66	226
	4p	-5.24	
	3d	-11.22	
Cu	4s	-11.4	227
	4p	-6.06	
	3d	-14.0	
Fe	4s	-9.10	226
	4p	-5.32	
	3d	-12.6	
H	1s	-13.6	23
I	5s	-18.0	228
	5p	-12.7	
Ir	6s	-11.36	24
	6p	-4.50	
	5d	-12.17	

(---continued)

Mn	4s	-9.75	229
	4p	-5.89	
	3d	-11.67	
Mo	5s	-8.34	226
	5p	-5.24	
	4d	-10.50	
N	2s	-26.0	23
	2p	-13.4	
Ni	4s	-9.17	230
	4p	-5.15	
	3d	-13.49	
O	2s	-32.3	23
	2p	-14.8	
P	3s	-18.6	226
	3p	-14.0	
Re	6s	-9.36	231
	6p	-5.96	
	5d	-12.66	
Rh	5s	-8.09	226
	5p	-4.57	
	4d	-12.50	
S	3s	-20.0	232
	3p	-11.0	
W	6s	-8.26	231
	6p	-5.17	
	5d	-10.37	

References

1. C. F. Barrientos-Penna, F. W. B. Einstein, D. Sutton and A. C. Willis, *Inorg. Chem.*, (1980), **19**, 2740.
2. C. F. Barrientos-Penna, F. W. B. Einstein, T. Jones and D. Sutton, *Inorg. Chem.*, (1982), **21**, 2740.
3. C. F. Barrientos-Penna, C. F. Campana, F. W. B. Einstein, T. Jones, A. S. Tracey and D. Sutton, *Inorg. Chem.*, (1984), **23**, 363.
4. C. F. Barrientos-Penna, F. W. B. Einstein, T. Jones and D. Sutton, *Inorg. Chem.*, (1982), **21**, 2578.
5. J. Chatt, J. R. Dilworth and R. L. Richards, *Chem. Rev.*, (1977), **78**, 589.
6. J. Chatt and R. L. Richards, *J. Organomet. Chem.*, (1982), **239**, 65.
7. G. W. Parshall, *J. Am. Chem. Soc.*, (1965), **87**, 2133.
8. A. B. Gilchrist, G. W. Rayner-Canham and D. Sutton, *Nature*, (1972), **235**, 42.
9. R. A. Henderson, G. J. Leigh and C. J. Pickett, *Adv. Inorg. Chem. and Radiochem.*, (1983), **27**, 197.
10. M. J. Nelson, P. A. Lindahl and W. H. Orme-Johnson, *Adv. Inorg. and Biochem.*, (1982), **4**, 1.
11. J. H. Enemark, *Nitrogen Fixation*, Ed. by W. E. Newton and W. H. Orme-Johnson, Vol. 1, University Park Press, Baltimore, (1980), p297.
12. M. M. Taqui Khan and A. E. Martell, *Homogeneous Catalysis by Metal Complexes*, Vol. 1, Academic Press, New York, (1974), p181.
13. D. Sutton, *Chem. Soc. Rev.*, (1975), **4**, 443
14. B. L. Haymore, *Ph.D Thesis*, Northwestern Univ. (1975), p30.
15. R. Yamashita, K. Kikukawa, F. Wada and T. Matsuda, *J. Organomet.*

- Chem.*, (1980), **201**, 463.
16. W. E. Carroll and F. J. Lalor, *J. Organomet. Chem.*, (1973), **54**, C37
 17. W. E. Carroll, F. A. Deeney and F. J. Lalor, *J. Organomet. Chem.*, (1980), **198**, 189.
 18. S. Krogsrud and J. A. Ibers, *Inorg. Chem.*, (1975), **14**, 2298.
 19. R. E. Cobblestick, F. W. B. Einstein, N. Farrell, A. B. Gilchrist and D. Sutton, *J. Chem. Soc., Dalton Trans.*, (1977), 373.
 20. A. Cusanelli and D. Sutton, *J. Chem. Soc., Chem. Comm.*, (1989), 1719.
 21. M. H. Whangbo, H. B. Schlegel and S. Wolfe, *J. Am. Chem. Soc.*, (1977), **99**, 1296.
 22. M. H. Whangbo and S. Wolfe, *Isr. J. Chem.*, (1980), **20**, 36.
 23. R. Hoffmann, *J. Chem. Phys.*, (1963), **39**, 1397.
 24. D. L. Dubois and R. Hoffmann, *Nouv. J. Chim.*, (1977), **1**, 479.
 25. F. W. B. Einstein, A. B. Gilchrist, G. W. Rayner-Canham and D. Sutton, *J. Am. Chem. Soc.*, (1972), **94**, 645.
 26. E. R. Möller and K. A. Jorgensen, *Acta Chem. Scand.*, (1991), **45**, 68.
 27. R. Hoffmann, *Angew. Chem., Int. Ed. Engl.*, (1982), **21**, 711.
 28. T. A. Albright, J. K. Burdett and M.-H. Whangbo, *Orbital Interactions in Chemistry*, John Wiley & Sons, New York, (1985).
 29. T. A. Albright, *Tetrahedron*, (1982), **38**, 1339.
 30. D. M. P. Mingos, *Adv. Organomet. Chem.*, (1977), **15**, 1.
 31. R. Hoffmann, *Science*, (1981), **211**, 995.
 32. J. K. Burdett, *Molecular Shapes*, John Wiley & Sons, New York, (1980)
 33. C. Römning, *Acta Chem. Scand.*, (1963), **17**, 1444.
 34. B. F. G. Johnson, B. L. Haymore and J. R. Dilworth, in *Comprehensive Coordination Chemistry*, G. Wilkinson, R. D. Gillard and J. A. McClevery,

- (Eds), Pergaman Press, Oxford, (1987), **Vol. 2**, pp.130 ~ 141.
35. N-N=1.232 Å, \angle N-N-C=120° are the average values from ~40 different singly bent diazenido complexes listed in reference 34.
 36. A. D. Walsh, *J. Chem. Soc.* (1953), 2260, 2266, 2288, 2296, 2301, 2318, 2321, 2325, 2330.
 37. G. L. Hillhouse, B. L. Haymore and W. A. Herrmann, *Inorg. Chem.* (1979), **18**, 2423.
 38. K. D. Schramm and J. A. Ibers, *Inorg. Chem.*, (1977), **16**, 3287.
 39. C. F. Barrientos-Penna and D. Sutton, *J. Chem. Soc., Chem. Comm.*, (1980), 111.
 40. R. E. Cobbleidick, F. W. B. Einstein, N. Farrell, A. B. Gilchrist and D. Sutton, *J. Chem. Soc., Dalton Trans.*, (1977), 373.
 41. A. P. Gaughan, B. L. Haymore, J. A. Ibers, W. H. Myers, T. E. Nappier and D. W. Meek, *J. Am. Chem. Soc.*, (1973), **95**, 6859.
 42. S. Krogsrud and J. A. Ibers, *Inorg. Chem.*, (1975), **14**, 2617.
 43. F. W. B. Einstein, X. Yan and D. Sutton, *J. Chem. Soc., Chem. Comm.*, (1990), 1466.
 44. J. V. McArdle, A. J. Schultz, B. J. Corden and R. Eisenberg, *Inorg. Chem.*, (1973), **12**, 1676.
 45. C. F. Barrientos-Penna, F. W. B. Einstein, T. Jones and D. Sutton, *Inorg. Chem.*, (1985), **24**, 632.
 46. J. Chatt, M. E. Fakley, P. B. Hitchcock, R. L. Richards and N. T. Luong-Thi, *J. Chem. Soc., Dalton Trans.*, (1982), 345.
 47. R. Mason, K. M. Thomas, J. A. Zubieta, P. G. Douglas, A R. Galbraith and B. L. Shaw, *J. Am. Chem. Soc.*, (1974), **96**, 260.
 48. V. F. Duckworth, P. G. Douglas, R. Mason and B. L. Shaw, *J. Chem. Soc.*,

- Chem. Comm.* (1970), 1083.
49. G. Avitabile, P. Ganis and M. Nemiroff, *Acta Crystallogr. Sect. B*, (1971), **27**, 725.
 50. F. J. Lalor, D. Condon, G. Ferguson and M. A. Kahn, *Inorg. Chem.*, (1981), **20**, 2178.
 51. A. V. Butcher, J. Chatt, J. R. Dilworth, G. J. Leigh, M. B. Hursthouse, S. A. A. Jayaweera and A. Quick, *J. Chem. Soc., Dalton Trans.*, (1979), 921.
 52. C. S. Day, V. W. Day, T. A. George and I. Tavanaiepour, *Inorg. Chim Acta*, (1980), **45**, L54.
 53. D. Carrillo, P. Gouzerh and Y. Jeannis, *Nouv. J. Chim.*, (1985), **9**, 749
 54. T. C. Hsieh and J. Zubieta, *Inorg. Chem.*, (1985), **24**, 1287.
 55. J. E. Huheey, *Inorganic Chemistry*, 3rd. Ed., Parper & Row, New York, (1983)
 56. P. S. Braterman, *Reactions of Coordinated Ligands*, Ed. by P. S. Braterman, Vol. 1, Plenum Press, New York, (1986).
 57. C. F. Barrientos-Penna, F. W. B. Einstein, T. Jones and D. Sutton, *Inorg. Chem.*, (1985), **24**, 632.
 58. C. Condon, M. E. Deane and F. J. Lalor, *J. Chem. Soc., Dalton Trans.*, (1977), 925.
 59. F. W. B. Einstein, R. H. Jones, Y. M. Zhang and D. Sutton, *Inorg. Chem.*, (1988), **27**, 1004.
 60. M. Sato, T. Kodama, M. Haidi and Y. Uchida, *J. Organomet. Chem.*, (1978), **152**, 239.
 61. F. A. Cotton and G. Wilkinson, *Advanced Inorganic Chemistry*, 5th Ed. John Wiley & Sons, New York, (1988), p12.
 62. E. L. Muetterties and R. A. Shunn, *Quart. Rev. Chem. Soc.*, (1966), **20**, 245.

63. E. L. Muetterties and L. J. Guggenberger, *J. Am. Chem. Soc.*, (1974), **96**, 1748.
64. L. Sacconi, *Pure Appl. Chem.*, (1968), **17**, 95.
65. J. S. Wood, *Progr. Inorg. Chem.*, (1972), **16**, 227.
66. J. R. Shapley and J. A. Osborn, *Accounts Chem. Res.*, (1973), **6**, 305.
67. M. R. Churchill and K.-K. G. Lin, *J. Am. Chem. Soc.*, (1974), **96**, 76.
68. S. A. Goldfield and K. N. Raymond, *Inorg. Chem.*, (1974), **13**, 770.
69. A. R. Rossi and R. Hoffmann, *Inorg. Chem.*, (1975), **14**, 365.
70. B. L. Haymore and J. A. Ibers, *Inorg. Chem.*, (1975), **14**, 1369
71. M. Cowie, B. L. Haymore and J. A. Ibers, *Inorg. Chem.*, (1975), **14**, 2617.
72. G. Albertin, S. Antoniutti, G. Pelizzi, F. Vitali and E. Bordignon, *J. Am. Chem. Soc.*, (1986), **108**, 6627.
73. M. Cowie, B. L. Haymore and J. A. Ibers, *J. Am. Chem. Soc.*, (1976), **98**, 7608.
74. A. R. Luixmor and M. R. Truter, *Acta Crystallogr.*, (1962), **15**, 1117.
75. C. Pedore and A. Sirigu, *Inorg. Chem.*, (1968), **7**, 2614.
76. L. Manojlovic-Muir, K. W. Muir and J. A. Ibers, *Discuss. Faraday Soc.*, (1969), **47**, 84.
77. G. B. Robertson and P. O. Whimp, *J. Chem. Soc., Dalton Trans.*, (1973), 2454.
78. B. Beagley, D. G. Schmidling and D. W. Cruickshank, *Acta Crystallogr., Sect. B*, (1973), **29**, 1499.
79. (a) F. A. Cotton and G. Wilkinson, *Advanced Inorganic Chemistry*, 5th Ed., John Wiley & Sons, New York, (1988), p742. (b) *ibid.*, p725. (c) *ibid.*, p918.
80. B. L. Haymore and J. A. Ibers, *Inorg. Chem.*, (1975), **14**, 2784.
81. D. J. Hodgson and J. A. Ibers, *Inorg. Chem.*, (1968), **7**, 2345.

82. S. D. Ittel and J. A. Ibers, *J. Am. Chem. Soc.*, (1974), **96**, 4808.
83. S. D. Ittel and J. A. Ibers, *Inorg. Chem.*, (1975), **14**, 636.
84. F. A. Cotton and G. Wilkinson, *Advanced Inorganic Chemistry*, 5th Ed., John Wiley & Sons, New York, (1988), p1388.
85. A. B. Gilchrist and D. Sutton, *Canad. J. Chem.*, (1974), **52**, 3387.
86. F. W. B. Einstein, A. B. Gilchrist, G. W. Rayner Canham and D. Sutton, *J. Chem. Soc., Dalton Trans.*, (1973), 434.
87. J. R. Dilworth, I. A. Latham, G. J. Leigh, G. Huttner and I. Jibril, *J. Chem. Soc., Chem. Commun.*, (1983), 1368.
88. T. Jones, A. J. Hanlan, F. W. B. Einstein and D. Sutton, *J. Chem. Soc., Chem. Commun.*, (1980), 1978.
89. J. Chatt, J. R. Dilworth, P. Dahlstrom and J. A. Zubieta, *J. Chem. Soc., Chem. Commun.*, (1985), 786.
90. R. R. Schrock, A. H. Liu, M. B. O'Regan, W. C. Finch and J. F. Payack, *Inorg. Chem.*, (1988), **27**, 3574.
91. F. W. B. Einstein, D. Sutton and K. G. Tyers, *Inorg. Chem.*, (1987), **26**, 111.
92. T. E. Glassman, M. G. Vale and R. R. Schrock, *Inorg. Chem.*, (1992), **31**, 1984.
93. J. R. Dilworth, *Coord. Chem. Rev.*, (1976), **21**, 19, and references therein.
94. M. G. Vale and R. R. Schrock, *Organometallics*, (1991), **10**, 1661.
95. B. L. Haymore, J. A. Ibers and D. W. Meek, *Inorg. Chem.*, (1975), **14**, 541.
96. J. Mason, in *Multinuclear NMR*, Ed. J. Mason, Plenum, New York, (1987), Chapter 12.
97. B. L. Haymore, M. Hughes, J. Mason and R. L. Richards, *J. Chem. Soc., Dalton Trans.*, (1988), 2935.
98. W. G. Proctor and F. C. Yu, *Phys. Rev.*, (1950), **77**, 717.

99. W. M. Litchman and M. Alei, *J. Chem. Phys.*, (1972), **56**, 5818.
100. D. M. P. Mingos and D. J. Sherman, *Adv. Inorg. Chem.*, (1989), **34**, 293.
101. G. C. Levy and R. L. Lichter, in '*Nitrogen-15 NMR Spectroscopy*', Wiley-Interscience, New York, (1979), p1.
102. G. C. Levy, J. J. Dichter and J. Kawalewski, *J. Am. Chem. Soc.*, (1978), **100**, 2308.
103. I. Ando and G. A. Webb, in '*Theory of NMR Parameters*', Academic Press, London, (1983), p10.
104. L. M. Ishol, T. A. Scott and M. Goldbatt, *J. Magn. Reson.*, (1976), **23**, 313.
105. S. D. Mtunzi, C. J. MacDonald, R. L. Richards, G. E. Hawkes and J. Mason, *J. Chem. Soc., Dalton Trans.*, (1985), 2473.
106. D. Sutton, unpublished data.
107. J. Mason, *Chem. Rev.*, (1981), **81**, 205.
108. M. Witanowski, L. Stefaniak and G. A. Webb, *Ann. Rep. NMR Spectrosc.*, (1981), **11B**.
109. M. Witanowski, L. Stefaniak and G. A. Webb, *Ann. Rep. NMR Spectrosc.*, (1986), **18**.
110. N. F. Ramsey, *Phys. Rev.*, (1953), **91**, 303.
111. J. O. Friedrich and R. E. Wasylshen, *J. Chem. Phys.*, (1985), **83**, 3707.
112. M. Karplus and J. A. Pople, *J. Chem. Phys.*, (1963), **38**, 2803.
113. T. Khin and G. A. Webb, *J. Magn. Reson.*, (1979), **33**, 159.
114. J. Müller and H. F. Schroder, *Z. Anorg. Allg. Chem.*, (1979), **450**, 149.
115. J. Müller, *Z. Naturforsch.*, (1978), **34b**, 437.
116. J. Müller, *Z. Naturforsch.*, (1979), **34b**, 531.
117. D. M. Kanjia, J. Mason, I. A. Stenhouse, R. E. Banks and N. D. Venayak, *J. Chem. Soc., Perkin Trans.*, (1981), **2**, 975.

118. J. R. Dilworth, S. Donovan-Mtunzi, C. T. Kan, R. L. Richards and J. Mason, *Inorg. Chim. Acta*, (1981), **53**, L161.
119. S. Donovan-Mtunzi, R. L. Richards and J. Mason, *J. Chem. Soc., Dalton Trans.*, (1984), 2724.
120. J. W. Lown and S. M. S. Chanhan, *J. Org. Chem.*, (1981), **46**, 5309.
121. J. W. Lown and S. M. S. Chanhan, *J. Org. Chem.*, (1983), **48**, 513.
122. S. Somova, R. Radeaglia and E. Fanghanel, *J. Prakt. Chem.*, (1982), **324**, 777.
123. Y. Kroda, H. Lee and A. Kuwae, *J. Phys. Chem.*, (1980), **84**, 3417.
124. N. A. Porter, G. R. Dubay and J. G. Green, *J. Am. Chem. Soc.*, (1978), **100**, 920.
125. J. M. Schulman, J. Ruggio and T. J. Venanzi, *J. Am. Chem. Soc.*, (1977), **99**, 2045.
126. J. M. Schulman and W. S. Lee, *J. Magn. Reson.*, (1982), **50**, 142.
127. J. R. Dilworth, C. T. Kan, R. L. Richards, J. Mason and I. A. Stenhouse, *J. Organomet. Chem.*, (1980), **201**, C24.
128. I. Ando and G. A. Webb, in '*Theory of NMR Parameters*', Academic Press, London, (1983), p 47.
129. R. K. Harris, in '*Nuclear Magnetic Resonance Spectroscopy*', Longman Scientific & Technical: Harlow, (1986), p13.
130. L. O. Andersson, J. Mason and W. van Bronswijk, *J. Chem. Soc., A*, (1970), 296.
131. D. G. Morris and A. M. Murray, *J. Chem. Soc., Perkin II*, (1976), 1579.
132. W. L. Jorensen, L. Salem, in '*The Organic Chemists' Book of Orbitals*', Academic Press: New York, (1973).
133. R. L. Lichter and J. D. Roberts, *J. Am. Chem. Soc.*, (1972), **94**, 4904.

134. C. J. Jameson and J. Mason, in '*Multinuclear NMR*', Plenum, New York, (1987), ch.3.
135. D. Sutton, unpublished data on $\text{Cp'Re}(\text{N}_2)\text{LL}'$, (Cp'= Cp or Cp*; L and L'=CO; PR_3 and $\text{P}(\text{OR})_3$).
136. A. P. Blumenfeld, W. S. Lemenko, B. Poree, I. Mjodus, M. Baren, B. G. Szur and M. E. Bolpin, *Dokl. Akad. Nauk. SSSR*, (1980), **251**, 611.
137. J. M. Manriquez, D. M. McAllister, E. Rosenberg, A. M. Shiller, K. L. Williamson, S. I. Chan and J. E. Bercaw, *J. Am. Chem. Soc.*, (1978), **100**, 3078.
138. K. R. Laing, S. D. Robinson and M. F. Uttley, *J. Chem. Soc., Dalton Trans.*, (1973), 2713.
139. A. P. Gaughan and J. A. Ibers, *Inorg. Chem.*, (1975), **14**, 352.
140. D. E. Samkoff, J. R. Shapley, M. R. Churchill and H. J. Wasserman, *Inorg. Chem.*, (1984), **23**, 397.
141. R. E. DeBlois, A. L. Rhinggold and D. E. Samkoff, *Inorg. Chem.*, (1988), **27**, 3506.
142. P. Legzdins and J. T. Malito, *Inorg. Chem.*, (1975), **14**, 1875
143. R. B. King and M. B. Bisnette, *J. Am. Chem. Soc.*, (1964), **86**, 5695
144. D. R. Fisher and D. Sutton, *Canad. J. Chem.*, (1973), **51**, 1697
145. B. L. Haymore and J. A. Ibers, *J. Am. Chem. Soc.*, (1973), **95**, 3052
146. W. E. Carroll, F. A. Deeney and F. J. Lalor, *J. Chem. Soc., Dalton Trans.*, (1974), 1430
147. W. E. Carroll and F. J. Lalor, *J. Chem. Soc., Dalton Trans.*, (1973), 1754
148. N. G. Connelly and Z. Demidowicz, *J. Organomet. Chem.*, (1974), **73**, C31
149. W. E. Carroll, M. E. Deane and F. J. Lalor, *J. Chem. Soc., Dalton Trans.*, (1974), 1837

150. W. A. Thomas, *Ann. Rev. NMR Spectrsc.*, (1968), **1**, 43
151. K. Moseley, J. W. Kang and P. M. Maitlis, *J. Chem. Soc.*, (1970), 2875
152. H. P. Weber, *Acta. Cryst.* (1969), **B25**, 1174
153. A. C. Larson, *Crystallographic Computing*, (1969), pp293
154. E. J. Gabe, A. C. Larson, F. L. Lee and Y. LePage, *NRC VAX Crystal Structure System*, National Research Council, Ottawa, Ontario, Canada, (1984)
155. *International Tables for X-ray Crystallography*, (1974), Kynoch Press, Birmingham, England, Vol. IV, Table 2.2B and 2.3.1
156. D. J. Watkin, J. R. Carruthers and P. W. Betteridge, *Crystals*, (1984), Chemical Crystallography Laboratory, University of Oxford, Oxford, England
157. H. Werner, *Angew. Chem. Int. Ed., Engl.*, (1983), **22**, 927
158. P. O. Stoutland and R. G. Bergman, *J. Am. Chem. Soc.*, (1988), **110**, 5732
159. F. A. Cotton, in *Dynamic Nuclear Magnetic Resonance Spectroscopy*, L. M. Jackman and F. A. Cotton, (Eds.), Academic Press, (1975), New York, pp377 ~ 440
160. R. Cramer, *J. Am. Chem. Soc.*, (1964), **86**, 217
161. R. Cramer, *J. Am. Chem. Soc.*, (1967), **89**, 5377
162. R. Cramer, J. B. Kline and J. D. Roberts, *J. Am. Chem. Soc.*, (1969), **91**, 2519
163. M. Mlekuz, P. Bougeard, B. G. Sayer, M. J. McGlinchey, C. A. Rodger, M. R. Churchill, J. W. Ziller, S-K. Kang and T. A. Albright, *Organometallics*, (1986), **5**, 656
164. M. J. S. Dewar, *Bull. Soc. Chim. Fr.*, (1951), **18**, C71
165. J. Chatt and L. A. Duncanson, *J. Chem. Soc.*, (1953), 2939

166. *Spec. Publ. - Chem. Soc.*, (1965), **No.18**, S16s
167. Reference 2, and there ref. 400
168. D. M. P. Mingos and J. A. Ibers, *Inorg. Chem.*, (1971), **10**, 1479
169. V. G. Albano, P. Bellon and M. Sanson, *J. Chem. Soc., (A)*, (1971), 2420
170. J. W. Kang, K. Moseley and P. M. Maitlis, *J. Am. Chem. Soc.*, (1969), **91**, 5970
171. This thesis, section 1.4.4.5 and references therein.
172. C. F. Barrientos-Penna, A. H. Klahn-Oliva and D. Sutton, *Organometallics*, (1985), **4**, 367
173. B. L. Haymore and J. A. Ibers, *J. Am. Chem. Soc.*, (1975), **97**, 5369
174. G. W. Parshall, *J. Am. Chem. Soc.*, (1967), **89**, 1822
175. H. Werner, *Angew Chem., Int. Ed. Engl.*, (1983), **22**, 927
176. F. W. B. Einstein, X. H. Zhang, X. Yan and D. Sutton unpublished results
177. F. W. B. Einstein, R. H. Jones, X. Zhang, X. Yan. R. Nagelkerke and D. Sutton, *J. Chem. Soc., Chem. Comm.*, (1989), 1424
178. M. R. Churchill and B. G. DeBoer, *Inorg. Chem.*, (1977), **16**, 878
179. M. R. Churchill and H. J. Wasserman, *Inorg. Chem.*, (1981), **20**, 1580
180. R. Mason and D. M. P. Mingos, *J. Organomet. Chem.*, (1973), **50**, 53
181. M. R. Churchill and S. A. Julis, *Inorg. Chem.*, (1977), **16**, 1488
182. M. R. Churchill and S. A. Julis, *Inorg. Chem.*, (1979), **18**, 1215
183. R. G. Ball, W. A. G. Graham, D. M. Heinekey, J. K. Hoyano, A. D. McMaster, B. M. Mattson and S. T. Michel, *Inorg. Chem.*, (1990), **29**, 2013
184. F. W. B. Einstein, D. Sutton and P. L. Vogel, *Inorg. Nucl. Chem. Lett.*, (1976), **12**, 671
185. G. C. Dobinson, R. Mason, G. B. Robertson, R. Ugo, F. Conti, D. Morelli, S. Cenini and F. Bonati, *J. Chem. Soc., Chem. Comm.*, (1967), 739

186. M. R. Churchill and K. G. Lin, *Inorg. Chem.*, (1975), **14**, 1133
187. J. R. Shapley, P. C. Adair and R. J. Lawson, *Inorg. Chem.*, (1982), **21**, 1702
188. W. A. G. Graham, *J. Organomet. Chem.*, (1986), **30**, 81 (*lit. value for $\nu(\text{CO})$ is 1996 cm^{-1} in cyclohexane*)
189. K. W. Kang and P. M. Maitlis, *J. Organomet. Chem.*, (1971), **26**, 393
190. *Lit. values of $\nu(\text{co})$: $1925, 2000\text{ cm}^{-1}$ and of $^1\text{H NMR}$, $\delta(\text{CDCl}_3)$: 2.19 ppm from Reference 170.*
191. R. G. Ball, W. A. G. Graham, D. M. Heinekey, J. K. Hoyano, A. D. McMaster, B. M. Mattson and S. T. Michel, *Inorg. Chem.*, (1990), **29**, 2023. (*Lit. values for (14), $\nu(\text{CO})$: $1930, 2005\text{ cm}^{-1}$ in CH_2Cl_2 , $1953, 2020\text{ cm}^{-1}$ in hexane and $^1\text{H NMR}$, $\delta(\text{CDCl}_3)$: 2.19 ppm . Lit. values for (15), $\nu(\text{co})$: 1670 cm^{-1} in CH_2Cl_2 , 1702 cm^{-1} in hexane and $^1\text{H NMR}$, $\delta(\text{CDCl}_3)$: 1.76 ppm , $\delta(\text{C}_6\text{D}_6)$: 1.76 ppm and $\delta(\text{CD}_2\text{Cl}_2)$: 1.76 ppm , MS: M^+ , M^+-CO , Anal. (calcd): C, 37.17, H, 4.25, (found): C, 37.14, H, 4.33).*
192. I. R. Lyatifov, G. I. Gulieva, E. I. Mysov, V. N. Babin and R. B. Materikova, *J. Organomet. Chem.*, (1987), **326**, 83
193. I. R. Lyatifov, G. I. Gulieva, E. I. Mysov, V. N. Babin and R. B. Materikova, *J. Organomet. Chem.*, (1987), **326**, 89
194. F. G. N. Cloke, J. P. Day, A. M. Greenway, K. P. Seddon, A. A. Shimran and A. C. Swain, *J. Organomet. Chem.*, (1989), **372**, 231
195. W. I. Bailey, Jr., D. M. Cllins, F. A. Cotton, J. C. Baldwin and W. C. Kaska, *J. Organomet. Chem.*, (1979), **165**, 373
196. A. Nuttin and P. M. Maitlis, *J. Organomet. Chem.*, (1979), **166**, C21
197. A. C. Bray, M. Green, D. R. Hankey, J. A. K. Howard, O. Johnson and F. G. A. Stone, *J. Organomet. Chem.*, (1985), **281**, C12

198. Spectroscopic data for $\text{Cp}^*\text{IrRh}(\text{CO})_2$, IR, $\nu(\text{CO})$: 1703 cm^{-1} in CH_2Cl_2 and $^1\text{H NMR}$, $\delta(\text{CDCl}_3)$: 1.55 s and 1.88 s ppm (2Cp*), MS (m/z): 622 (M^+), 592 ($\text{M}^+ - \text{CO} - 2\text{H}$), 564 ($\text{M}^+ - 2\text{CO} - 2\text{H}$), 562 ($\text{M}^+ - 2\text{CO} - 4\text{H}$), 560 ($\text{M}^+ - 2\text{CO} - 6\text{H}$), 463 ($[\text{Cp}^*\text{IrCp}^*]^+$), 373 ($[\text{Cp}^*\text{RhCp}^*]^+$).
199. Spectroscopic data for $\text{Cp}^*\text{IrCpIr}(\text{CO})_2$, IR, $\nu(\text{CO})$: 1695 cm^{-1} in CH_2Cl_2 and $^1\text{H NMR}$, $\delta(\text{C}_6\text{D}_6)$: 1.58 s (15H, Cp*) and 5.14 s (5H, Cp)
200. C. Galli, *Chem. Rev.*, (1988), **88**, 765
201. F. A. Cotton and G. Wilkinson, *Advanced Inorganic Chemistry*, 5th edition, (1988), John Wiley & Sons, p1036
202. F. A. Cotton and G. Wilkinson, *Advanced Inorganic Chemistry*, 5th edition, (1988), John Wiley & Sons, p1125
203. J. Holton, M. Lappert, R. Pearce and P. I. W. Yarrow, *Chem. Rev.*, (1983), **83**, 135
204. W. A. Herrmann, *Angew. Chem., Int. Ed. Engl.*, (1978), **17**, 800
205. M. P. Brown, J. R. Fisher, S. J. Franklin, R. J. Puddephatt and K. R. Seddon, *J. Chem. Soc., Chem. Comm.*, (1978), 749
206. W. A. Herrmann, I. Schweizer, M. Creswick and I. Bernal, *J. Organomet. Chem.*, (1979), **165**, C17
207. M. D. Rausch, R. G. Gastinger, S. A. Gardner, R. K. Brown and J. S. Wood, *J. Am. Chem. Soc.*, (1977), **99**, 7870
208. G. Perego, G. Del Piero, M. G. Clerici and E. Perrotti, *J. Organomet. Chem.*, (1973), **54**, C51
209. A. F. Wells, *Structural Inorganic Chemistry*, 5th. edition, (1984), Clarendon Press, Oxford, p920
210. A. F. Wells, *Structural Inorganic Chemistry*, 4th. edition, (1975), Clarendon Press, Oxford, p727

211. R. B. King and M. B. Bisnette, *Inorg. Chem.*, (1966), **5**, 300
212. G. N. Schrauzer, *Chem. Ber.*, (1961), **94**, 1891
213. J. C. Clark and R. C. Cookson, *J. Chem. Soc.*, (1962) 686
214. A. N. Nesmeganov, Y. A. Clapovski and L. G. Makarova, *Izv. Akad. Nauk., SSSR, Ser. Khim.*, (1965), 1310
215. E. W. Abel, C. A. Burton, M. R. Churchill and K. G. Lin, *J. Chem. Soc., Chem. Comm.*, (1974), 268
216. C. F. Barrientos-Penna, A. B. Gilchrist, A. H. Klahn-Oliva, A. J. L. Halan and D. Sutton, *Organometallics*, (1985), **4**, 478
217. R. Hoffmann, *J. Chem. Phys.*, (1963), **40**, 2474
218. J. C. Slater, *Phys. Rev.*, (1930), **36**, 57
219. C. Zener, *Phys. Rev.*, (1930), **36**, 51
220. A. Rauk, *EHMO86— The Extended Huckel Program*
221. H. Basch and H. B. Gray, *Theoret. Chim. Acta*, (1966), **4**, 367
222. E. Clementi and C. Roetti, *At. Data Nucl. Data Tables*, (1974), **14**, 177
223. E. Clementi, C. L. Raimondi and W. P. Reinhardt, *J. Chem. Phys.*, (1967), **47**, 1300
224. J. W. Richardson, W. C. Nieuwpoort, R. R. Powell and W. F. Edgell, *J. Chem. Phys.*, (1962), **36**, 1057
225. J. Hinze and H. H. Jaffé, *J. Chem. Phys.*, (1963), **67**, 1501
226. R. H. Summerville and R. Hoffmann, *J. Am. Chem. Soc.*, (1976), **98**, 7240
227. P. J. Hay, J. C. Thibeault and R. Hoffmann, *J. Am. Chem. Soc.*, (1975), **97**, 4884
228. E. Canadell and O. Eisenstein, *Inorg. Chem.*, (1983), **22**, 2398
229. M. Elian and R. Hoffmann, *Inorg. Chem.*, (1975), **14**, 1058
230. J. W. Lauher, M. Elian, R. H. Summerville and R. Hoffmann, *J. Am. Chem.*

Soc., (1976), **98**, 3219

231. A. Dedieu, T. A. Albright and R. Hoffmann, *J. Am. Chem. Soc.*, (1979),
101, 3141

232. M. M. L. Chen and R. Hoffmann, *J. Am. Chem. Soc.*, (1976), **98**, 1647